TECHNICAL REPORT STANDARD TITLE PAGE

1. Report No.	2. Government Accession No.	3. Recipient's Catalog No.
FHWA/TX-86/78+350-1		

4. Title and Subtitle	5. Report Date
BEHAVIOR OF ONTARIO-TYPE BRIDGE DECKS ON STEEL GIRDERS	January 1986
	6. Performing Organization Code
7. Author(s)	8. Performing Organization Report No.
I.-K. Fang, J. A. Worley, N. H. Burns, and R. E. Klingner	Research Report 350-1
9. Performing Organization Name and Address	10. Work Unit No.
Center for Transportation Research The University of Texas at Austin Austin, Texas 78712-1075	11. Contract or Grant No. Research Study 3-5-83-350
	13. Type of Report and Period Covered
12. Sponsoring Agency Name and Address Texas State Department of Highways and Public Transportation; Transportation Planning Division P. O. Box 5051 Austin, Texas 78763	Interim
	14. Sponsoring Agency Code

15. Supplementary Notes

Study conducted in cooperation with the U. S. Department of Transportation, Federal Highway Administration. Research Study Title: "Behavior of Concrete Bridge Decks on Steel Beams—Verification of the Ontario Bridge Deck Design (With and Without Panels)"

16. Abstract

An experimental and analytical investigation was conducted regarding the behavior of reinforced concrete bridge decks designed in accordance with the Ontario Highway Bridge Deck Design provisions. Detailed finite element models of the specimen were developed for both the cast in place and precast deck cases. Cracking of the deck was followed using a smeared cracking model. Results predicted by the analytical models correlated well with experimental observations. In brief, the following conclusions were reached: (1) a full-scale bridge deck (both cast-in-place and precast), detailed in accordance with the Ontario Highway Bridge Design provisions and having about 60 percent of the reinforcement required by the current AASHTO code, performed satisfactorily under current AASHTO design load levels; (2) under service and overload conditions (about three times the current AASHTO design wheel load) the behavior of the deck slab was essentially linear, and was not affected by fatigue loading, nor by the presence of midspan diaphragms or additional diaphragms; (3) analytical predictions and experimental results agreed closely, showing that the analytical models of the bridge specimen are satisfactory, and can be extended to other bridge configurations; and (4) compressive membrane forces did not significantly affect the performance of the bridge at loads below cracking. The effects of arching action on the ultimate capacity of the bridge deck are discussed in further reports for the project.

17. Key Words	18. Distribution Statement
bridge decks, reinforced concrete, behavior, experimental, analytical, Ontario, design, composite	No restrictions. This document is available to the public through the National Technical Information Service, Springfield, Virginia 22161.

19. Security Classif. (of this report)	20. Security Classif. (of this page)	21. No. of Pages	22. Price
Unclassified	Unclassified	210	

Form DOT F 1700.7 (8-69)

BEHAVIOR OF ONTARIO-TYPE BRIDGE DECKS ON STEEL GIRDERS

by

I.-K. Fang, J. A. Worley, N. H. Burns, and R. E. Klingner

Research Report No. 350-1

Research Project 3-5-83-350

"Behavior of Concrete Bridge Decks on Steel Beams - Verification of the Ontario Bridge Deck Design (With and Without Panels)"

Conducted for

Texas

State Department of Highways and Public Transportation

In Cooperation with the
U.S. Department of Transportation
Federal Highway Administration

by

CENTER FOR TRANSPORTATION RESEARCH
BUREAU OF ENGINEERING RESEARCH
THE UNIVERSITY OF TEXAS AT AUSTIN

January 1986

The contents of this report reflect the views of the authors who are responsible for the facts and accuracy of the data presented herein. The contents do not necessarily reflect the official views or policies of the Federal Highway Administration. This report does not constitute a standard, specification, or regulation.

PREFACE

Recent research in the U.S. and Canada has suggested that the flexural capacity of bridge decks is increased by in-plane compressive forces, created when the cracked deck is restrained by supports that cannot move laterally. This phenomenon, commonly referred to as "arching action", is the basis for the semi-empirical design provisions of the current Ontario (Canada) Bridge Design Code. That code permits the use of less flexural steel than would be required by current AASHTO Specifications, resulting in bridge decks which are generally more economical and resistant to corrosion.

Previous research on arching action has been carried out mainly using small-scale models with artificial boundary conditions. The overall objective of Research Project 3-5-83-350 was to study the performance of full-scale bridge decks designed taking arching action into account. Using a full-scale model of a realistic prototype highway bridge, both cast-in-place and precast, prestressed panel decks were considered. The specific objectives addressed in Report 350-1 were:

1. To study the pre- and post-fatigue behavior of the cast-in-place and panel decks under service load and overload conditions;

2. To develop analytical models of the bridge, and to test these models against the observed behavior of the bridge;

3. To use the analytical models to conduct parametric studies involving one bridge design feature (diaphragm spacing); and

4. To assess, experimentally and analytically, the significance of compressive membrane action in a real bridge deck at service load and overload levels. Ultimate behavior is not considered in this report, but is discussed in other reports for this project.

SUMMARY

An experimental and analytical investigation was conducted regarding the behavior of reinforced concrete bridge decks designed in accordance with the Ontario Highway Bridge Deck Design provisions.

In the experimental part of the investigation, a full-scale composite bridge (concrete deck on steel girders) was built using a cast-in-place deck at one end, and a precast, prestressed panel deck with cast-in-place topping at the other end. The bridge was simply supported on a 49-ft span, and loaded vertically at four points. The bridge was first loaded statically to about three times the current AASHTO design wheel load (to study its response under service and overload conditions), after which it was subjected to 5 million cycles of sinusoidal fatigue loading with a maximum value of about 125% of current design wheel loads, and a minimum value close to zero. After that, the bridge was again loaded statically, to about twice the design load level, to study its service and overload behavior after fatigue cracking.

Detailed finite element models of the specimen were developed for both the cast-in-place and precast deck cases. Cracking of the deck was followed using a smeared cracking model. Results predicted by the analytical models correlated well with experimental observations.

In brief, the following conclusions were reached:

1. A full-scale bridge deck (both cast-in-place and precast), detailed in accordance with the Ontario Highway Bridge Design provisions (and having about 60 percent of the reinforcement required by the current AASHTO code), performed satisfactorily under current AASHTO design load levels;

2. Under service and overload conditions (about three times the current AASHTO design wheel load) the behavior of the deck slab was essentially linear, and was not affected by fatigue loading, nor by the presence of midspan diaphragms or additional diaphragms;

3. Analytical predictions and experimental results agreed closely, showing that the analytical models of the bridge specimen are satisfactory, and can be extended to other bridge configurations; and

4. Compressive membrane forces did not significantly affect the performance of the bridge at loads below cracking. The effects of arching action on the ultimate capacity of the bridge deck are discussed in further reports for this project.

IMPLEMENTATION

Cast-in-place and precast, prestressed panel bridge decks similar to the one tested in this study, and detailed with Ontario-type reinforcement, can be built in the field. Their field performance should be evaluated by the Texas SDHPT.

To obtain a broader understanding of the behavior of bridge decks before the new deck design is completely incorporated in Texas SDHPT design provisions, parametric studies should be conducted involving variables such as the span to thickness ratio of the deck, the effects of line loads, skew bridge behavior, and the stiffness of integral barriers. Work needs to be completed on the effects of arching action on ultimate capacity, and on crack widths and reinforcement stresses at higher load levels.

TABLE OF CONTENTS

Chapter

Page

Chapter

Page

LIST OF TABLES

LIST OF FIGURES

LIST OF FIGURES (continued)

Figure

Page

LIST OF FIGURES (continued)

LIST OF FIGURES (continued)

LIST OF FIGURES (continued)

LIST OF FIGURES (continued)

LIST OF FIGURES (continued)

CHAPTER 1

INTRODUCTION

1.1 General

Over the past decade, considerable research has been devoted to a reassessment of the load-carrying capacity of reinforced concrete bridge decks. Such decks have traditionally been designed by conventional beam theory (1.1). Recent research in the U.S. and Canada has suggested that the flexural capacity of bridge decks may be increased by the presence of in-plane compressive forces, created when the deck is restrained by supports that cannot move laterally. This phenomenon is referred to in much of the literature (and therefore in this report as well) as "arching action". It is the basis for the semi-empirical design provisions of the current Ontario (Canada) Bridge Design Code (1.2). According to that code, arching action permits the use of less flexural steel than would be required by current AASHTO specifications (1.1). In addition to reduced costs for material and placement, lower required areas of flexural reinforcement can lead to fewer problems with corrosion, since the reduced steel area has less tendency to cause popouts and spalling of the deck's wearing surface.

In view of these possible advantages, the Texas State Department of Highways and Public Transportation (SDHPT) and the Federal Highway Administration (FHWA) have begun to investigate the performance of bridge decks reinforced in accordance with the Ontario design provisions.

1.2 Research Objectives and Scope

As described in the literature review of Chapter 2, most specimens used in previous tests were either small-scale panels or isolated full-scale panels with special edge restraints. When these tests were evaluated in planning the experimental program, it was felt that those special circumstances would make it difficult to infer the behavior of an actual bridge deck from available experimental results. Also, sufficient studies of actual full-scale bridge deck behavior are still not available, and the long-term effects of fatigue loading are difficult to test in the field. In addition, very little analytical confirmation of those results was available. It was therefore believed necessary to study experimentally the behavior of a full-

scale bridge deck with realistic support conditions, and to develop analytical models capable of accurately reproducing the observed behavior.

Given the deficiencies of the existing research, the primary objective of this research was to verify the Ontario bridge deck design procedures for the case of cast-in-place (CIP) and precast prestressed panel decks on steel girders. The specific objectives were:

1. To study the pre- and post-fatigue behavior of the CIP deck under service load and overload conditions;

2. To study the pre- and post-fatigue behavior of the precast panel deck under service load and overload conditions;

3. To develop analytical models of the CIP deck and precast panel deck, and to test these models against the observed behavior of the bridge;

4. To use the models to conduct parametric studies involving one bridge design feature (diaphragm spacing); and

5. To assess, experimentally and analytically, the significance of compressive membrane action in a real bridge deck at service load and overload levels. Ultimate behavior is not discussed here.

The behavior of bridge decks detailed in accordance with the Ontario empirical method is being studied in a series of research investigations conducted at the Ferguson Structural Engineering laboratory of The University of Texas at Austin. Other investigations are devoted specifically to a study of girder moments in such bridges (1.3), to the behavior of such bridge decks under negative moment regions (1.4), and to the ultimate capacity of such bridge decks under concentrated loads (1.4). Those investigations are not discussed further here.

1.3 Summary of Current AASHTO Bridge Deck Design Provisions

According to the current AASHTO Code (1.1), deck slabs of highway bridges must be designed to resist wheel loads plus their own dead weight. Live load moments in concrete bridge decks are evaluated differently for each of the three main types of slabs: 1) slabs whose main reinforcement is placed perpendicular to the traffic; 2) slabs whose main reinforcement is placed parallel to the traffic; and 3) cantilever slabs.

For slabs and girder bridges, the deck slab is considered as a one-way slab spanning transversely and supported by the girders. The main reinforcement is therefore placed transversely. Only this type of slab will be discussed hereafter.

According to the AASHTO Code, the maximum transverse design moment per foot of such slabs is given by:

$$M = ((S + 2)/32)\ P \qquad \text{(Section 1.3.2. of Ref. (1.1))}$$

where S is the effective slab span in ft; and P is the concentrated wheel load. For slabs supported on steel stringers, S is the distance between edges of flanges plus one-half of the stringer flange width. Dynamic effects are included by multiplying those moments by an impact factor of 1.3. Design moments may be reduced by a continuity factor of 0.8 for slabs supported over three or more supports. Once the design moment has been calculated, the main reinforcement can be proportioned.

According to the AASHTO provisions, slabs proportioned as above are considered satisfactory in bond and shear. The above procedures have long been used in the design of bridge decks. However, recent research, described in the literature review of Chapter 2, has suggested that current AASHTO design procedures are conservative, and result in unnecessarily high reinforcement requirements in the typical deck slabs of slab and girder bridges.

1.4 Summary of Empirical Method of Current Ontario Highway Bridge Deck Design

The limit state concept has been adopted in the design of bridge structures in the current Ontario Bridge Design Code (OHBDC) (1.2). According to the current (1983) Ontario design provisions, concrete deck slabs shall be designed for the ultimate limit state of strength and the serviceability limit state of cracking. The use of the empirical method is emphasized if the bridge system satisfies certain criteria. This empirical method is based mainly on the presumption of significant compressive membrane action in the deck slab. Design of the deck slab simply involves prescribing 0.3% reinforcement in both directions, as shown in Fig. 1.1.

The prerequisites for the empirical method are as follows:

1. The girder spacing should not exceed 3.7 m (12.1 ft). The cantilever portion of the slab should extend at

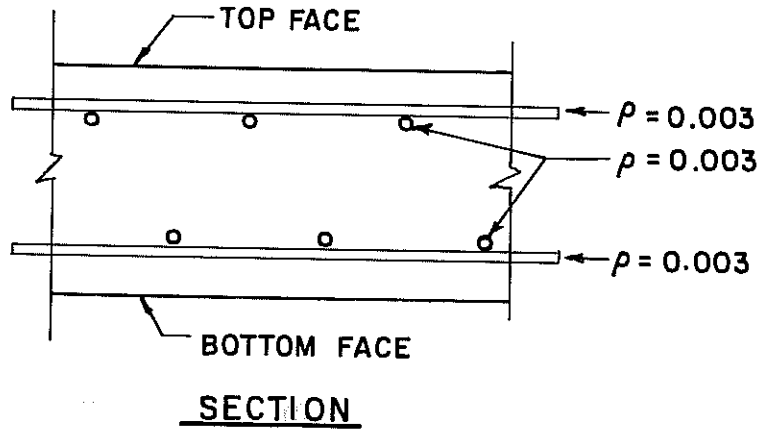

SECTION

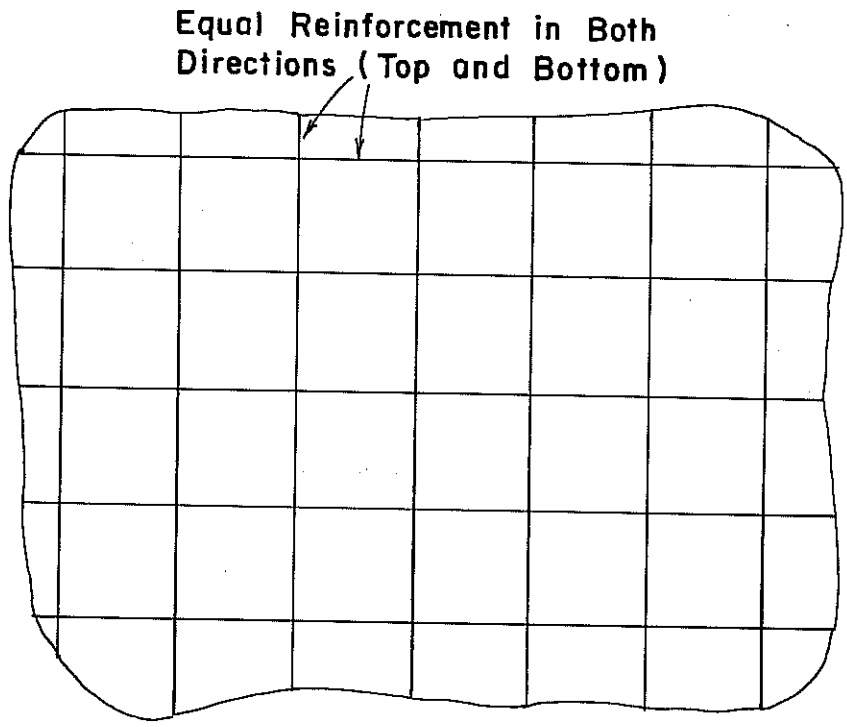

PLAN

Fig. 1.1 Reinforcement layout prescribed by empirical method

least 1 m (3.3 ft) beyond the centerline of the exterior. The curb integral with the slab may be used instead of the 1 m overhang, provided that the combined cross-sectional area of the curb, plus the slab beyond the centerline of the external girder, is not less than the cross-sectional area of a 1 m length of the deck slab.

2. The span length to thickness ratio of the slab should not exceed 15. In skew slabs, the skew span shall be used in calculating this ratio.

3. For skew angles greater than 20 degrees, the end portions of the deck slab shall be provided with 0.6% isotropic reinforcement.

4. Slab thickness is not less than 225 mm (9 in.), and spacing of the isotropic reinforcement bars in each face does not exceed 300 mm (12 in.). In earlier versions of the OHBDC, this minimum thickness was specified as the equivalent of 7-1/2 in. Owing to durability considerations (for Ontario) rather than stuctural considerations, the minimum required thickness was increased in the 1983 OHBDC to the equivalent of 9-in.

5. Diaphragms shall extend throughout the transverse cross section of the bridge between external girders, and the maximum spacing of such diaphragms shall be 8 m (26 ft) for steel I-beams and box girders. The diaphragms shall be provided at the supports for reinforced and prestressed concrete girders.

6. Edge stiffening shall be provided in accordance with the Code provisions.

Deck slabs designed in accordance with the empirical method need not be analyzed, are presumed to have met crack control requirements, and to have adequate shear resistance.

When the empirical method is not applicable, ultimate resistance should be determined by yield line methods rather than elastic analyses. The serviceability limit state of cracking should also be checked. Since crack control is a very important requirement for a durable deck slab, the cross-section of the deck shall be proportioned so that the maximum calculated crack widths meet the Code requirements.

To prevent excessive cracking at the ultimate limit state, the ratio of unfactored flexural resistance at a support to that at midspan in the same direction should be between 1.0 and 1.5 (1.2).

When the empirical method is not applicable, the deck design moments can be calculated using the provisions of Chapter 3 of the current OHBDC. Those calculations are beyond the scope of this research, and are not discussed further here.

1.5 Comparison of the Reinforcement Required by AASHTO Code and Ontario Code (Empirical Method)

As mentioned before, one of the possible advantages of the Ontario Code's empirical design method is that smaller amounts of deck reinforcement can be used. This section is intended to compare typical reinforcement requirements for bridge decks designed according to the AASHTO Code and the Ontario Code (empirical procedure). For simplicity, the comparison will be presented only for deck slabs supported on steel girders and prestressed concrete girders. Supporting calculations are given in Appendix A, and the results are summarized in Fig. 1.2.

As shown in that figure, the required reinforcement in decks detailed using the AASHTO Code weighs about 5 to 5.3 lbs/sq. ft. for girder spacing ranging from 5.66 ft to 9.64 ft. The average reinforcement required using the Ontario Code (empirical method) weighs about 3.3 lbs/sq. ft. Although this requirement increases slightly for girder spacings beyond 8 ft, the amount of steel required by the Ontario Code is typically less than 60% of that required by the current AASHTO Code.

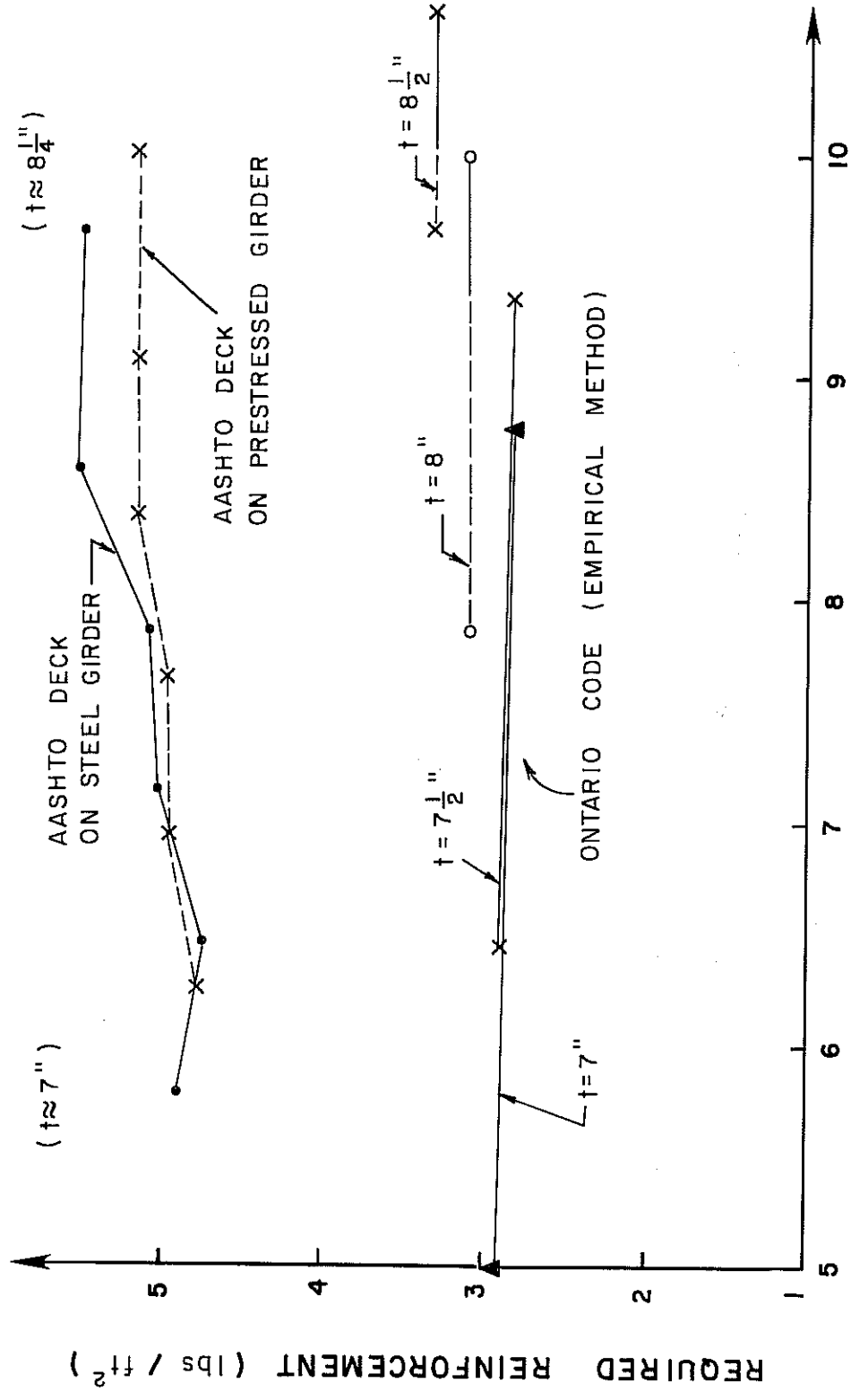

Fig. 1.2 Comparison of deck reinforcement required for interior span of slab and girder bridge

CHAPTER 2

BACKGROUND

2.1 General

This chapter is intended to give a historical review of research into the phenomenon of "arching action" as applied to reinforced concrete elements.

2.2 Reinforced Concrete Beams

2.2.1 Uncracked. As shown in Fig. 2.1, a simply supported beam under vertical loads can undergo unrestrained elongation of its bottom fiber if there is no horizontal restraint at the end supports. Such a beam is normally analyzed as a line segment subject only to flexure and shear. No axial restraint force is developed in such a beam.

As shown in Fig. 2.2(a), if the same simply supported beam is restrained against elongation of its neutral axis by horizontal supports, no axial axial restraint force is developed as long as small-deflection theory is applied. If, however, as shown in Fig. 2.2(b), the bottom fiber of the same beam is restrained against elongation by horizontal supports, compressive axial force will be present, along with the flexure and shear. The axial force is due to the fact that the depth of the element is considered, and it is present even if deflections are small. This axial compression is commonly referred to in bridge literature as "arching action", even though the element may be relatively shallow.

2.2.2 Cracked. A typical fixed-fixed reinforced concrete beam is shown in Fig. 2.3. If the external load is high enough, some cracks will form at the sagging (ends) and hogging (midspan) moment regions. If the beam is idealized as a line element restrained at its neutral axis, it will behave as in Fig. 2.2(a), and no arching action will be developed, even after flexural cracking.

However, if the thickness of the beam is considered, flexural cracking will produce compressive membrane forces. Because of flexural cracking, the neutral axis of the beam will be shifted towards the bottom fiber at the supports, and towards the top fiber at midspan. Under load, each uncracked portion of the beam will rotate

A) SUPPORTS AT NEUTRAL AXIS
(THICKNESS NEGLECTED)

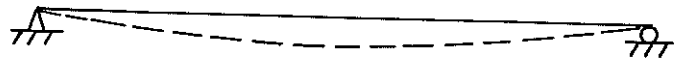

B) SUPPORTS AT BOTTOM FIBER
(THICKNESS CONSIDERED)

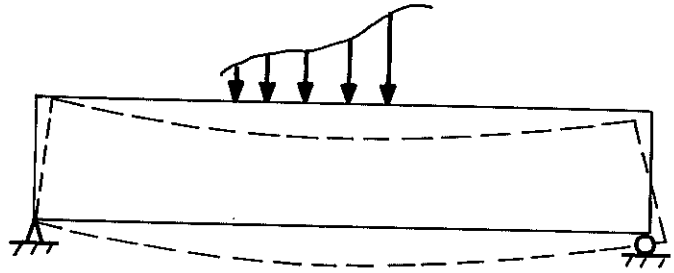

WITHOUT ARCHING ACTION

Fig. 2.1 Simply supported beam, no horizontal restraint at supports

A) SUPPORTS AT NEUTRAL AXIS
(THICKNESS NEGLECTED)

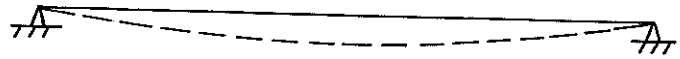

B) SUPPORTS AT BOTTOM FIBER
(THICKNESS CONSIDERED)

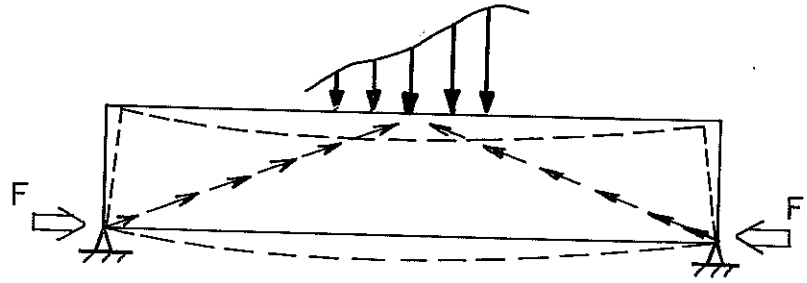

WITH ARCHING ACTION

Fig. 2.2 Simply supported beam with horizontal restraint at supports

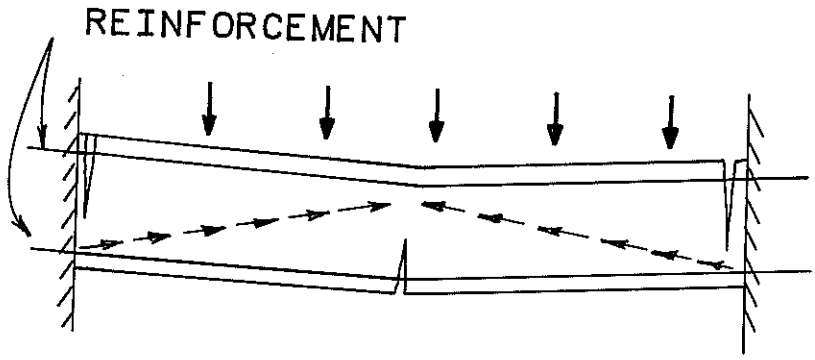

Fig. 2.3 Arching action in cracked beam

about the point where its neutral axis hits the support (Fig. 2.3). Because of the off-center location of the neutral axis, compressive membrane forces will be produced even by small displacements of the beam. This is illustrated by a numerical example in Subsection 4.3.7.

2.3 Reinforced Concrete Slabs

2.3.1 Uncracked. In small-deflection plate theory, all loads and supports are assumed to act on the middle of the plate. This middle plane is assumed to be unstretched, and to remain neutral during loading. This last assumption is satisfied only if the plate is bent into a developable surface, such as a cylindrical surface (2.1). In other cases, bending of a plate is accompanied by tensile strain in the middle plane. An example of this, shown in Fig. 2.4, involves a simply supported square plate, subjected to a concentrated out-of-plane load at its center. In addition to flexural deformations, the central part of this plate is stretched, and is in membrane tension (2.2). This tensile membrane force is balanced by compression in the outer compressive ring. This membrane action exists even in the absence of in-plane restraint at the supports.

However, the magnitude of such membrane stress is often small in comparison to the bending stress, provided that the deflection of the plate is small in comparison to its thickness.

Now suppose that same plate is simply supported at its bottom surface. If the thickness of the plate is considered, the solution will differ from that discussed immediately above. As for the beams discussed in Section 2.2, restraint of the bottom surface will produce additional membrane compression in the plate ("arching action"), even if deflections are small.

2.3.2 Cracked. As shown in Fig. 2.5, flexural cracking of a reinforced concrete slab can cause its neutral surface to move away from the center, toward the top or bottom surface. Since reinforced concrete slabs are usually not heavily reinforced, the neutral surface will be very close to the slab's compressive surface. Analogous to the cracked beam discussed above, these shifts in the height of the neutral surface will produce compressive membrane forces in a cracked slab, even if deflections are small. These membrane forces will increase with applied load.

Near the collapse load, slab deflections become very large, the slab resists loads primarily through membrane tension in the reinforcement. This resistance mechanism is not discussed further here.

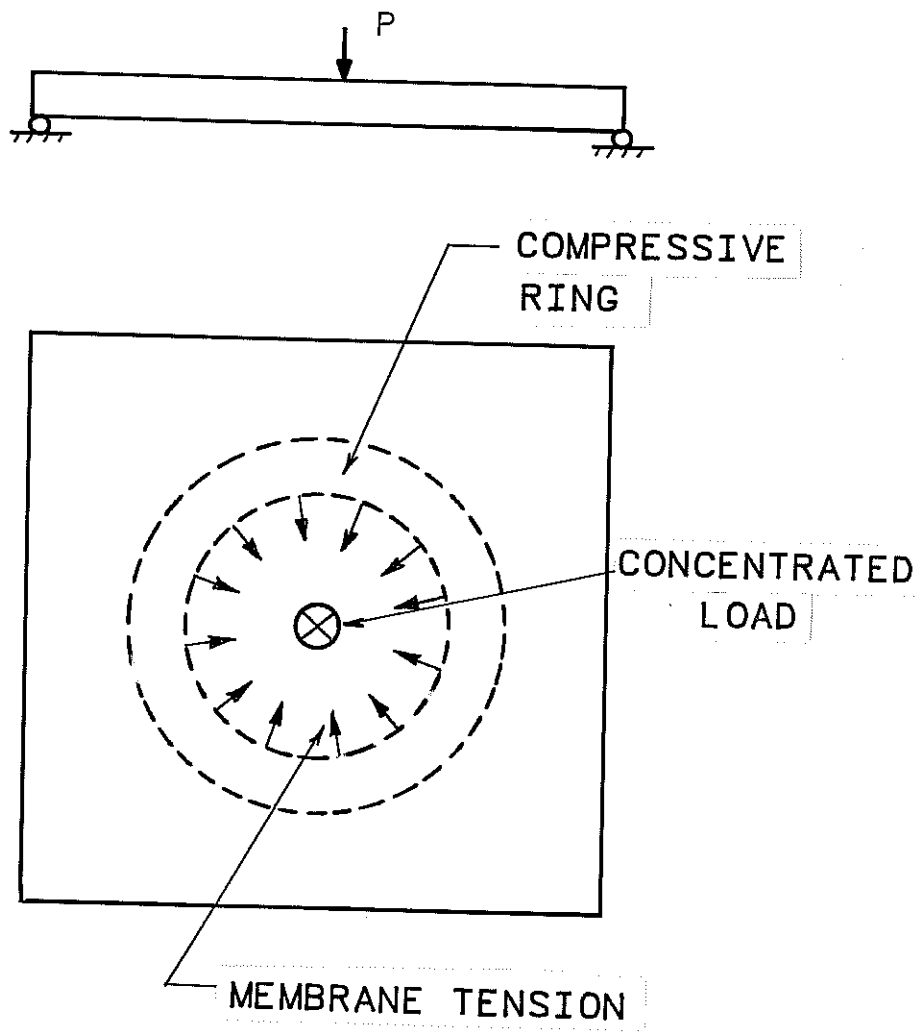

Fig. 2.4 Membrane tension in centrally loaded plate

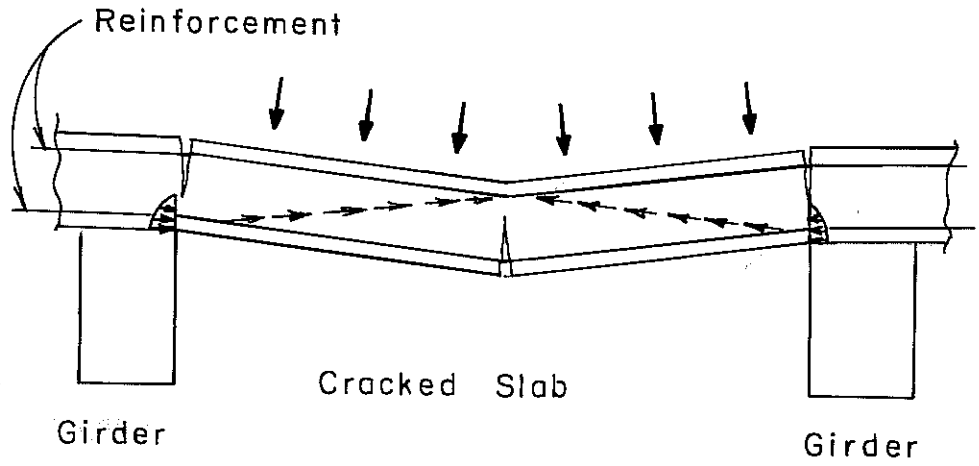

Fig. 2.5 Arching action in cracked slab

2.4 Historical Review

The effect of in-plane forces on the load-carrying capacity of reinforced concrete slabs has been an active field of structural engineering research for several decades. In 1956, Ockleston (2.3) tested a three-story reinforced concrete building in Johannesberg, South Africa, and recorded collapse loads three or four times the capacities predicted by yield-line theory. Ockleston (2.4) also identified this phenomenon as the effect of compressive membrane forces. In 1957, Liebenberg, Robertson and McGraw (2.5) conducted tests on the old Alliance House in Cape Town, South Africa. Fifty slab panels were tested to destruction prior to the demolition of the building. These test results also confirmed the existence of compressive membrane action, and its beneficial effect on the load-carrying capacity of the floor system. After a study of the behavior of continuous prestressed concrete slabs, Guyon (2.6) suggested that arching action should be taken into account in designing such slabs to resist concentrated out-of-plane loads. Other experimental verifications of this were also carried out by Christiansen, Fredericksen (2.7, 2.8) and Park (2.9, 2.10, 2.11, 2.12, 2.13).

To predict the strength of edge-restrained slabs, several approximate analytical techniques were proposed and verified using small-scale models. For instance, Park attempted to analyze two-way rectangular slabs for compressive membrane action using rigid-plastic strips running along the short and long directions of the slab. The slab's ultimate capacity was then obtained from a virtual work equation (2.12).

In the late 1950's, tests were conducted on single panels by Sozen and Gamble (2.14, 2.15) at the University of Illinois. When bounded by elements which could develop horizontal reactions, such reinforced concrete panels were found to have flexural capacities considerably in excess of the load calculated by Johanson's yield line theory. The additional capacity was attributed primarily to the effect of in-plane forces.

Research in this field originally concentrated on the behavior of building floor systems, and most tests were conducted using small-scale models (2.16, 2.17, 2.18). At the end of 1975, the Ontario Ministry of Transportation and Communications decided to develop a code for designing highway bridges in that province. A series of tests were undertaken by academic researchers and the Ministry's Research and Development Division. Bridge design loads were reevaluated using survey data of actual truck loadings in Ontario (2.19, 2.20, 2.21). A new bridge design load, adopted for the current OHBDC (2.22), is shown in Fig. 2.6.

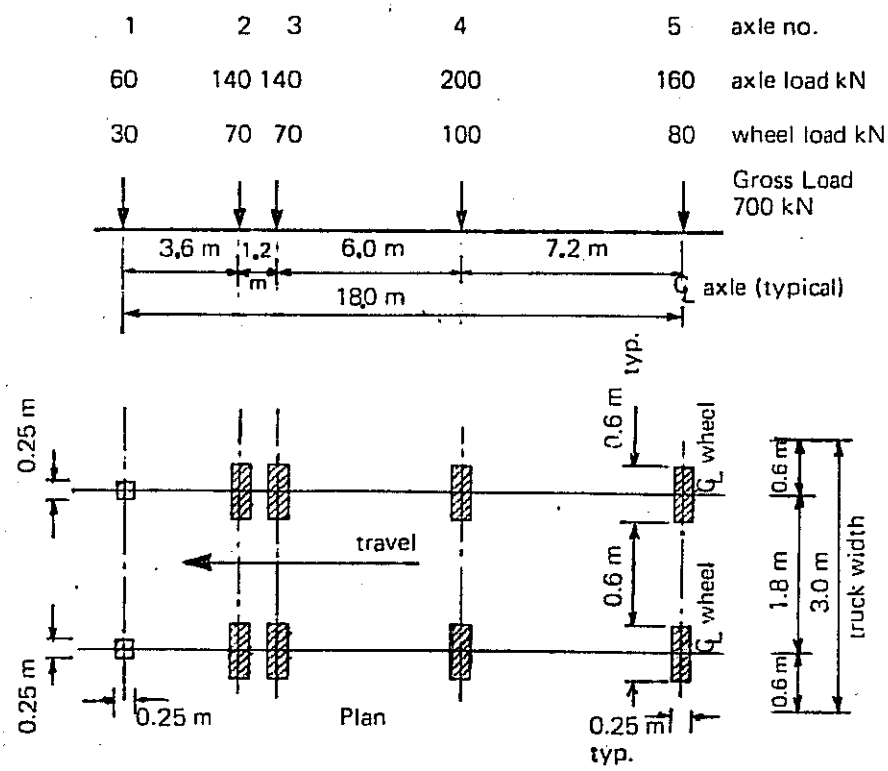

A) OHBD TRUCK LOADING

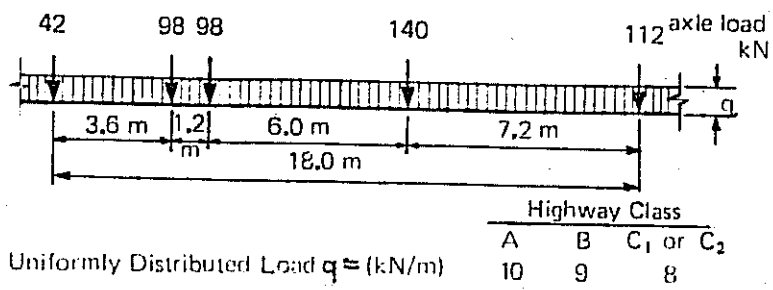

B) OHBD LANE LOADING

Fig. 2.6 Current (1983) Ontario Highway Bridge Design Load (Fig. 2-4.3.1.2 of Ref. 2.22)

Since 1969, many bridges have been tested in the field by the Structural Research Section of the Ontario Ministry of Transportation and Communications (2.23). The load-carrying capacities of these bridges, and the performance of their structural components, have been evaluated.

From field tests, it was observed that thin concrete deck slabs supported by beams or girders were generally capable of carrying concentrated wheel loads far in excess of capacity predicted by traditional methods of analysis, even if the deck had considerably deteriorated, or a large percentage of the reinforcing steel had been lost due to corrosion.

Under the sponsorship of the Ontario Ministry of Transportation and Communication, a series of studies was conducted at Queen's University, Kingston, Ontario, using 1/8-scale models (2.24, 2.25, 2.26, 2.27). Results showed that large reserves of strength existed in deck slabs under static and fatigue loadings.

This research work was supplemented by field tests of actual bridges (2.28,2.29,2.30). It was concluded that a slab's load-carrying capacity was increased by in-plane restraint.

Based on these findings, an empirical design method was proposed, involving an isotropic reinforcement layout in the deck. Required reinforcement is considerably less than that specified by the AASHTO Code (2.31). Some bridge decks in Ontario have been designed using the proposed empirical method.

Recent field tests of a trapezoidal box girder bridge in Canada (2.32), conducted by the Ontario Highway Department, have shown that a bridge deck detailed with the 0.3% isotropic reinforcement performed satisfactorily. Under the maximum wheel load of 100 kips, the maximum observed transverse reinforcing steel stress was 18.64 ksi, and the longitudinal stress, 14.5 ksi. The load-deflection relationship at the loaded point was very linear up to that load level.

Field tests were also recently conducted in Canada on a composite prestressed concrete girder bridge with a deck detailed in accordance with the empirical method (2.33). The load-deflection curve at the loaded point was again very linear up to about 100 kips wheel load level. The maximum observed stresses in reinforcement were less than 20 ksi at that load level.

The convenience in construction of such decks, and the savings in the amount of reinforcement required, have attracted the attention of researchers in the United States. The New York Highway

Department has recently conducted a study of the strength of highway bridge decks (2.34). Both the proposed Ontario reinforcing details and those consistent with current AASHTO design procedures were tested, using reduced-scale bridge decks. Tests were conducted on uncracked and cracked slabs. The uncracked-slab test was intended to simulate the behavior of the deck slab under vehicular overload, and to better study steel strains.

Under design loads, the stress in reinforcement was found not to exceed 12 ksi. When loaded to ultimate, all locations bounded by longitudinal girders failed by punching shear. Regardless of the reinforcing pattern used, failure loads always exceeded six times the design wheel load for slabs bound by girders.

CHAPTER 3

TEST SPECIMEN

3.1 Development of Test Specimen

The design of the bridge specimen for the experimental testing program took into account the known details suggested by the Ontario Highway Department's research. In the Ontario design method, the deck design is reduced to a prescription of the isotropic reinforcement (3.1). The Texas-proposed highway bridge deck details (following the Ontario code quite closely) showed two layers of reinforcement in a 7-1/2 in. thick deck slab (3.2). The slab thickness was set at 7-1/2 rather than 9-in. for two reasons: a) the 7-1/2 in. thickness was adequate from a structural viewpoint; and b) durability requirements for Texas did not demand the additional thickness deemed necessary for Ontario. In addition, use of the thinner slab resulted in a more severe test of the system's structural performance. This slab was to be made composite with the steel girders by means of shear studs. Figures 3.1 and 3.2 show the plan and elevation views of the test specimen, and Fig. 3.3 shows the composite bridge cross-section.

Another design consideration for the experimental program was that precast-prestressed concrete deck panels were to be included in some portions of the deck of the test specimen. Figure 3.4 shows the cross-section with panels used for the south half of the deck. Previous studies by Buth et al. (3.3 through 3.12) and, more recently, Bieschke and Klingner (3.13), had shown excellent behavior of bridge decks incorporating precast panels. Experience in the field has followed the experimenal work, and 4-in. thick panels (see detail, Fig. 3.5) have become standard products in Texas for use in construction of composite deck slabs similar to the one in this experimental program. It was decided that this test slab would need to be full-sized (7-1/2 in. thick) in order to allow use of the standard precast-prestressed panels for half the bridge. Use of the full-size bridge deck, as indicated above, was also designed to take advantage of standard materials and avoid complications due to scaling in the interpretation of test results.

A typical bridge could be simulated with three girders, an interior girder and two exterior ones. Due to the space limitations inherent in full-scale testing, it was decided to use a bridge specimen having only three girders. For the Ontario deck design, a

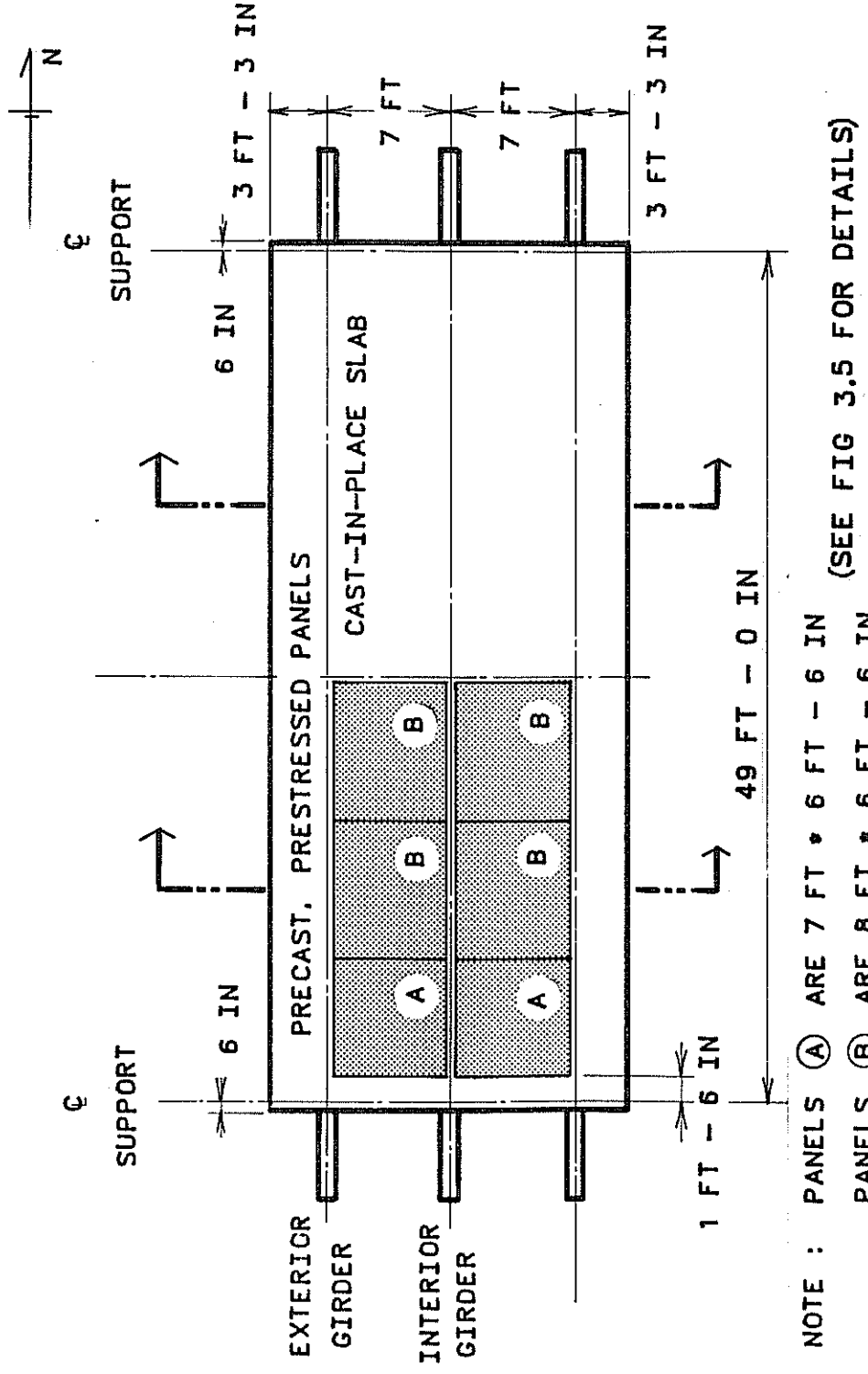

Fig. 3.1 Plan view of laboratory specimen

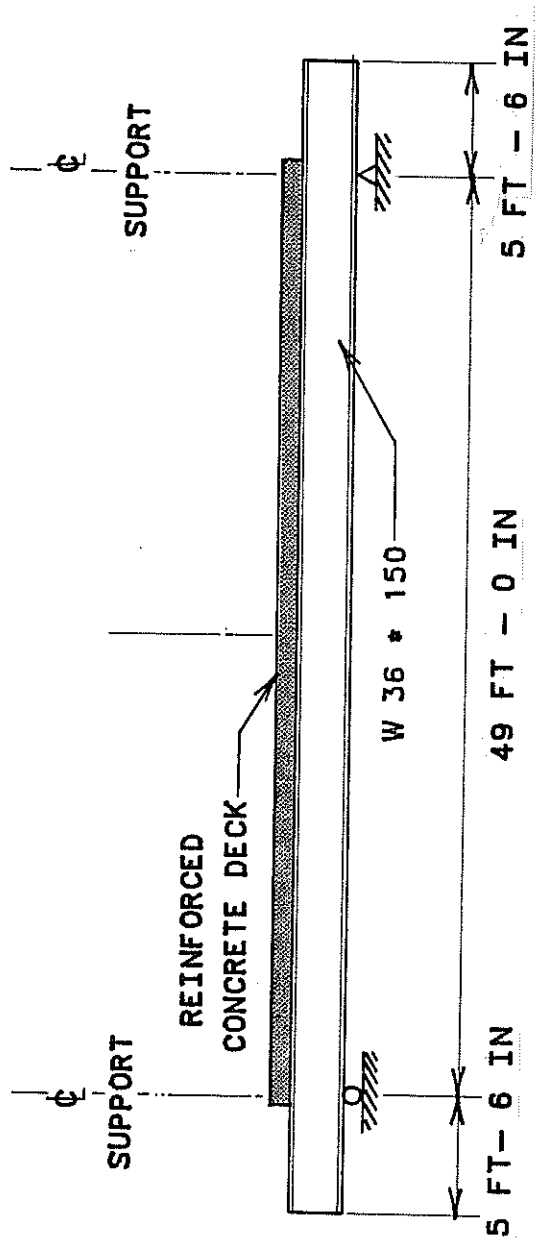

Fig. 3.2 Elevation view of laboratory specimen

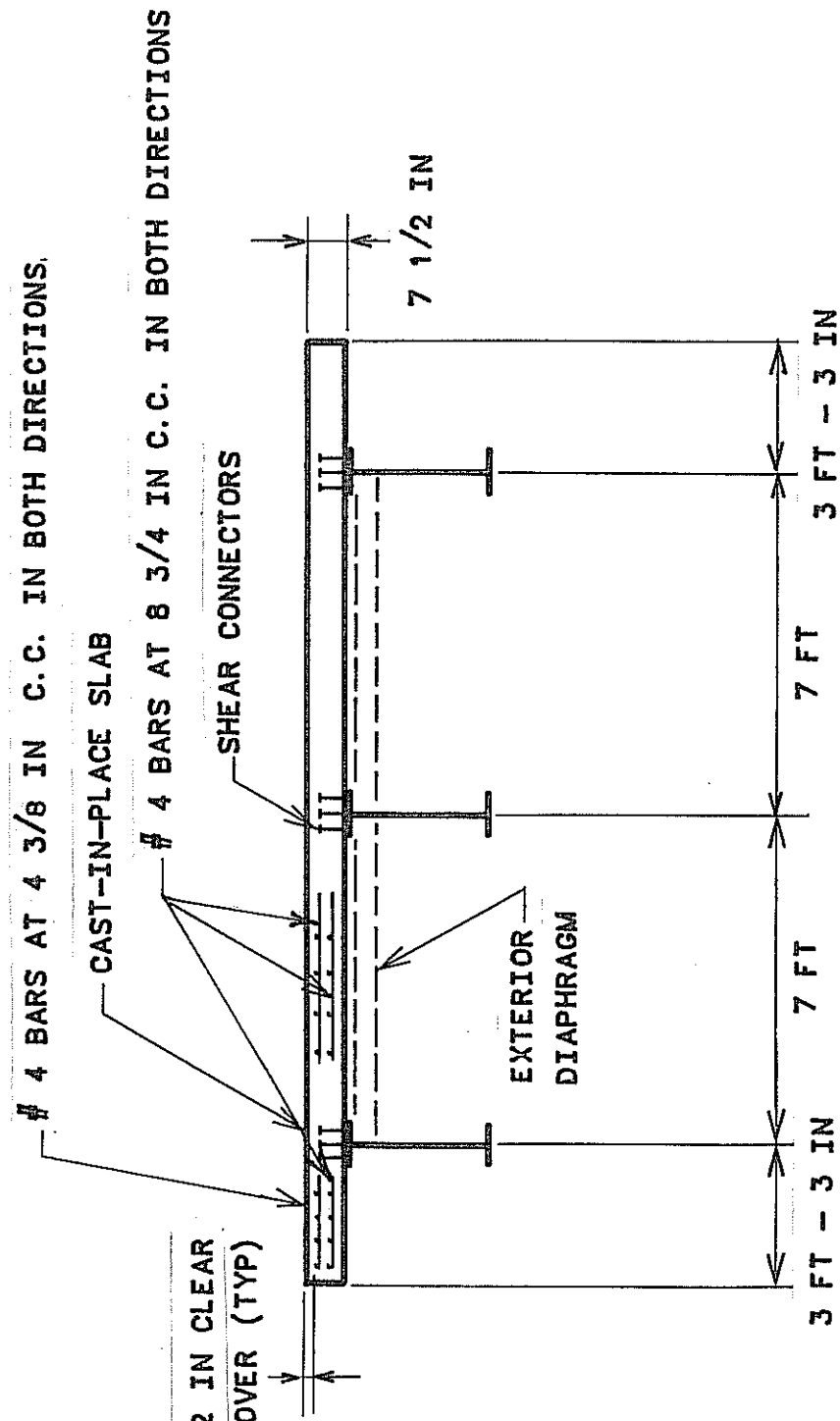

Fig. 3.3 Cross section of laboratory specimen showing cast-in-place deck

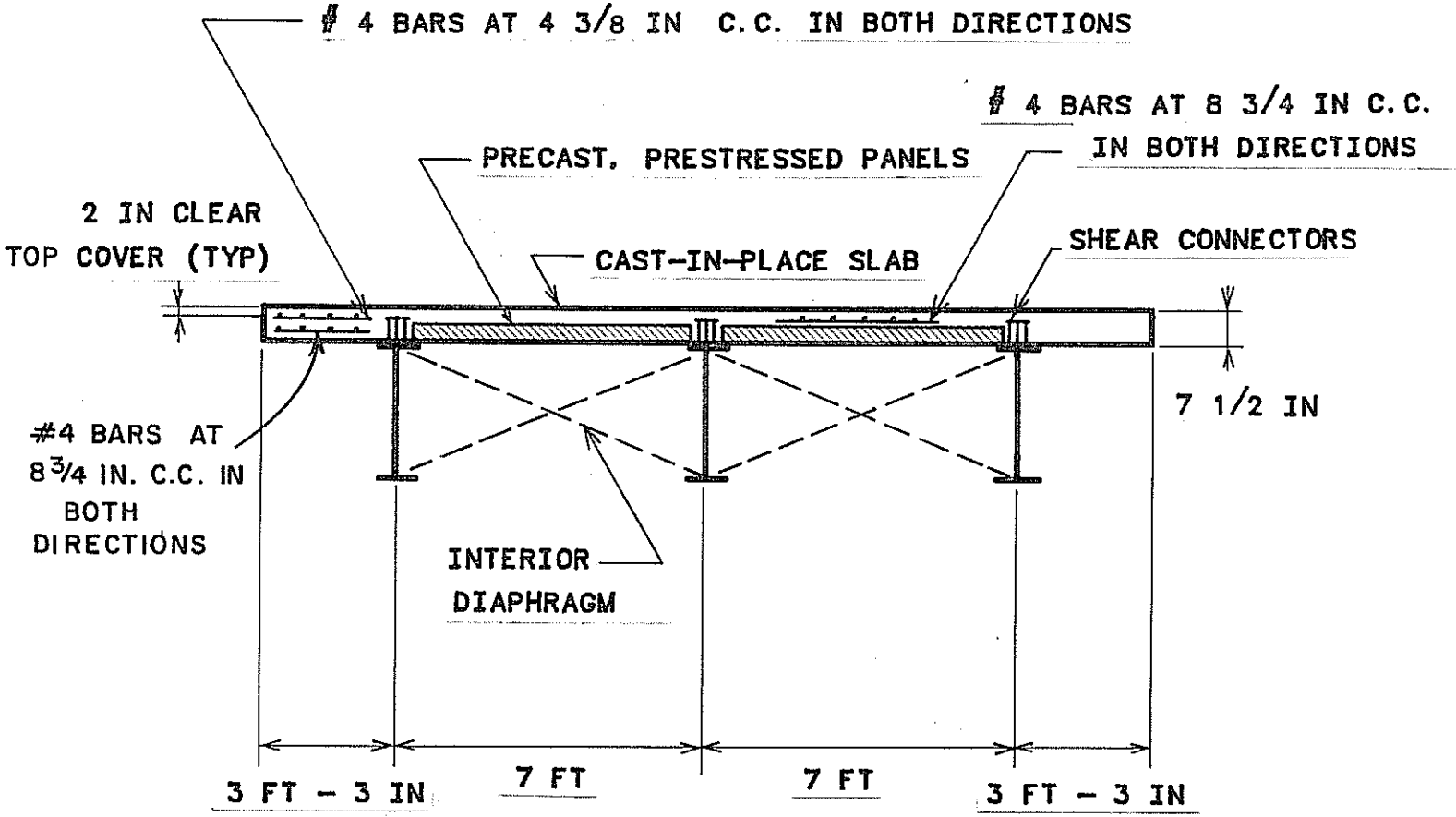

Fig. 3.4 Cross section of laboratory specimen showing precast, prestressed panels

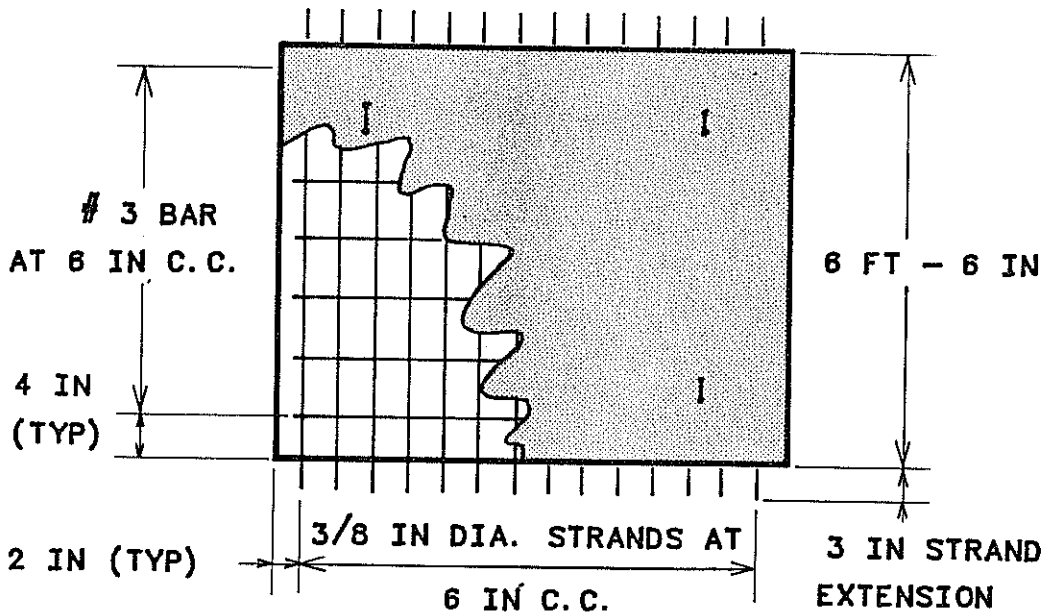

Fig. 3.5 Precast, prestressed panels

minimum overhang width of about 3 ft was required to satisfy the demands for transferring of in-plane forces from wheel load locations to the adjacent deck. The width between beams was made 7 ft, a representative spacing for many Texas bridges (with and without panels). As is typical, diaphragms were placed at support and midspan locations of the 49-ft span.

The deck between steel girders was built with conventional forms for half the bridge (Fig. 3.3) and with precast-prestressed panels (Fig. 3.4) for the other half. Where panels were used, the reinforcing steel placed in the deck slab consisted of only the top layer of the two-layer reinforcing steel used in the 7-1/2 in. thick cast-in-place portion.

The full-sized deck was connected to three W36x150 girders using standard, 7/8-in. welded studs. The girders were 60 ft long, spanning 49 ft between simple supports. The studs were placed in groups of three per row along the top flange, and their design for composition action in the region of the deck containing precast panels took into account the reduced flange width available. In the southern half of the bridge, in which panels were used (Fig. 3.1), the rows of studs were placed diagonally to allow adequate spacing between the panels. Details of stud placement are shown in Fig. 3.7.

As shown in Fig. 3.3, the deck was reinforced in accordance with Texas SDHPT details for Ontario-type decks. The cast-in-place deck had two layers of steel (running both ways), supported by chairs from the forms. The overhangs had reinforcement extended from the interior spans, plus some additional steel (Fig. 3.3). They were cast-in-place (full 7-1/2 in. thickness) for the entire 49 ft span, plus an additional 6-in. length of deck beyond the support at each end.

3.2 Construction of Test Specimen

The bridge specimen was constructed at the Ferguson Structural Engineering laboratory, Balcones Research Center, The University of Texas at Austin. Three 60-ft girders (W36x150) were donated to the project by the Texas Department of Highways and Public Transportation, District 14. These girders, recovered from a bridge which had been replaced, were in excellent condition for use in this composite bridge. Neoprene pads provided the required simple support conditions. The bearing pads were set on concrete supports resting on the test slab and simulating pier caps. After positioning the three girders at 7-ft spacing and installing diaphragms at ends and midspan (Fig. 3.6), the shear studs needed to assure composite action were welded to the top flanges. Rented equipment allowed full-penetration

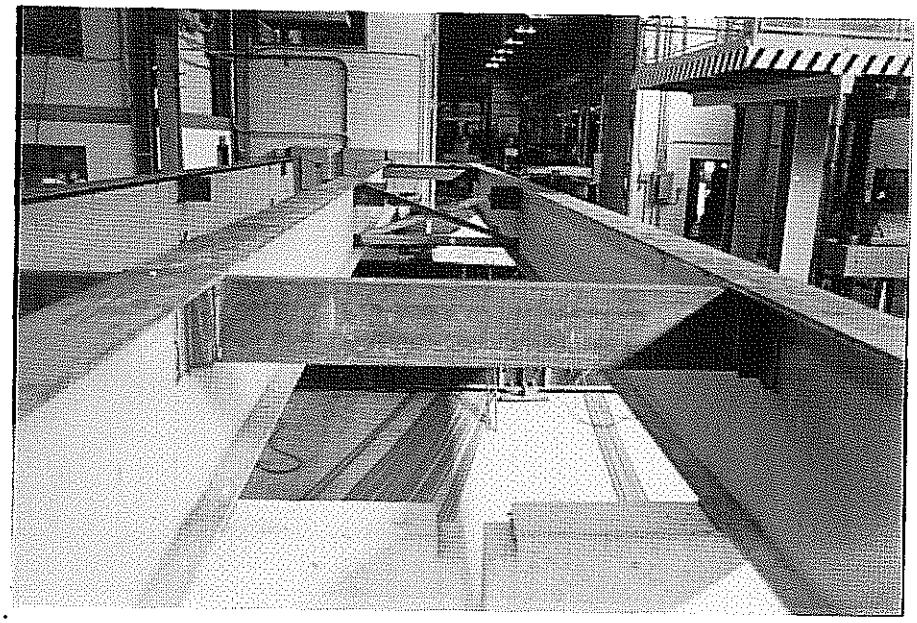

Fig. 3.6 Construction of intermediate and end diaphragms

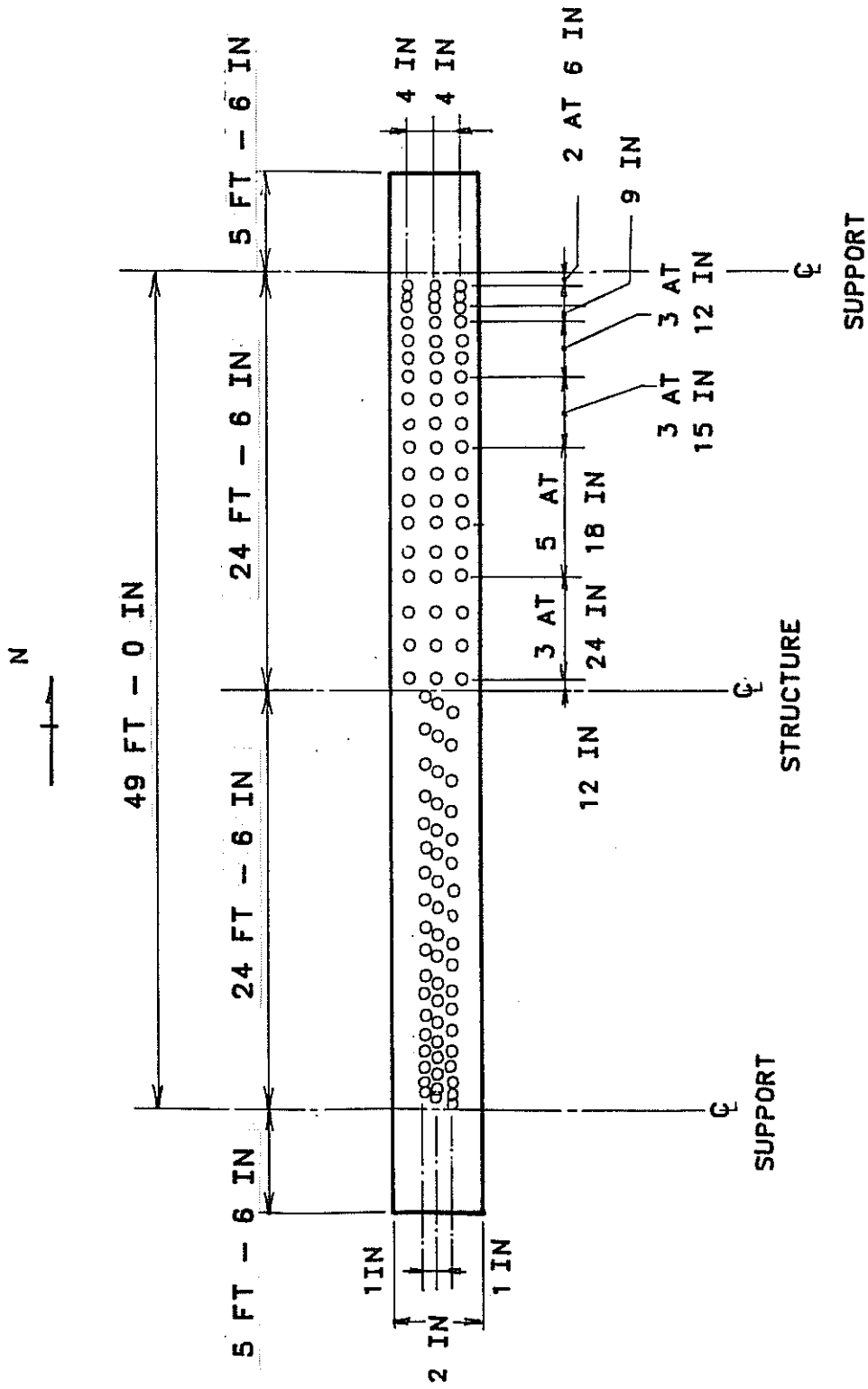

Fig. 3.7a Layout of shear studs on the steel girders

welding, and all welds were checked for soundness. Fig. 3.7 shows the shear studs used.

On the northern half of the bridge, plywood forms stiffened by 2x4 and 2x6 members were used to form the cast-in-place overhangs on each side, and also the spaces between the steel girders. On the southern half of the bridge, the 6.5-ft wide precast-prestressed panels were placed on the top flanges of the girders (Figs. 3.8 and 3.9). Bearing strips placed along the tips of the girder top flanges supported the panels with approximately 1-1/2 in overhangs, as shown in Fig. 3.7b. The forms supported the two layers of bars in each direction in the cast-in-place slab. The precast-prestressed concrete panels replaced the bottom layer of bars for the southern half of deck between steel girders, and the top layer of steel was supported just above the top of the panels. All reinforcing bars were Grade 60, and wire ties were used to secure the bars in each direction into a mat which was securely supported by chairs at the desired position in the slab to provide 2 in. clear cover. Figures 3.10 and 3.11 show the deck slab reinforcement on the cast-in-place and precast panel ends respectively.

As is described later, strain gages needed in the experimental program were mounted on bars at the desired locations and waterproofed for protection prior to placing the bars. Wires leading to all instrumentation in concrete were marked to identify gage locations, and were taken out through holes in the forms prior to placing the concrete. All tiedown hardware for the loading rams under the test bridge was positioned carefully, and securely bolted to the test floor prior to casting the deck on the girders.

Concrete was carried from the readymix trucks to the forms by overhead crane, using a concrete bucket. The desired thickness was maintained with a motorized vibrating screed, moved longitudinally. A fairly smooth surface was obtained without the texturing which would normally be done for a bridge deck slab. Cylinders and beams, taken at intervals during the casting period, were tested at various ages during the testing period to allow the strength to be evaluated accurately at each stage.

Other instrumentation was then mounted. Using a coring bit, holes were drilled in the deck to allow loading equipment to pass through. Cores obtained at the panel end showed good bond between precast panels and cast-in-place concrete.

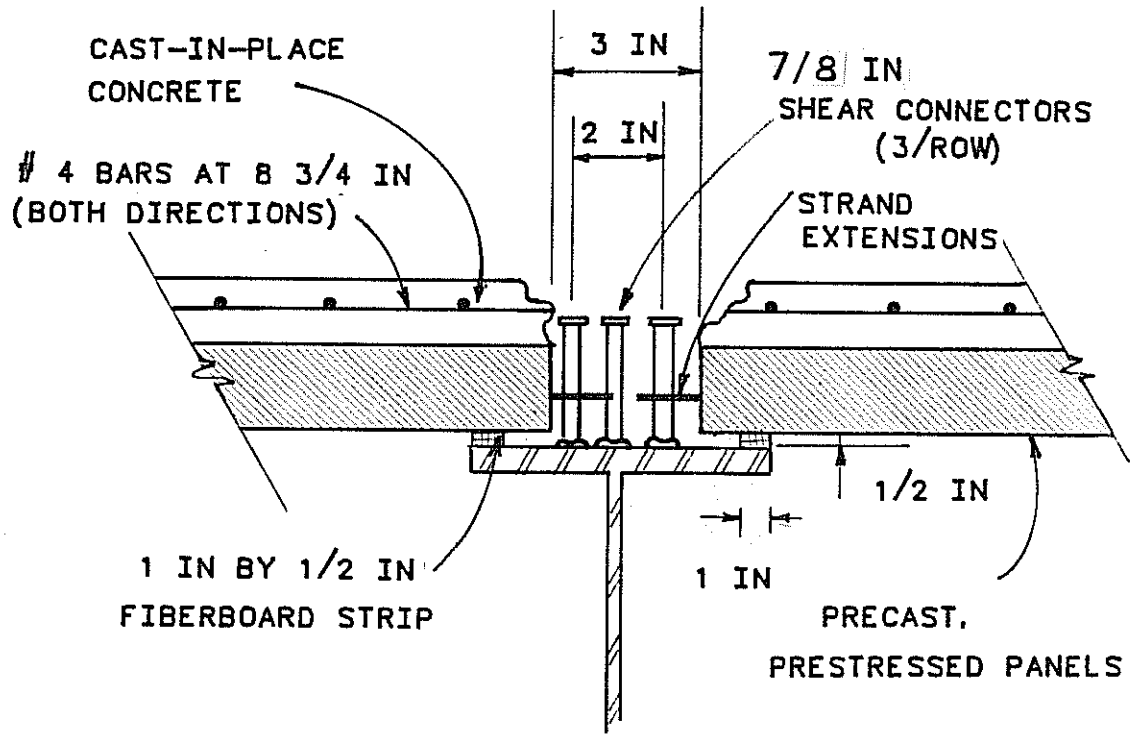

Fig. 3.7b Detail of connection between girders and panels

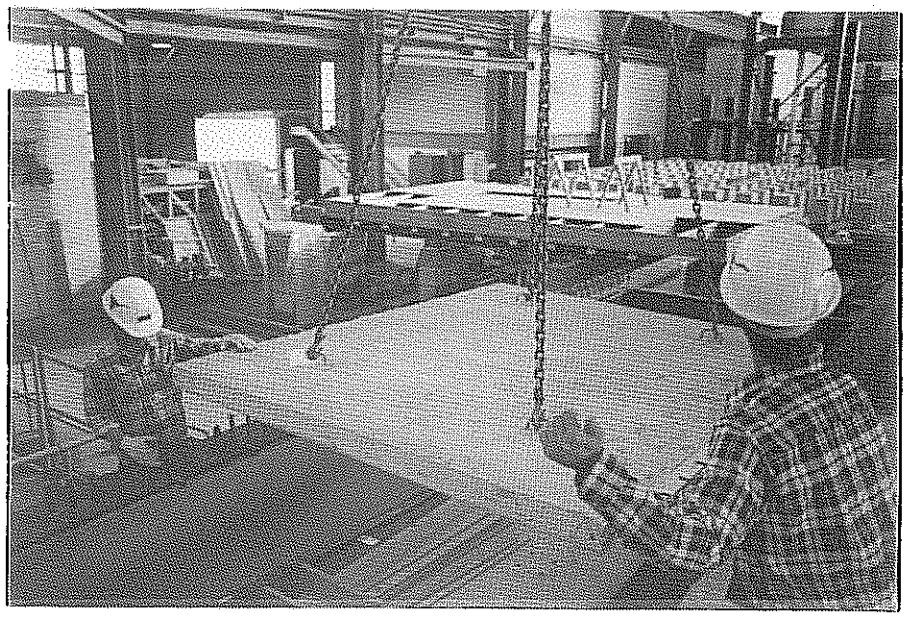

Fig. 3.8 Placement of precast panels

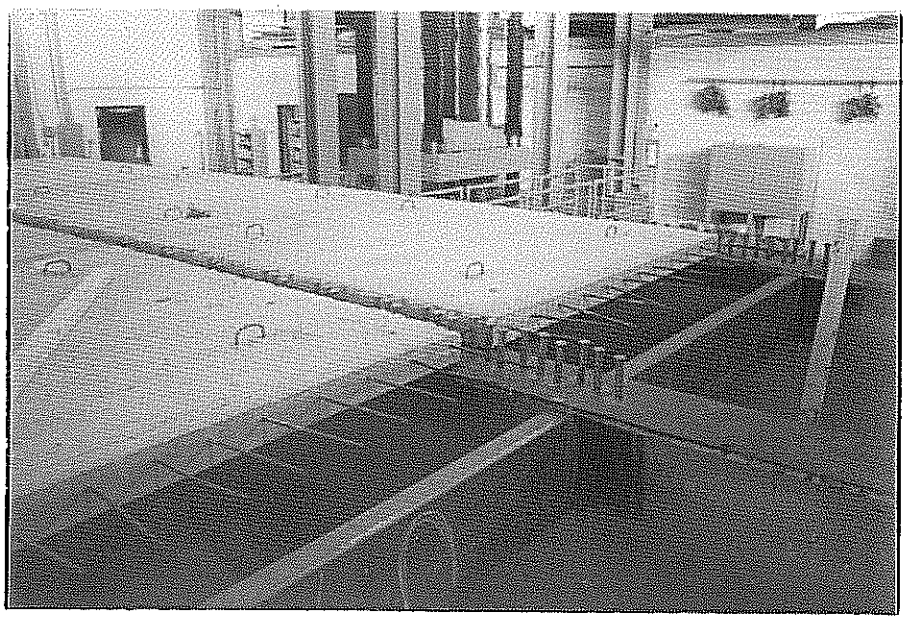

Fig. 3.9 Precast panels in position near south end of the bridge specimen

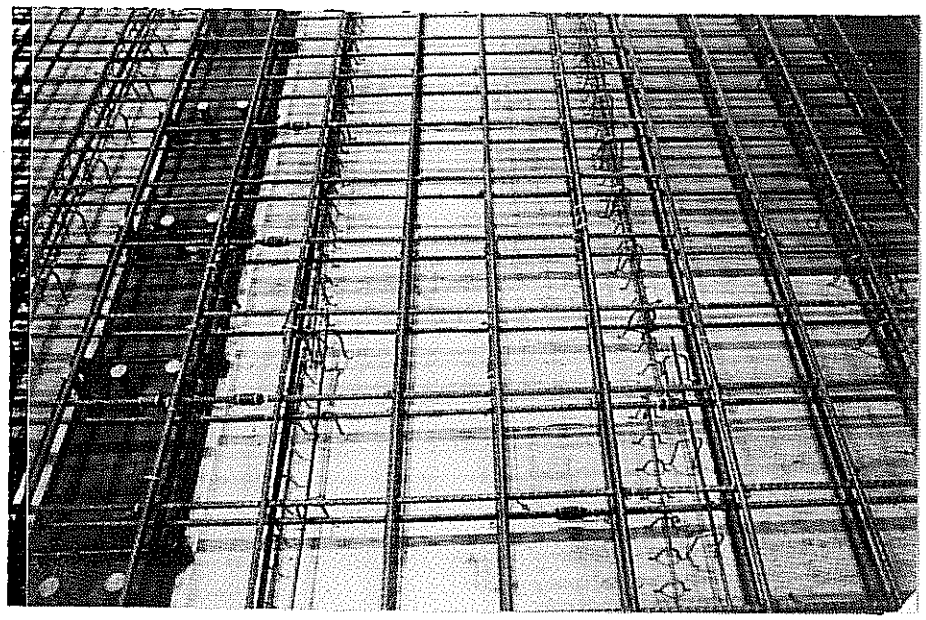

Fig. 3.10 Layout of reinforcing bars in CIP deck

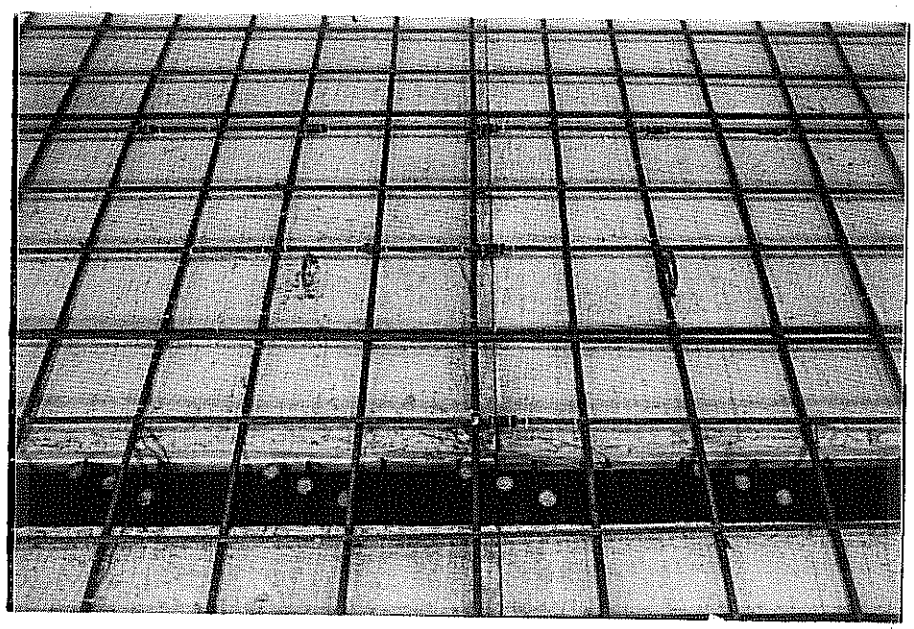

Fig. 3.11 Layout of reinforcing bars in panel deck

3.3 Material Characteristics

The material properties of the cast-in-place concrete and precast panels are detailed in Appendix B.

3.3.1 Cast-in-Place Concrete. The 28-day design compressive strength was 3600 psi. The concrete used for the deck, supplied by a local readymix plant, met the Specifications of the Texas Department of Highways and Public Transportation for Class C concrete (3.14). Twenty-one cylinders and nine beams, taken at intervals during casting, were tested at various stages during the testing period to allow the strength to be evaluated accurately at each stage. The 28-day cylinder tests showed 4240 psi average strength. The test results at all days tested are shown in Appendix B.

3.3.2 Reinforcement for Cast-In-Place Deck. All steel reinforcement used for the cast-in-place deck and the top mat of panel deck came from a single heat, and met the requirements of ASTM A-615 for Grade 60 steel. The yield strength of the steel reinforcement was 73 ksi, based on laboratory tests.

3.3.3 Precast, Prestressed Panels. Six precast, transversely-prestressed panels, fabricated by J. D. Abrams Precast (Austin) spanned between longitudinal girders (Figs. 3.5, 3.8 and 3.9). The panels were 6.5 ft wide by either 7 or 8 ft long. They were of 6000-psi concrete, 4 in. thick, and were later covered by a 3-1/2 in. topping of CIP concrete.

CHAPTER 4

ANALYSIS OF BRIDGE SPECIMEN

4.1 General

Because of the time and expense needed to build a full-sized bridge, it was considered important, from the very beginning of this project, to develop analysis procedures for computing the response of the whole bridge, not just at the discrete points where instrumentation had been placed. This chapter is intended to describe the analysis of the whole bridge specimen.

To analyze a bridge sructure, several methods can be used, depending on the bridge's structural characteristics, geometric configuration and support conditions. The principal methods are orthotropic plate theory, folded plate method, finite element method, finite strip method, grillage method and space frame method (4.1, 4.2, 4.3).

Since one of the primary objectives of this research was to assess the effect of compressive membrane action in the deck slab, the modeling of that slab becomes more significant. The finite element method was considered from the beginning for analysis of the composite structure (including the deck slab) because of its power and versatility.

Although the deflections and stresses of the test bridge (and of corresponding real bridges) are low under service loads, a conventional linear elastic analysis is insufficient for close comparison with experimental results, because it cannot predict the effect of cracking on the specimen's behavior. Because the bridge's deflections are small, geometrical nonlinearity is not significant, and analysis incorporating geometrical as well as material nonlinearity was judged expensive and unnecessary. As is explained shortly, the bridge was analyzed using a sequence of linear elastic analyses, each conducted using SAPIV, a computer program which is widely available on a non-proprietary basis (4.4).

As is explained in the following sections, cracking of the deck was modeled using a smeared cracking model (4.5, 4.6), extended to a three-dimensional stress state. The validity of this cracking model was verified using examples involving a reinforced concrete beam with thickness and reinforcement ratio similar to those of the bridge

deck. Computer results for deflections and stresses showed good agreement with the results of hand calculations based on the cracked and uncracked transformed section. Two finite element models were developed to simulate the CIP deck and precast panel deck test specimen respectively.

4.2 Verification of Analytical Models

4.2.1 Evaluation of Thick Shell Element in the Modeling of Arching Action.

As mentioned in Chapter 2, cracking of a lightly reinforced concrete slab can cause its neutral surface to shift up or down depending on the sense of the applied moment. To reproduce the arching action caused by in-plane restraint at the boundaries of a cracked concrete segment, it was proposed to model the deck using three-dimensional finite elements.

To evaluate this idea, the three-dimensional thick shell element in SAPIV was used to model a simply supported slab, first unrestrained and then restrained horizontally at the edges, and subjected to a uniformly distributed load (Figs. 4.1, 4.2). To permit comparison with the beam-theory solution, the Poisson's ratio of the slab was set to zero. The combination of bending and axial effects produce longitudinal stresses in the slab. The resulting stresses at the top and bottom surfaces of the slab are plotted in Figs. 4.3 and 4.4. As shown in Fig. 4.3, the compressive stress at the top surface of both the unrestrained and restrained slabs, modeled using thick shell elements, agreed quite well with that predicted by beam theory. As shown in Fig. 4.4, good agreement was also obtained for the tensile bottom fiber stresses.

This excellent agreement indicated that the thick shell element could accurately model a slab with edge restraint. It was therefore decided to consider using the thick shell element in modeling the concrete deck slab.

When three-dimensional elements are used to model a large structure, one of the principal concerns is how to reduce computational time and cost, yet also retain satisfactory accuracy.

The SAPIV program provides several options for the number of nodal points needed to describe a thick shell element. The maximum number of nodal points is 21. A typical 21-node thick shell element is shown in Fig. 4.5. As will be discussed in a later section, since the thickness of the elements used was only about 3.5 in., it was judged unnecessary to retain the midside nodes between the top and bottom surfaces.

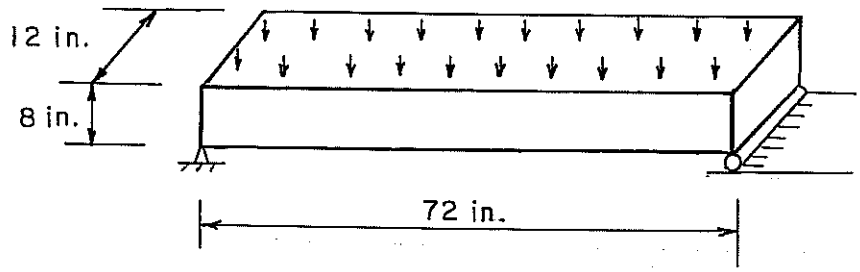

UNRESTRAINED SLAB OF UNIT WIDTH

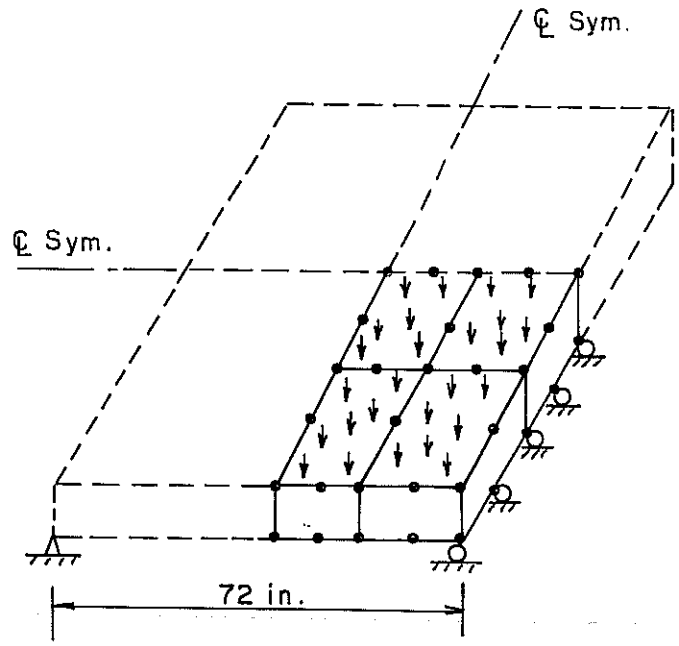

COMPUTER MODEL OF UNRESTRAINED SLAB USING THICK SHELL ELEMENTS (POISSON RATIO ν=0)

Fig. 4.1 Modeling of unrestrained slab using thick shell elements

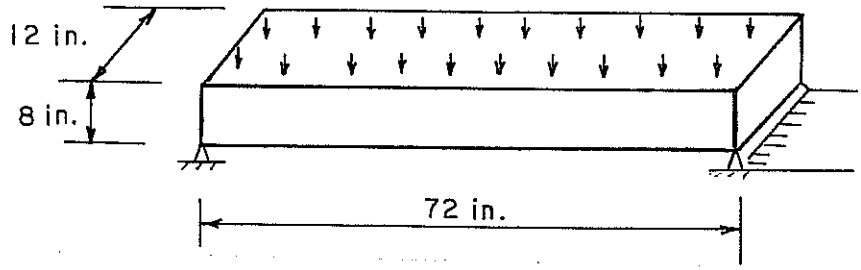

RESTRAINED SLAB OF UNIT WIDTH

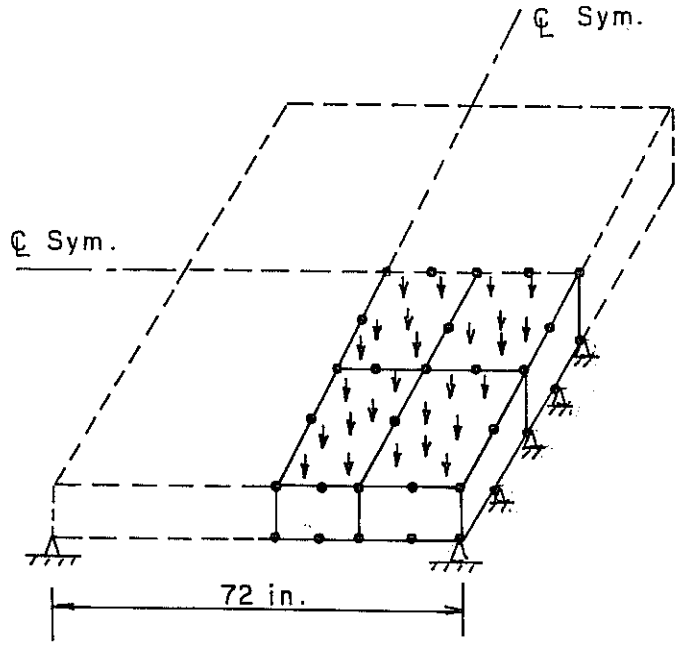

COMPUTER MODEL OF RESTRAINED SLAB USING THICK SHELL ELEMENTS (POISSON RATIO ν=0)

Fig. 4.2 Modeling of restrained slab using thick shell elements

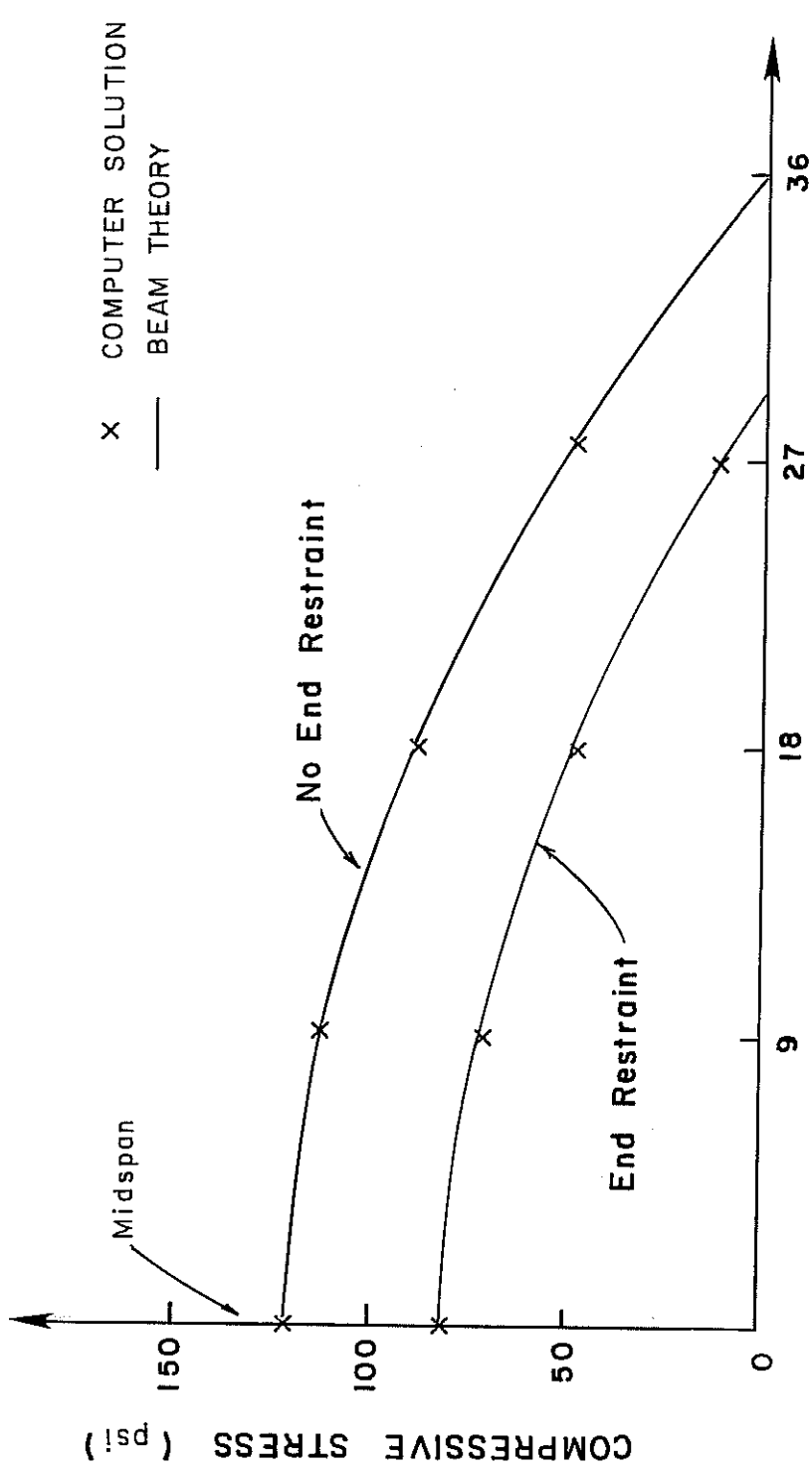

Fig. 4.3 Computed top fiber stress, restrained and unrestrained slabs

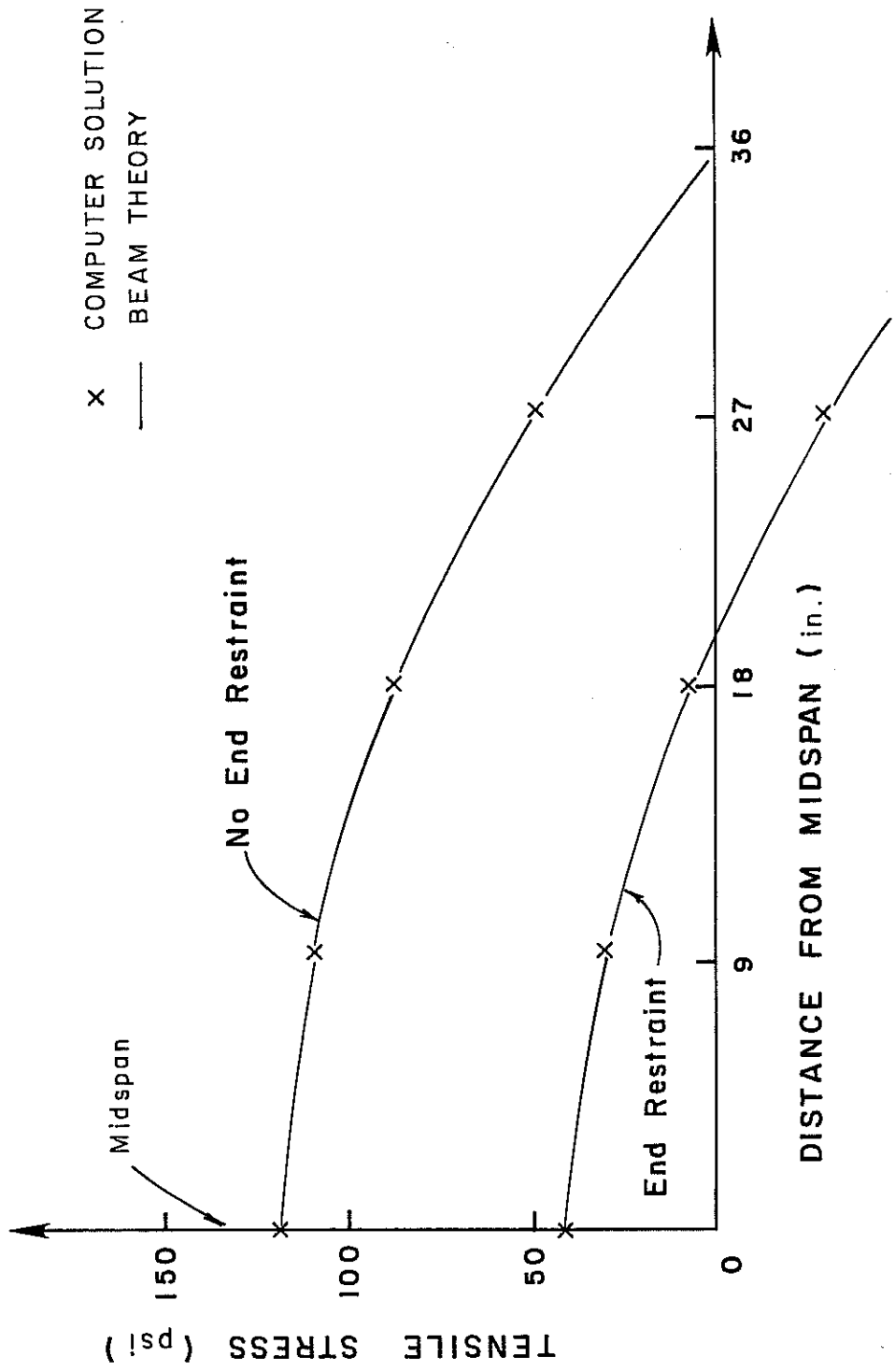

Fig. 4.4 Computed bottom fiber stress, restrained and unrestrained slabs

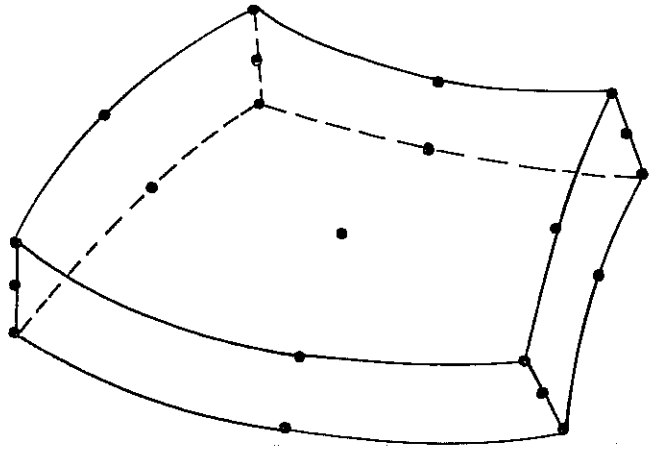

A) 3D THICK SHELL ELEMENT IN SAP IV

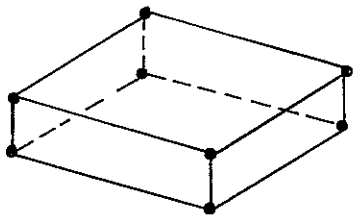

B) 8-NODE ELEMENT

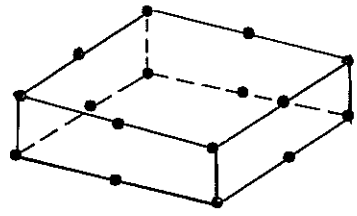

C) 16-NODE ELEMENT

Fig. 4.5 Possible nodal arrangements for thick shell elements in SAP IV

As shown in Fig. 4.6, the 8-node brick element and the 16-node quadratic element were then compared with respect to computational time and rate of convergence, using the analysis of a homogeneous, elastic cantilever beam as an example.

As shown in Figs. 4.7 and 4.8, an 8-element model using 16-node elements gave computed displacements very close to those predicted by beam theory, using relatively little computation time. The 16-node element was therefore used for all models of the deck slab.

4.2.2 Modeling of Composite Girders. The overall structural behavior of the test specimen in the longitudinal direction is essentially determined by the composite action of the deck slab and steel girders. The need for a model which could account for this behavior, and also produce the complex in-plane restraint of the deck in both directions, significantly influenced the modeling decisions.

The composite action of the deck slab and girder was modeled using a combination of thick shell element and three-dimensional beam elements, shown schematically in Fig. 4.9. In modeling the girder, no slip was assumed to take place between the slab and the girders. As will be discussed, this assumption was verified experimentally. The steel girder is discretized using a series of three-dimensional beam elements with the same properties as the girder, and located at the girder midheight.

The beam elements were then connected to the thick shell element at the corresponding nodel points using rigid links, satisfying typical assumptions for plane sections.

As shown in Fig. 4.10a, this modeling concept was tested using a simply supported, composite girder. Fig. 4.10b shows the calculated distribution of longitudinal bending stresses at top surface of the deck and also the midspan deflection. Both calculated longitudinal stress and midspan deflection agree well with the values calculated using beam theory.

This example indicates that a composite girder can be modeled using a combination of thick shell elements and three-dimensional beam elements. Therefore, this technique was used for the bridge specimen.

4.3 Modeling of Cracked Bridge Deck Slab

4.3.1 General. In the literature review of Chapter 2, it was noted that cracking of reinforced concrete slabs is related to the

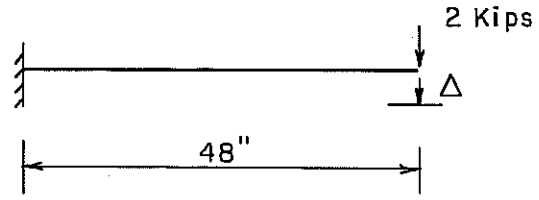

A) PROTOTYPE BEAM

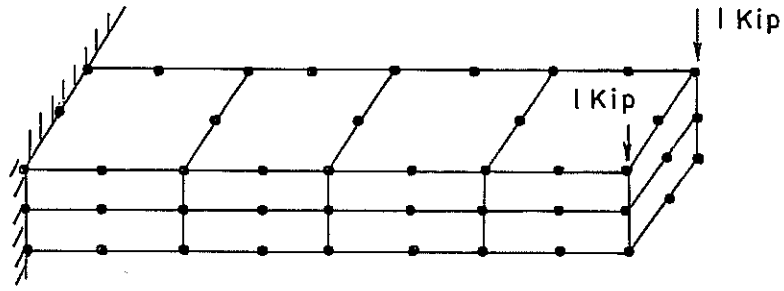

B) COMPUTER MODEL USING EIGHT 16-NODE THICK SHELL ELEMENTS

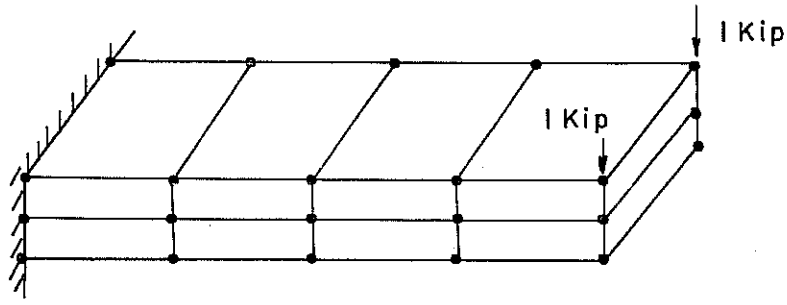

C) COMPUTER MODEL USING EIGHT 8-NODE THICK SHELL ELEMENTS

Fig. 4.6 Computer modeling of a beam using thick shell elements

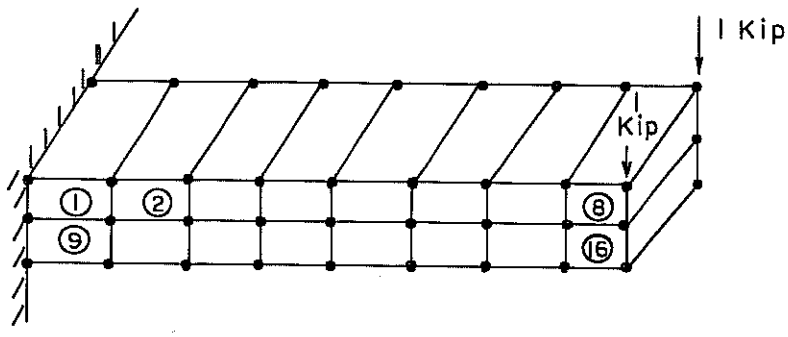

D) COMPUTER MODEL USING 16 8-NODE THICK SHELL ELEMENTS

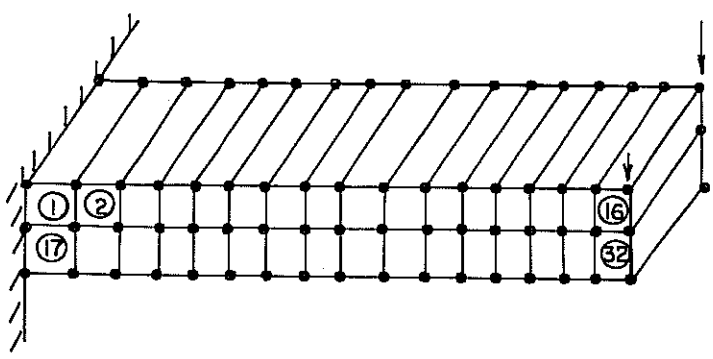

E) COMPUTER MODEL USING 32 8-NODE THICK SHELL ELEMENTS

Fig. 4.6 Computer modeling of a beam using thick shell elements (conti.)

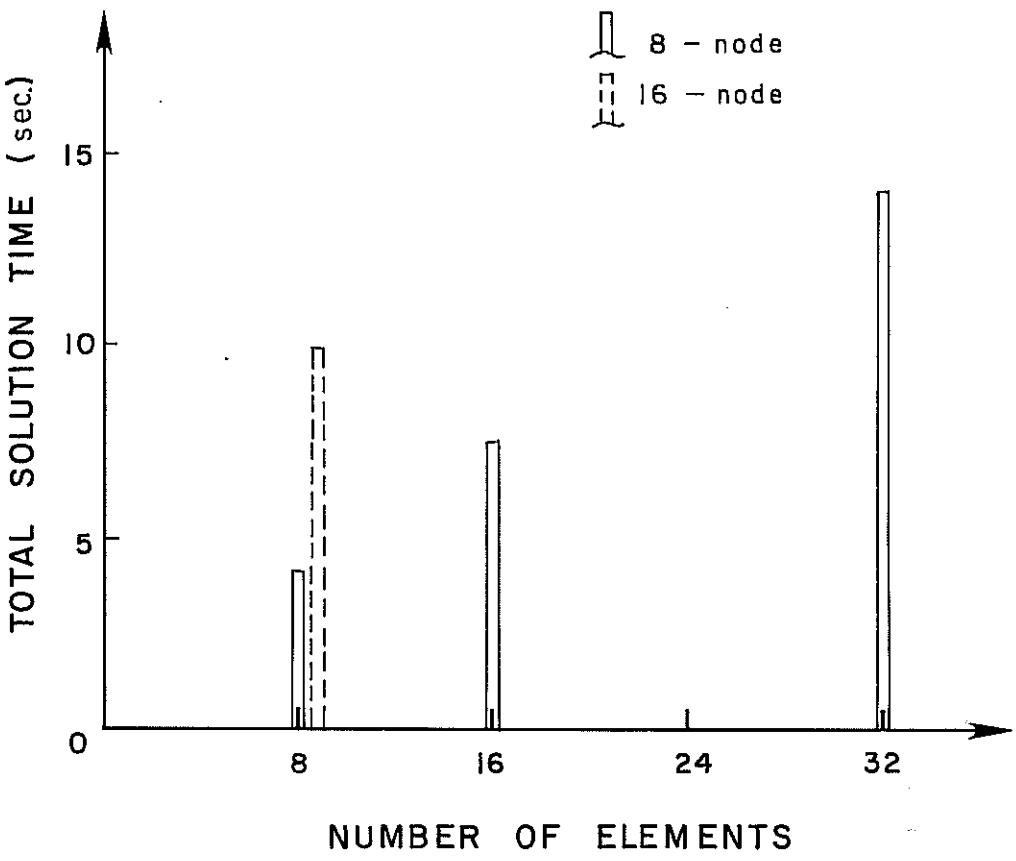

Fig. 4.7 Comparison of total solution times for cantilever beam model

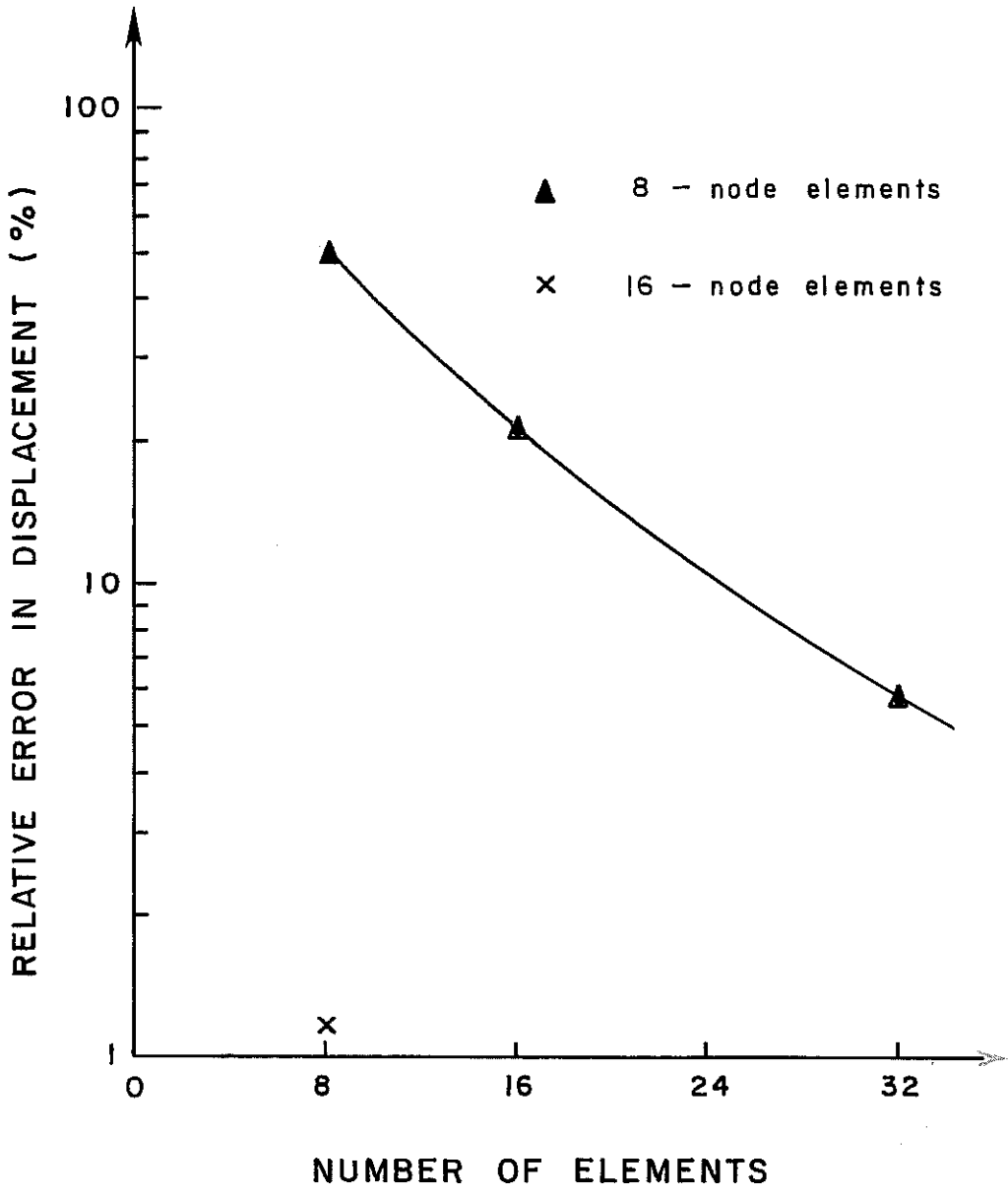

Fig. 4.8 Comparison of accuracy between 8-node and 16-node thick shell elements

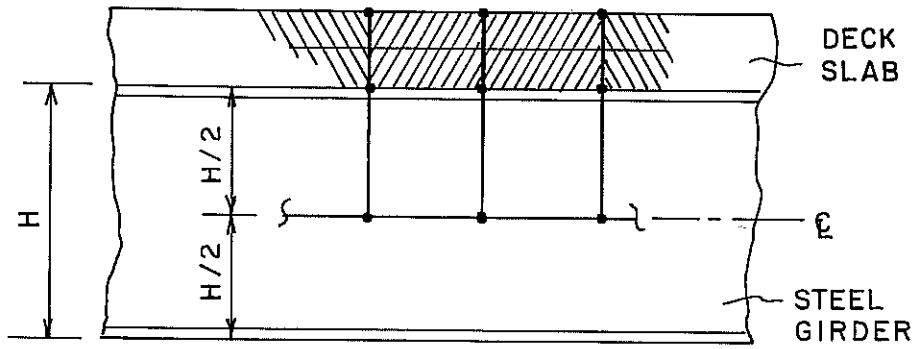

ACTUAL COMPOSITE GIRDER

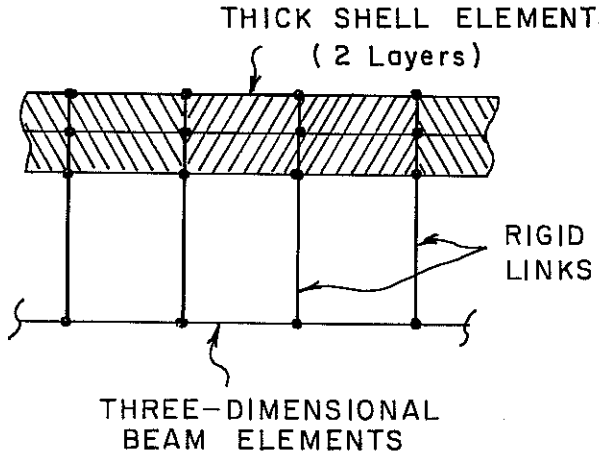

FINITE ELEMENT MODEL

Fig. 4.9 Schematic representation of finite element model of composite girder

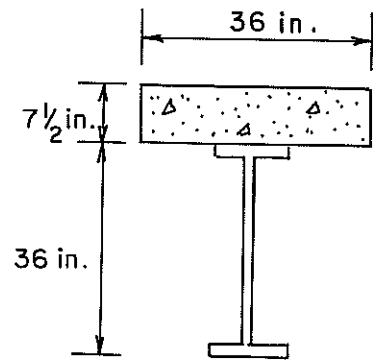

A) CROSS SECTION OF MODEL

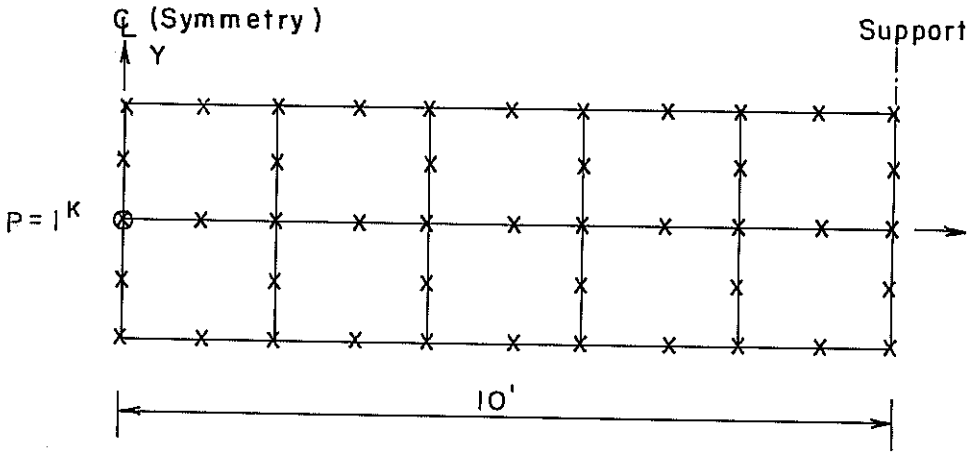

C) PLAN VIEW OF FINITE ELEMENT MESH

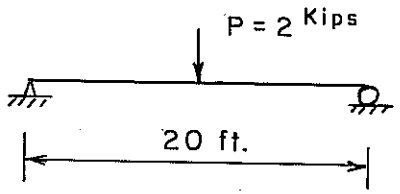

B) SIDE VIEW OF MODEL

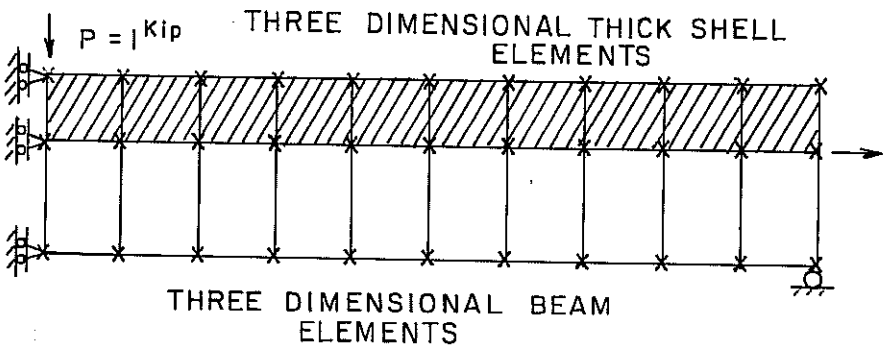

D) LONGITUDINAL SECTION OF FINITE ELEMENT MODEL

Fig. 4.10a Finite element modeling of composite girder

E) LONGITUDINAL STRESS

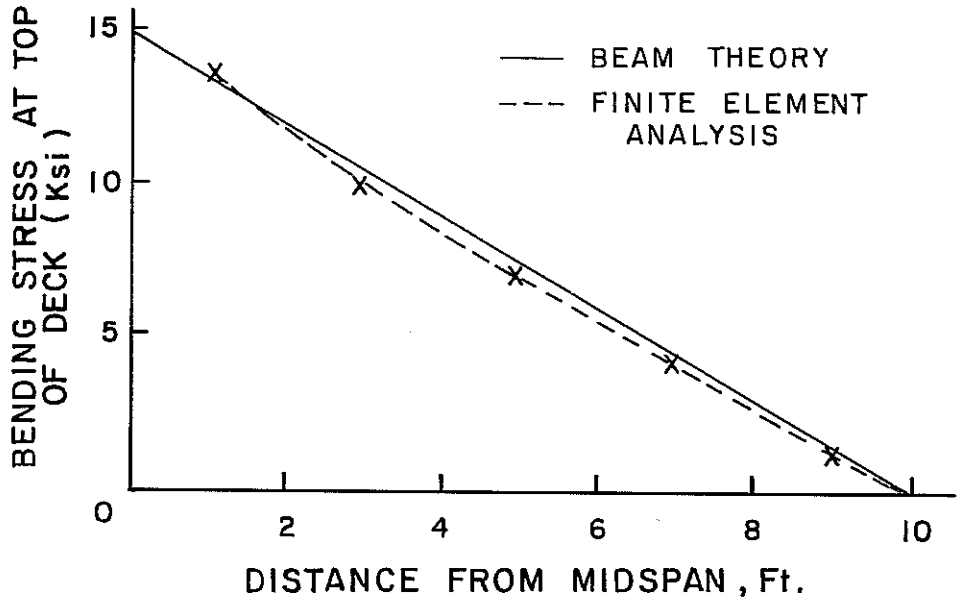

F) MIDSPAN DEFLECTION

$\Delta_{model} = -14.99 \times 10^{-4}$ in. (FINITE ELEMENT MODEL)

$\Delta = -14.24 \times 10^{-4}$ in. (BEAM THEORY)

Fig. 4.10b Comparison of longitudinal stress and midspan deflection

development of compressive membrane action. It was therefore decided that the effects of concrete cracking should be included in modeling the deck slab.

This section has the following objectives: a) to give a brief historical review of the techniques used to model cracking in reinforced concrete; b) to explain the smeared cracking model which was selected, and to justify that choice; and c) to explain the sequential linear approach which was used with the smeared cracking model to analyze the cracked bridge deck. As is discussed later in this section, several numerical examples were used to validate these procedures.

4.3.2 Historical Review. Modeling of cracking using the finite element method has been studied by many researchers in the past decade (4.5). Each proposed model has three distinguishing features: 1) crack initiation criteria; 2) crack representation; and 3) representation of crack propagation. Most models use a strength criterion for determining crack initiation.

For crack representation, two methods are generally used: discrete crack models and smeared crack models. Crack propagation is generally represented using either strength criteria or fracture mechanics parameters (4.7, 4.8, 4.9, 4.10, 4.11).

In deciding on the best crack representation, the following points were considered: in the discrete crack model, cracks are modeled by separating nodal points as shown in Fig. 4.11. One obvious difficulty in such an approach is that the location and orientation of the cracks are not known in advance. Although it can be improved to some extent by redefining the element nodes, it is still complex and time-consuming to redefine the structural topology following the formation of a crack. When the topology of these models changes, redefinition of the nodal points alters the banded nature of the structural stiffness matrix, and can greatly increase the required computational effort. Therefore, the discrete crack model is restricted to some special areas. For those problems involving a few dominant cracks, it can offer a more realistic representation of the cracks. For instance, the effect of aggregate interlock and dowel force can generally be well modeled using this approach (4.12, 4.13).

In the smeared cracking model, the cracked concrete is assumed to remain continuous, and the cracks are "smeared" as shown in Fig. 4.12. If the overall load-deflection behavior of the structure is desired, the smeared crack approach is the best choice. The details of this approach will be presented later in Section 4.3.4.

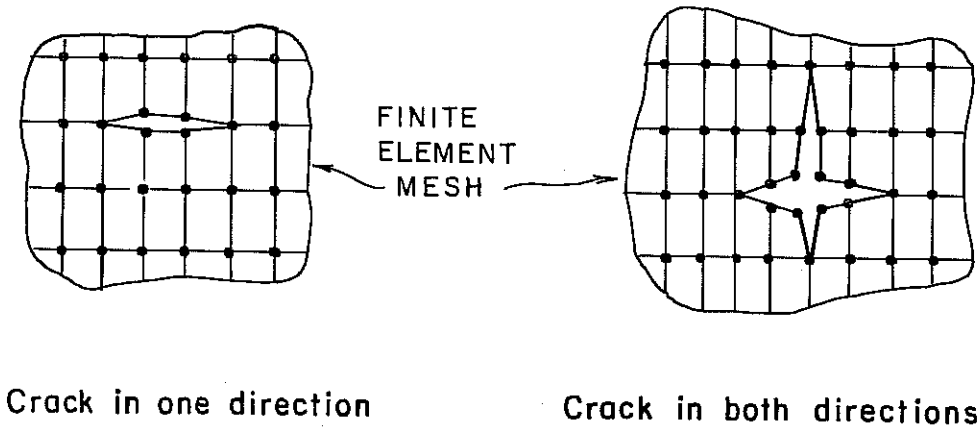

Fig. 4.11 Schematic representation of discrete crack model

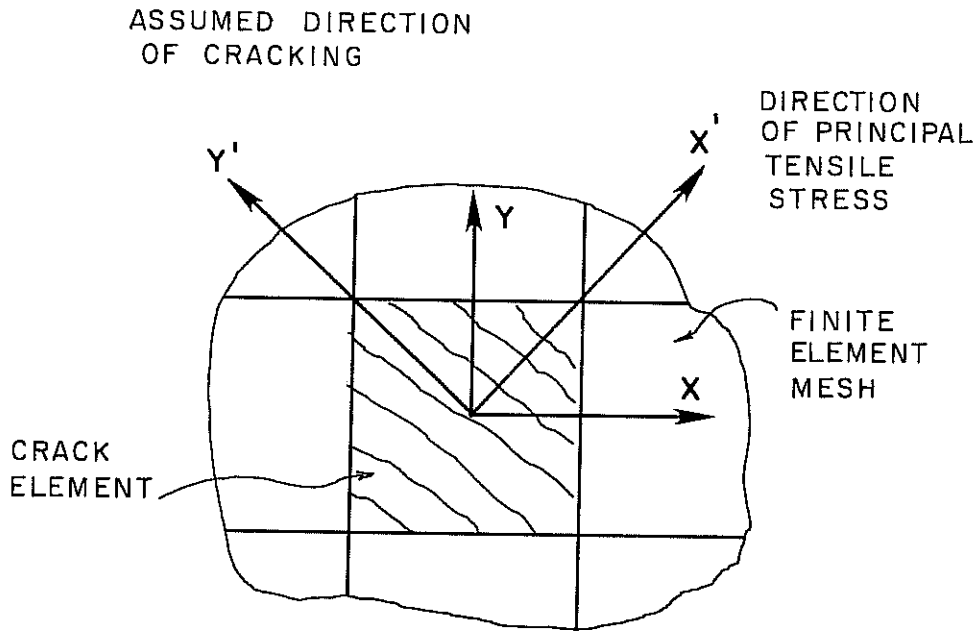

Fig. 4.12 Schematic representation of smeared crack model

4.3.3. Cracking Criteria. The cracking of concrete can be predicted by various measures of its tensile strength, such as split cylinder tests, modulus of rupture tests, and biaxial stress tests.

As is noted later, an analytical solution of the bridge model showed that the deck was essentially in a state of plane stress. Therefore, Kupfer's biaxial failure envelope (4.14) was used to detect cracking in the deck. At each load level, the maximum principal stress at the center of each element is calculated and compared with the biaxial cracking criterion proposed by Kupfer and shown in Fig. 4.13. As shown in Fig. 4.12, once the maximum principal tensile stress in any element exceeds the failure value, the entire element is treated as cracked perpendicular to the direction of that stress.

At one end of the bridge, the deck slab was composed partially of precast panels. The greater strength in the precast panels, and the existence of prestressing force in one direction, required a slightly different approach in detecting cracking in the panels. The effect of the transverse prestressing force in the panels was included in the crack-detection part of the analysis by superposing the prestress and live-load stress. This superposition of stresses was incorporated in a separate program which was used to check the cracking criterion.

4.3.4 Smeared Crack Model for Reinforced Concrete. As mentioned in Subsection 4.3.1, the cracking of concrete can be represented either by the discrete crack model or by smeared crack model. Each approach has distinctive features in the modeling of cracks.

The smeared crack model was initially introduced by Rashid (4.15). An entire element is assumed to crack when the principal stress anywhere in that element exceeds some maximum value. As shown in Fig. 4.12, cracks are assumed to form perpendicular to the direction of the principal tensile stress. After cracking, the stiffness of the entire element is set to zero in the direction perpendicular to the principal tensile plane. This concept was initially applied to plane-stress problems. For isotropic materials, the original plane stress constitutive matrix can be expressed in terms of x,y coordinate system as follows:

$$\begin{Bmatrix} \sigma_x \\ \sigma_y \\ Z_{xy} \end{Bmatrix} = \begin{bmatrix} \upsilon E_c & \upsilon E_c & o \\ E_c & E_c & o \\ o & o & G \end{bmatrix} \begin{Bmatrix} \epsilon_x \\ \epsilon_y \\ \gamma_{xy} \end{Bmatrix} \qquad (4.1)$$

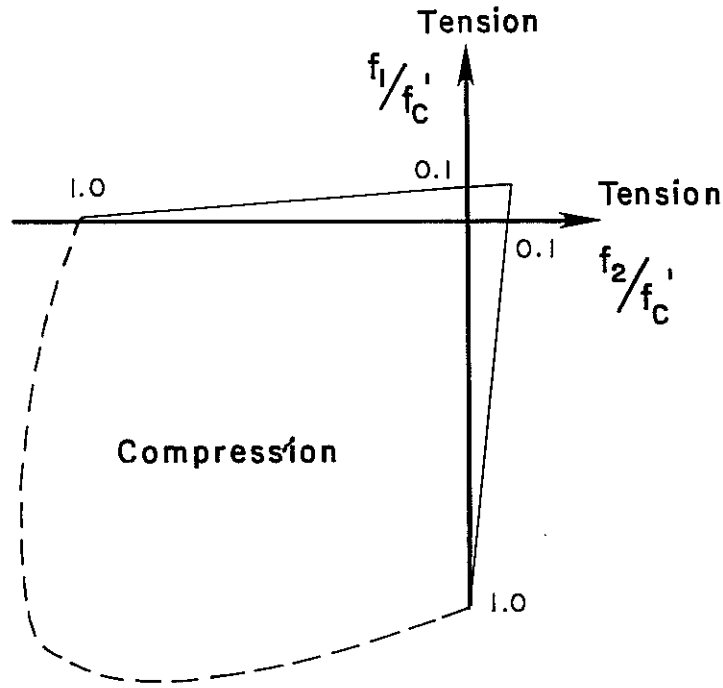

Fig. 4.13 Kupfer's biaxial stress criterion

However, after cracks form perpendicular to the x' axis (Fig. 4.12), the matrix becomes:

$$\begin{Bmatrix} \sigma_x^1 \\ \sigma_y^1 \\ Z_{x\,y}^1 \end{Bmatrix} = \begin{bmatrix} o & o & o \\ o & E_c & o \\ o & o & o \end{bmatrix} \begin{Bmatrix} \epsilon_x^1 \\ \epsilon_y^1 \\ \gamma_{x\,y}^1 \end{Bmatrix} \tag{4.2}$$

This cracking model has been used satisfactorily by some investigators (4.16, 4.17, 4.18, 4.19), but has sometimes caused numerical difficulties (4.20, 4.21). A reduced shear modulus has therefore been incorporated (4.20, 4.22, 4.23):

$$\begin{Bmatrix} \sigma_x^1 \\ \sigma_y^1 \\ Z_{x\,y}^{1\,1} \end{Bmatrix} = \begin{bmatrix} o & o & o \\ o & E_c & o \\ o & o & \beta G \end{bmatrix} \begin{Bmatrix} \epsilon_x^1 \\ \epsilon_y^1 \\ \gamma_{x\,y}^{1\,1} \end{Bmatrix} \tag{4.3}$$

where β is a reduction factor representing the remaining shear stiffness in the cracked plane, due to aggregate interlock and dowel action. A value of 0.5 has often been used for β, and is used in this research (4.24, 4.25).

The tensile stiffness of reinforcement crossing the smeared cracking plane has also been included by some investigators (4.26, 4.27, 4.28) giving a matrix as follows:

$$\begin{Bmatrix} \sigma_x^1 \\ \sigma_y^1 \\ Z_{x\,y}^{1\,1} \end{Bmatrix} = \begin{bmatrix} \rho_{eff} E_s & o & o \\ o & E & o \\ o & o & \beta G \end{bmatrix} \begin{Bmatrix} \epsilon_x^1 \\ \epsilon_y^1 \\ \gamma_{x\,y}^{1\,1} \end{Bmatrix} \tag{4.4}$$

where ρ_{eff} is the effective tensile steel ratio perpendicular to the cracking plane as shown in Fig. 4.14.

In effect, a smeared cracking model idealizes cracked reinforced concrete as an orthotropic material, with reduced tensile stiffness perpendicular to the cracking orientation, and reduced shear stiffness parallel to it.

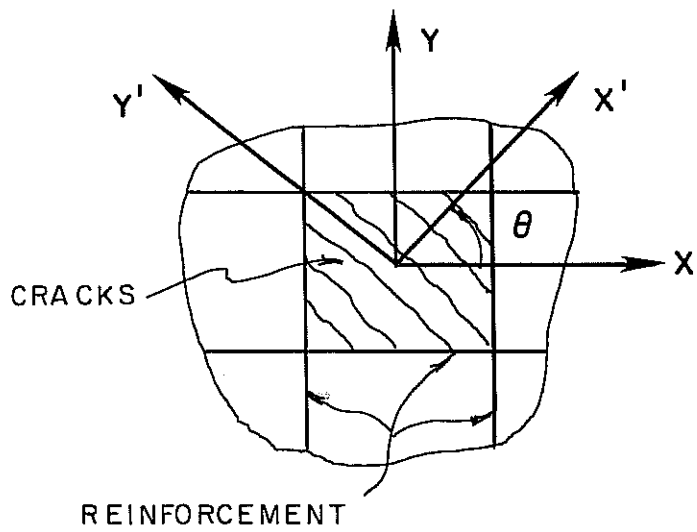

$$\rho_{eff} = \rho_x \cos^2\theta + \rho_y \sin^2\theta$$

ρ_{eff}: Effective tensile steel ratio perpendicular to cracking plane

$$\rho_x = \frac{A_{sx}}{bdx}, \rho_y = \frac{A_{sy}}{bdy}$$

A_{sx}: Area of reinforcement running in the x-direction within a width b

A_{sy}: Area of reinforcement running in the y-direction within a width b

d_x, d_y: Effective depth of slab in the x and y directions

Fig. 4.14 Effective tensile steel ratio perpendicular to cracking plane

In this research, it was proposed to extend this smeared cracking model to three dimensions. The flexibility matrix of a three-dimensional material is given by:

(4.5)

$$\begin{Bmatrix} \varepsilon_x \\ \varepsilon_y \\ \varepsilon_z \\ \gamma_{xy} \\ \gamma_{yz} \\ \gamma_{zx} \end{Bmatrix} = \left[\begin{array}{ccc|ccc} \frac{1}{E_x} & \frac{-\upsilon_{yx}}{E_y} & \frac{-\upsilon_{zx}}{E_z} & & & \\ \frac{-\upsilon_{xy}}{E_x} & \frac{1}{E_y} & \frac{-\upsilon_{zx}}{E_z} & & \underset{\sim}{0} & \\ \frac{-\upsilon_{xz}}{E_x} & \frac{-\upsilon_{yz}}{E_y} & \frac{1}{E_x} & & & \\ \hline & & & \frac{1}{G_{xy}} & 0 & 0 \\ & \underset{\sim}{0} & & 0 & \frac{1}{G_{yz}} & 0 \\ & & & 0 & 0 & \frac{1}{G_{zx}} \end{array}\right] \begin{Bmatrix} \sigma_x \\ \sigma_y \\ \sigma_z \\ \tau_{xy} \\ \tau_{yz} \\ \tau_{zx} \end{Bmatrix}$$

Before any crack forms, the concrete deck is assumed isotropic, and the above flexibility matrix is independent of the orientation of the coordinate axes. Once cracks form at an arbitrary orientation x', y' with respect to the slab reinforcement (Fig. 4.14), the above flexibility matrix becomes:

(4.6)

$$\begin{Bmatrix} \varepsilon_x^1 \\ \varepsilon_y^1 \\ \varepsilon_z \\ \gamma_{x\,y}^{1\,1} \\ \gamma_{y\,z}^{1} \\ \gamma_{zx}^{1} \end{Bmatrix} = \left[\begin{array}{ccc|ccc} \frac{1}{E_x} & 0 & \frac{-\upsilon_{x\,z}^{1}}{E_x} & & & \\ 0 & \frac{1}{\rho_{eff} E_s} & 0 & & \underset{\sim}{0} & \\ \frac{-\upsilon_{zx}^{1}}{E_x} & 0 & \frac{1}{E_z} & & & \\ \hline & & & \frac{1}{\beta G_{x\,y}^{1\,1}} & 0 & 0 \\ & \underset{\sim}{0} & & 0 & \frac{1}{G_{y\,z}^{1}} & 0 \\ & & & 0 & 0 & \frac{1}{\beta G_{zx}^{1}} \end{array}\right] \begin{Bmatrix} \sigma_x^1 \\ \sigma_y^1 \\ \sigma_z \\ \tau_{x\,y}^{1\,1} \\ \tau_{y\,z}^{1} \\ \tau_{zx}^{1} \end{Bmatrix}$$

As mentioned above, the uncracked concrete deck is considered isotropic. Therefore, the moduli of elasticity E_x, E_y, E_z in the three directions can be expressed in terms of the unique concrete modulus of elasticity E_c. The shear moduli G_{xy}, G_{yz}, and G_{zx}, are all identical to G. Under such simplification, Eq. (4.6)

$$\begin{Bmatrix} \varepsilon_x^1 \\ \varepsilon_y^1 \\ \varepsilon_z \\ \gamma_{xy}^{11} \\ \gamma_{yz}^1 \\ \gamma_{zx}^1 \end{Bmatrix} = \left[\begin{array}{ccc|ccc} \frac{1}{E_c} & o & \frac{-\upsilon}{E_c} & & & \\ o & \frac{1}{\rho_{eff}E_s} & o & & \underset{\sim}{o} & \\ \frac{-\upsilon}{E_c} & o & \frac{1}{E_c} & & & \\ \hline & & & \frac{1}{\beta G} & o & o \\ & \underset{\sim}{o} & & o & \frac{1}{G} & o \\ & & & o & o & \frac{1}{\beta G} \end{array}\right] \begin{Bmatrix} \sigma_x^1 \\ \sigma_y^1 \\ \sigma_z \\ z_{xy}^{11} \\ z_{yz}^1 \\ z_{zx}^1 \end{Bmatrix} \qquad (4.7)$$

In effect, cracked concrete is treated as an orthotropic material whose axes of orthotrophy coincide with the cracking orientation.

4.3.5 Sequential Linear Approach. Since SAPIV is a linear elastic program, the nonlinear behavior associated with crack information was handled using a sequence of linear elastic analyses. A schematic representation of this sequential approach is shown in Fig. 4.15. The bridge model was first subjected to a given load, and would deflect linearly along path 1 shown in Fig. 4.15. In each element, the maximum principal stress was compared to the maximum allowable stress of Kupfer's biaxial stress criterion. Elements having maximum ratios of calculated to failure stress greater than unity were regarded as cracked, while maximum while ratios less than unity corresponded to uncracked conditions. The first cracking load, P_1, was then calculated by scaling the load to give a maximum ratio of unity (one cracked element) or slightly greater than unity (possibly more than one cracked element). The cracking orientation of each cracked element was calculated, and its element stiffness matrix was reformed following the procedures for the smeared cracking model given earlier in this chapter. The model was then unloaded to the origin.

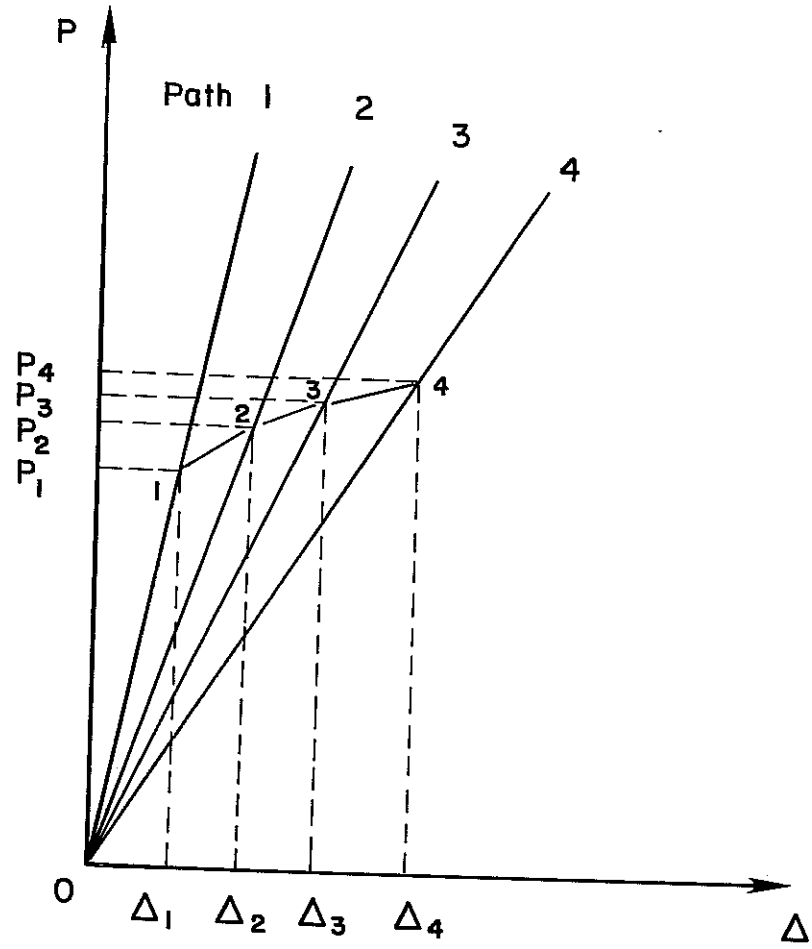

Fig. 4.15 Schematic representation of sequential linear approach

Upon reloading, since the model's stiffness would be reduced due to cracking, it would deflect linearly along Path 2 of Fig. 4.15. The maximum principal stress was then calculated in each uncracked element and compared with Kupfer's biaxial stress criterion. The maximum ratio was again used to predict the next cracking load P_2, and its corresponding deflection 2.

After unloading back to the origin, this process was repeated for Paths 3, 4, and so forth, as shown in Fig. 4.15. The points 1, 2, etc. then represent a series of accurate load-deflection combinations assuming loading and unloading as described above.

Now suppose that the specimen were loaded monolithically rather than as described above. If its behavior were path independent, the load deflection curve would go from the origin through points 1,2,3 and so forth in succession.

To the extent that behavior is path-independent, that path represents a close approximation of the actual nonlinear behavior. This approach can be almost as accurate as a true nonlinear analysis. It is much faster and cheaper in terms of computer time, but less so in terms of the human effort involved. The human effort can be reduced by selecting the loads P_1, P_2, etc. to allow simultaneous cracking of groups of elements with similar stress magnitudes.

4.3.6 Evaluation of Proposed Cracking Model. The validity of the proposed cracking model and the sequential approach was verified using examples involving a reinforced concrete beam with thickness and reinforcement ratio similar to those of the bridge deck. Fig. 4.16 shows a reinforced concrete cantilever beam, modeled using two layers of thick shell elements. The poisson's ratio of the concrete was assumed to be 0.15. The magnitude of the tip load was adjusted so that it would just produce cracking at the right-hand edge of element "1" of the beam (Fig. 4.17) , and therefore place that entire element in the cracked state. Using the proposed cracking model discussed above, the appropriate coefficients in the material matrix of element 1 were modified, after which the load was again applied to the beam. The resulting stress distribution along the top and bottom surface of the beam was again calculated, and is compared in Fig. 4.17 with the values obtained using beam theory and transformed sections.

The results predicted using the smeared cracking model agree reasonably well with those predicted using beam theory. The model could reflect the stress increase at the bottom surface of the beam near the fixed end due to the crack at the top surface.

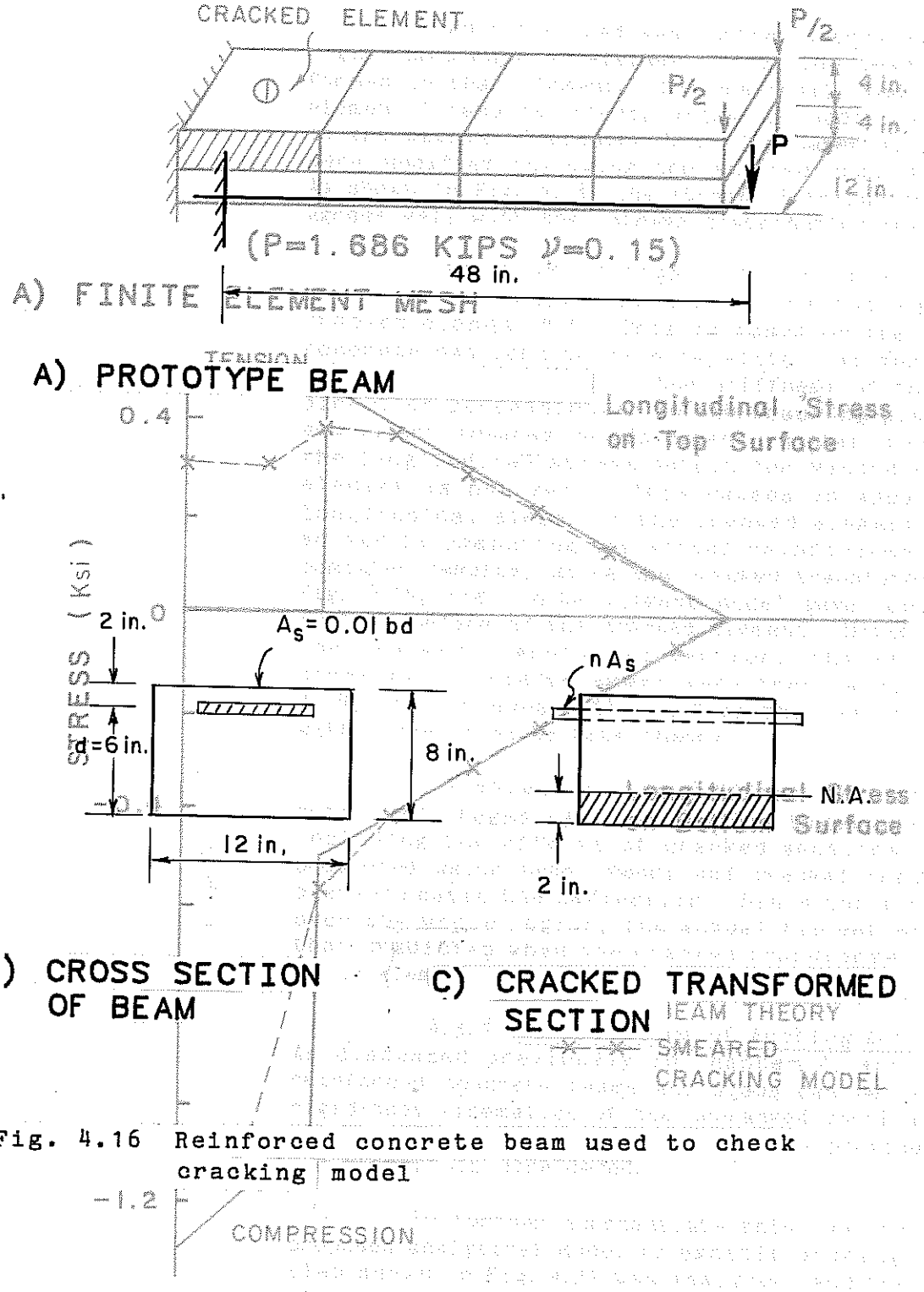

Fig. 4.16 Reinforced concrete beam used to check cracking model

Fig. 4.17 Flexural stresses in beam model, one element cracked

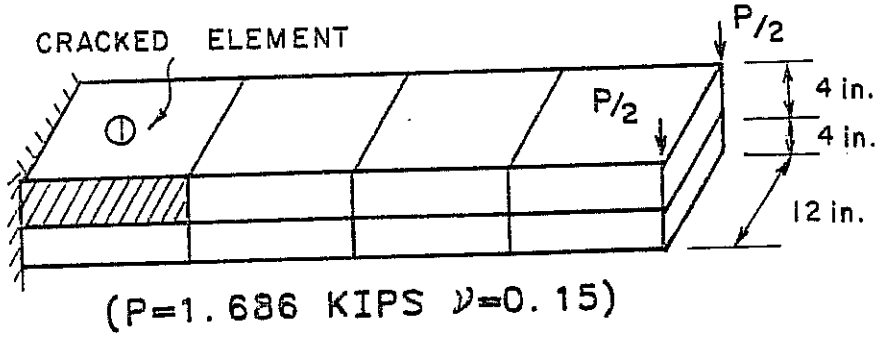

A) FINITE ELEMENT MESH

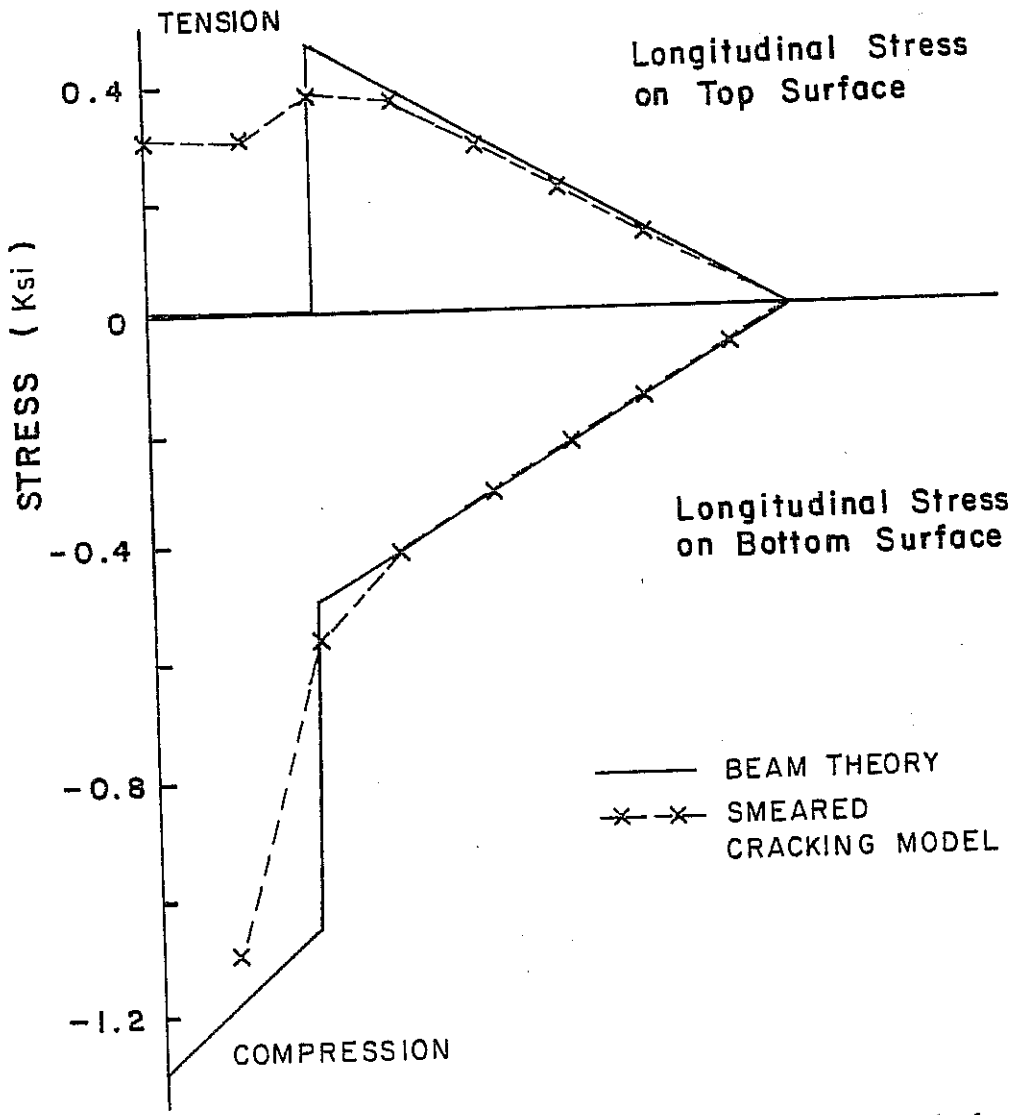

Fig. 4.17 Flexural stresses in beam model, one element cracked

When the load was further increased, causing cracking at the right-hand edge of element "2" of the beam (Fig. 4.18), new cracks formed in that element. The previously modified element stiffness of element 1 remains intact, while the modification procedure is applied to the matrix of element "2". The material properties of element "2" were modified following the smeared cracking model discussed above. As shown in Fig. 4.18, the stress distribution from the proposed model agrees well with the stress distribution predicted by beam theory.

As shown in Figs. 4.17 and 4.18, beam theory predicts a longitudinal tensile stress on the top surface of zero over the cracked element "1". This is based on the assumption that cracked concrete has zero tensile capacity. As described earlier, for the finite element solution, the stiffness of the cracked element in the direction perpendicular to the cracking plane is determined by the equivalent smeared reinforcement in that direction. Because of this the longitudinal stress output corresponding to the top of cracked element is not zero. This causes an apparent discrepancy in the longitudinal stress in the cracked elements. This problem can be solved by computing the actual reinforcement stress implied by the computer results, using the cracked transformed section. As shown in Fig. 4.19, the finite element model gave compressive stresses at the bottom surface of the cracked element. Using the neutral position for the cracked transformed section, the strains and corresponding stresses in reinforcement were then calculated. As shown in Fig. 4.19, the stresses obtained from the computer results agree closely with those given by beam theory.

As shown in Figs. 4.20 and 4.21, the tip deflections from both load stages agree well with those predicted by beam theory, including the effects of cracked sections. The deflection curve predicted using beam theory and cracked transformed sections always overestimates the deflection. Since the actual beam is not cracked over the whole region, the actual tip deflection will be less than that predicted when the cracked transformed section is used for the whole element.

4.3.7 Verification of Arching Action in Continuous Slabs. As discussed previously in Chapter 2, arching action in cracked, reinforced concrete beams and slabs can be explained in terms of the rigid-body kinematics of the uncracked portions of those elements. It exists even if deflections are small, provided that the thickness of the element is considered.

To further substantiate this, and to test the ability of the proposed analytical model to exhibit arching action, the continuous slab shown in Fig. 4.22 was analyzed, and the net membrane force was plotted as a function of load in Fig. 4.23.

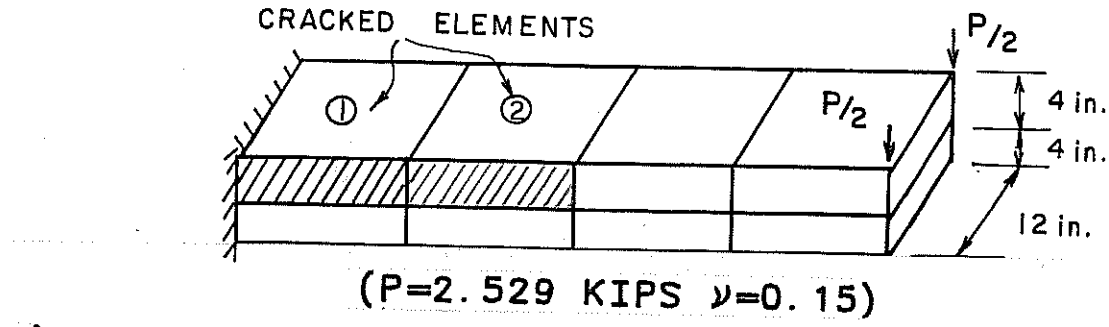

A) FINITE ELEMENT MESH

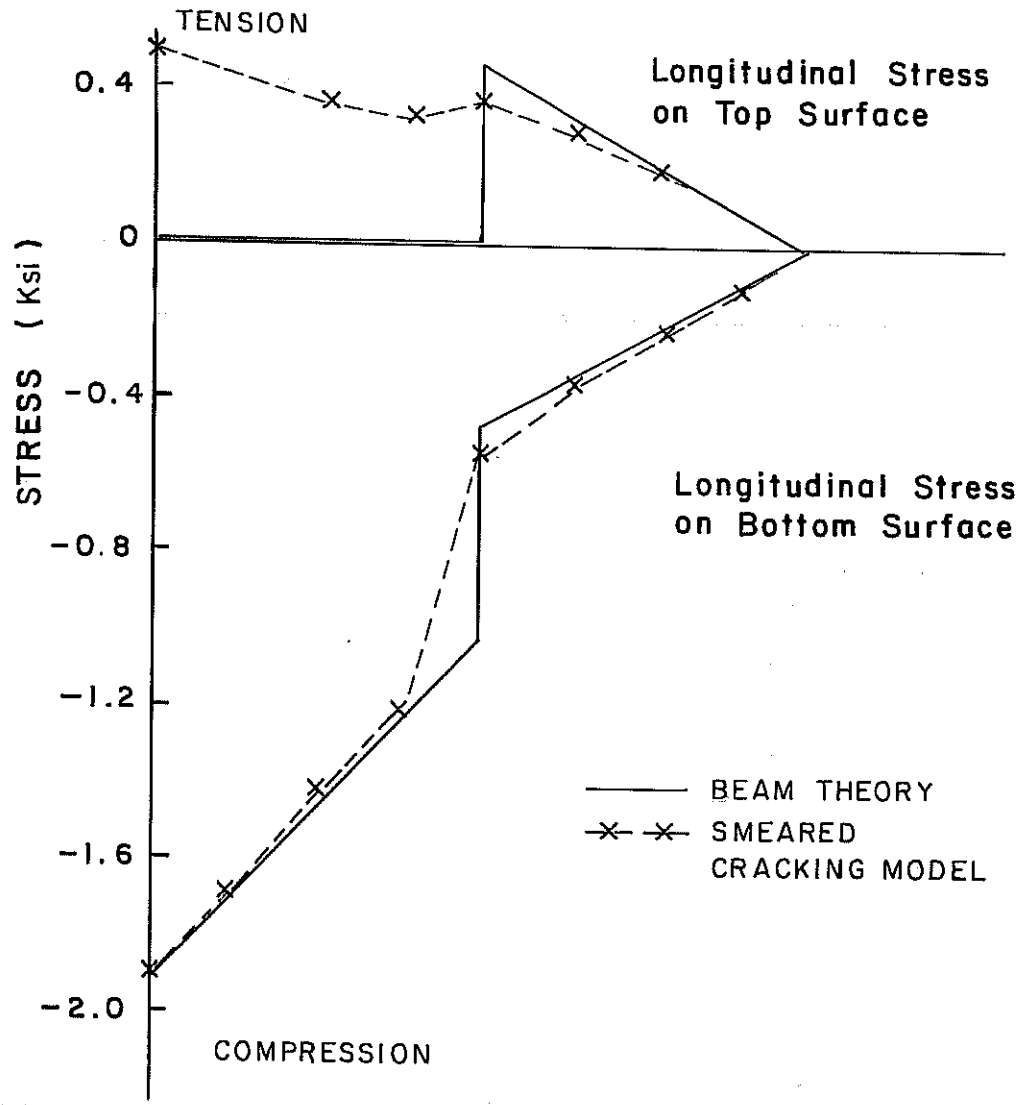

Fig. 4.18 Flexural stresses in beam model, two elements cracked

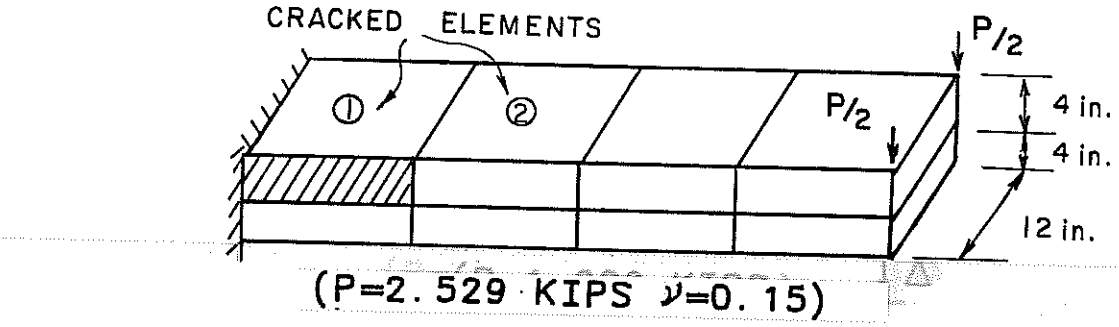

A) FINITE ELEMENT MESH

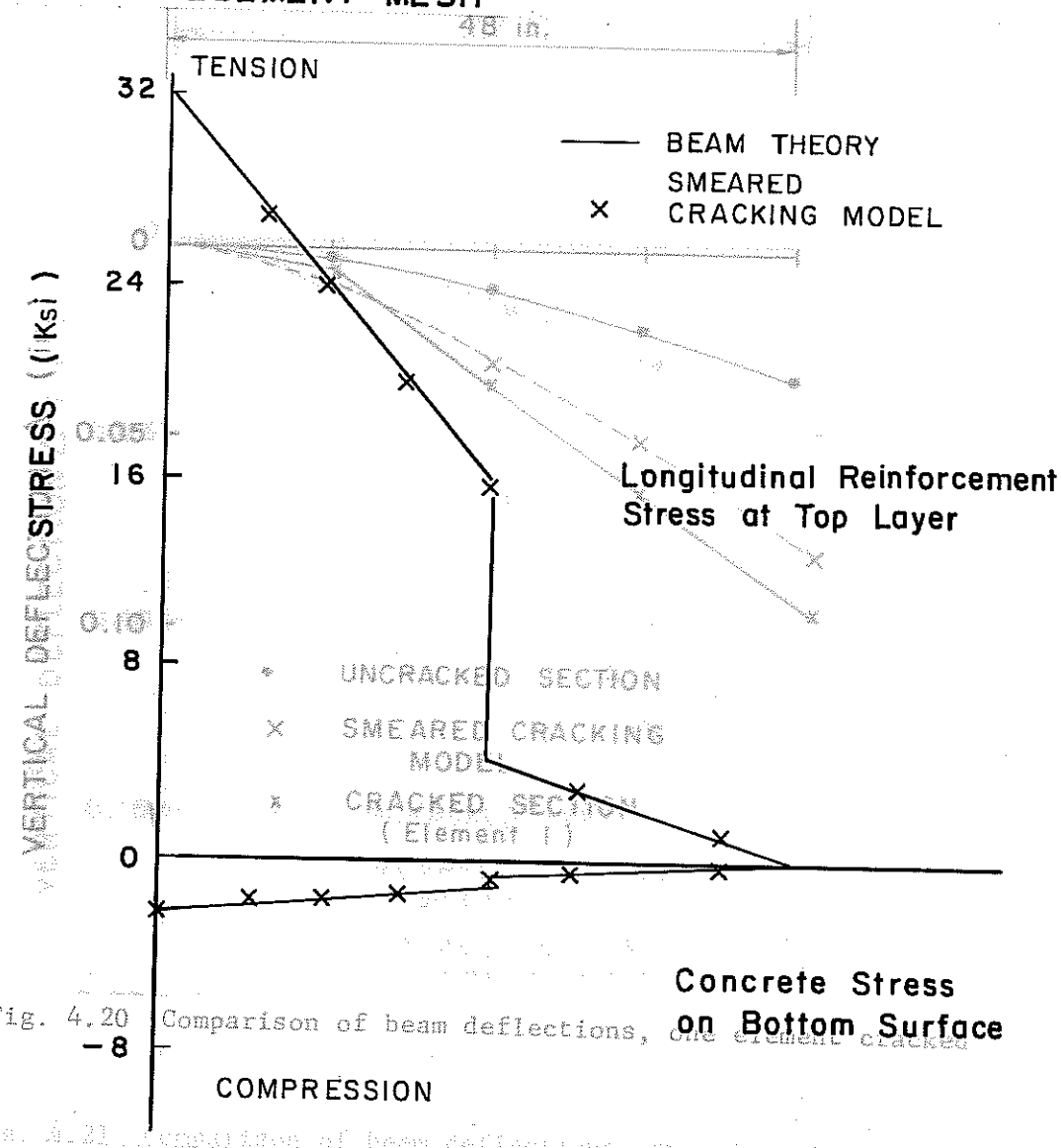

Fig. 4.19 Stresses in reinforced concrete beam model

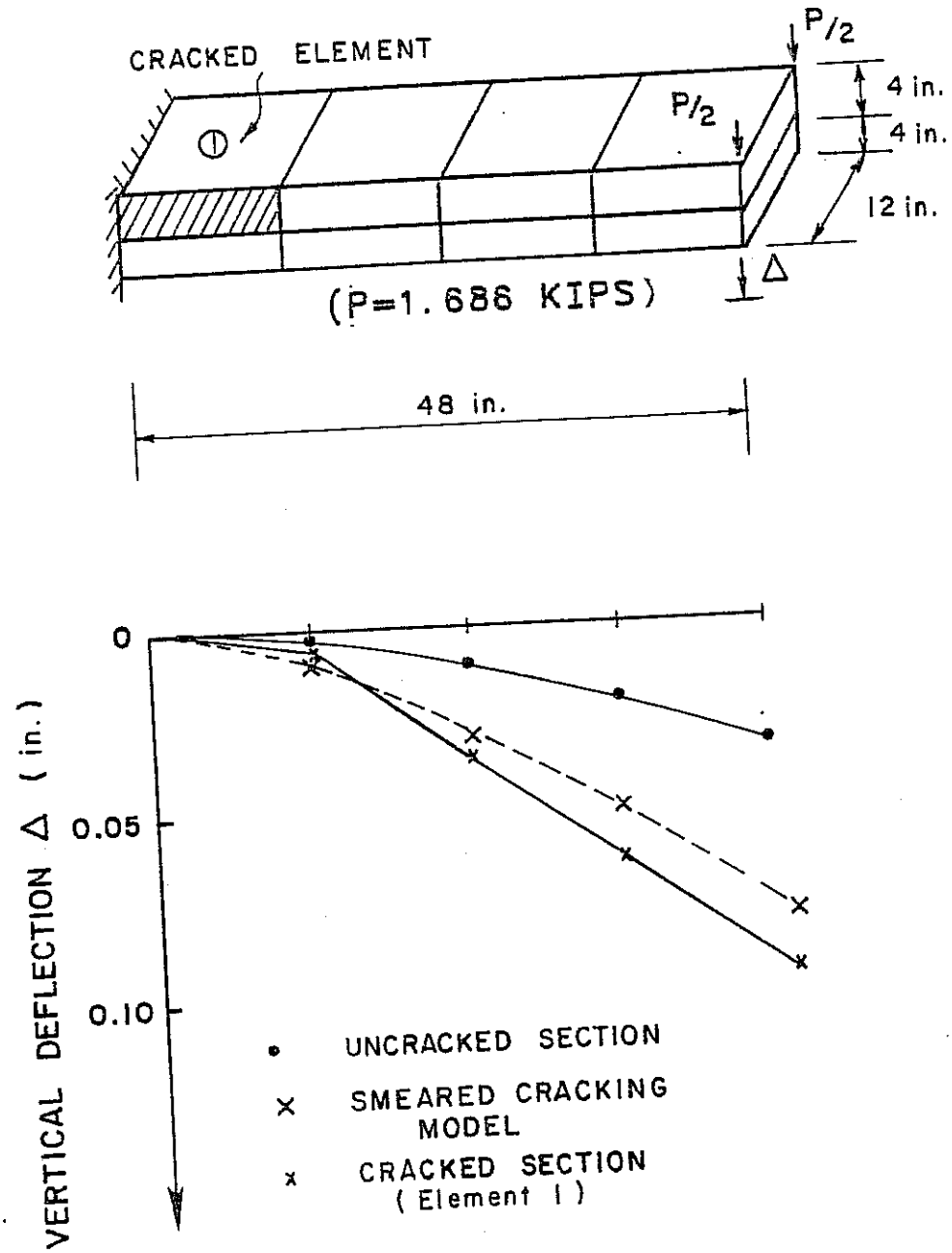

Fig. 4.20 Comparison of beam deflections, one element cracked

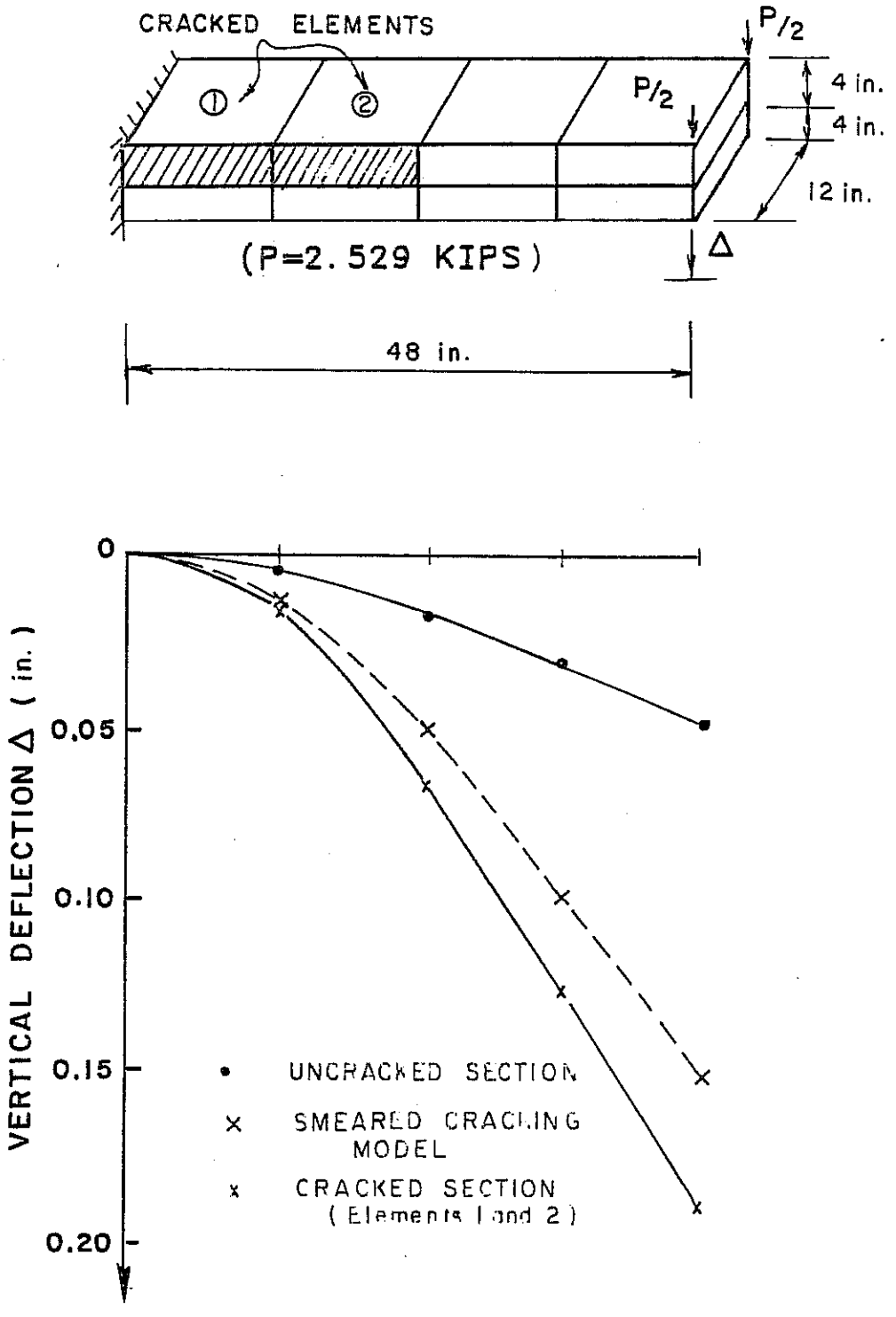

Fig. 4.21 Comparison of beam deflections, two elements cracked

A) UNCRACKED

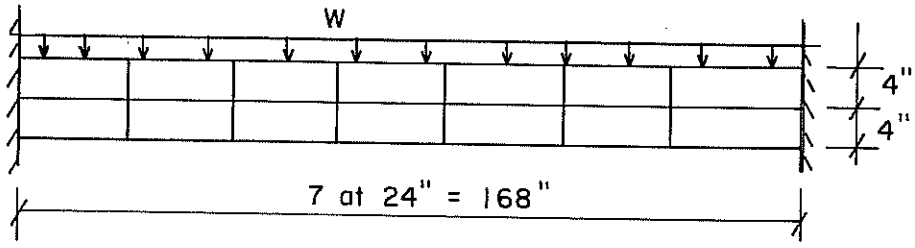

B) CRACKED AT ENDS

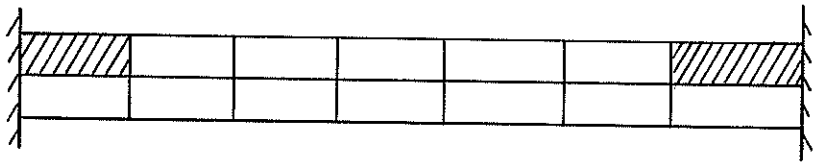

C) CRACKED AT ENDS AND MIDDLE

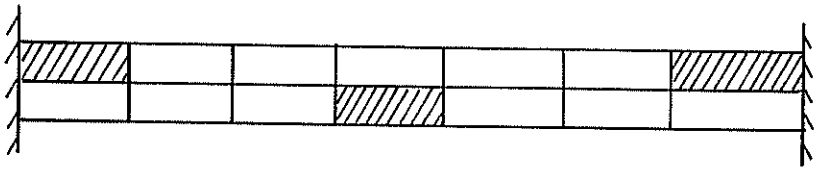

Fig. 4.22 Model used to verify arching action in continuous slab

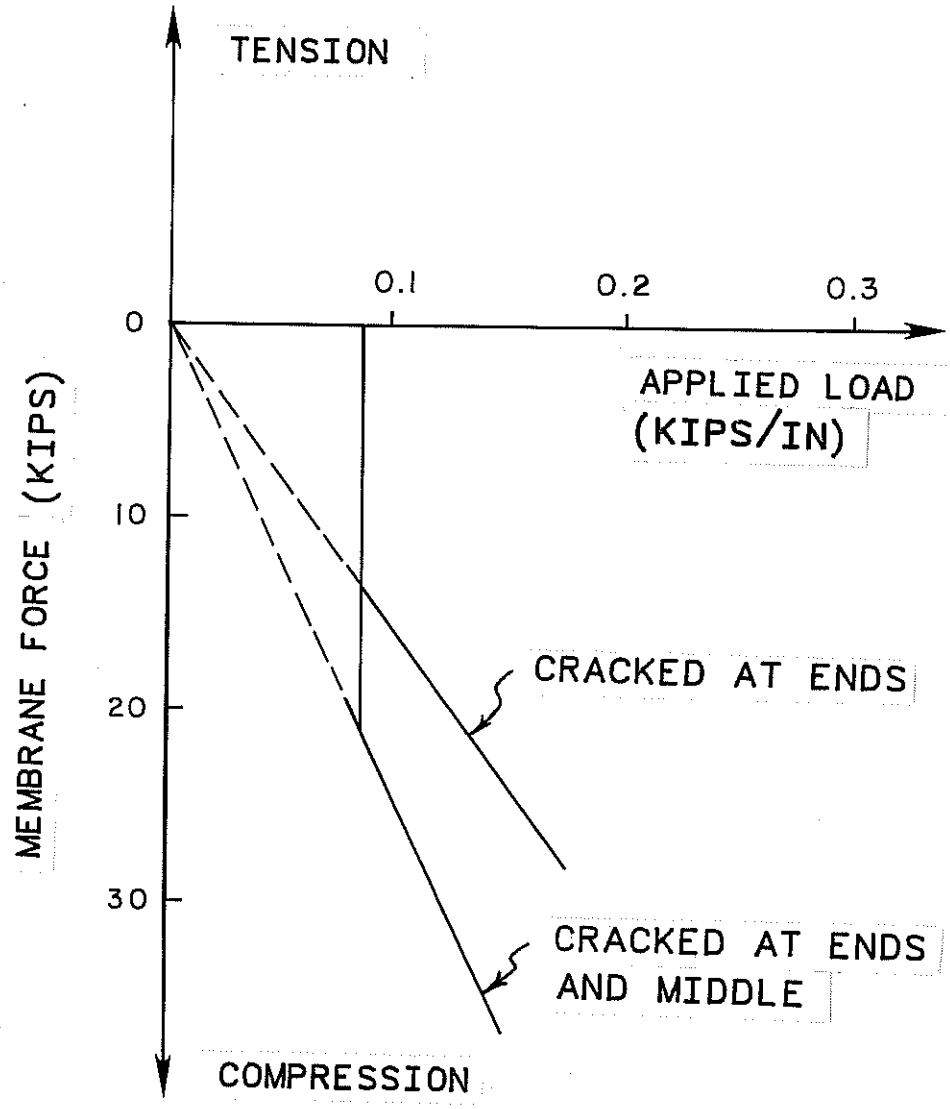

Fig. 4.23 Membrane force vs. applied load

As shown in Fig. 4.23, net membrane force in the uncracked slab (Fig. 4.22(a)) is essentially zero. However, after application of a load sufficient to produce flexural cracking at the supports (Fig. 4.22(b)), a compressive membrane force was produced in the slab. When further load was applied, the slab cracked at midspan (Fig. 4.22(c)), producing another increase in compressive membrane (Fig. 4.23).

As shown by this example, compressive membrane forces do exist in cracked reinforced concrete slabs, and this analytical model can show them.

4.4 Modeling of Bridge Specimen

4.4.1 General Description of Mesh. The real bridge, having one end cast-in-place and the other with precast panels, is not symmetrical in north-south (longitudinal) direction. To model such a bridge specimen, different material properties, geometric configuration and prestressing force should be used for the northern and southern halves of the bridge. Even taking advantage of transverse symmetry, half of the bridge needs to be modeled. To reduce computational effort, the bridge was simplified as consisting entirely of panels, or entirely of CIP concrete. The assumption behind this technique (that the local behavior of the bridge near a load would be relatively unaffected by whether the other half was composed of panels or CIP concrete) was later verified by comparing results for the two models. Two types of bridge models (CIP and precast panel) were developed individually, as shown in Fig. 4.24. Equivalent concentrated loads for the loaded region are shown in Fig. 4.25. Because the idealized bridge was symmetric in both directions, each model could consist of only a quarter of the bridge, with appropriate boundary conditions, as shown in Fig. 4.26.

The deck slab could be cracked at either the top or bottom surface, depending on the sense of the moment in the slab. Therefore, the CIP deck was modeled using 156 thick-shell elements, placed in two layers as shown in Fig. 4.27. As discussed earlier in this chapter, the composite girder can be effectively modeled using combination of thick shell elements and three dimensional beam elements, as illustrated in Fig. 4.28. This modeling concept was applied to the bridge specimen. The steel girder was modeled using 300 three-dimensional beam elements. Transverse and longitudinal sections of the bridge model are shown in Figs. 4.27 and 4.28.

To avoid input complexity due to a refined mesh near the load point, it was decided to use a simple but satisfactory mesh discretization, verified using simpler finite element models, and

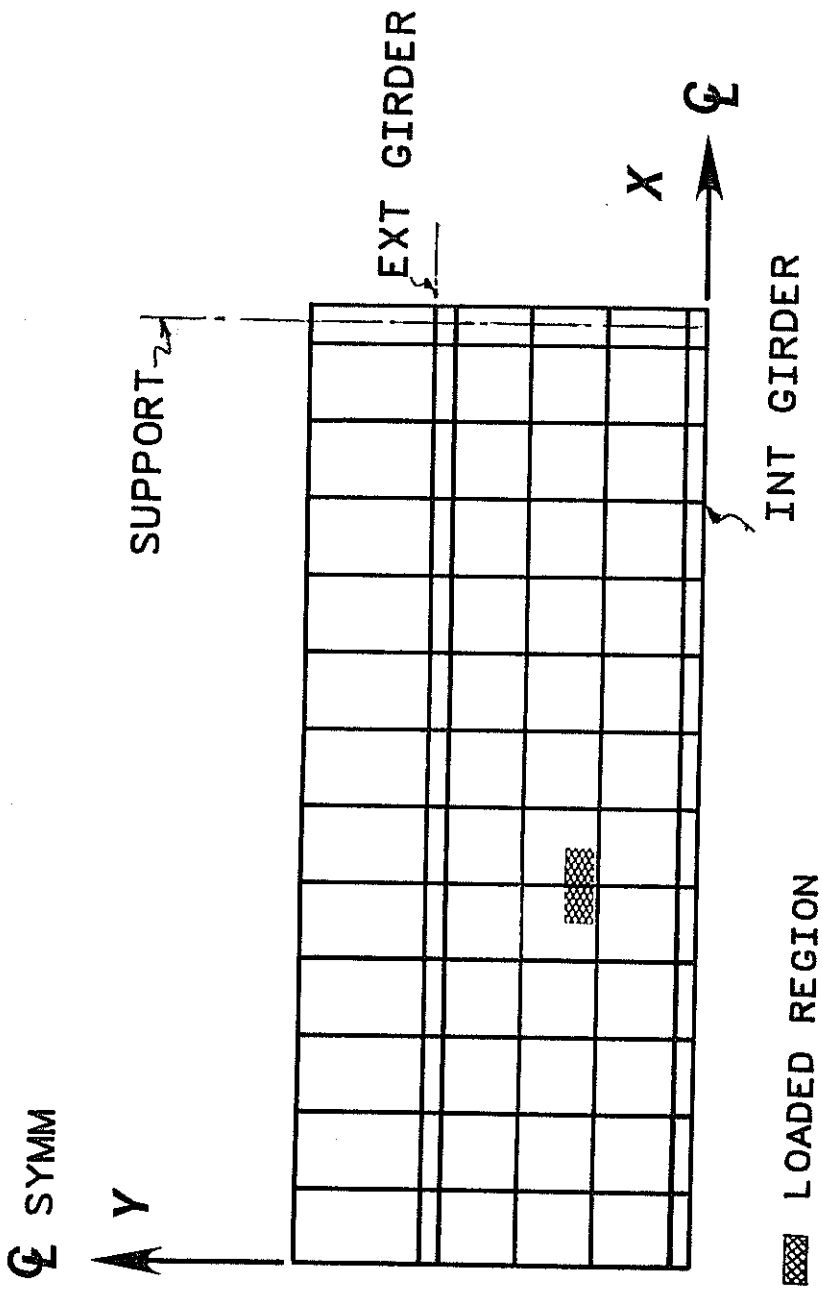

Fig. 4.24 Finite element mesh of quarter bridge specimen

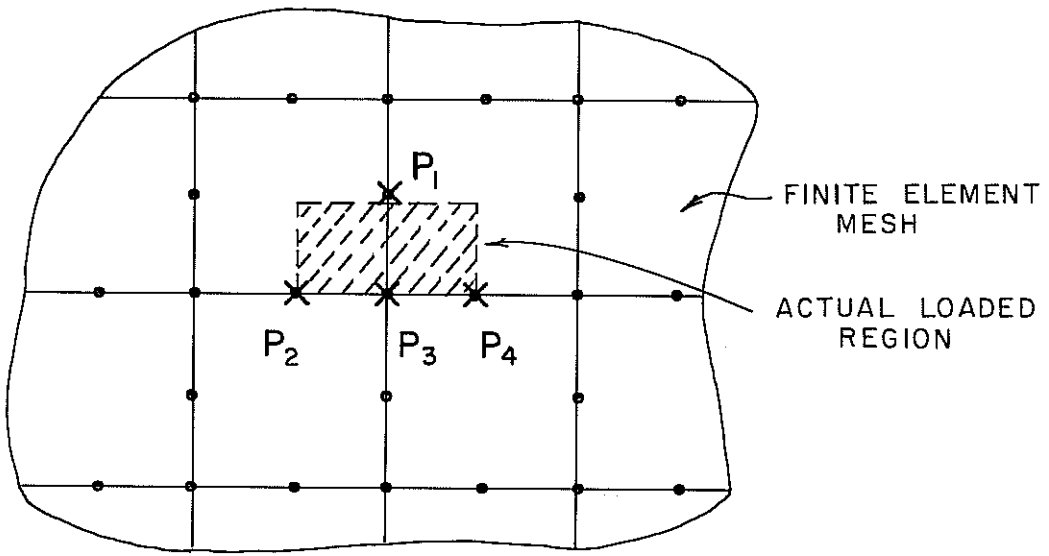

100-Kip Total Load

X : Equivalent Concentrated Load

P_1 = 50 Kips ; P_3 = 25 Kips ; P_2 = 12.5 Kips ; P_4 = 12.5 Kips

Fig. 4.25 Equivalent concentrated loads for loaded region

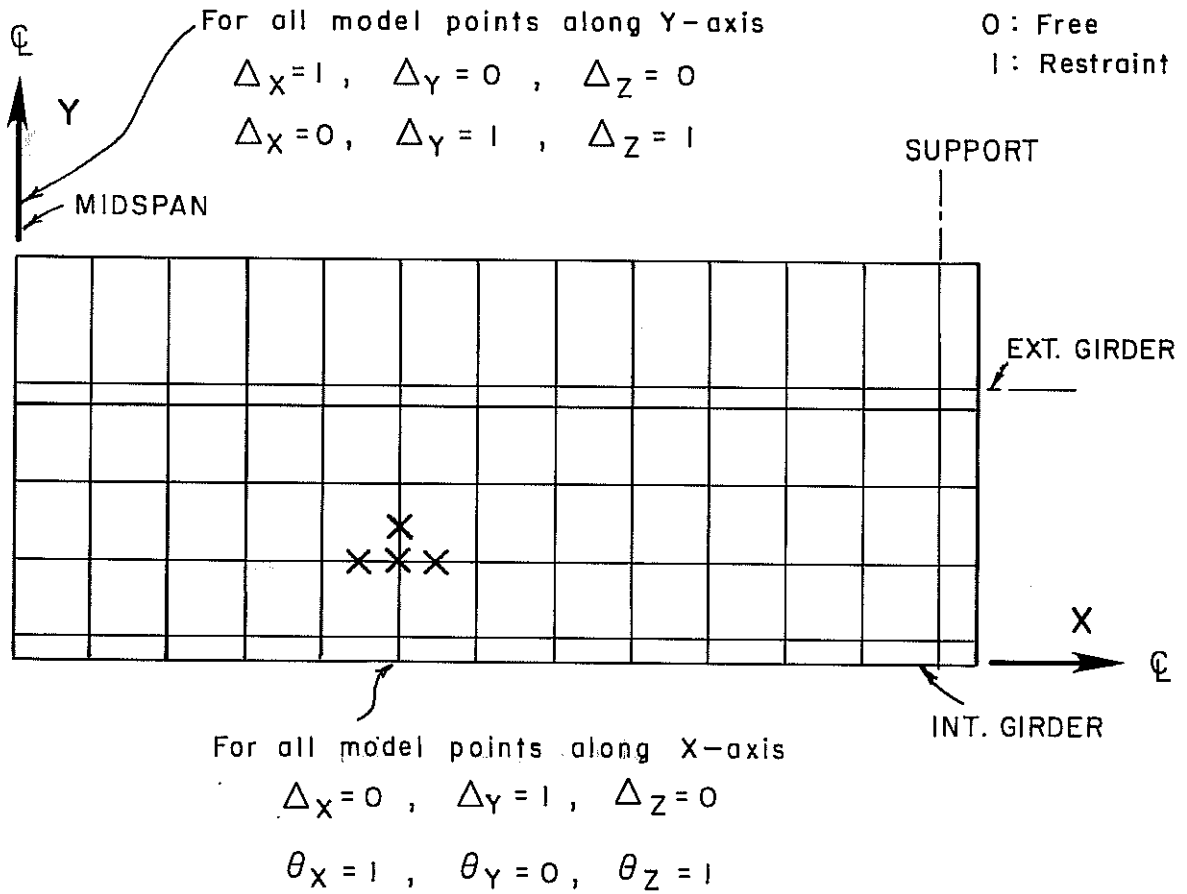

Fig. 4.26 Boundary conditions of quarter bridge model

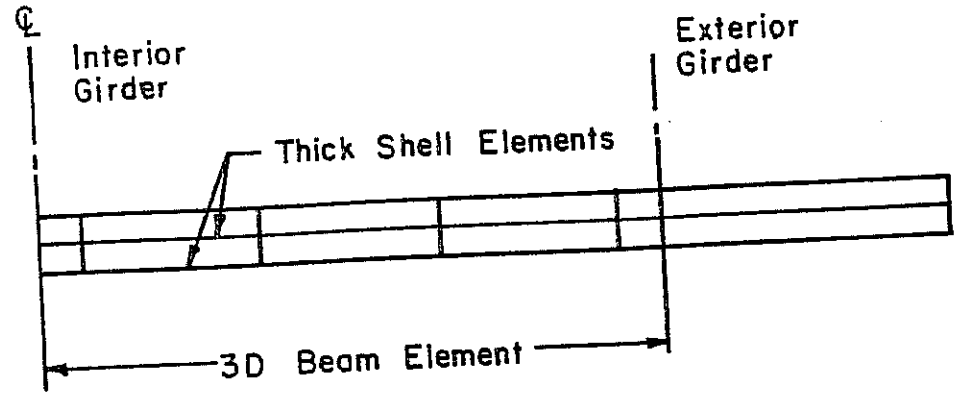

Fig. 4.27 Transverse section of bridge model

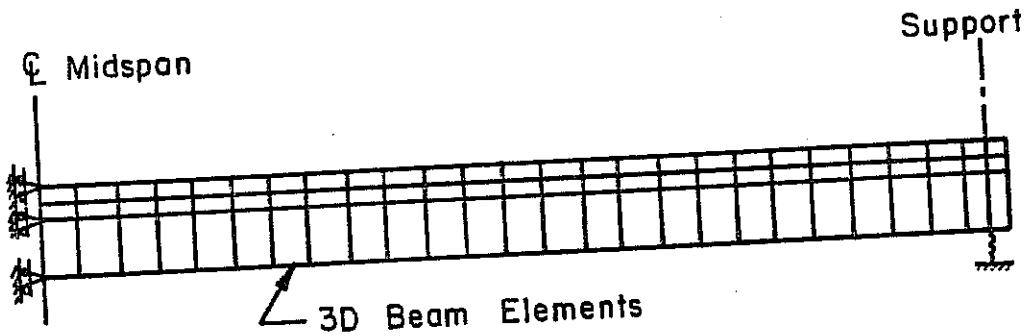

Fig. 4.28 Longitudinal section of bridge model

shown in Figs. 4.24 and 4.25. In the actual bridge specimen, load was applied at each load position through a 8- by 20-in. loading plate whose location and patch size do not match the mesh of the bridge model. The uniformly distributed load was simulated using four equivalent concentrated nodal loads. To obtain the appropriate combination of concentrated nodal loads, the bending stress distribution of a simply supported slab with a distributed patch load was compared with those obtained using various combinations of concentrated nodal loads. The best equivalent combination of concentrated nodal loads was then applied to the bridge model as shown in Fig. 4.25.

The end and intermediate diaphragms were modeled using two three-dimensional beam elements as illustrated in Fig. 4.29. The flexural and axial stiffnesses of those beam elements were adjusted to reproduce the flexural and axial stiffness of the real X-brace diaphragms. The neoprene pads at the supports were modeled using axial springs. The axial stiffness of these pads was obtained from the experimental data in Ref. 4.29.

4.4.2 Modeling of Prestressed Panel Deck. A typical bridge deck slab designed using the precast prestressed panel is shown in Fig. 3.4. Once the panels had been placed in position, a cast-in-place concrete topping was poured to create a monolithic deck.

In modeling this type of bridge deck, different moduli of elasticity were used to represent the different stiffness of the CIP concrete and the precast panels. Since the precast panels were placed end to end without continuity in the longitudinal direction, the panel gaps were modeled using two separate rows of nodal points, so that the closeness of the gap could be simulated. A schematic representation of the modeling of panel gaps is shown in Fig. 4.30.

The rest of the modeling concept was the same as that used for the cast-in-place deck. To save computation time, the same number of thick shell elements as before was used for the deck slab. The steel girders were modeled as before.

As noted earlier, the analytical representation of cracking in the panel deck was identical to that used in the CIP deck, with the following modifications. First, the transverse precompression due to prestressing was taken into account in computing the principal stress magnitude and orientation in the panels. Second, the higher compressive (and therefore tensile) strength of the panels was considered when applying the cracking criterion.

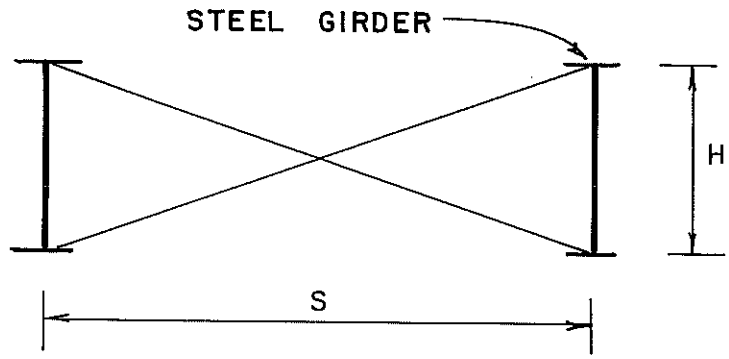

ACTUAL DIAPHRAGM

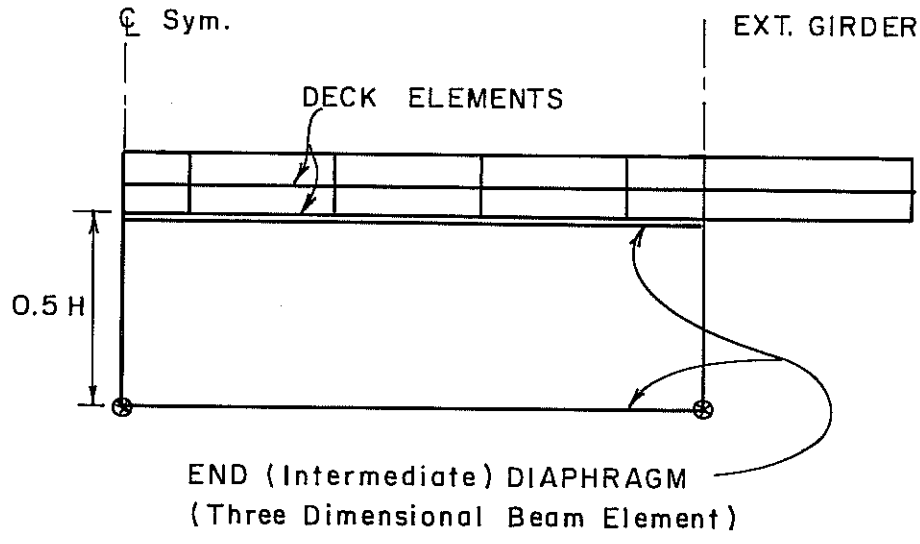

FINITE ELEMENT MODEL OF DIAPHRAGM

Fig. 4.29 Model of end (intermediate) diaphragm

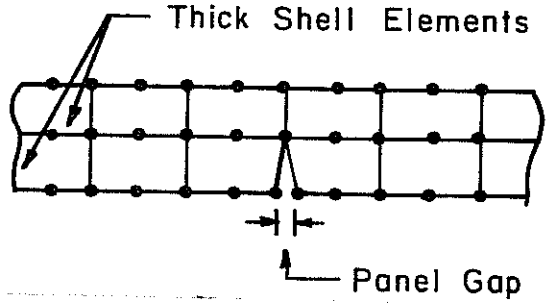

Fig. 4.30 Modeling of panel gaps

CHAPTER 5

TEST PROCEDURE

5.1 Load Magnitude and Points of Load Application

Fatigue and static loadings were developed based on standard AASHTO truck loadings. An HS20 truck produces a maximum wheel load of 16 kips. When multiplied by the maximum AASHTO impact factor of 1.30, this results in a maximum service wheel load of 20.8 kips. This is referred to in this study as the "design wheel load". Static tests were conducted using multiples of this service load (design wheel load). To be conservative in the experimental program, fatigue tests were conducted using a maximum wheel load of 26 kips, 25 percent higher than the service load. The load was applied simultaneously to four locations on the deck. Wheel lines were 6 ft apart transversely, and a longitudinal spacing of 20 ft was used between axles as shown in Fig. 5.1. The wheel lines were thus located 3 ft on either side of the center steel girder, or 6 in. from the midspan of the girder spacing. From the viewpoint of overall moment on the bridge, this loading simulated the worst possible position of the four wheel loads on this bridge.

5.2 Loading System

To avoid using a large overhead reaction frame, loads were applied to the bridge from below at four locations (Figs. 5.1, 5.2). As shown in Figs. 5.3 and 5.4, the hydraulic actuators were attached at their bottom ends to the structural test slab underneath the bridge, and at their top ends, to rods passing through holes in the bridge deck and held in place by nuts. Each actuator had a static capcity of about 60 kips, and a fatigue capacity (governed by the fatigue life of the tensile rods connecting the actuators to the bridge) of about 35 kips. Hydraulic fluid at 3000 psi was supplied by two Shore-Western pumps. The actuators were controlled using a closed-loop feedback system, operating under load control. Load feedback from a fatigue-rated load cell was input to a Short-Western servocontroller (Fig. 5.5), which compared it to the sinusoidal command signal from a function generator. The resulting error signal operated a single 60-gpm Moog servovalve, which fed all four actuators through a common manifold. The interconnected hydraulic actuators are shown schematically in Fig. 5.6.

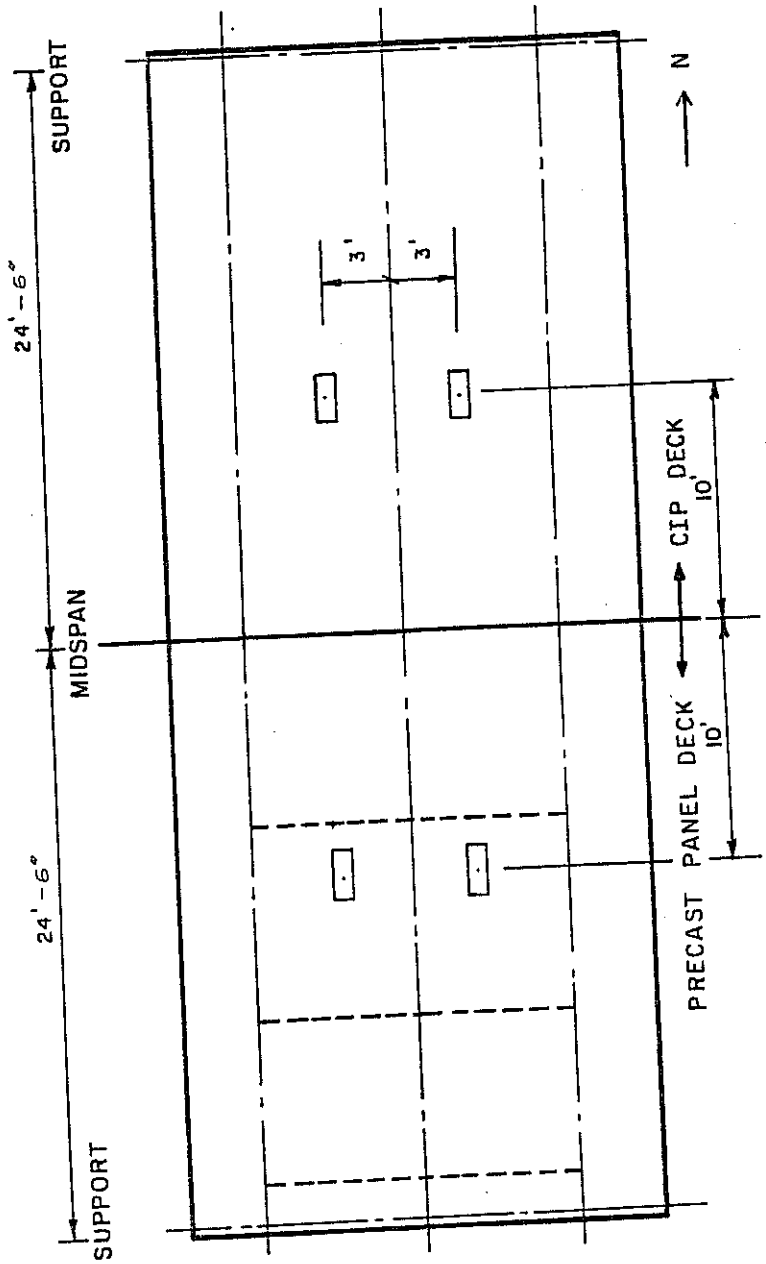

Fig. 5.1 Placement of loads

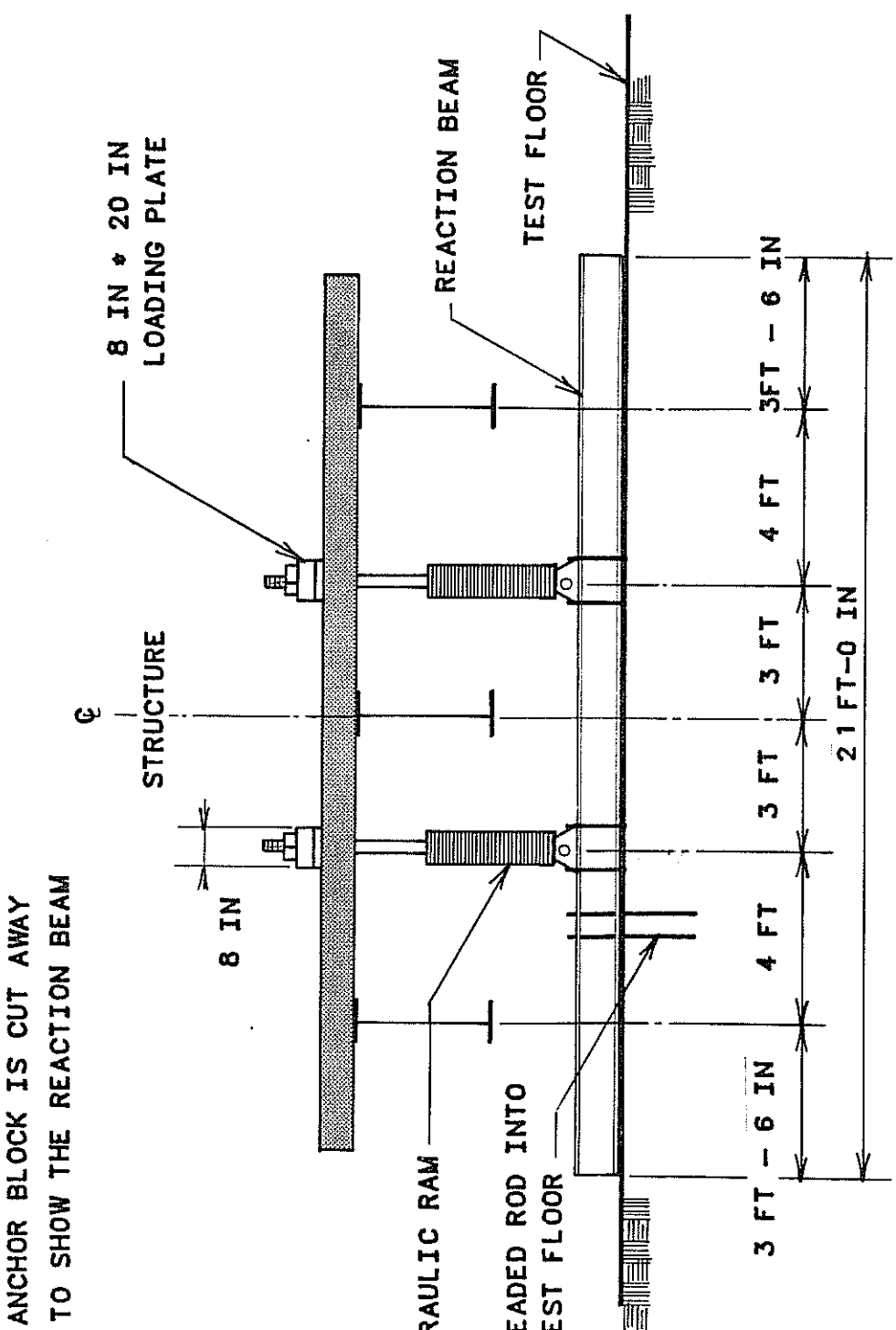

Fig. 5.2 Cross section of test setup

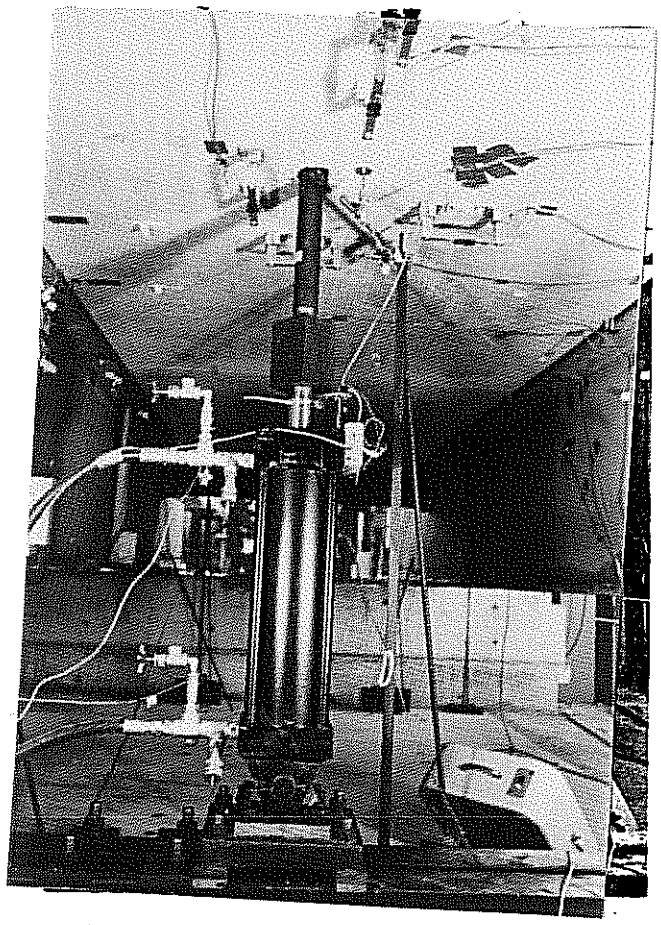

Fig. 5.3 Typical hydraulic actuator

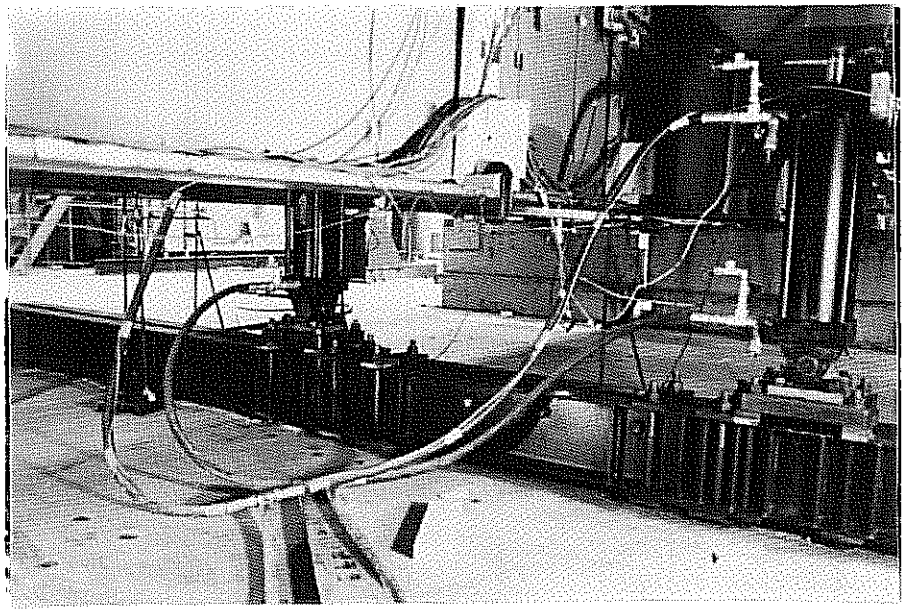

Fig. 5.4 Reaction beam

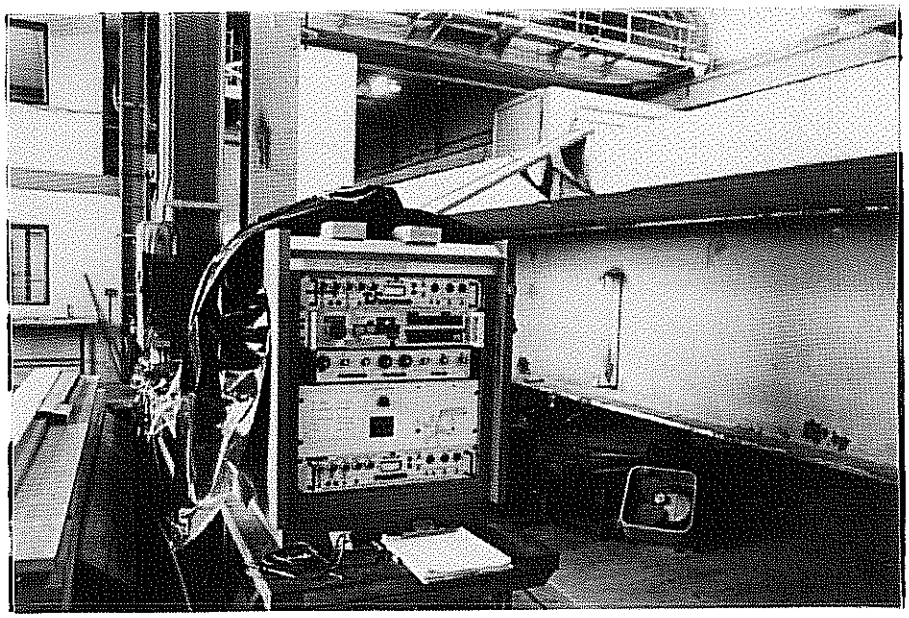

Fig. 5.5 Load control console

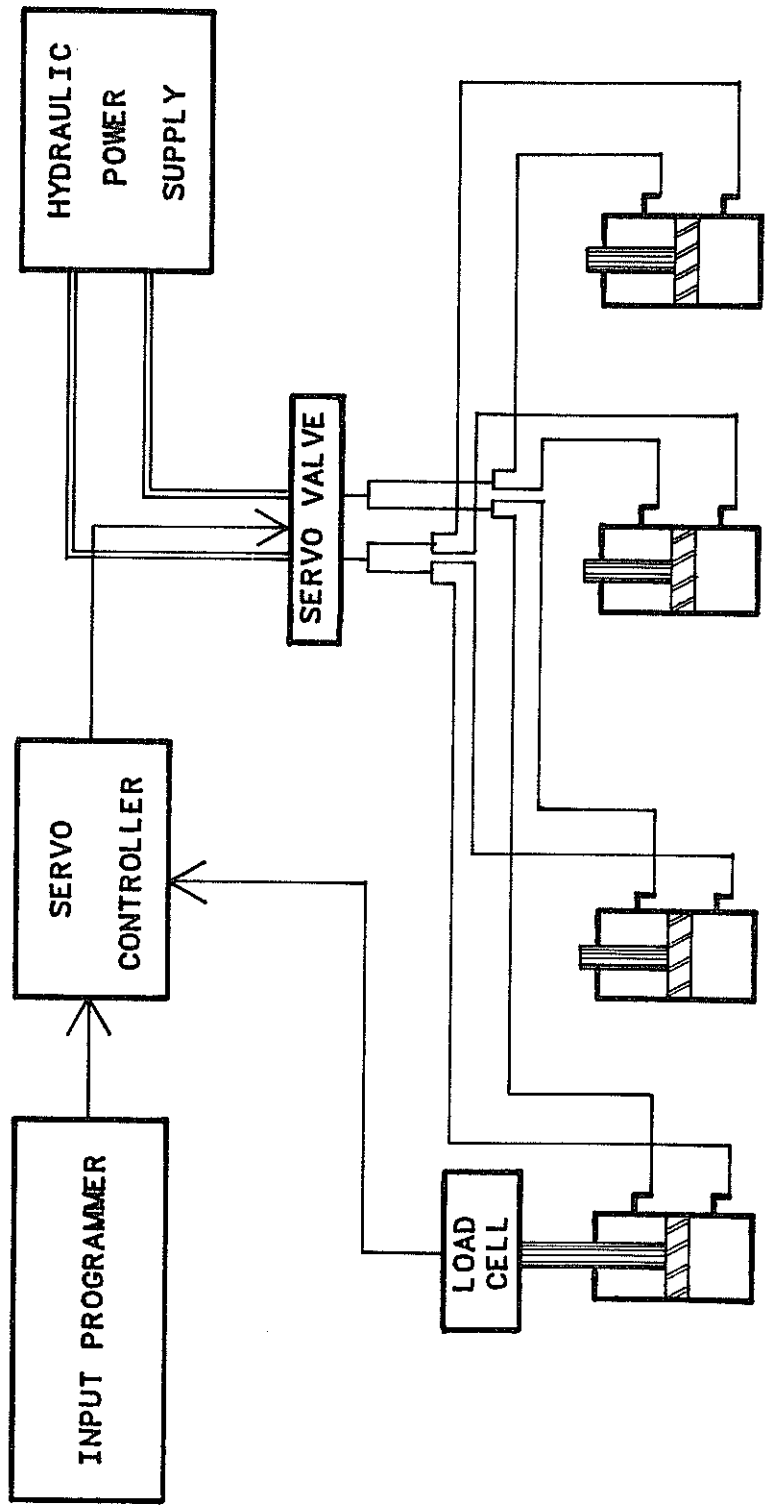

Fig. 5.6 Schematic of loading system

5.3 Instrumentation

The specimen was heavily instrumented in order to obtain sufficient data to monitor its behavior during the test and correlate the experimental and analytical results. The desired data were: applied load; deflections of the deck and steel girder; strain of concrete and steel; cracking pattern and crack width; slip between deck and girder; and local deformation of precast panel deck.

5.3.1 Loads. In the closed-loop hydraulic system, the load was monitored by a 200-kip fatigue-rated load cell (Strainset), connected to one of the hydraulic actuators. Loads were measured using two 5000-psi pressure transducers attached to the high- and low-pressure sides of the actuators. Before tests, the load cell and both pressure transducers were calibrated using the Laboratory's 600-kip universal loading machine and dead weight pressure gage tester. Tests have shown that actuator friction is much less then the loads applied to the bridge in this test. Because all rams were interconnected through a common manifold, they were assumed to have equal pressure, and thus to apply equal load. A single load cell was therefore sufficient to control the four equal loads applied at the positions shown in Fig. 5.1.

5.3.2 Deflections. The vertical deflections of deck and steel girder were measured using a 2-in. linear potentiometer and an 0.001-in. dial gage. The instrumented locations are shown in Fig. 5.7.

5.3.3 Strains. As shown in Fig. 5.8, strain gages were mounted on the reinforcement and on the concrete surface. Reinforcement strains were measured using 0.32-in. (Precision Measurement W-32) paper-backed strain gages. Concrete surface strains were measured using 2.5-in. (PL-60) surface-mounted gages. Three-wire hookups were used to provide temperature compensation for all gages. Near the loaded points, strain gages were installed longitudinally and transversely to detect the strain of the deck in both directions. Numerous gages were also installed near the interior and exterior girders to detect possible membrane forces at the boundary of the deck. Gages were also installed at the panel gaps and the interface of the precast panel and cast-in-place concrete, to detect possible cracking and deck deterioration at these local regions. To avoid loss of gages due to concrete cracking in regions of the deck subjected to tensile strains, those regions were instrumented using clip gages.

At almost every gaged location, three gages were installed to permit verification of the strain gradient through the deck.

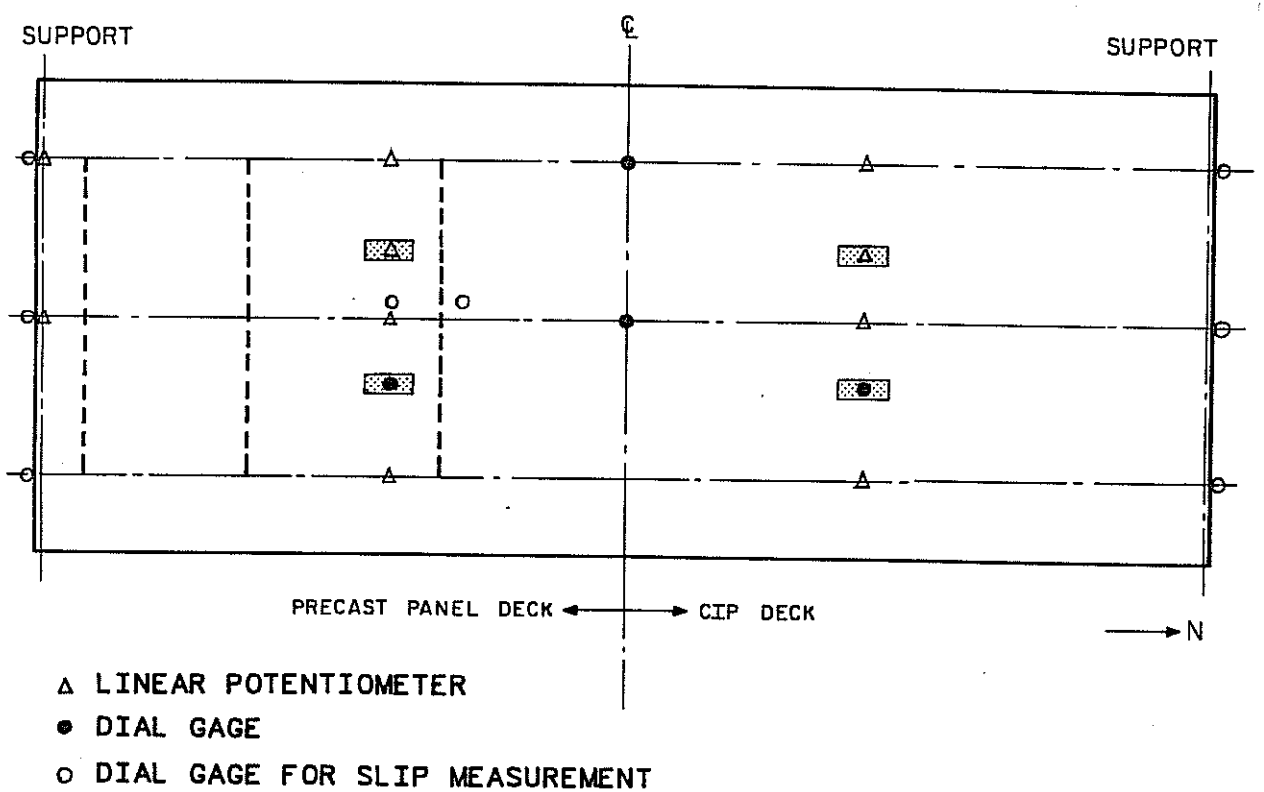

Fig. 5.7 Instrumented locations for deflection measurement

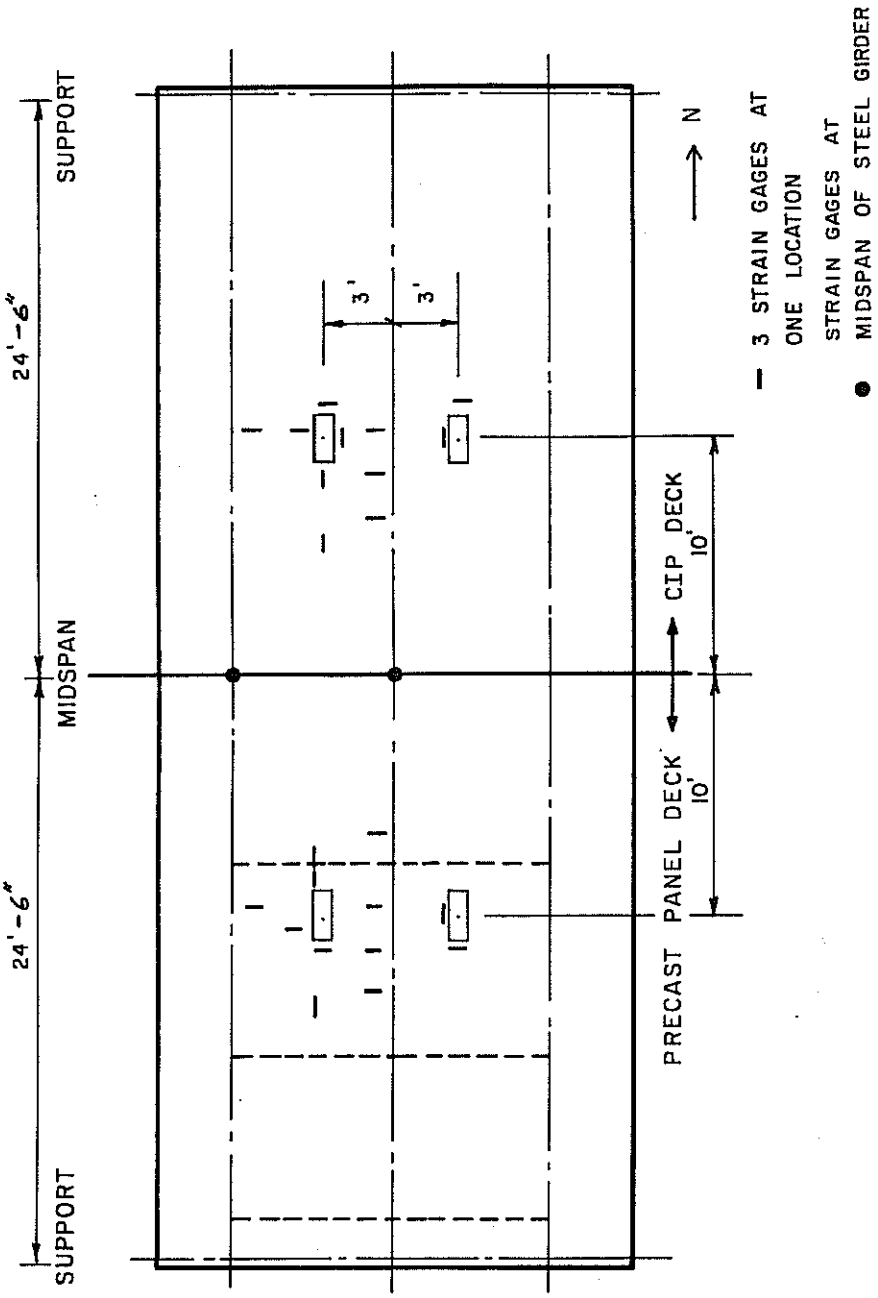

Fig. 5.8 Strain gage locations

5.3.4 Slip Between Deck and Girder. The slip between deck and girder was measured using 0.001-in. dial gages at each end of the deck. Because more space was needed on the girder flanges to allow placement of the precast panels on the girder, the shear studs in the southern end were placed closer togethe, toward the middle of the flange. Therefore, several more dial gages were installed across the load and near the panel gap to observe the possible loss of bond near those points (Fig. 5.9).

5.3.5 Cracking of Deck. Cracking due to shrinkage was carefully recorded before testing. During the tests, crack propagation was documented at each load stage. Crack widths were also measured using a crack-width template whose smallest scale is 0.002 in.

5.4 Data Acquisition

A total of 99 channels of instrumentation were used. Data were read and recorded electronically by an Acurex digital voltmeter connected to a reed-type scanner and controlled by a CompuPro microcomputer. Test data for all 99 channels were scanned in approximately 10 seconds, avoiding changes in readings due to creep. Digitized data were written immediately onto the microcomputer's diskette, and were also converted to engineering units for immediate review during a test. Data were transferred to the main computer on the UT campus for further processing and automatic plotting.

5.5 Test Program

As shown in Fig. 5.10, the test program involved the following sequence of loading:

1. The bridge was tested statically to a maximum load of 60 kips on each of the 4 actuators. This load level represented about 3 times the service live load of 20.8 kips, including impact factors;

2. As shown in Fig. 5.11, the bridge was subjected to 5 million cycles of fatigue loading, varying sinusoidally between 5 to 26 kips on each actuator. The maximum fatigue loading of 26 kips represented the service live load level of 20.8 kips, plus a 25 percent overload for conservatism. At intervals of about 1 million cycles, the bridge was loaded statically to 30 kips on each actuator (an overload condition), to document the effects of fatigue loading on bridge performance; and

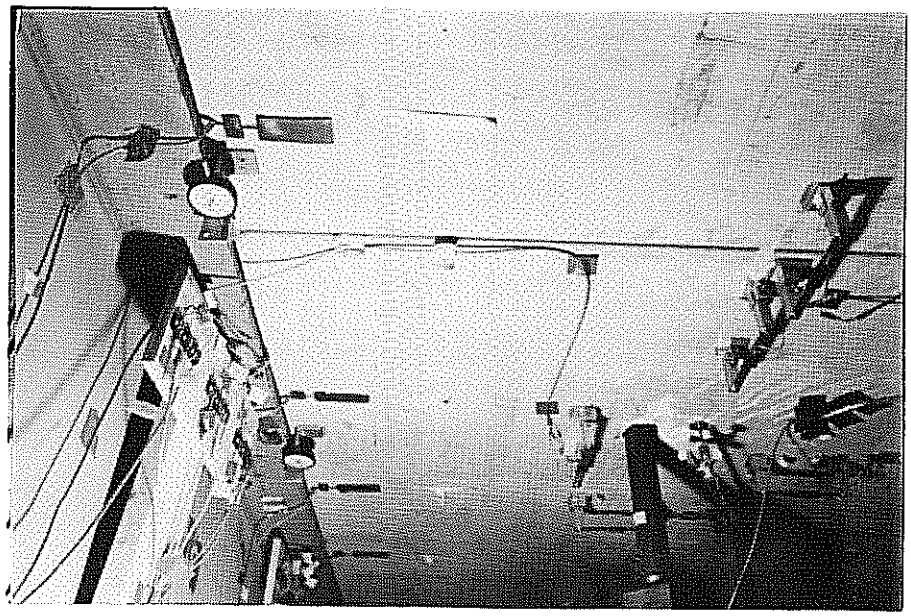

Fig. 5.9 Slip gages near panel gap and load point

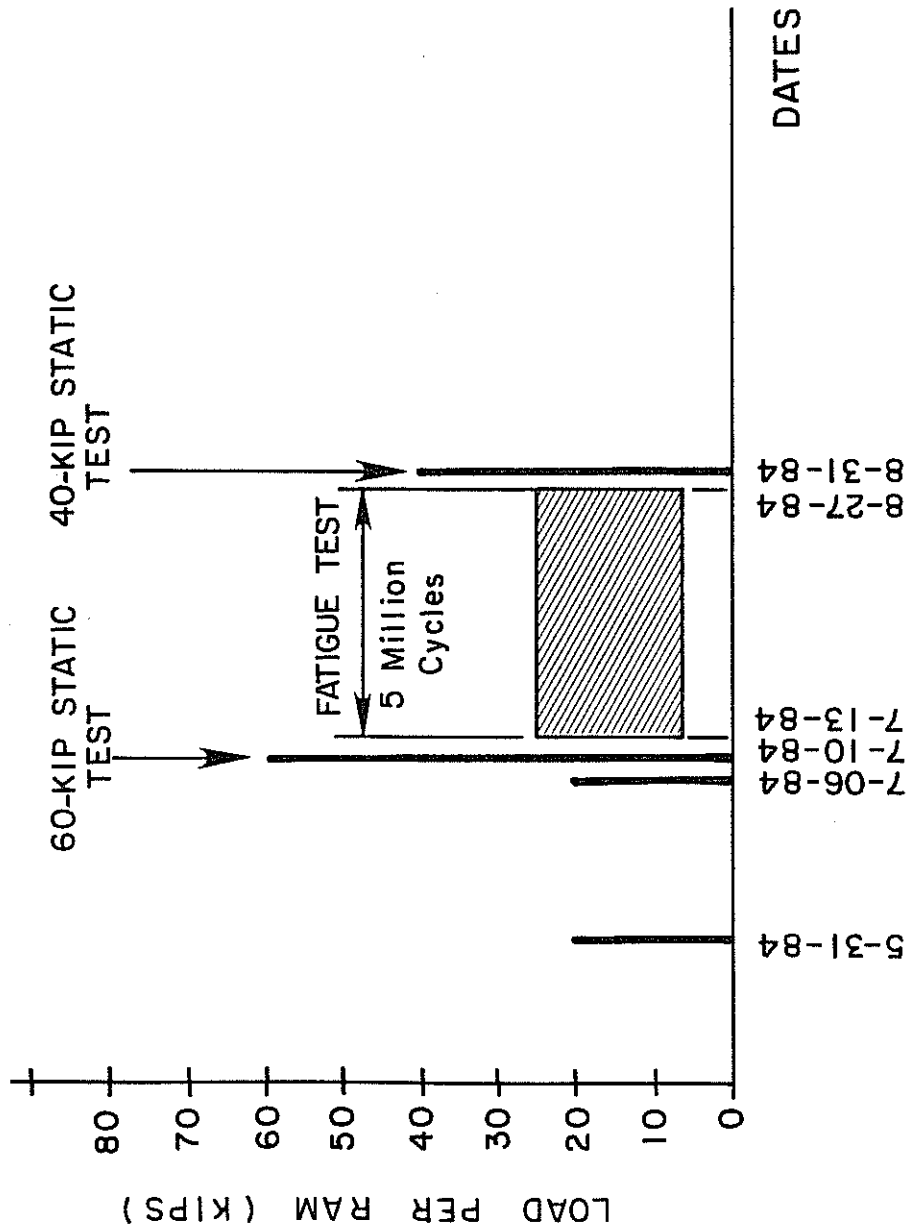

Fig. 5.10 History of loading

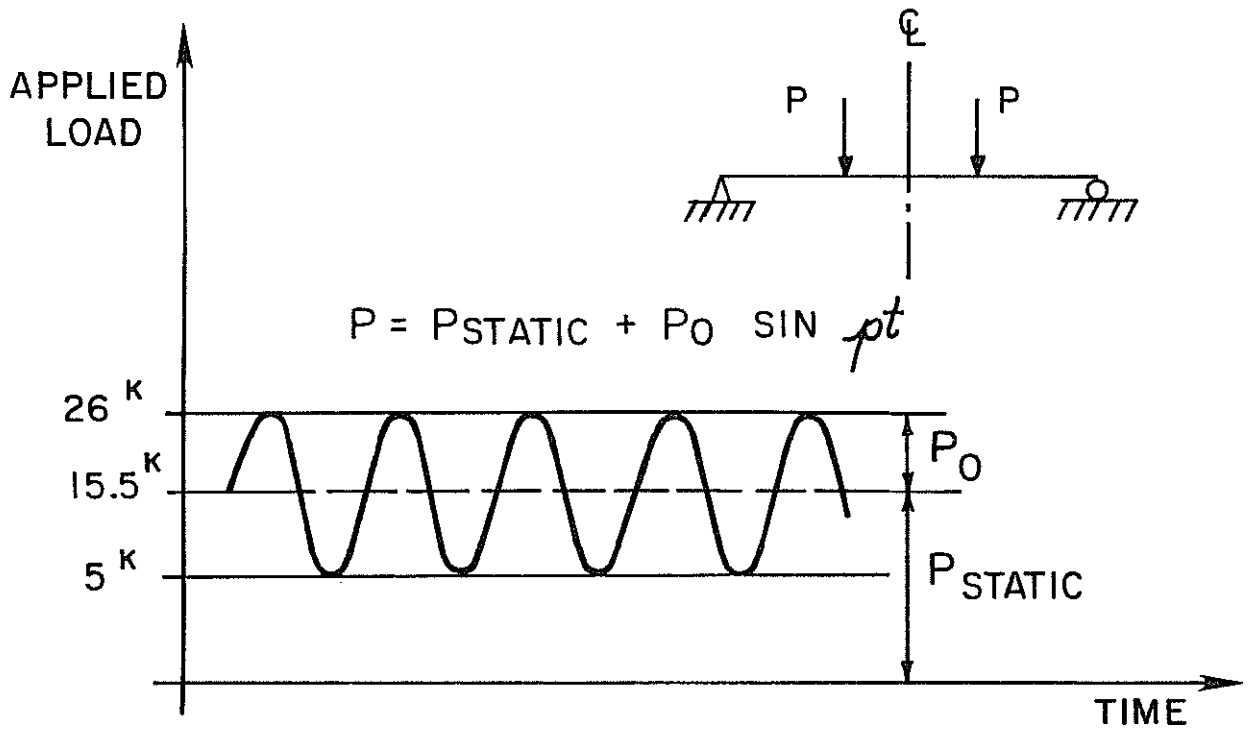

Fig. 5.11 Range of loading during fatigue test

3. Following the 5 million cycles, the bridge was tested statically to 40 kips on each actuator (Fig. 5.10). This load level represented almost twice the service live load of 20.8 kips (including impact factors).

   In every static test, the following data were obtained:

   a) loads applied at one actuator;

   b) vertical displacements at various points on the bridge;

   c) strain profiles at various points on the bridge deck;

   d) slip between the deck and steel girders at various points;

   e) strain at various points along the steel girders; and

   f) crack widths and extensions over the bridge deck.

The experimental program outlined above allowed the acquisition of sufficient data to document the actual performance of the Ontario Bridge Deck under both static and fatigue loadings. The initial static loading of 60 kips, followed by the application of 5 million cycles of fatigue loading with a maximum load of 26 kips, was designed to produce the worst possible loading sequence for the deck.

CHAPTER 6

BEHAVIOR OF SPECIMEN

6.1 Introduction

In this chapter, results and observations from the tests of the specimen are presented and discussed. During the test sequence described earlier, the following observations were made:

1. First Static Test: At a load of about 38 kips per ram, the bottom of the CIP deck near the load started to crack. The top surface of the CIP deck did not crack until about 55 kips per ram. At the panel end, the first top surface cracks also occurred at a load of about 55 kips per ram, and no bottom cracks developed in the panels. The weld between the intermediate diaphragms and the center girder broke at a load between 57.5 and 60 kips per ram, and the test was then stopped.

2. Fatigue Test: The bridge was then subjected to fatigue loads which varied sinusoidally from 5 to 26 kips per ram. The intermediate diaphragm had been re-welded, but broke again very early in the fatigue loading. It was then left broken for the rest of the fatigue loading, simulating an unfavorable situation for the bridge with respect to the lack of lateral restraint at midspan. At approximately million-cycle intervals, the bridge was loaded statically to 30 kips per ram, to monitor possible deterioration due to fatigue loading.

3. Final Static Test: After the 5 million cycles of fatigue loading, the intermediate diaphragm of the bridge was rewelded. A static load test was then undertaken, up to a load of about 40 kips per ram.

In every static test, data were obtained to monitor load, deflections, strains, and cracking as listed in the previous chapter.

The strains at the concrete surface and on the reinforcement were used to calculate: stresses in concrete and reinforcement at various locations; the strain profile through the deck; the longitudinal and transverse moments in the deck; and the location of the neutral surface in the deck. The measured strains in the steel

girder were used to calculate the curvature and moment at various locations, and the distribution of load to the interior and exterior girder. These are discussed in Ref. 1.3. In this chapter, typical results are presented to illustrate the overall and local behavior of the specimen.

6.2 Load-Deflection Data

At each load stage, readings from 10 linear potentiometers and 4 dial gages were used to measure the vertical deflections of the deck and the steel girders. Typical load-deflection relationships at various locations are shown in Figs. 6.1 through 6.4.

Load-deflection data for the CIP deck at the first (precracked) static test is shown in Fig. 6.1. The load-deflection relationships for the exterior and interior girders across the loaded section are essentially linear up to about three times the design wheel load of 20.8 kips. Cracking of the deck, which occurred at a load of about 38 kips/ram, does not seem to have influenced this linear behavior. The change in slope (while loading to 60 kips) of the load-deflection curves for both girders is attributable to the weld failure of one of the center diaphragms. During the tests, the stand holding the linear potentiometer at the loaded point in the CIP deck was inadvertently moved; therefore, only partial results are shown for load-deflection at that point.

Load-deflection results before and after 5 million cycles of fatigue loading are compared in Fig. 6.2. The two load-deflection curves (before cracking and after fatigue) almost coincide. This implies that cracking of the deck did not significantly change the stiffness of the deck at the loaded point, even after fatigue loading. The load-deflection behavior of the bridge did not change significantly as a result of the fatigue loading.

At the precast panel end, similar linear load-deflection behavior was also observed, as can be seen in Figs. 6.3 and 6.4. As before, fatigue loading did not significantly change the stiffness of the deck at the loaded point.

As will be discussed in Section 6.6, the effectiveness of compressive membrane action can be limited by excessive vertical deflection of the deck with respect to the girders. In this test, the relative deflections between deck and exterior girder under a service-level load of 20.8 kips per ram were approximately 0.043 in. in the CIP deck, and 0.033 in. in the precast panel deck. These correspond to ratios of relative deflection to transverse span of 1/1810 and 1/2290 respectively.

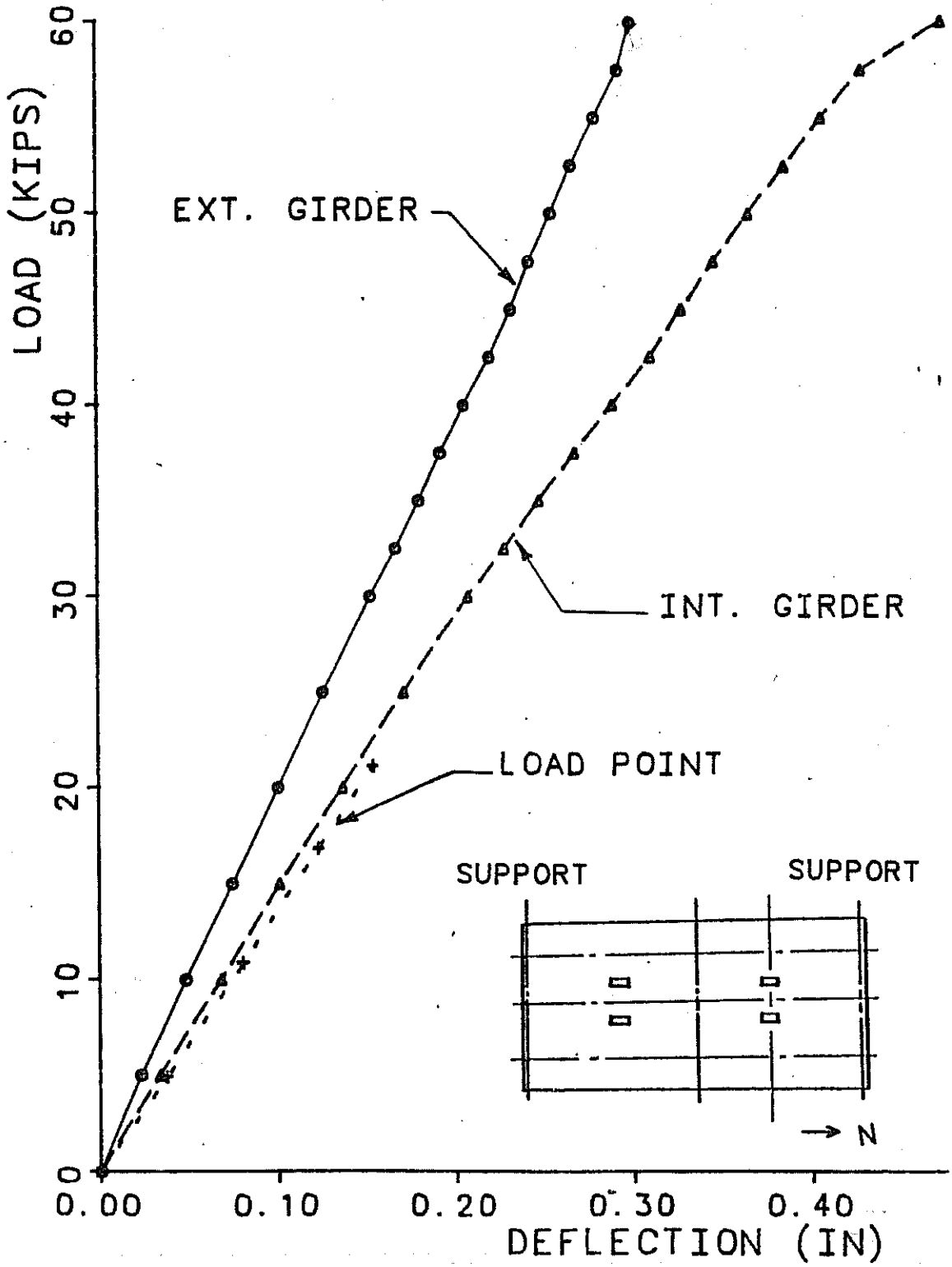

Fig. 6.1 Experimental load-deflection results, CIP end, transverse section through loaded points

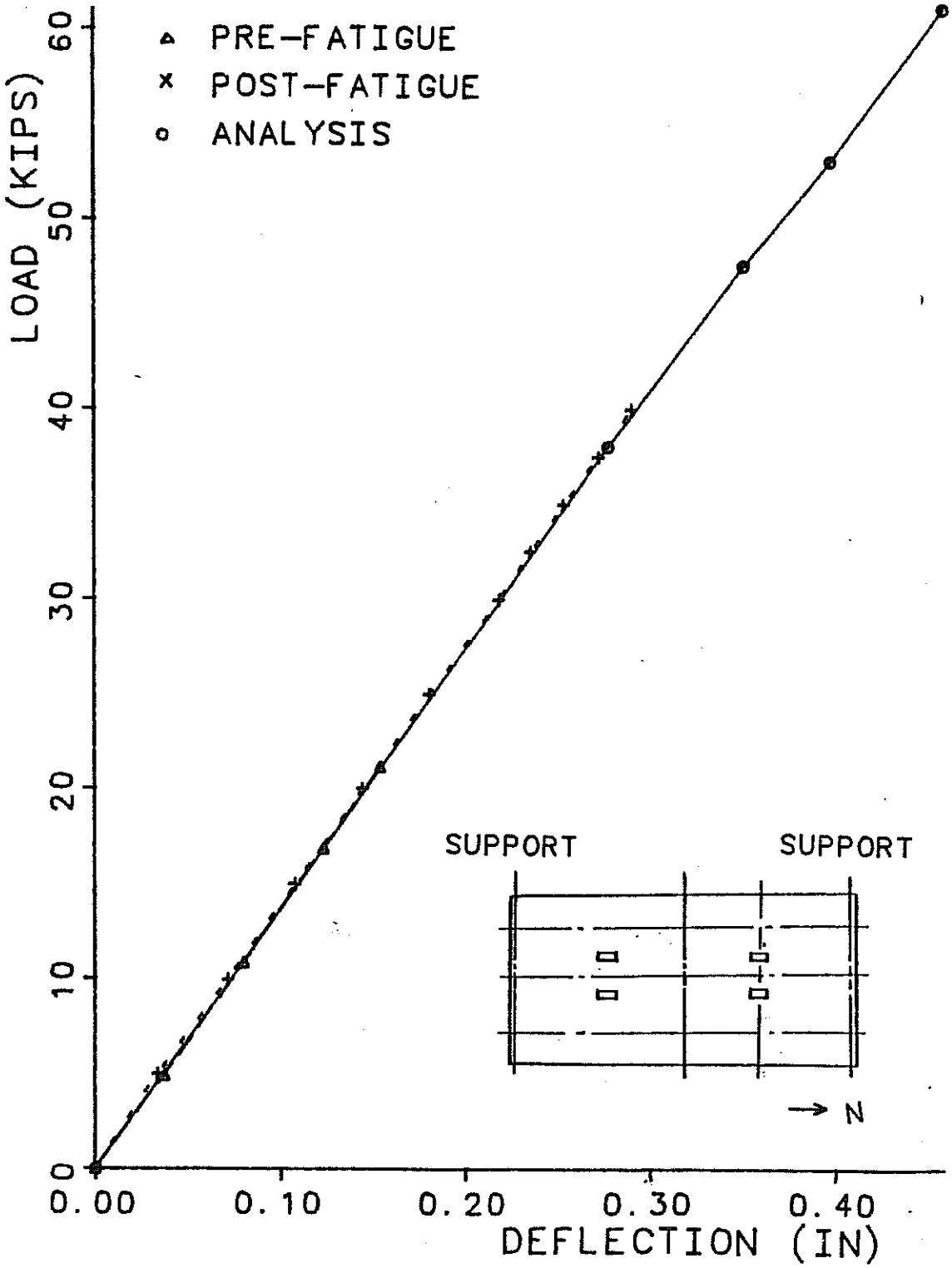

Fig. 6.2 Deflection at loaded point, CIP end

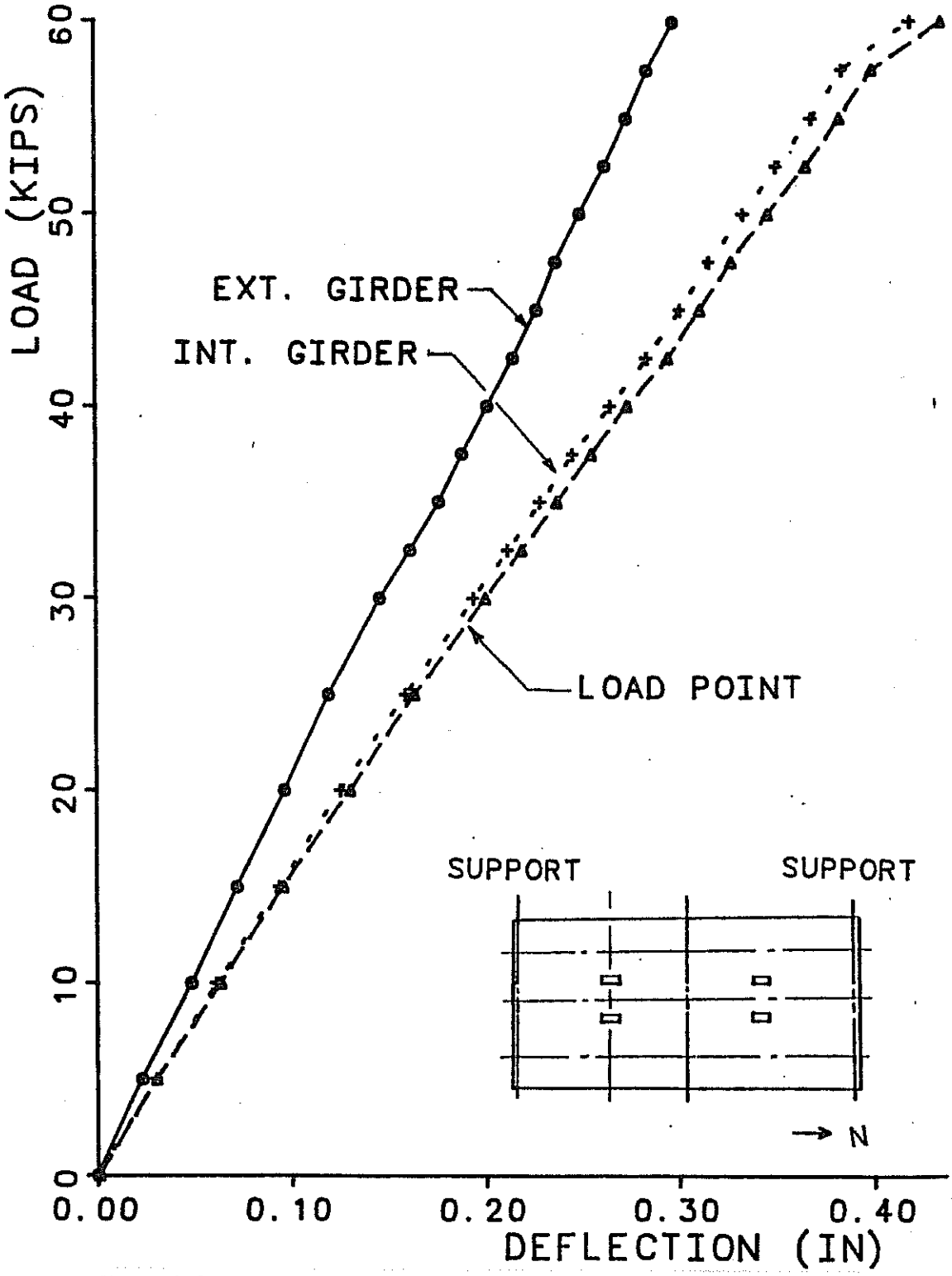

Fig. 6.3 Experimental load-deflection results, panel end, transverse section through loaded points

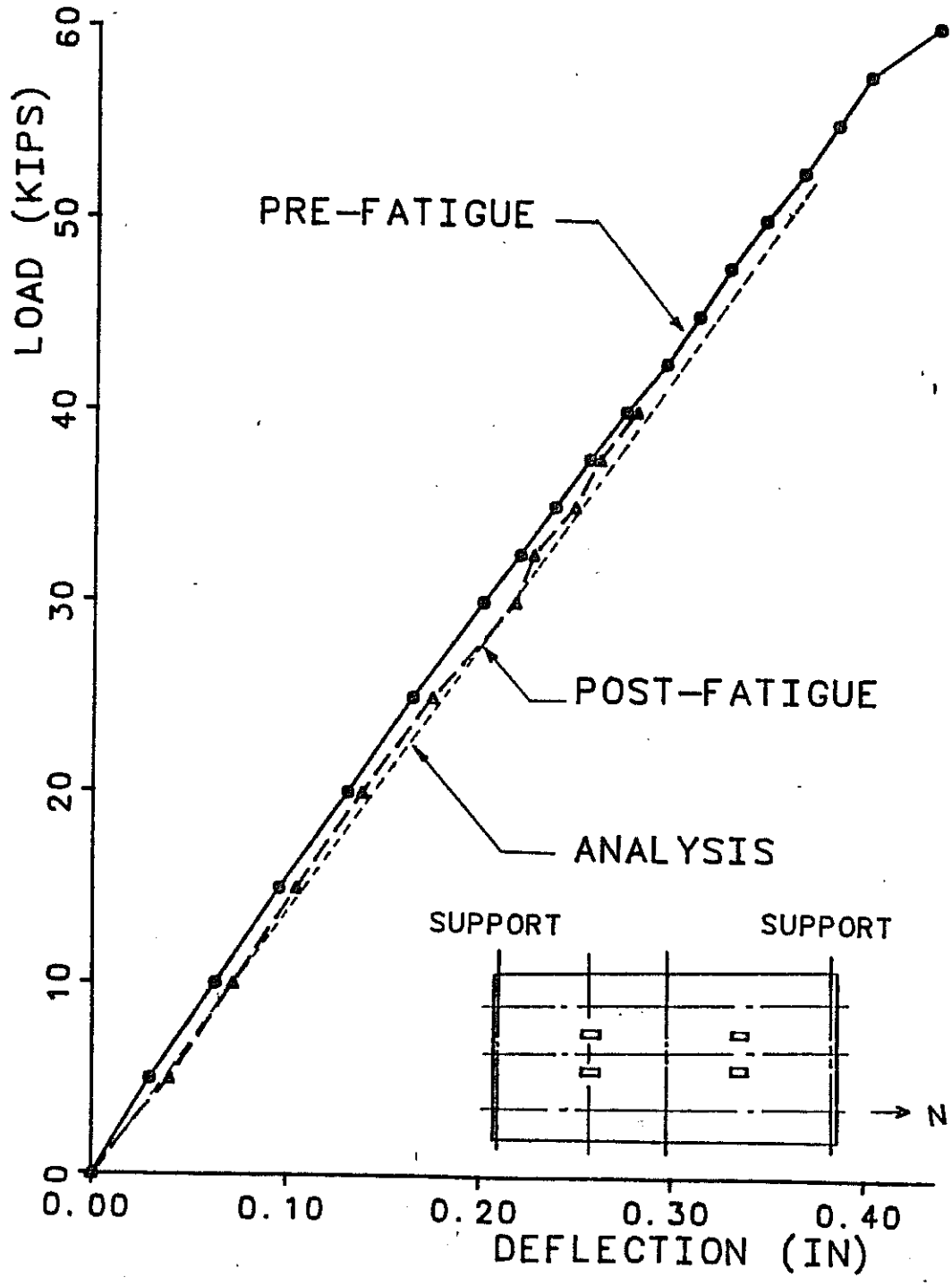

Fig. 6.4 Deflection at loaded point, panel end

As can be seen by comparing Figs. 6.2 and 6.4, the analytically predicted deflections agreed almost exactly with measured values. This was a first step in verifying the validity of the analytical model as applied to the entire bridge.

At the precast panel end, the center of the loading plate was located only two feet longitudinally from the nearest gap. Comparison of Figs. 6.2 and 6.4 shows that the closeness of this gap to the loaded point did not significantly increase the deflection of the loaded point.

6.3 Cracking of the Deck

According to the current Ontario Highway Bridge Design Code (OHBDC) (6.1), deck slabs should be designed for the ultimate limit state of strength, and also for the serviceability limit state of cracking. The requirement of the serviceability limit state of cracking need not be considered for slabs detailed in accordance with the empirical design.

However, cracking of the deck was important in this study for two reasons. First, the thickness of the deck proposed by the Texas SDHPT is less than the 9-in minimum required by the revised OHBDC. Second, it was important to determine the effects of compressive membrane action on crack widths.

Before loading the specimen, the top and bottom surfaces of the deck were carefully examined for shrinkage cracks. Only a few transverse hairline shrinkage cracks were found on the top surface of the CIP deck. The panel deck had shrinkage cracks less than 0.002 in. wide along the panel gaps.

Crack propagation was monitored carefully at each load stage during the tests. The first cracking in the CIP deck was observed at the bottom surface under the loaded point, as shown in Fig. 6.5. The cracking load, about 37.5 kips per ram, was very close to that predicted by the analyical model. As the load increased, these cracks divided into two cracks, each of which propagated longitudinally toward the midspan and end of the bridge. The first crack on the top of the deck occurred at a load of 55 kips per ram, and was oriented longitudinally. At almost the same load, some fine cracks formed at the top of precast panel deck, near the interior girder. When the load was increased to 60 kips per ram, very fine longitudinal cracks were observed at the bottom of the precast panel deck near the load.

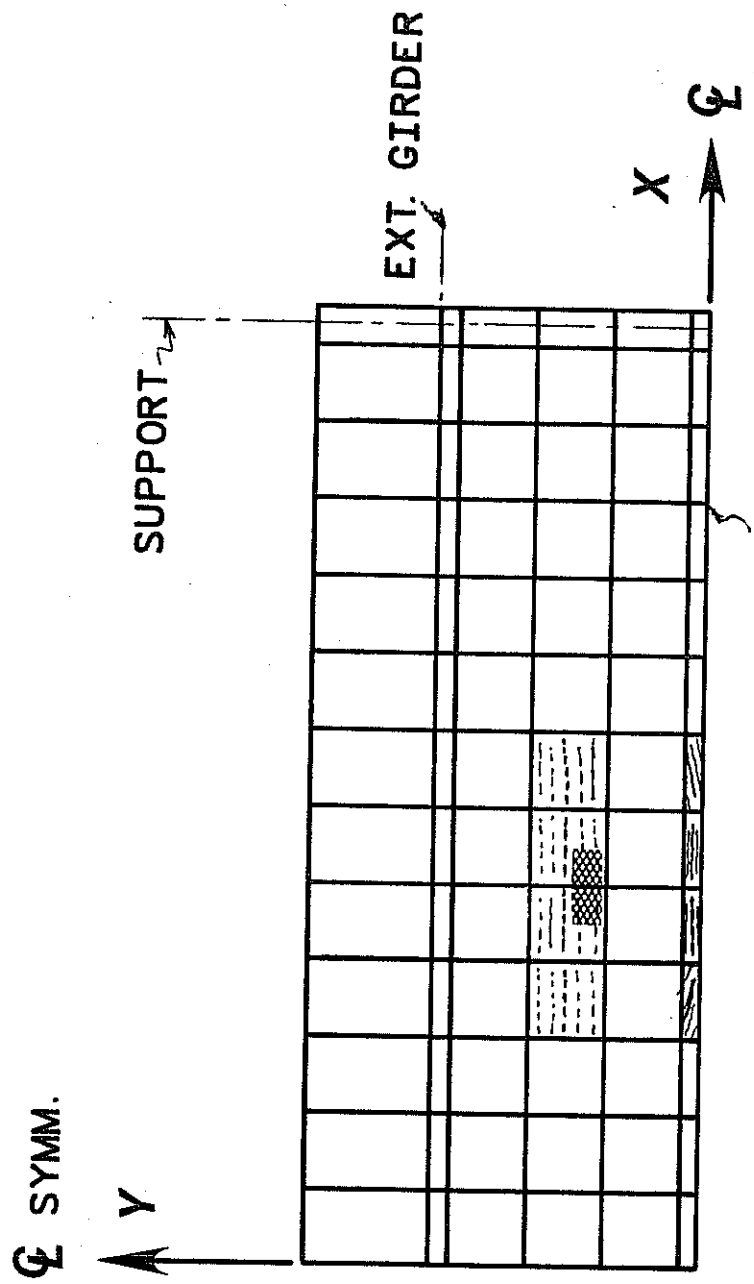

Fig. 6.5 Analytically predicted cracking pattern

Crack propagation was monitored periodically during the 5 million cycles of fatigue loading. No crack propogation was found at the top of the CIP deck. However, many crack extensions were found at the bottom of the deck. On the precast panel end, no clear extension of the cracks was found (either at the top or the bottom), but the cracks at the panel gaps widened slightly.

After the 5 million cycles of fatigue loading, crack widths were measured during a 40 kip per ram static test. Crack widths are shown in Table 6.1 corresponding to the service load (including impact factors) of about 20 kips. Crack widths in the deck were clearly well below the maximum allowable crack widths of Ref. 6.1 (0.014 in. for interior exposure and 0.010 in. for severe exposure). Approximate crack locations and orientations at the 60-kip load were also computed analytically, and are shown in Fig. 6.6.

6.4 Local Stresses in the Deck

6.4.1 General. Strain readings from the concrete and reinforcing steel were used to study the typical load stresses in the deck slab near the loaded point, interior girder and exterior girder. The maximum concrete stress near the loaded point in both the CIP and panel decks was about 0.4 ksi under the design wheel load of 20.8 kips per ram. The maximum stress in reinforcement near the load was only about 1.8 ksi at that load level. At the panel end, deck cracking did not cause any significant change in concrete.

TABLE 6.1 Crack Widths at 20 kip/ram Load Stage

	CIP Deck		Precast Panel Deck		
	Top	Bottom	Top	Bottom	Panel Gaps
Crack Width (in.)	0.003	0.008	0.003	0.003	0.004

and steel stresses near the loaded points. However, deck cracking did cause some nonlinear variation of the corresponding stresses at the CIP end.

The 5 million cycles of fatigue load did not cause significant change in the concrete and steel stresses in the deck or girders, even at twice the design load level.

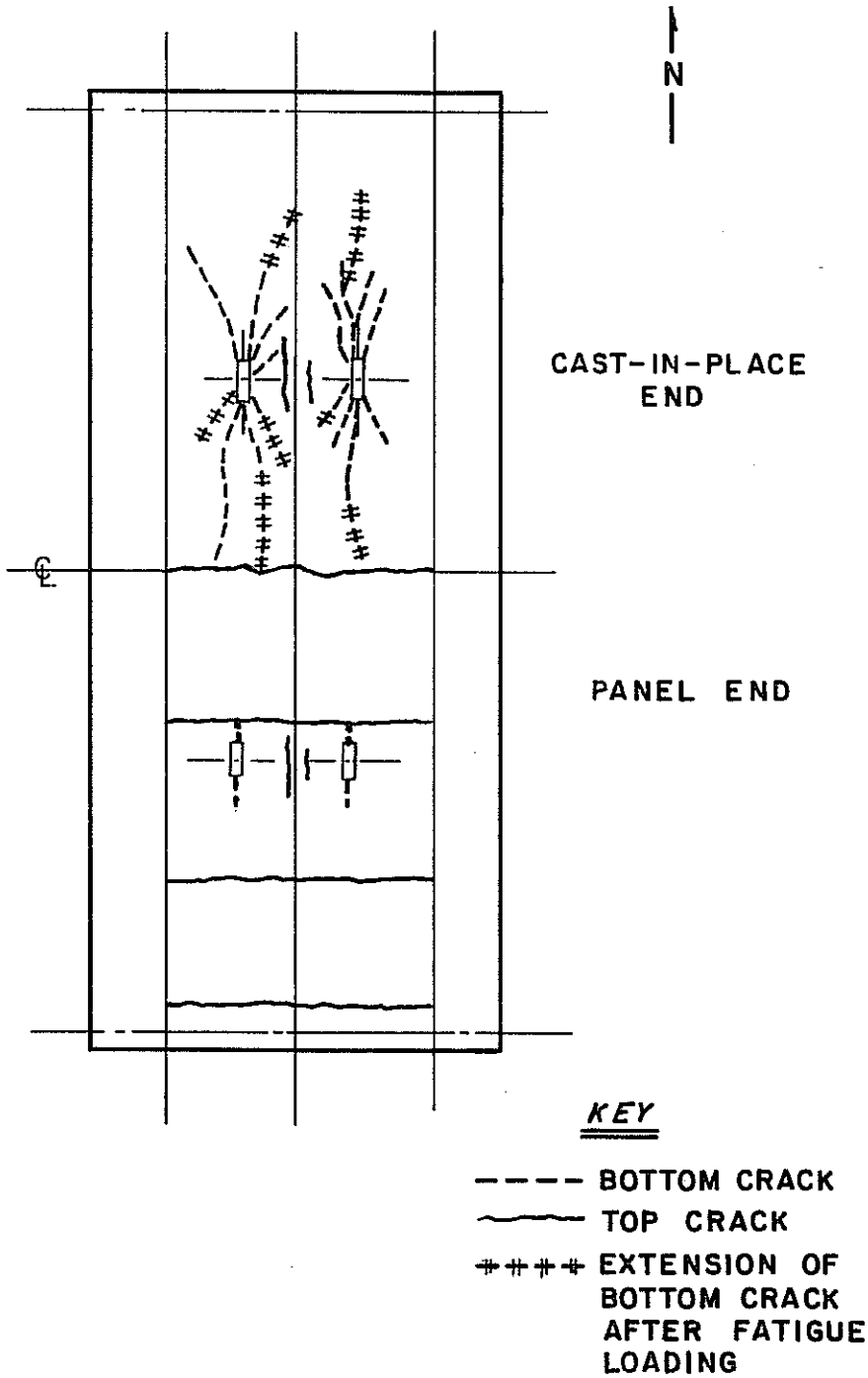

Fig. 6.6 Deck cracking before and after fatigue loading

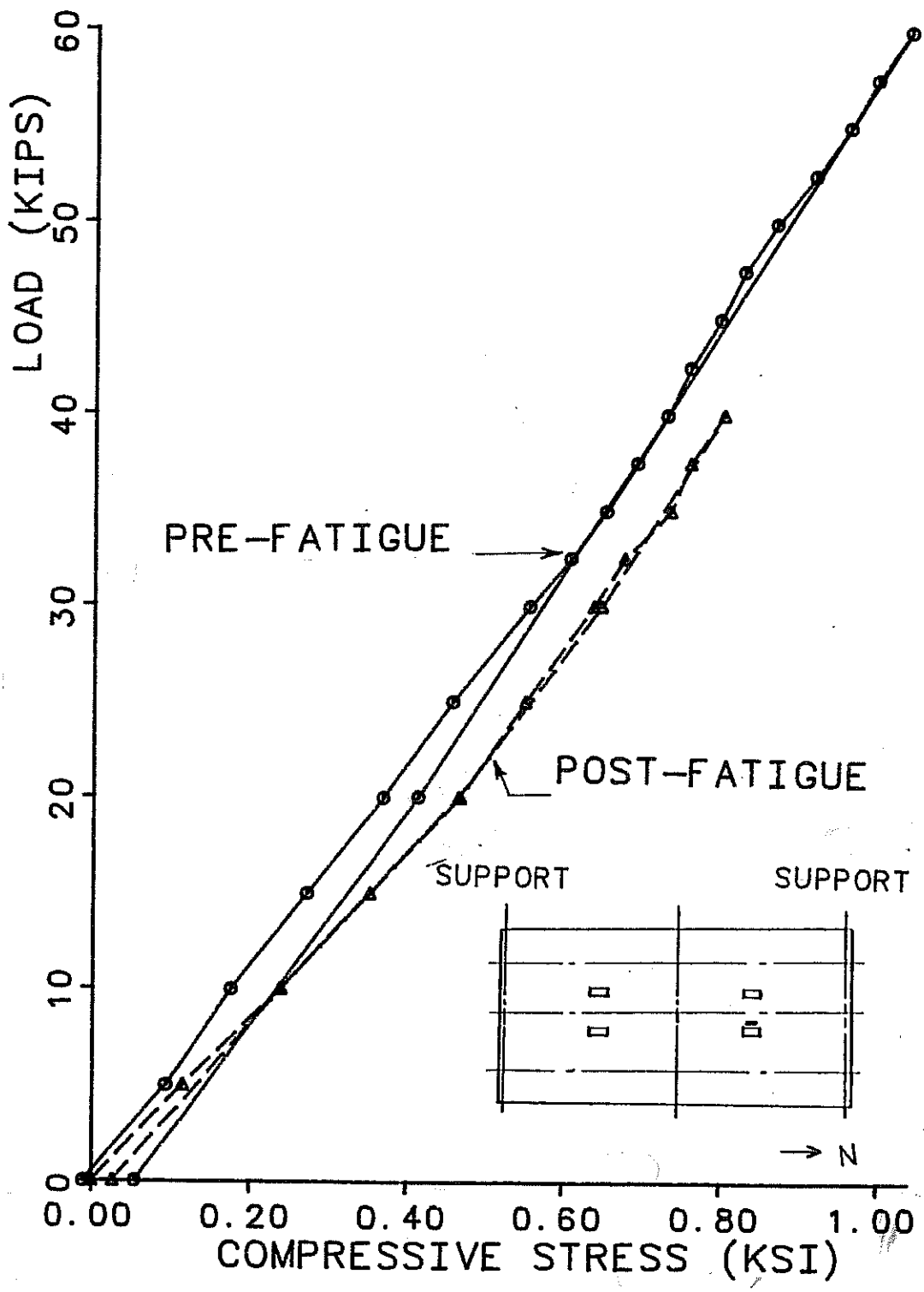

Fig. 6.7 Concrete stress in longitudinal direction, CIP end, near loaded point (top surface)

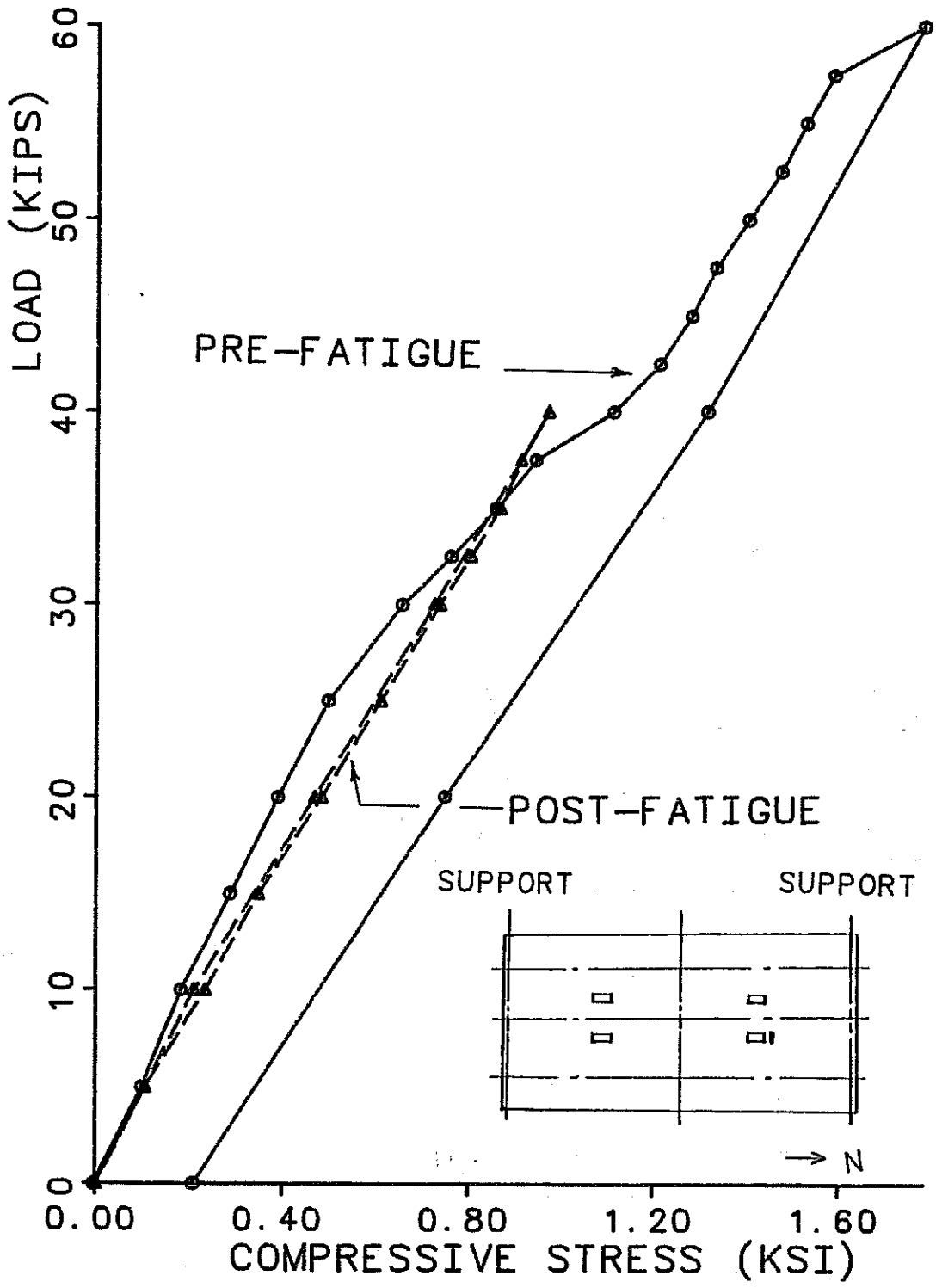

Fig. 6.8 Concrete stress in transverse direction, CIP end, near loaded point (top surface)

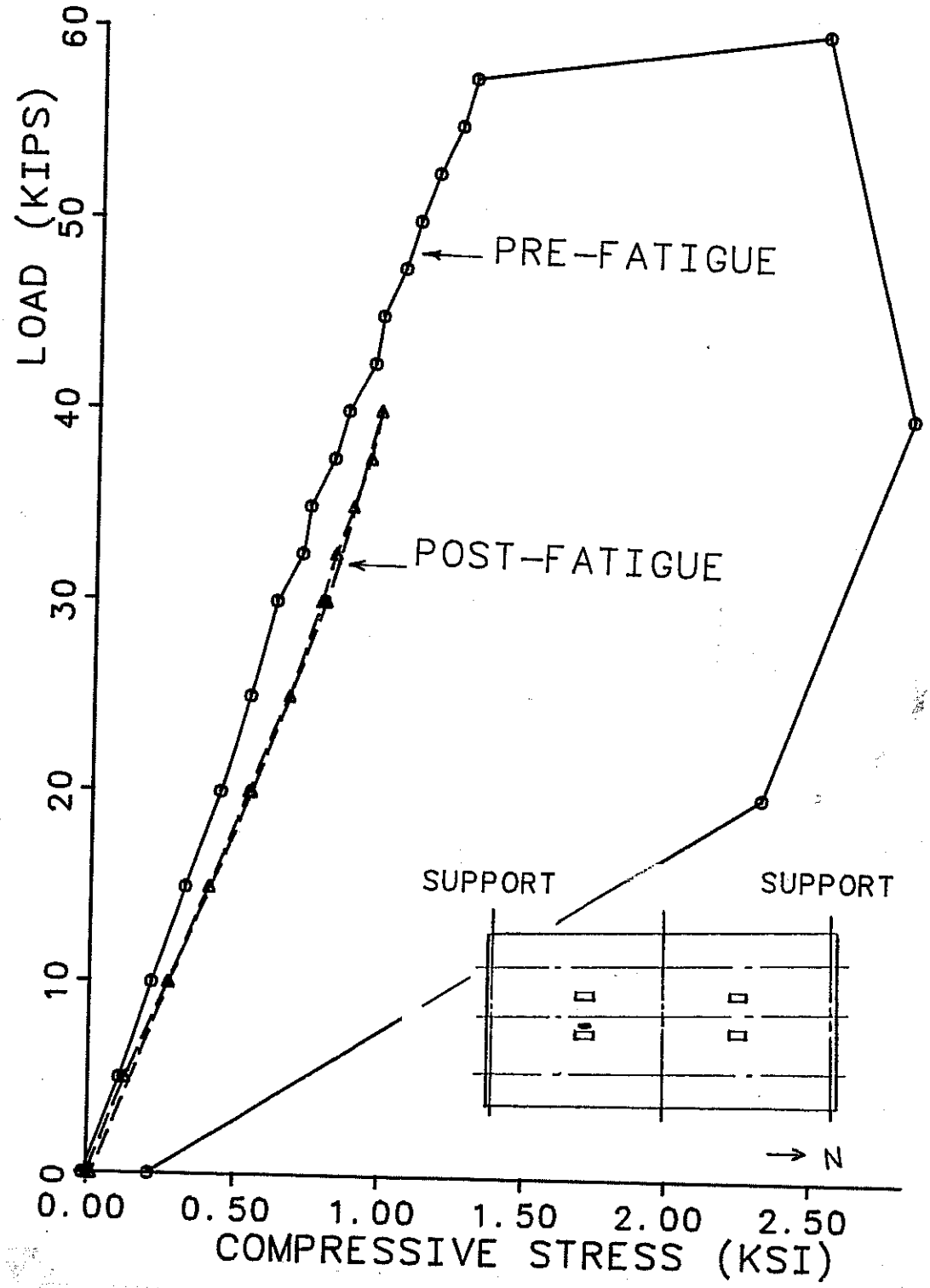

Fig. 6.9 Concrete stress in longitudinal direction, panel end, near loaded point (top surface)

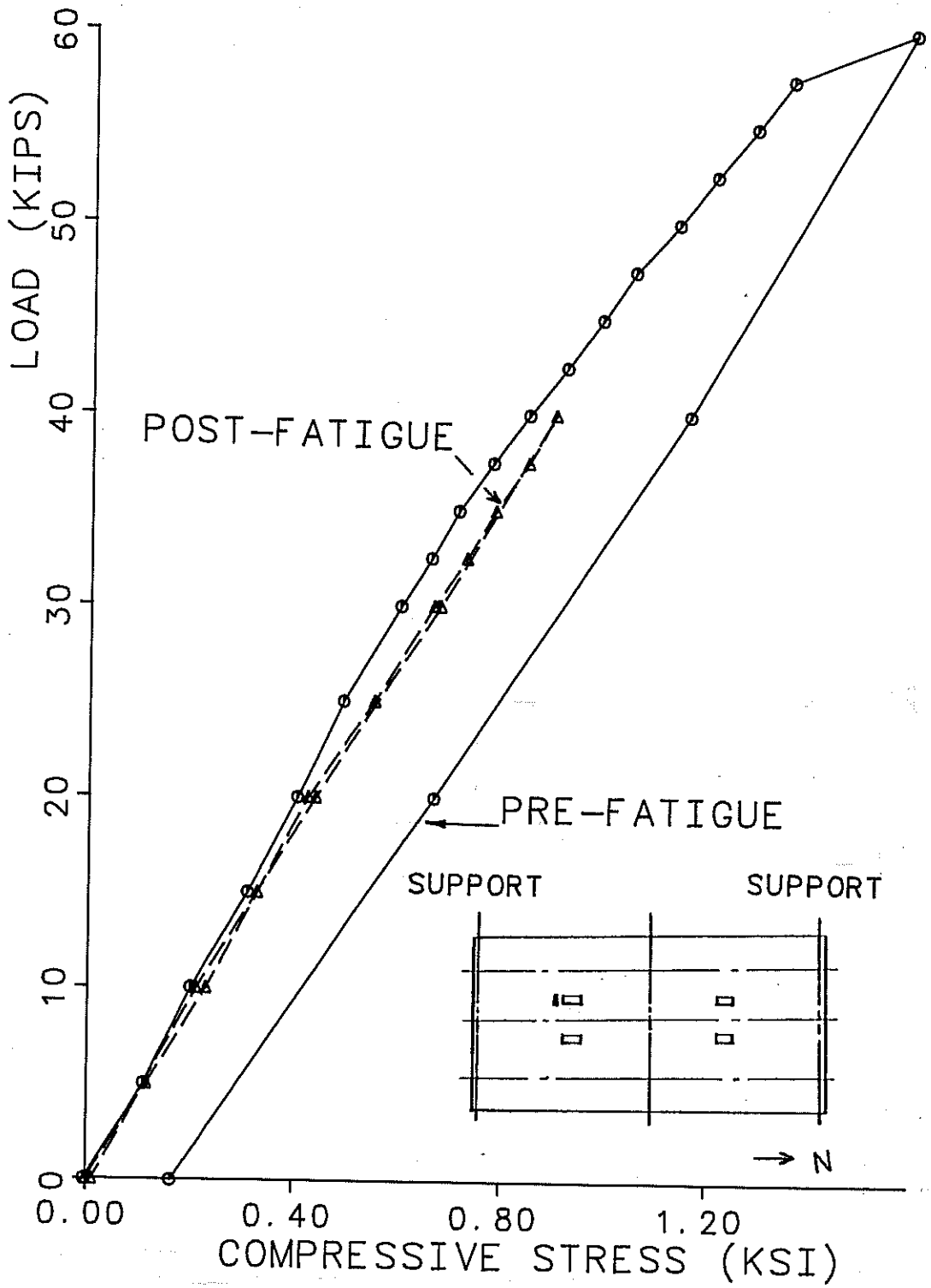

Fig. 6.10 Concrete stress in transverse direction; panel end, near loaded point (top surface)

6.4.2 Local Stresses Near Loaded Points. The compressive stress of concrete in the transverse and longitudinal direction near the loaded point at both ends of the bridge are shown in Figs. 6.7 through 6.10. Under the design load of 20.8 kips per ram, the concrete stress under the load is only about 0.4 ksi in both the longitudinal and transverse directions. As mentioned previously, the cracking loads (around 38 kips per ram in the CIP deck and 60 kips per ram in the panel deck), are much higher than the design load. The maximum compressive stresses in concrete near the loaded point are very similar for both types of deck. Comparisons of Figs. 6.8 and 6.10 show that the effects of cracking on the transverse stress in concrete are more pronounced in the CIP deck than in the precast panel deck. Examination of Fig. 6.7 through 6.10 shows that service load-level concrete stresses near the loaded point did not change significantly as a result of fatigue loading, either for the CIP or for the panel deck.

Figure 6.10, and other similar figures in this Chapter, show a non-zero residual stress after the first static load. This is due to internal stress redistribution following cracking of the deck and failure of the diaphragms. Post-fatigue tests were conducted several months after the prefatigue test. To monitor sress changes over such a long period of time would have been impractical and also unnecessary, since stresses were so low. All strain gage readings were therefore re-zeroed before the post-fatigue test. For this reason, all post-fatigue curves begin at the origin.

Stresses in transverse reinforcement near the loaded point in the CIP and panel decks are shown in Figs. 6.11 and 6.12 respectively. As shown in Fig. 6.11, the stress in the transverse reinforcement near the load in the CIP deck in the pre-fatigue test is only about 1.8 ksi at the service load of 20.8 kips. The curve of that figure is linear up to a load of about 45 kips per ram, after which a very pronounced change in slope occurs, due to cracking near the loading point. Examination of Fig. 6.11 shows significant differences between the initial slopes of the pre- and post-fatigue curves. However, the difference is due to cracking under overload, rather than fatigue. The unloading portion of the prefatigue curve reflects the decreased difference due to cracking. The post-fatigue curve has almost the same slope as the unloading portion of the prefatigue curve, implying little change in behavior due to fatigue. Stresses in reinforcement were very low before and after fatigue with a maximum tensile stress in the reinforcement of only 3.3 ksi at service loads (20.8 kips). The variation of stress in reinforement in the panel deck near the loaded point, shown in Fig. 6.12, is similar to that observed at the CIP end, except that the effects of cracking are reduced due to the transverse prestress of the panels. Since the panel end had only one layer of reinforcing bars placed above the

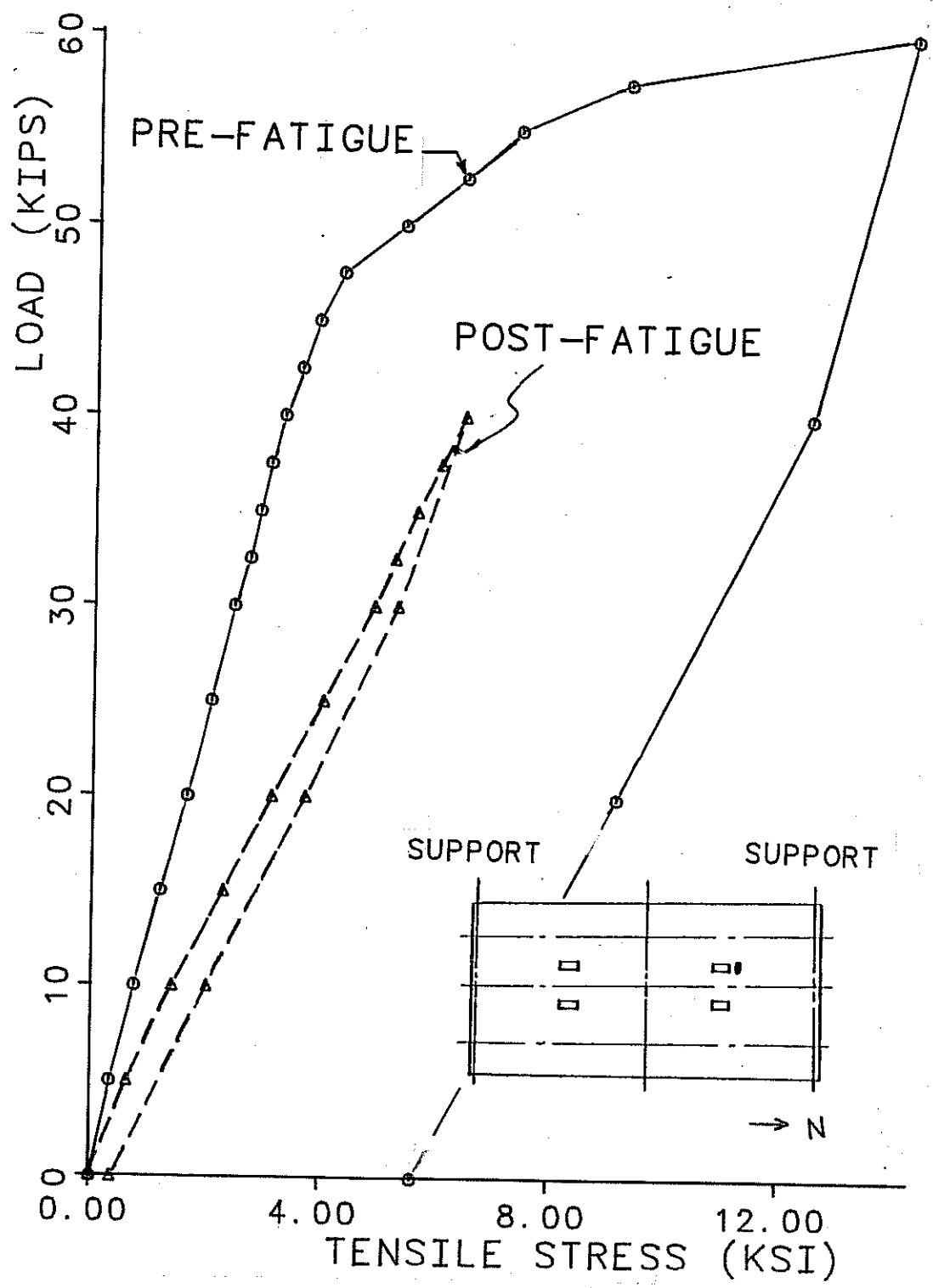

Fig. 6.11 Reinforcement stress in transverse direction, CIP end, near loaded point (bottom layer)

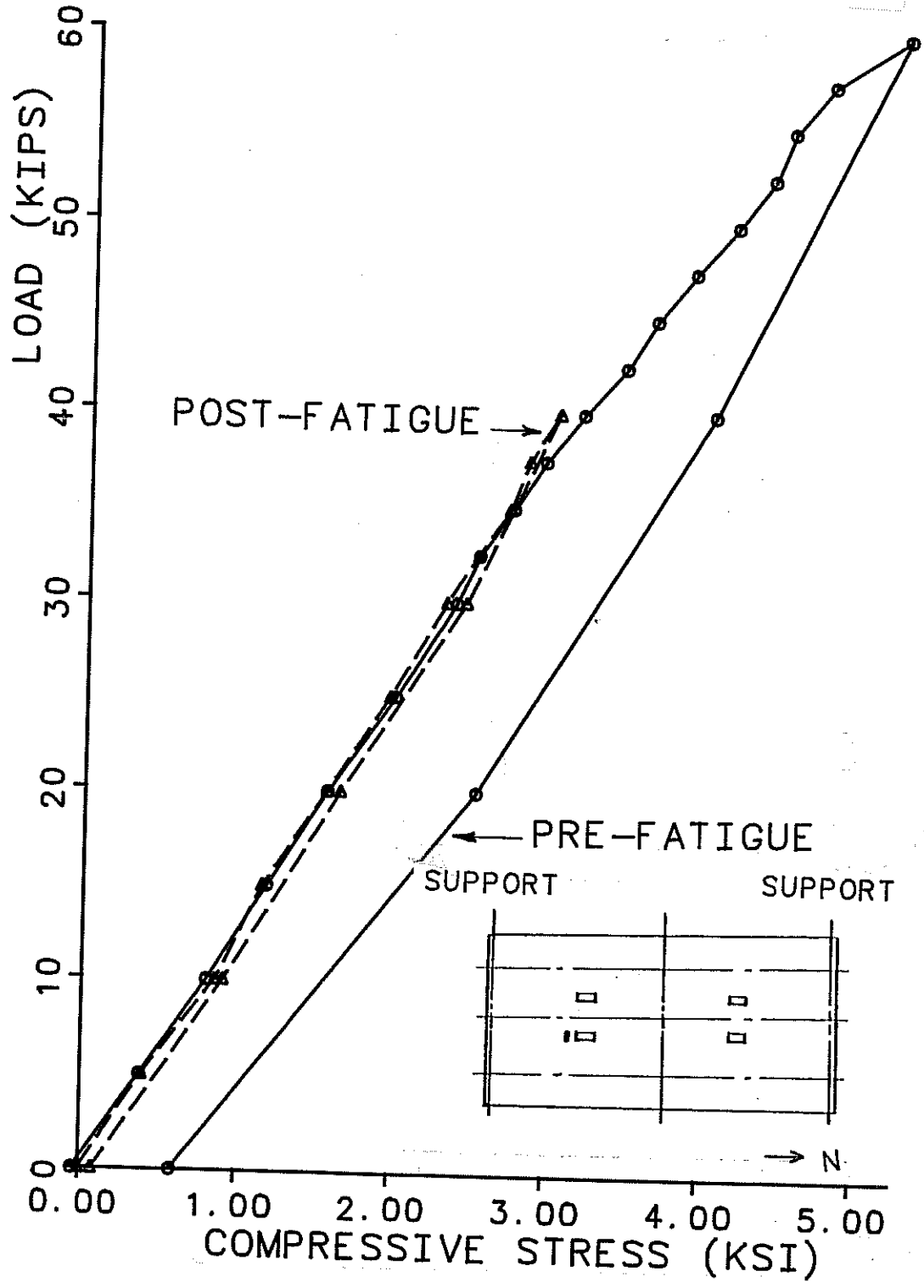

Fig. 6.12 Reinforcement stress in transverse direction, panel end, near loaded point (top layer)

precast panels, that reinforcement acts in compression. The stress varied linearly up to a load of about 57.5 kips/ram (higher than that corresponding to the CIP deck) because of the prestress. For the panel end, fatigue loading did not significantly influence the stress in deck reinforcement near the load as shown in Fig. 6.12.

6.4.3 Local Stresses Near Interior Girder. Transverse stresses in concrete at a section across the load near the interior girder in the CIP and panel decks are shown in Figs. 6.13 and 6.14 respectively. As shown in both figures, the stresses are much lower than those near the loaded point. By comparing the load-stress results of both figures, it was found that the stresses in the CIP end are higher than at the panel end. This is due to the lower cracking load in the CIP deck, which could have reduced the overall bending of the deck in the transverse direction over this region. Fatigue loading did not significantly change the concrete stresses near the interior girder.

Stresses in transverse reinforcement near the interior girder in both types of deck are shown in Figs. 6.15 and 6.16 respectively. In the CIP end (Fig. 6.15), the stresses varied very linearly up to a load of about 50 kips per ram, after which the slope of the curve changed abruptly. This is primarily due to the cracking of the deck at the top surface over the interior girder. Since only very fine cracks had formed at the loaded point and over the interior girder in the panel end, load-stress data varied linearly up to a load of about 60 kips per ram. Fatigue loading did not cause significant change in stresses in the reinforcement near the interior girder. At service load of 20.8 kips maximum reinforcement stress was less than 3 ksi at the CIP end (Fig. 6.15), and less than 1.5 ksi at the panel end (Fig. 6.16).

6.4.4 Local Stresses Near Exterior Girder. As shown in Fig. 6.17, the transverse stress in the deck concrete above the exterior girder increases linearly with load up to a load of about 35 kips per ram, after which the slope of the curve decreases due to cracking near the loaded point. At the current design load level of 20.8 kips per ram, the stress is only about 0.05 ksi. The post-fatigue loading did not cause significant transverse compressive stress in bottom fiber of concrete above the exterior girder in the CIP deck (Fig. 6.17), with only 0.12 ksi compression at 20.8 kips per ram. In Fig. 6.18, the transverse concrete stress near the exterior girder is seen to vary linearly up to a load of 57.5 kips per ram, after which the slope of the curve decreases abruptly due to the failure of the intermediate diaphragm. That diaphragm was repaired before the post-fatigue curve of Fig. 6.18 was obtained. Comparison of the pre- and post-fatigue results show that fatigue loading did not significantly affect transverse stresses in the deck near the exterior girders.

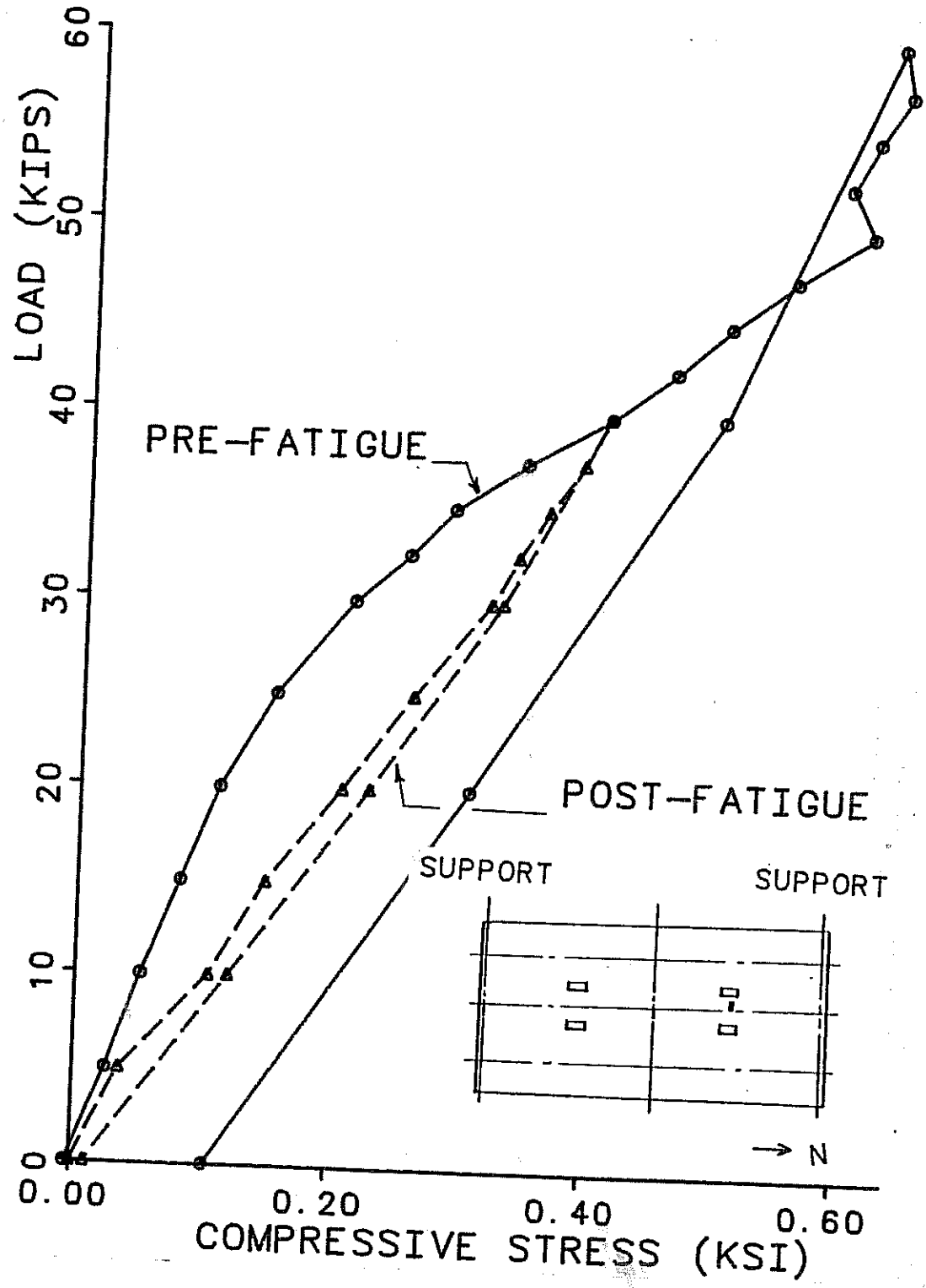

Fig. 6.13 Concrete stress in transverse direction, CIP end, near loaded point (bottom surface)

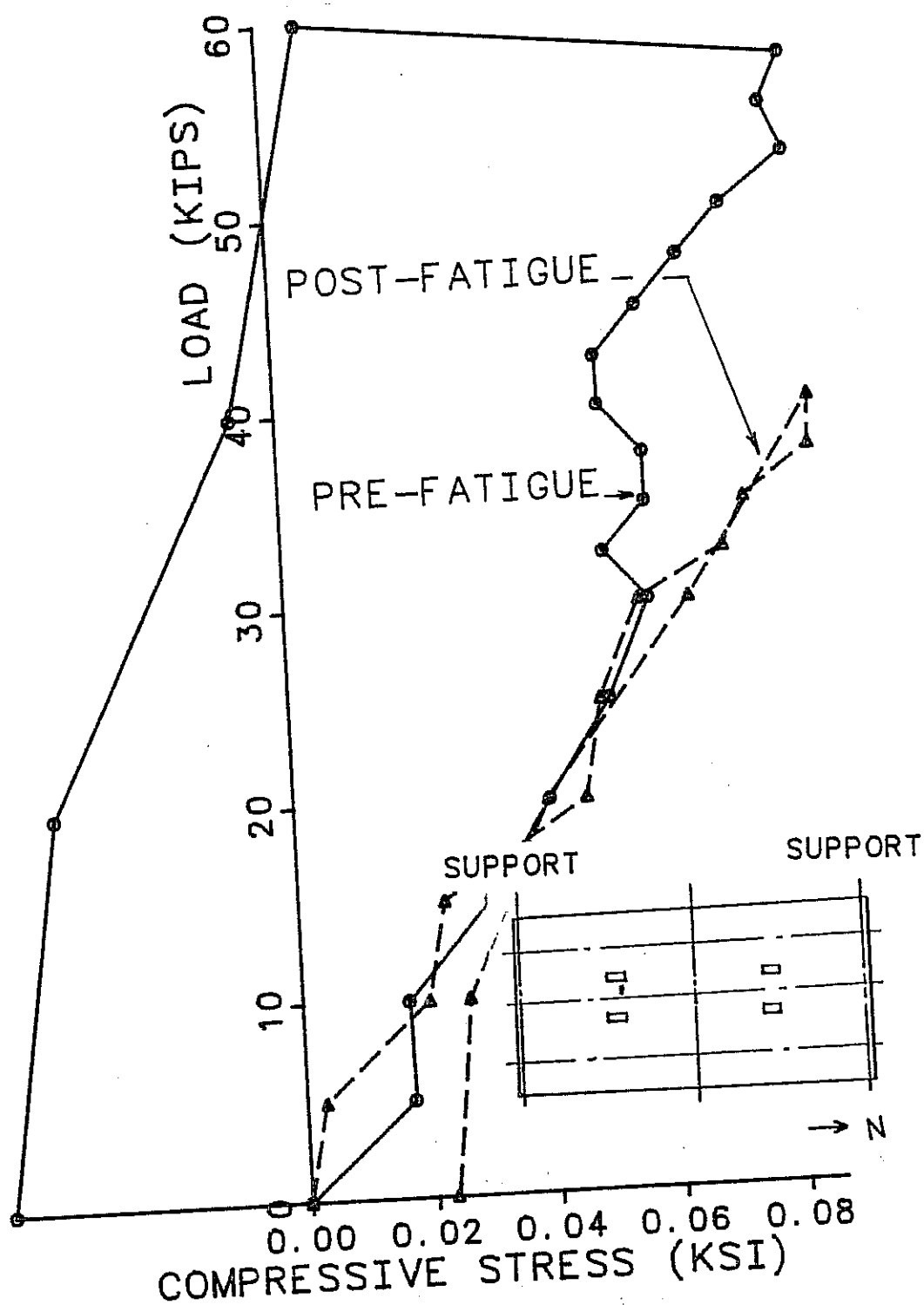

Fig. 6.14 Concrete stress in transverse direction, panel end, near loaded point (bottom surface)

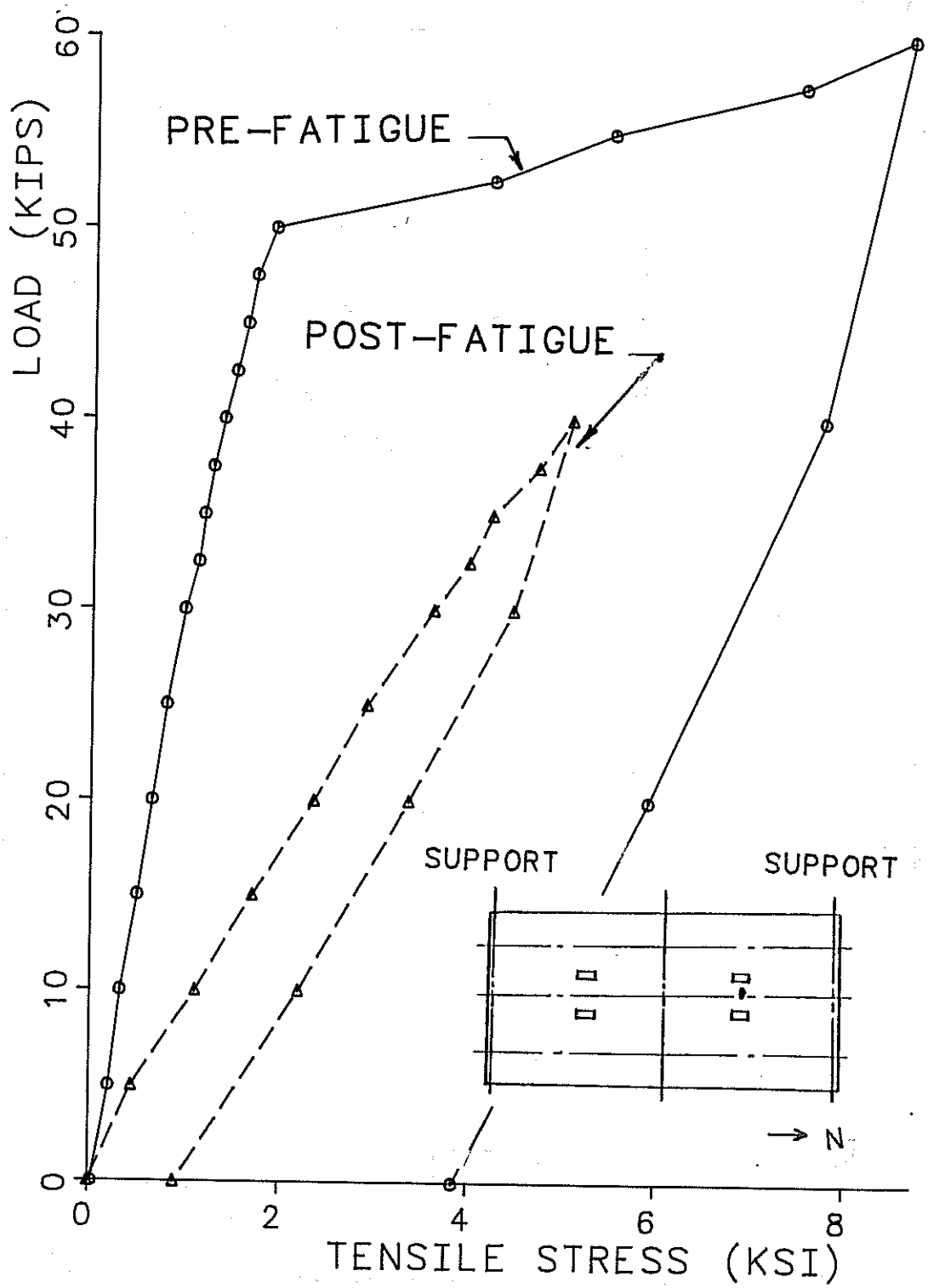

Fig. 6.15 Reinforcement stress in transverse direction, CIP end, above interior girder (top layer)

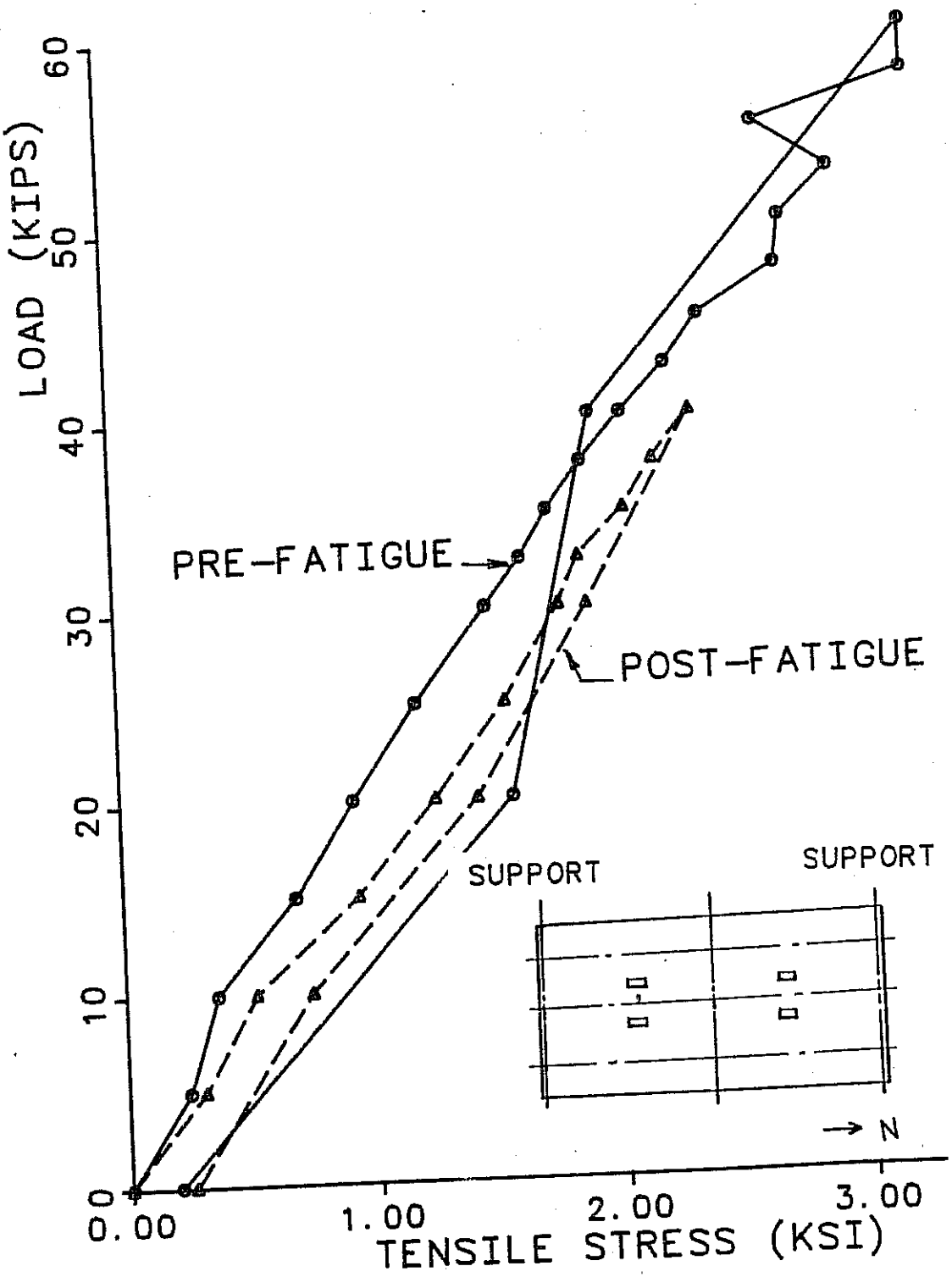

Fig. 6.16 Reinforcement stress in transverse direction, panel end, above interior girder (top layer)

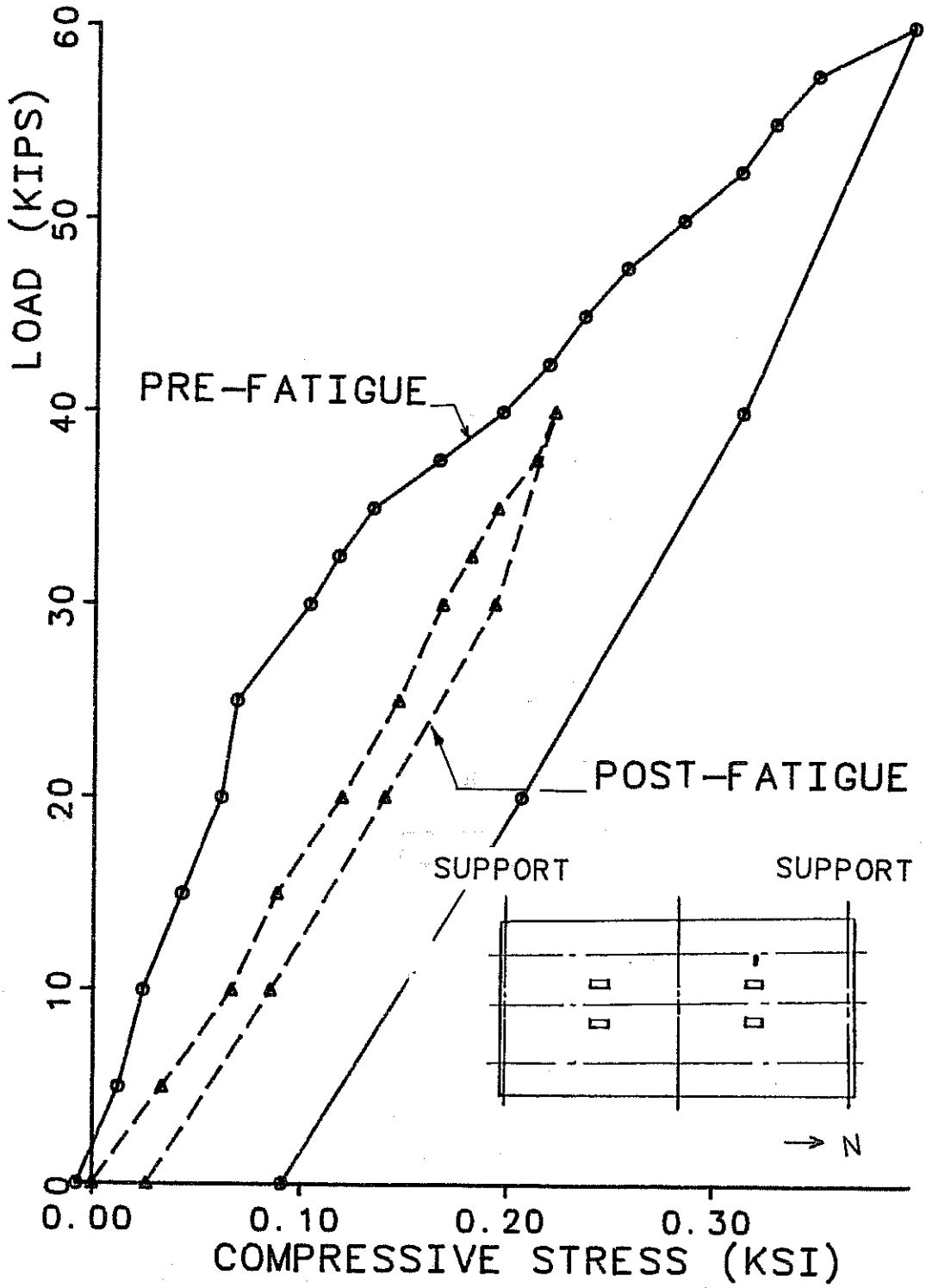

Fig. 6.17 Concrete stress in transverse direction, CIP end, near exterior girder (bottom surface)

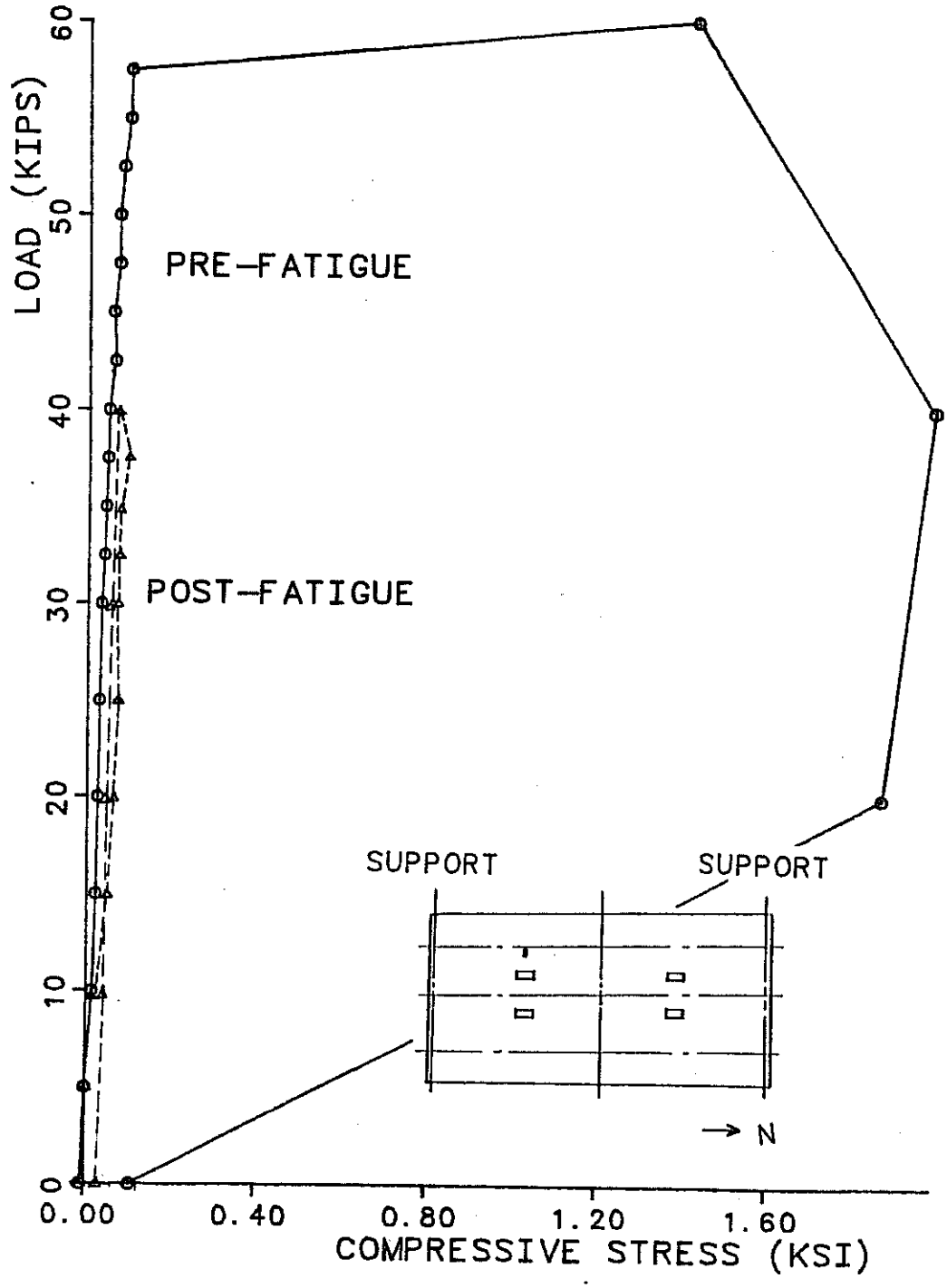

Fig. 6.18 Concrete stress in transverse direction, panel end, near exterior girder (bottom surface)

6.5 Distribution of Moment in the Deck

6.5.1 Computation of Moments from Experimental Data. At all gage locations on the CIP end of the bridge (Fig. 5.8), three types of strain gages were installed to measure strains in concrete and reinforcement. A typical strain gage layout is shown schematically in Figs. 6.19 and 6.20. Strain gages were placed on the longitudinal and transverse reinforcement. The strain gradient was constructed by assuming a linear variation between the strain at the concrete surface and on the reinforcement. As is discussed later, some of the clip gage readings were found to be erratic, and information from this type of gage was used for reference only. On the panel end of the bridge, it was not possible to install strain gages on the panel reinforcement. Because of this, strain gradient readings were less reliable at that end, and fewer graphs are presented. However, very little stress was observed at the panel end, indicating low stress levels in steel and concete. This was also corroborated by analytical results.

As shown in Fig. 6.20, the assumed linear strain gradient defines the location of the neutral axis, and can also be used to predict the maximum tensile strain of the concrete, and the strain in the other layer of reinforcement. Given the experimentally determined strain gradients, the corresponding stresses were then calculated. Concrete was assumed to be cracked, and to carry zero stress, if its tensile strain exceeded the cracking strain of $7.5\ f_c/E_c$. The modulus of concrete, E_c, was calculated using the formula of the ACI Code (6.2). Once the stresses in concrete and reinforcement had been calculated, the axial force and bending moment were obtained by equilibrium of the cross-section. The middle surface of the deck was used as a reference. An example of this calculation is shown in Appendix D.

6.5.2 Computation of Moments from Analytical Results. As discussed in Chapter 4, the bridge deck was modeled using two layers of thick shell elements. For this part of the study, stresses were requested at the middle of the top and bottom faces of each element. Because the stress output for such points is obtained by extrapolating from stresses inside the element, it is possible to get slightly different calculated stresses at the same point on the interface between the two layers. As shown in Fig. 6.21, in this situation the strain gradient was computed assuming a linear variation between the values on the top and bottom surfaces of the deck. The interface strains computed using this procedure were always very close to the average of the two strain values at the interface. Once the strain values had been computed, axial forces and moments were computed by equilibrium, again using the middle surface of the deck as a reference.

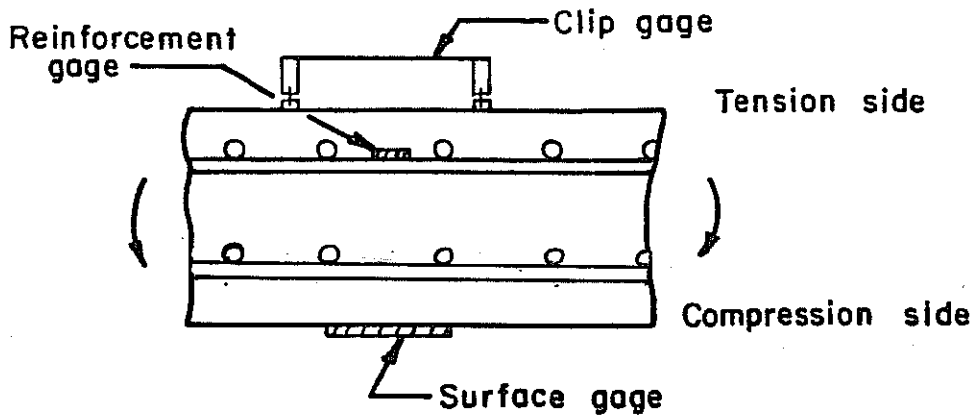

Fig. 6.19 Schematic illustration of strain gage layout

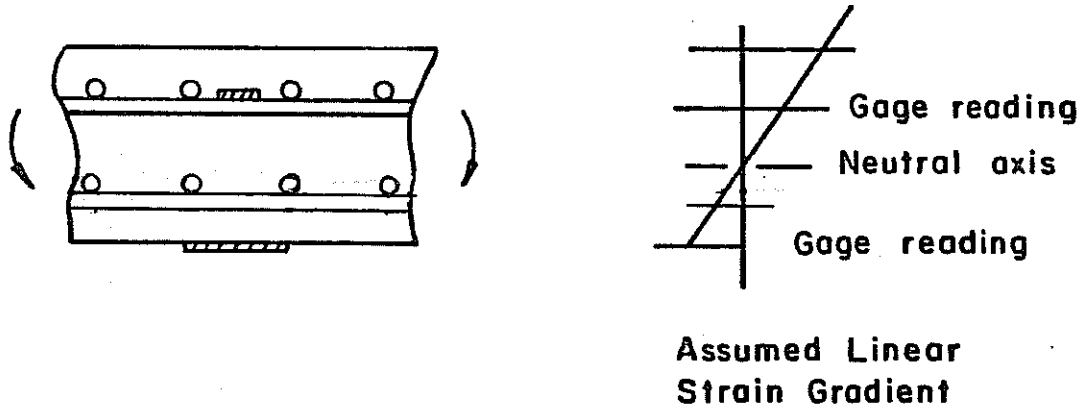

Fig. 6.20 Strain gradient from gage readings

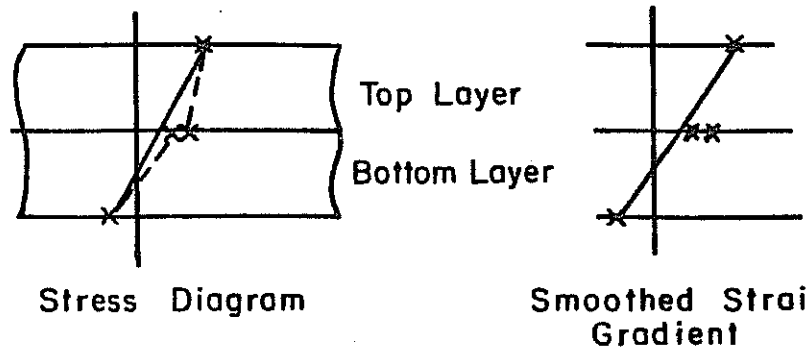

Fig. 6.21 Procedure used to obtain strain gradient from analytical model

6.5.3 Load-Moment Relationship. Typical relationships between the applied load and transverse moment in the CIP deck at the loaded point are shown by the solid line in Fig. 6.22. The slope of the load-moment relationship changes slightly at loads above about 30 kips per ram, due to the effects of initial cracking of the deck. After that point, the slope of the curve returned to its original value, even though cracks continue to form at the bottom of the deck. The abrupt change in slope of the curve just before the last load stage was primarily due to failure of the intermediate diaphragm at that load level. As shown by the dashed line in Fig. 6.22, after the 5 million cycles of fatigue test, the load-moment relationship is similar to that observed after cracking in the first static test to a load of 60 kips per ram.

As typified by Fig. 6.23, similar load-moment relationships were observed for the precast panel deck in pre-fatigue and post-fatigue tests.

6.5.4 Distribution of Transverse and Longitudinal Moment. After load-moment relationships such as those shown above were obtained at every gage location, figures were constructed showing the distribution of longitudinal and transverse moment in the deck at each load stage.

In Figs. 6.24 and 6.25, the experimentally determined distribution of transverse moments in the CIP deck are compared with the analytical predictions. The experimental and calculated values agree closely. As shown by the negative transverse moments over the interior and exterior girders near the loaded points, the diaphragms and cantilever overhangs provided some rotational restraint to the slabs in the transverse direction, even after cracking of the deck. Under the service-level load of 20.8 kips per ram, the peak value of transverse moment is about 2 kip-ft/ft, much less than the current AASHTO design value of 5.85 kip-ft/ft. Peak moments increase slightly after the 5 million cycles of fatigue load. As shown by Fig. 6.26, the transverse moment variation is similar at the panel end.

The distribution of longitudinal moment in the CIP deck before cracking and after fatigue is shown in Figs. 6.27 and 6.28. As before, experimental and analytical values agree well. Maximum moments occurred in a very small region near the load, and decreased very quickly away from the load.

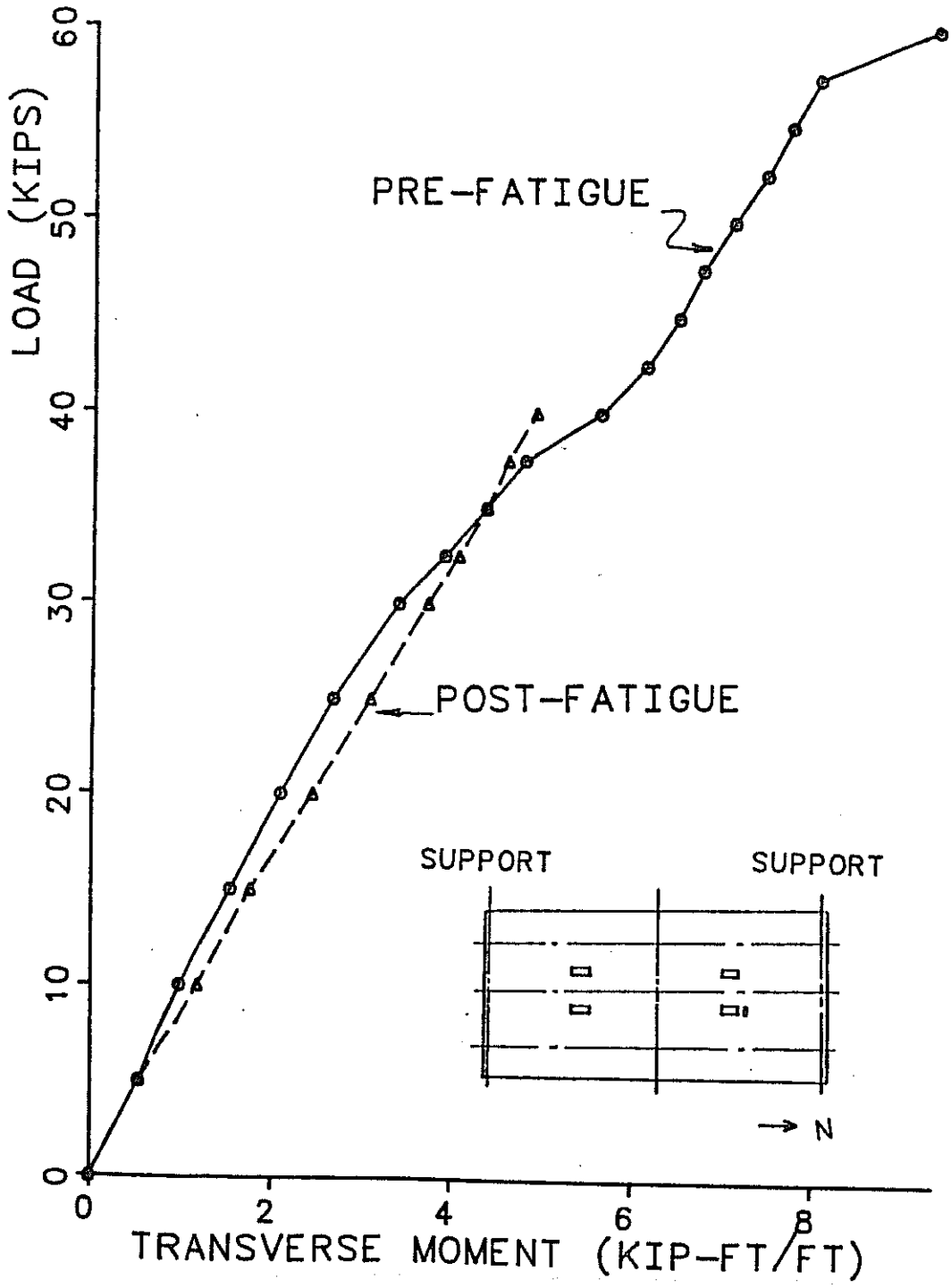

Fig. 6.22 Transverse moment in CIP deck at loaded point

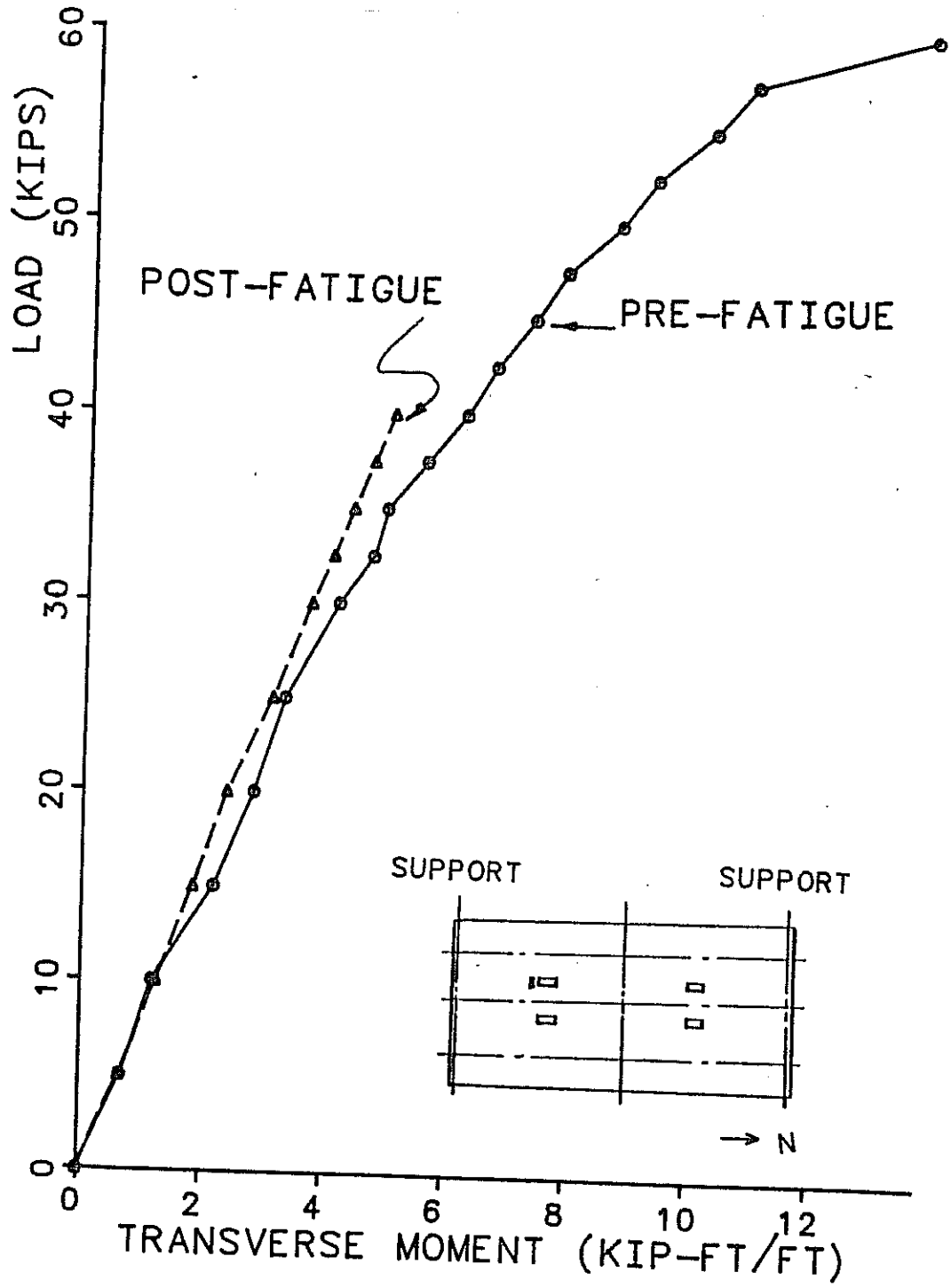

Fig. 6.23 Transverse moment in precast panel deck at loaded point

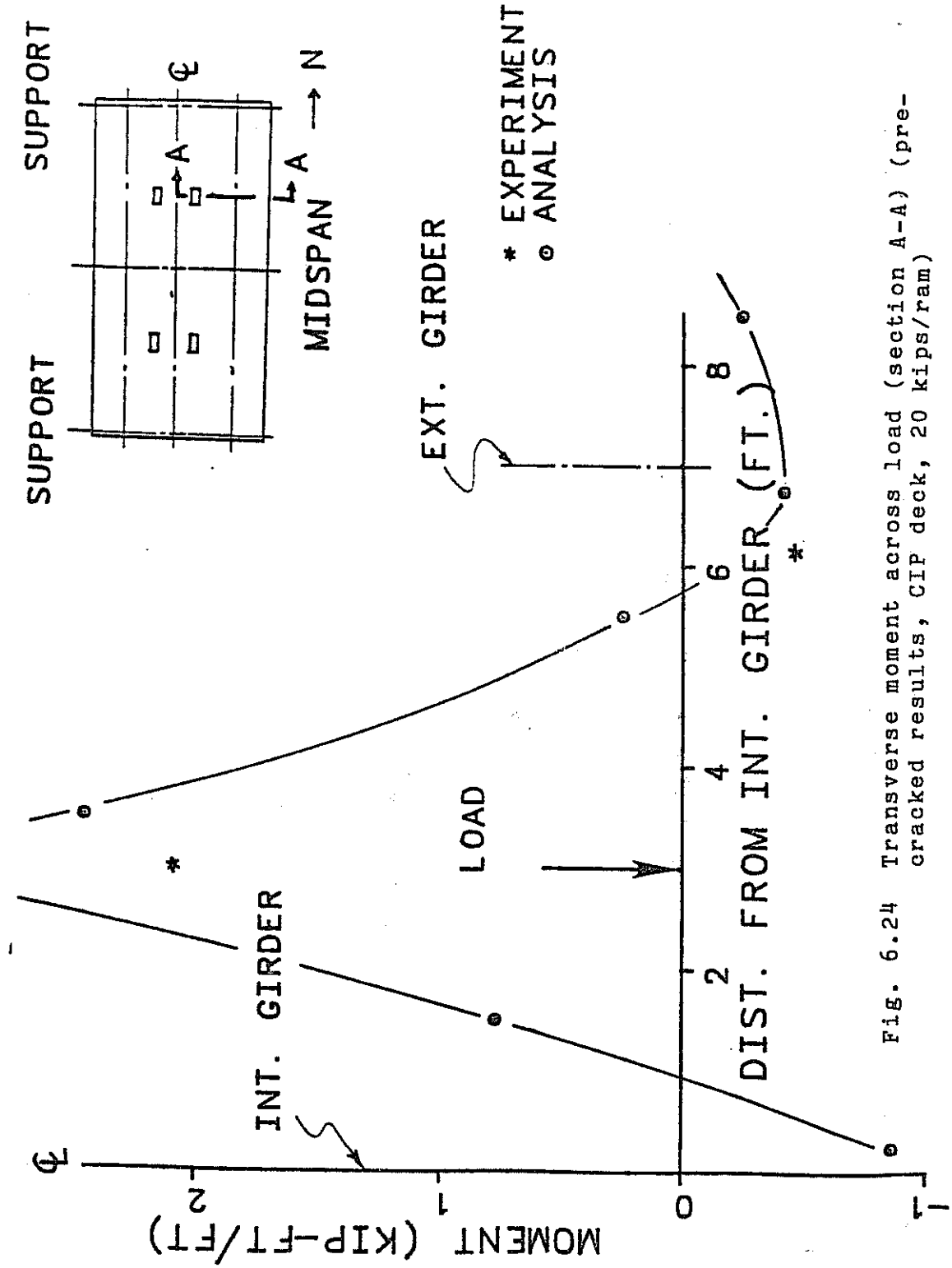

Fig. 6.24 Transverse moment across load (section A-A) (pre-cracked results, CIP deck, 20 kips/ram)

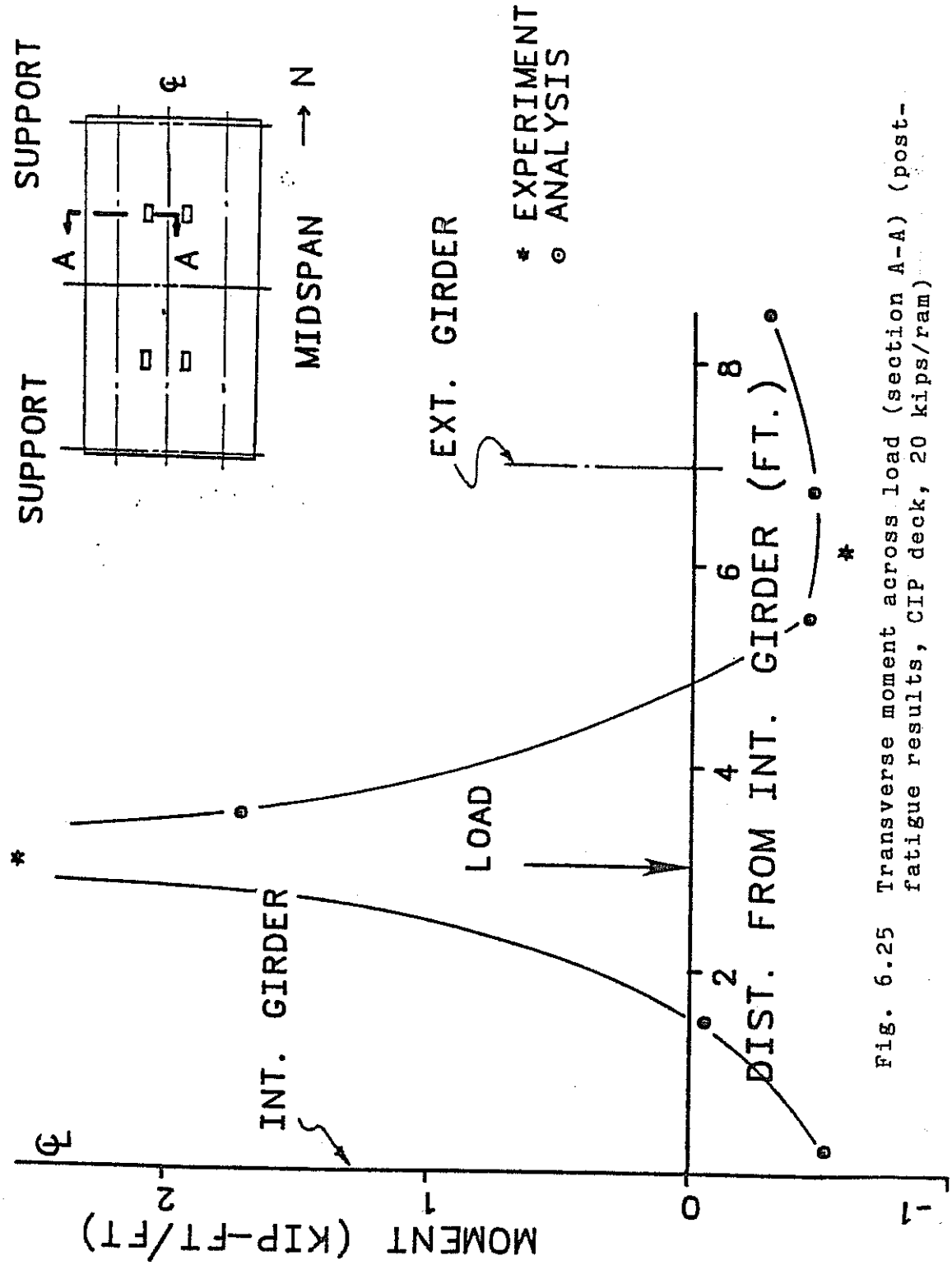

Fig. 6.25 Transverse moment across load (section A-A) (post-fatigue results, CIP deck, 20 kips/ram)

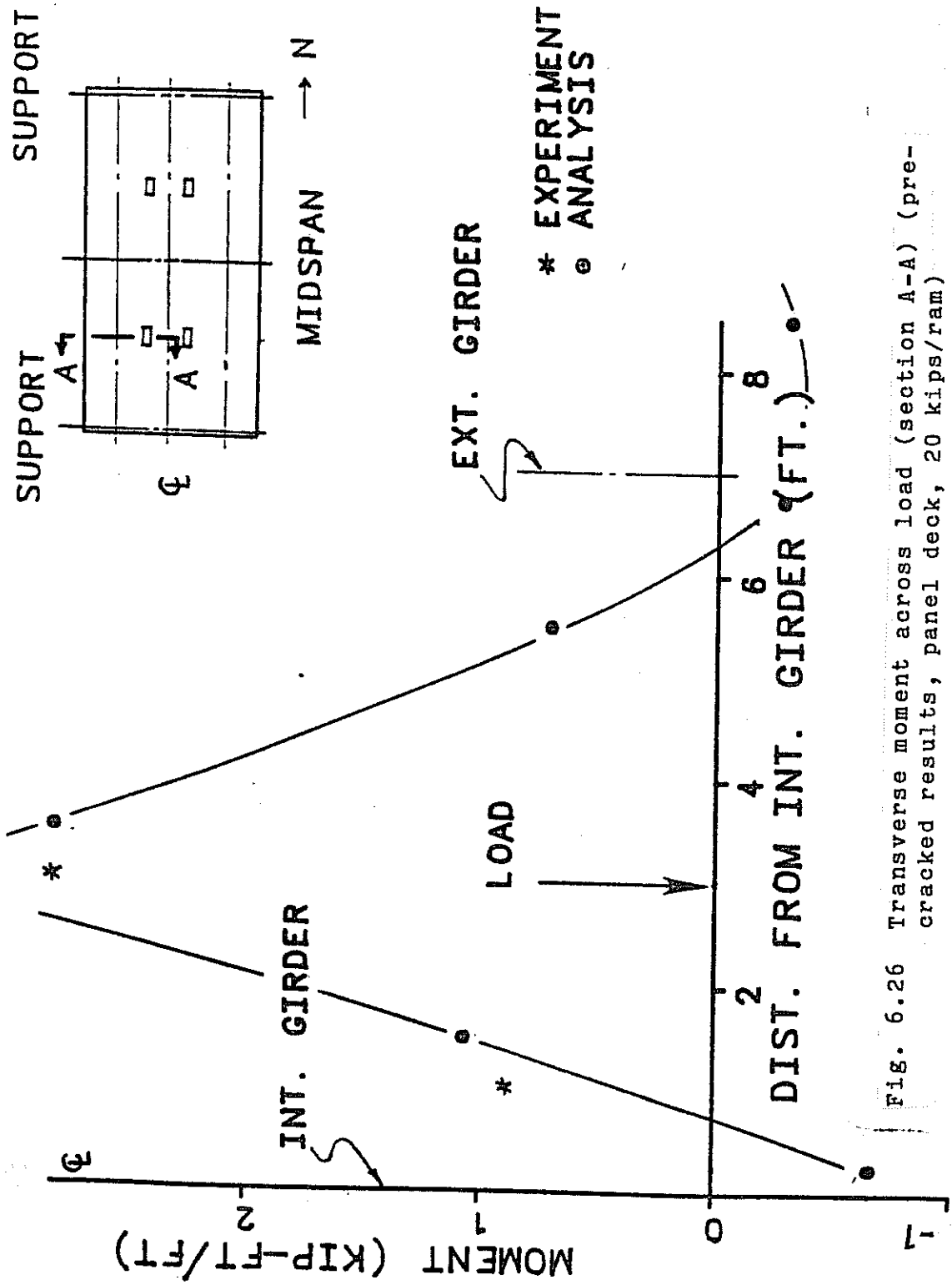

Fig. 6.26 Transverse moment across load (section A-A) (pre-cracked results, panel deck, 20 kips/ram)

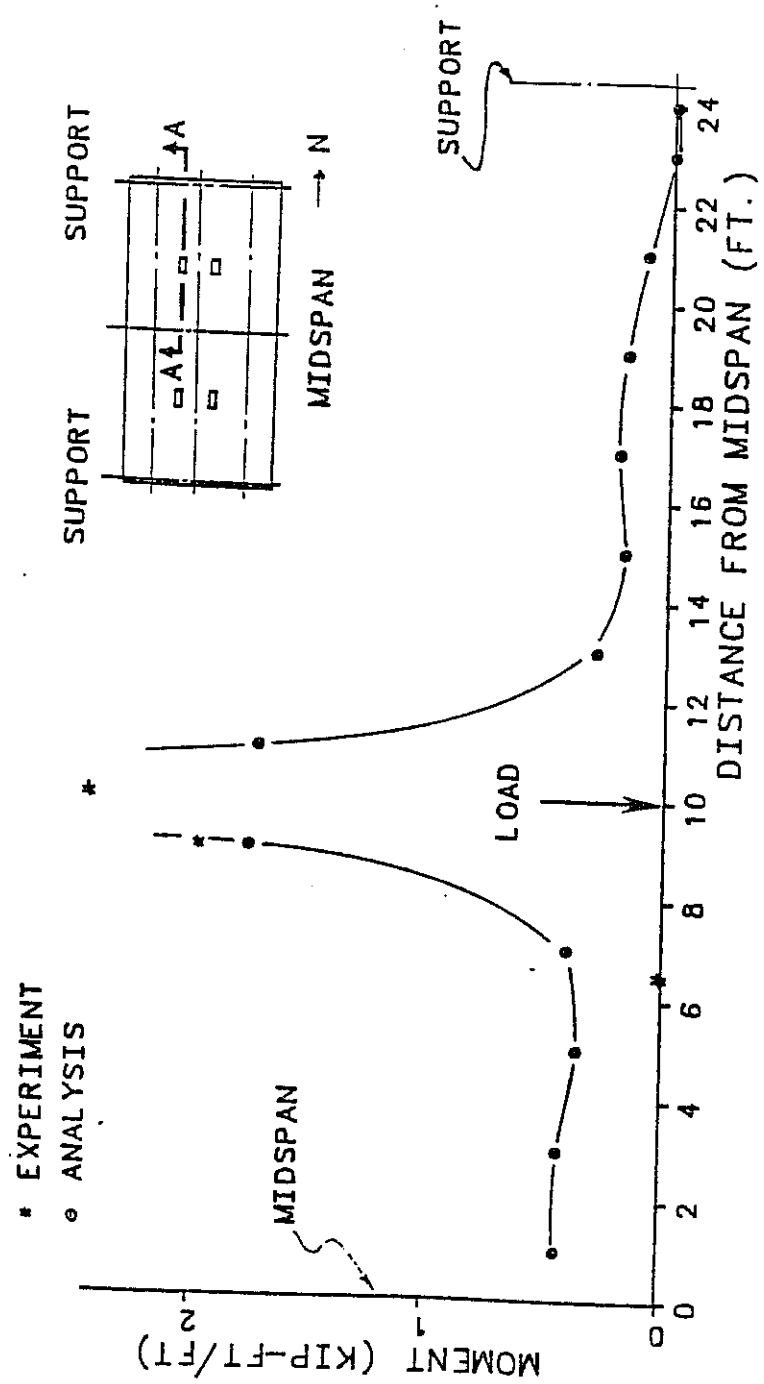

Fig. 6.27 Longitudinal moment along load (section A-A) (pre-cracked results, CIP deck, 20 kips/ram)

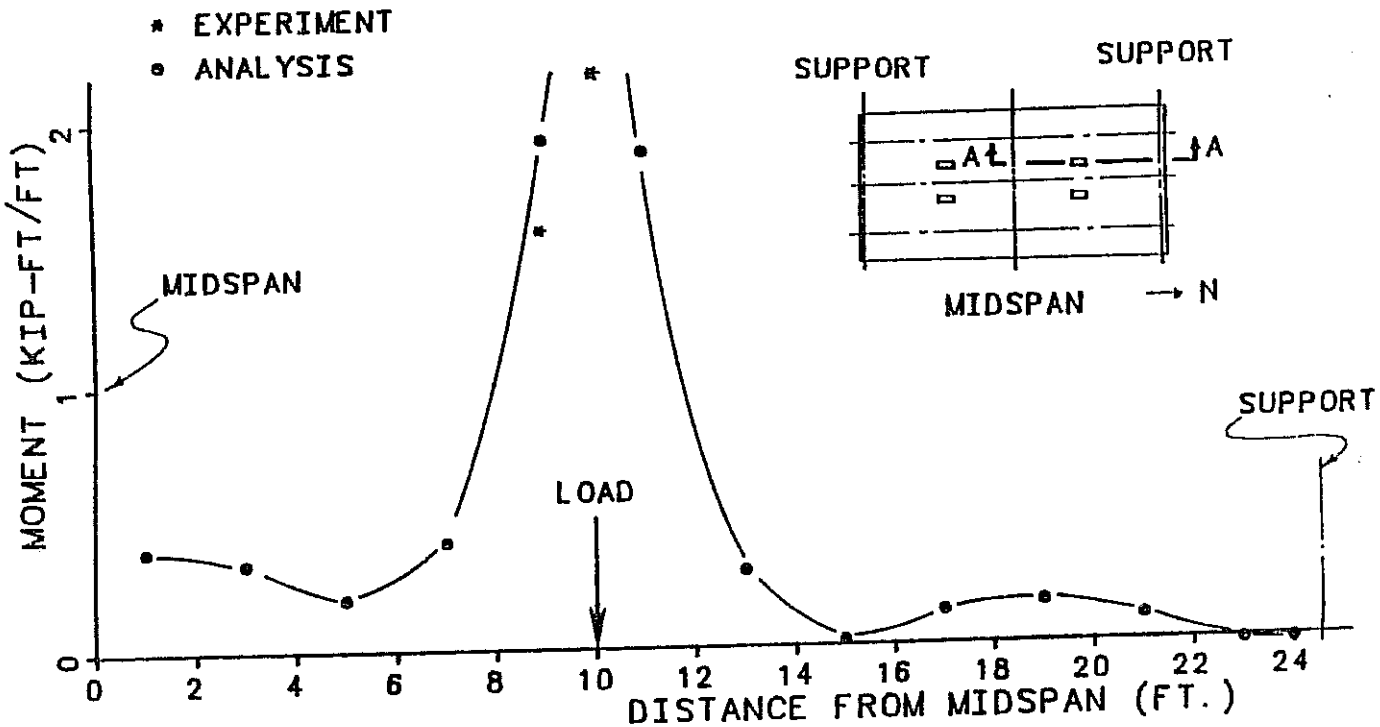

Fig. 6.28 Longitudinal moment along load (section A-A) (post-fatigue results, CIP deck, 20 kips/ram)

6.6 Compressive Membrane Force in the Deck.

After computing axial forces in the slab as explained in Sec. 6.5, figures were drawn showing the variation of membrane force in the bridge deck, in each direction, at each load stage.

6.6.1 Load-Membrane Force Relationship. Fig. 6.29 shows the relationship between load and transverse membrane force per unit width at a gage location near the loaded point. As shown by the solid line (before fatigue loading), the membrane forces are all in tension up to a load of 50 kips per ram, when significant cracking occurred in the deck. Due to cracking, the membrane force then changed from tension to compression. The dashed line shows that after cracking, transverse membrane forces near the load are all compressive, and increase as the load increases.

Also shown in Fig. 6.33 is the analytically predicted variation of transverse membrane force (CIP end) with load. It can be seen that a slight tensile force was present initially becoming compressive after the deck was significantly cracked.

Transverse membrane forces in the panel deck are typical of those shown in Fig. 6.30, corresponding to a gaged location about 3 ft from the loaded point. In contrast to the behavior at the CIP end, transverse membrane forces at the panel end were always tensile, and increased with increasing applied load. The abrupt increase in tensile membrane force near the 60-kip load level (pre-fatigue curve), corresponds to failure of a diaphragm weld. In Chapter 2, it was hypothesized that significant compressive membrane action could be developed only after slab cracking. For the CIP end, this is borne out by Fig. 6.29. For the panel end, which did not crack significantly, transverse membrane forces remained tensile, and did not change significantly as a result of fatigue loading. This is also shown in the analytically predicted curve of the same figure.

6.6.2 Distribution of Transverse Membrane Force. Using such graphs of load or membrane force at each gage location at every load stage, the distribution of transverse membrane force per unit width along the interior girder can be plotted, as shown in Fig. 6.31. Analytical and experimental results, plotted on the same figure, agree reasonably well. From this figure, the variation of sign and magnitude of the membrane force at various locations can be clearly seen. The area under the compressive part of the curve is approximately equal to that under the tensile part. As shown by that comparison, compressive membrane forces must be balanced by tensile membrane forces acting in adjacent sections of the deck.

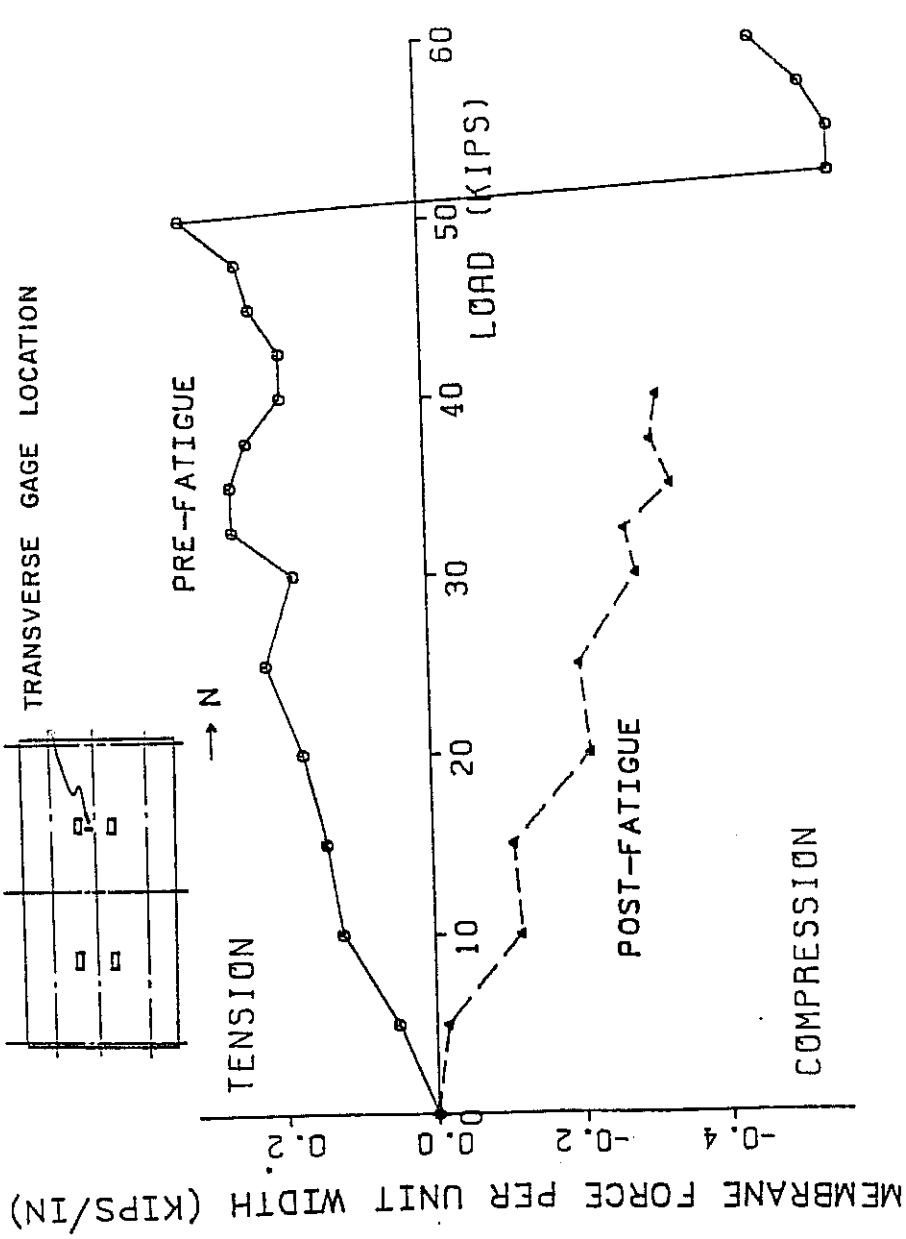

Fig. 6.29 Load vs. transverse membrane force (CIP deck)

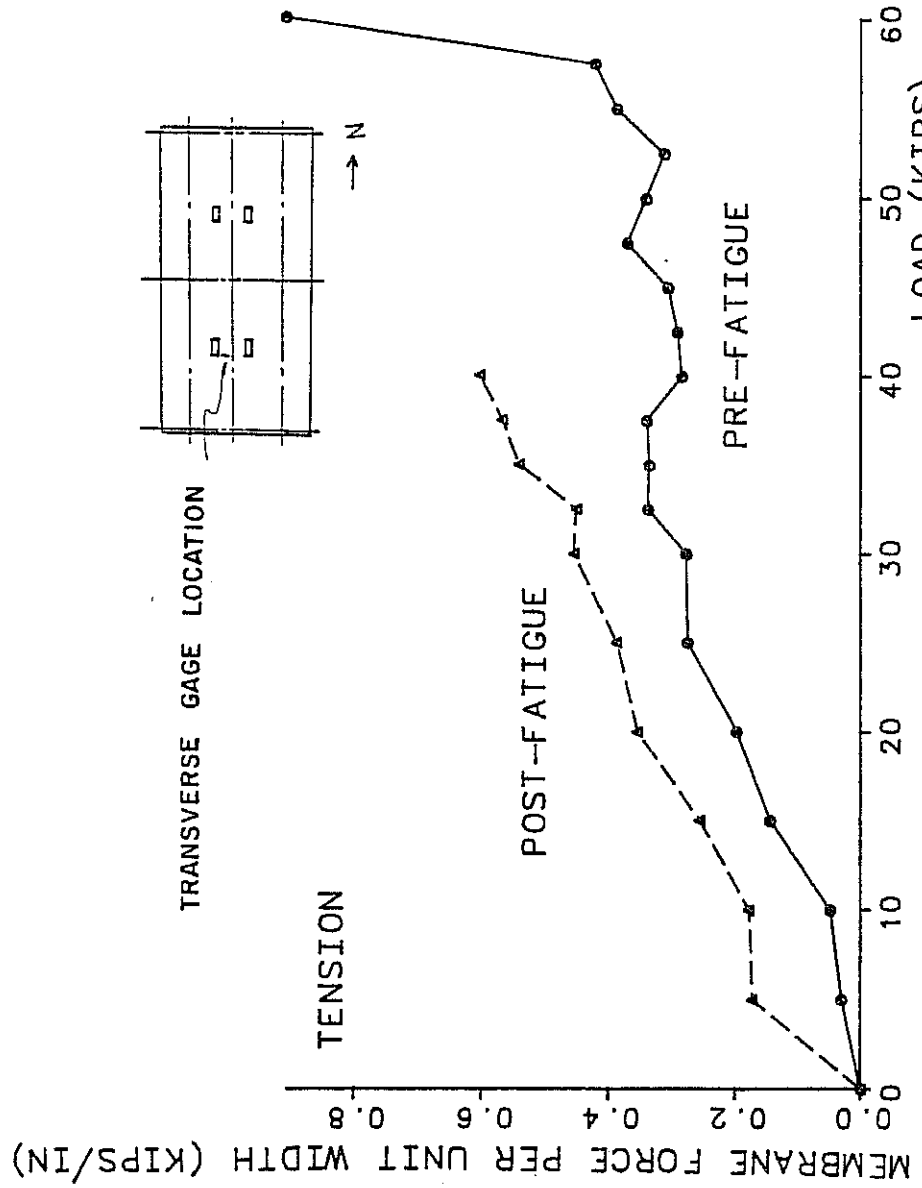

Fig. 6.30 Load vs. transverse membrane force (panel deck)

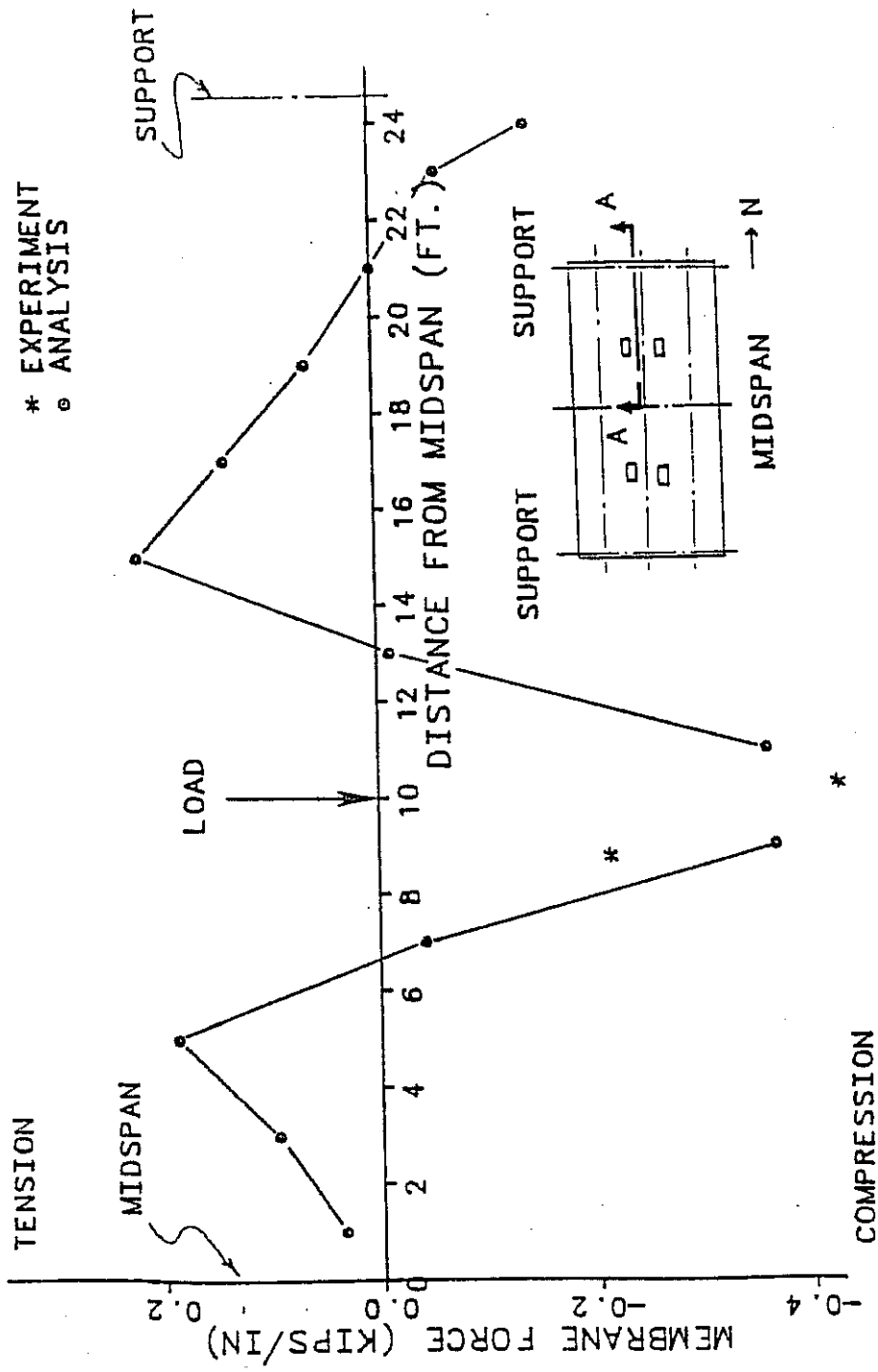

Fig. 6.31 Distribution of transverse membrane force (post-fatigue results, CIP deck, 20 kips/ram)

6.6.3 Total Transverse Compression. By summing the areas under the compressive zone near the load in curves like that of Fig. 6.31, at different load stages, a diagram of load versus total compressive membrane force can be constructed, as shown in Fig. 6.32. Experimental and analytical results are shown in the same figure, and agree closely.

Since there was not much cracking at the panel end, little compressive membrane force was evident there, even though the deck was loaded up to about three times the design load. Some tensile membrane force was also seen in this type of deck.

6.7 Effect of Transverse Membrane Forces on Deck Behavior

6.7.1 Introduction. The foregoing figures and previous analytical examples clearly show that transverse membrane forces are negligible in an uncracked deck, and that significant transverse compressive forces can only exist after the deck has cracked. The importance of these transverse compressions depends on the extent to which they can increase the flexural strength of the deck slab.

The research discussed in Chapter 2 indicates that under some circumstances, the flexural strength of deck slabs can be increased as much as 3 or 4 times the values predicted by yield line theory. The mechanism behind this can be visualized in terms of the moment-axial force interaction diagram for a lightly reinforced concrete slab, a typical example of which is shown in Fig. 6.34. Axial loads less than the balanced axial load produce an increase in flexural capacity. Since bridge decks behave predominantly as one-way slabs spanning in the transverse direction, transverse compressive membrane forces will increase their flexural capacity. How much the flexural capacity is increased will depend on the magnitude of the compressive membrane force.

6.7.2 Flexural Capacity of Bridge Deck. A transverse section of the CIP deck of the bridge tested in this project is shown in Fig. 6.33. Using the actual material characteristics of steel and concrete, and assuming a maximum concrete strain of 0.003, the axial force-moment interaction diagram shownin Fig. 6.36 was calculated.

6.7.3 Probable Variation of Transverse Compressive Force and Transverse Moment with Load. As shown in Fig. 6.31, experiment and analysis both predict transverse membrane compressions which change rapidly in the longitudinal direction. Because of inelastic moment redistribution, it is likely that flexural capacity depends on average values of membrane compression occurring over a relatively wide zone of the deck. Such average values can be extracted from Fig.

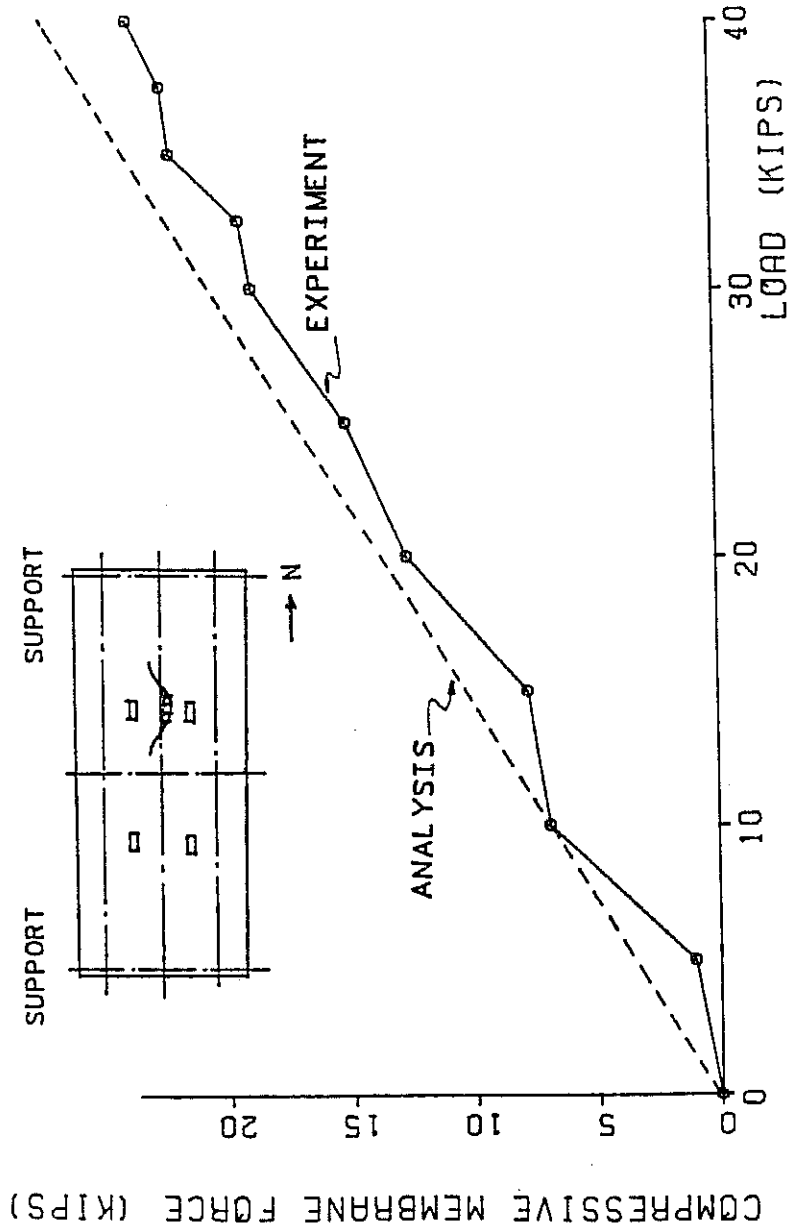

Fig. 6.32 Applied load vs. transverse membrane force (post-fatigue results, CIP deck)

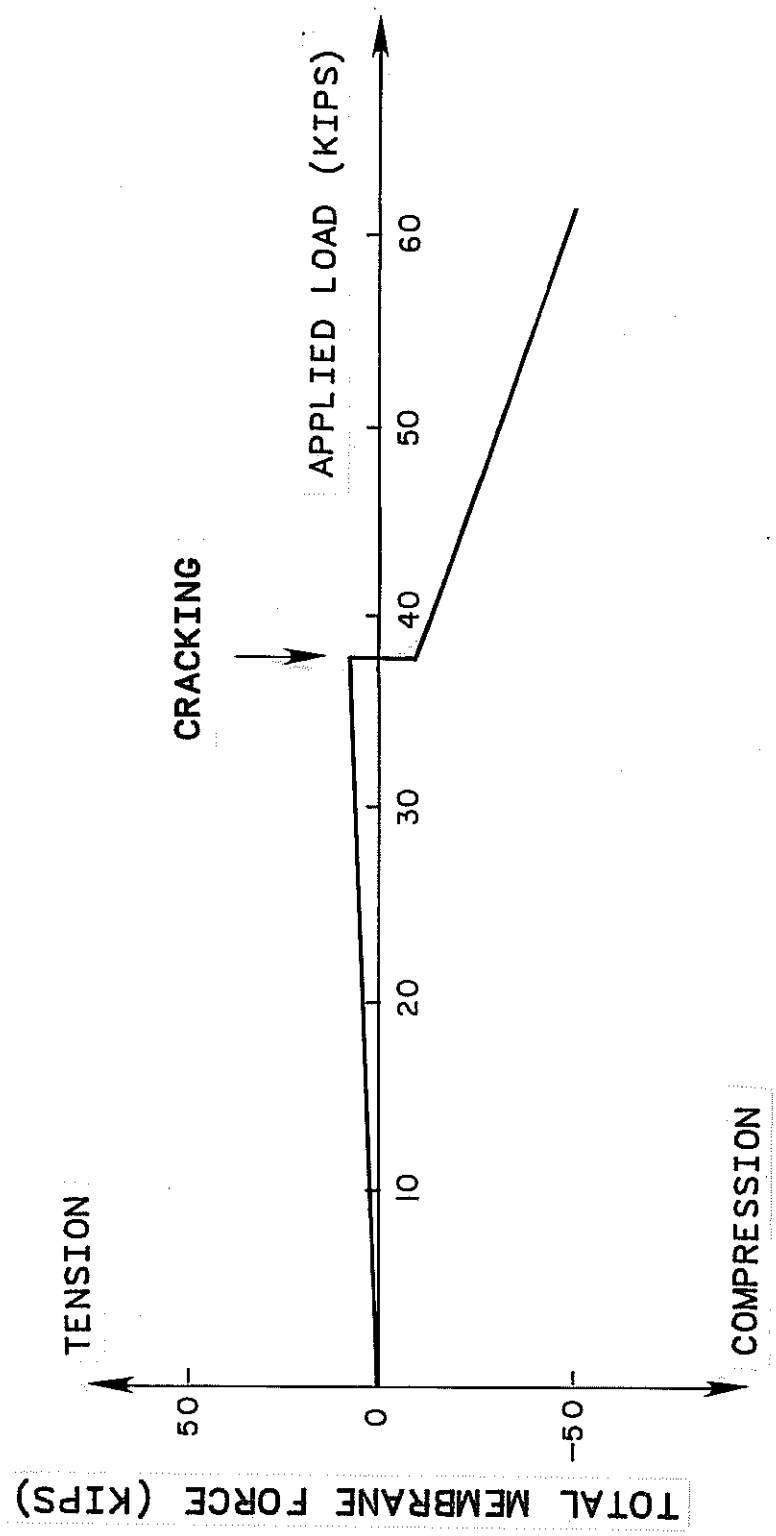

Fig. 6.33 Envelope of total predicted transverse membrane force vs. applied load

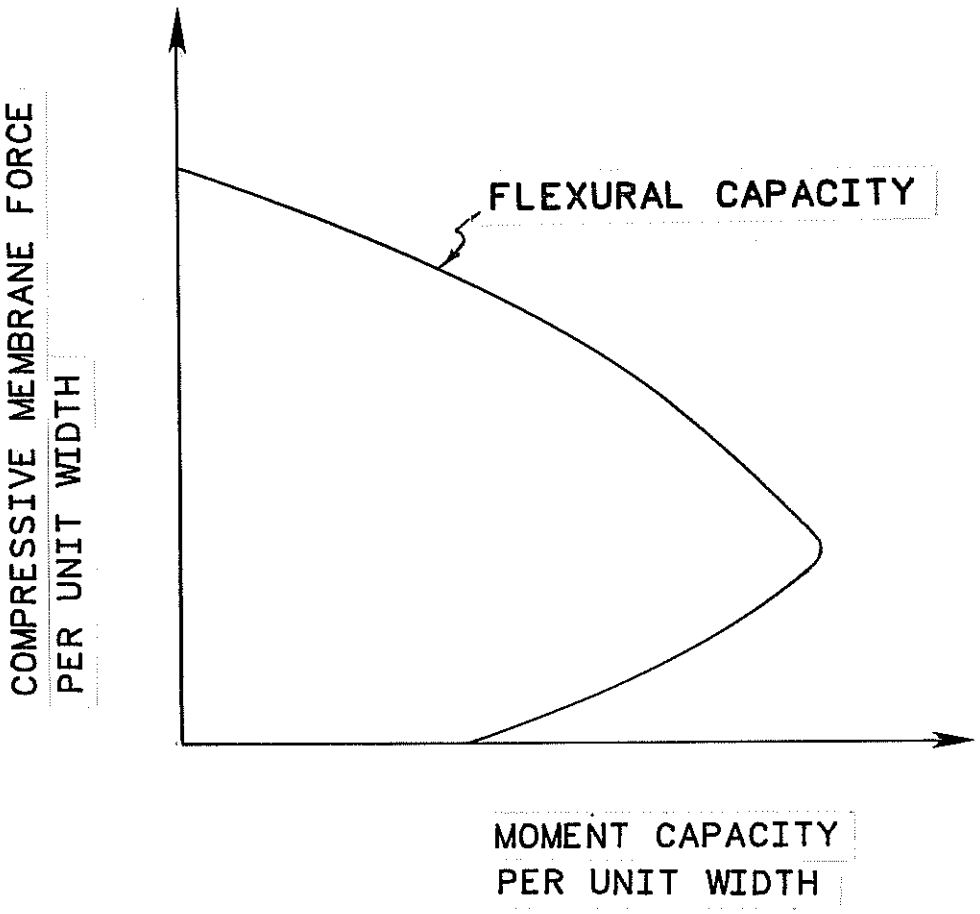

Fig. 6.34 Typical moment-axial force interaction diagram for lightly reinforced slab

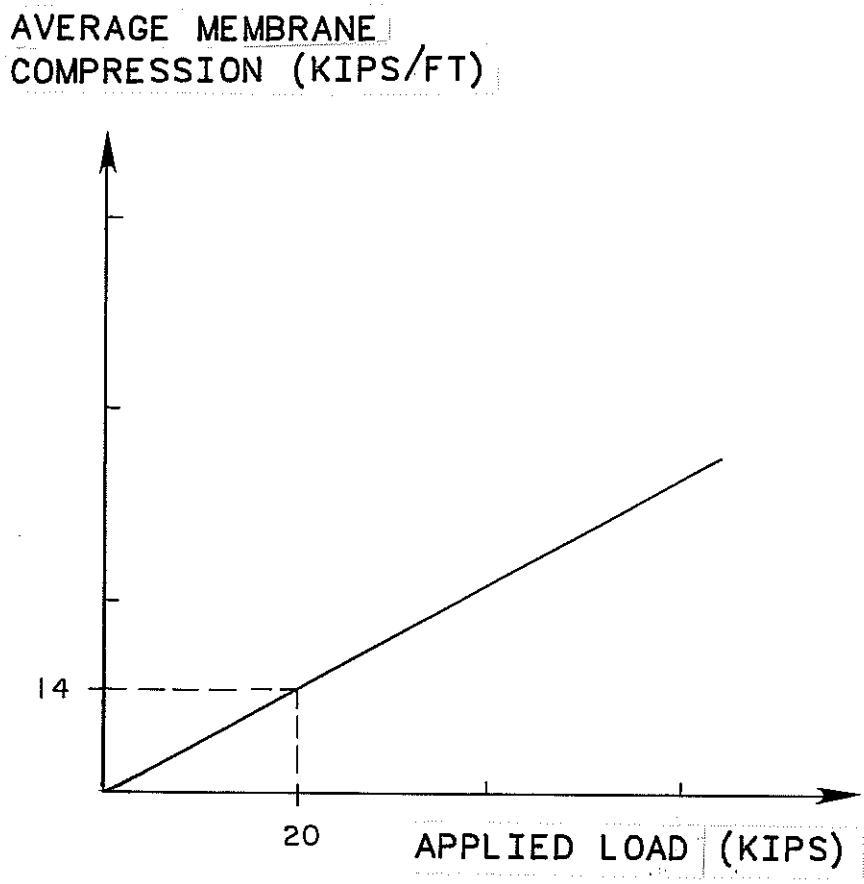

Fig. 6.35 Variation of average transverse membrane compression, CIP deck

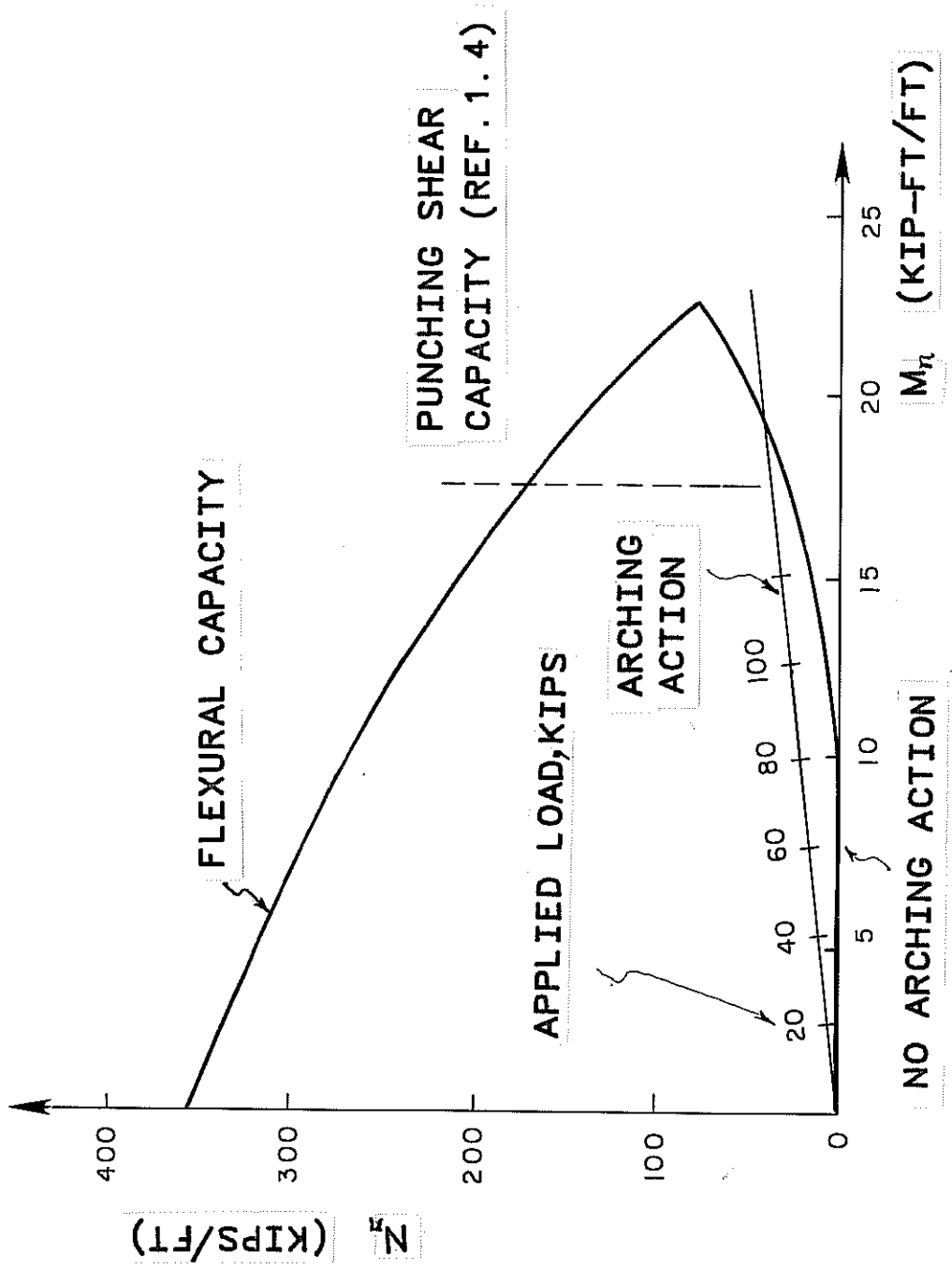

Fig. 6.36 Increase in flexural capacity of underreinforced slab due to compressive membrane force

6.32, which shows values of total transverse compression in the cracked CIP deck over a width of about 6 ft (also see Fig. 6.31). Dividing the compressive forces given in that figure by the 6-ft width over which they act, reasonable values of average transverse compression per unit width can be obtained as a function of applied load. For example (using the analytical curve of Fig. 6.32), an applied load of 20 kips would produce an average compressive membrane force of about 14 kips/ft.

The top surface of the CIP deck was only slightly cracked at an applied load of 60 kips per ram. At any given applied load, transverse membrane stresses were observed to increase with increased cracking. The straight line of Fig. 6.35 corresponds to a constant level of cracking (that is, at 60 kips), and would therefore give a conservative (low) estimate of membrane force at failure.

The transverse moments corresponding to those transverse compressions can be obtained by comparing Figs. 6.31 and 6.25. The peak observed transverse compression of about 0.4 kips/in. (5.0 kips/ft) corresponds to a peak experimental transverse moment of 2.5 kip-ft/ft. To be consistent, peak values were compared.

6.7.4 Probable Increase in Flexural Capacity Due to Transverse Membrane Compression. The curves of Figs. 6.34 and 6.35 are combined in Fig. 6.36. The interaction diagram is taken directly from Fig. 6.34. The straight line showing applied actions combines the load vs transverse compression and transverse compressio vs transverse moment relationships discussed immediately above. Applied moments are related to transverse compressive forces by the ratio of 2.5 kip-ft/ft (moment) to 5.0 kips/ft (transverse force). That ratio determines the slope of the line. Transverse compression is related to applied load by the ratio of 14 kips (tranverse compression) to 20 kips (applied load). That ratio determines the spacing of the load scale along the line.

Also included in Fig. 6.36 is a second load line, corresponding to the complete absence of arching action. That load line has zero slope, since any applied load whatsoever is assumed to produce no transverse compression for that case.

Examination of Fig. 6.36 clearly shows that the presence of arching action can significantly increase the flexural capacity of the deck. Evaluation of the numerical value of the increase would have to be conducted by a yield-line analysis of the slab, and is beyond the scope of this report. However, it is clear that the flexural capacity per unit width of the slab, and hence its collapse load by yield-line analysis, would be significantly increased because of arching action.

Whether or not this increase in flexural capacity is actually reflected in the failure load of the deck, depends on the deck's punching shear resistance. While further discussion of this is beyond the scope of this report, that value was determined in Ref. 1.4 to be about 140 kips, and is also shown in Fig. 6.36.

6.8 Summary of Specimen Behavior

From the overall observation of the bridge specimen tested, the behavior of the bridge can be stated briefly as follows:

The load-deflection relationship for points near the load was very linear up to about three times the current design wheel load of 20.8 kips per ram. Fatigue loading did not significantly change this relationship. More cracks formed at the bottom of CIP deck than the panel deck. Only a few cracks were found in the panel deck when the bridge was loaded up to about three times the design loading. Under fatigue loading, crack propagation occurred only at the bottom of the CIP deck. The maximum crack width observed at the bottom of CIP deck was about 0.008 in., within the allowable limit of the current Ontario Highway Bridge Design Code. No significant widening of cracks was observed under fatigue.

Under the current design wheel load of 20.8 kips per ram, the maximum compressive concrete stress near the load in both types of deck was about 0.4 ksi. At the same load level, the maximum stress in the reinforcement near the load was about 1.8 ksi. The stresses in reinforcement and concrete near the interior girder and exterior girder were much smaller than those near the loaded point, and did not change significantly as a result of fatigue loading.

Because the panel deck never cracked significantly, transverse membrane stresses at that end of the bridge were always tensile.

The peak measured transverse and longitudinal moment, about 2 kip-ft/ft, is less than the current AASHTO design value. At both the CIP and panel ends of the bridge, the transverse membrane force acted in tension before the deck cracked. After the CIP deck had significantly cracked, the transverse membrane forces near the load became more compressive, and increased as the load increased.

CHAPTER 7

EFFECTS OF INTERMEDIATE DIAPHRAGMS ON DECK BEHAVIOR

7.1 Introduction

In previous chapters of this report, experimental results and analytical predictions are compared. In this chapter, an example is presented of the use of the verified analytical model to answer further questions about the bridge behavior. In particular, this chapter concerns the question of recommended diaphragm spacing. What diaphragm spacing should be used with Ontario-type decks?

Using the measured test results and verified computer model, this chapter is intended to study the effects of intermediate diaphragms on the behavior of the bridge deck. Two cases are considered:

1) midspan diaphragms placed as in the test specimen; and

2) additional diaphragms placed at to the loaded points.

The first case is studied using the test results from the fatigue test with the midspan diaphragm broken, together with the behavior predicted analytically using the verified bridge model. The second case is studied using the analytically predicted behavior of a bridge model with and without extra diaphragms at the loaded points. The specific objective of this study is to investigate the effects of diaphragms on the local stiffness, moment distribution, local stresses, and compressive membrane force in the deck slab.

7.2 Effect of Intermediate Diaphragms on Local Deck Stiffness

Measured load-deflection data for the CIP deck with and without midspan diaphragm (Fig. 7.1), indicated that the local stiffness at the loaded point was not significantly changed by the presence of midspan diaphragms. The same figure also shows that even without the midspan diaphragm, there was no significant change in the load-deflection relationship between 2 million and 5 million cycles of fatigue loading. As can be seen in Fig. 7.2, similar behavior was

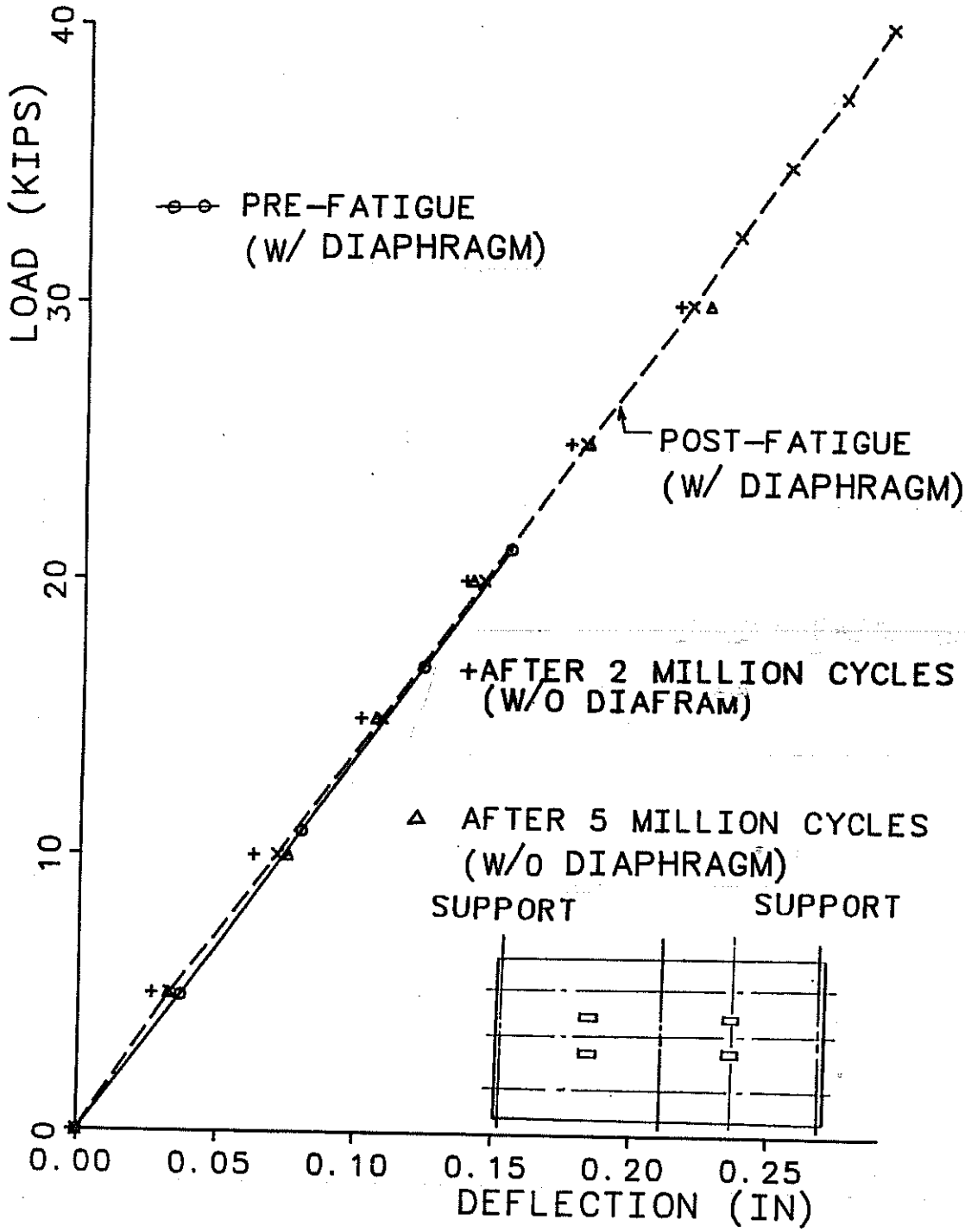

Fig. 7.1 Measured deflection of loaded point of CIP deck with and without midspan diaphragm

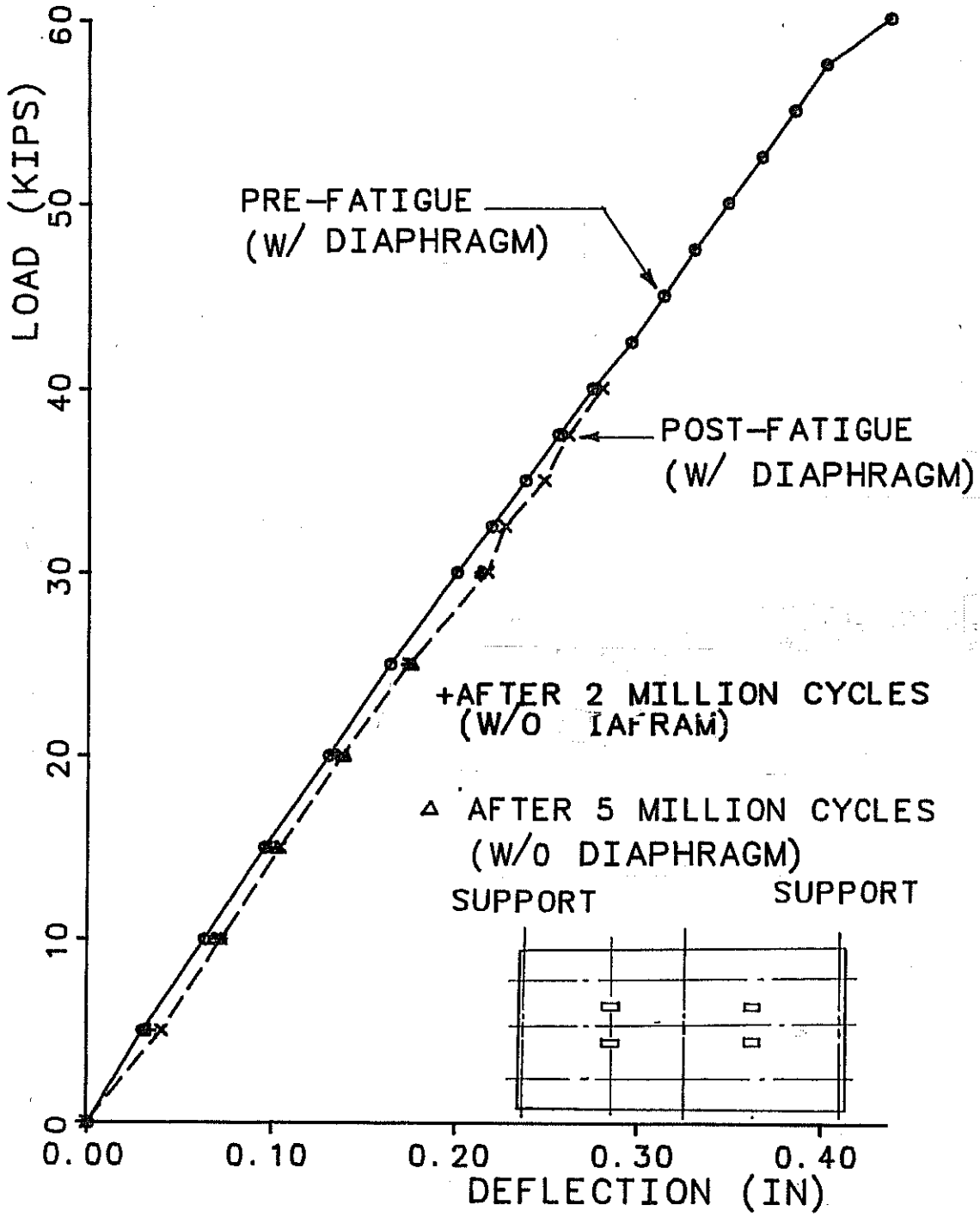

Fig. 7.2 Measured deflection at loaded point of panel deck with and without midspan diaphragm

observed at the panel end. The presence of midspan diaphragms did not significantly change the local stiffness of the deck at the loaded point.

To study analytically the effects of changes in diaphragm location with respect to the loaded point, diaphragms were put directly at the loaded point on the previously verified bridge model. The predicted load-deflection relationship at the loaded point is shown in Fig. 7.3. The presence of additional diaphragms at the loaded point has an insignificant effect on the local stiffness.

7.3 Effects of Intermediate Diaphragm on Deck Slab Moments

The relationship between applied load and longitudinal moment in the CIP deck with and without midspan diaphragm was calculated using the analytical bridge model, and is shown in Fig. 7.4. The presence of midspan diaphragms did not significantly affect the distributions of longitudinal moments in the deck slab. Similar observations also apply to the transverse moments, as shown in Fig. 7.5.

Figs. 7.6 and 7.7 show the effects of additional diaphragms placed at the loaded points. From both figures, it is found that additional diaphragms at the loaded points do not significantly affect the magnitude nor the distribution of moment.

7.4 Effects of Intermediate Diaphragms on Local Slab and Girder Stresses

Local stresses in bridge deck concrete and reinforcement near the loaded point were measured when the bridge specimen was tested without a midspan diaphragm. Figs. 7.8 and 7.9 show the relationship between applied load and measured concrete stress near the loaded point for the CIP and panel decks respectively. From both figures, it can be seen that the stress in concrete near the loaded point did not change significantly between 2 million and 5 million cycles of load in the absence of midspan diaphragms. Also, the presence of midspan diaphragms did not significantly change the deck concrete stresses. As shown by Figs. 7.10 and 7.11, similar observations apply to stresses in reinforcement.

Bending stresses in the steel girders at midspan were monitored throughout each test. As shown in Fig. 7.12, due to the breakage of the diaphragm, stress in the interior girder increased as additional load went to it instead of being transferred by the diaphragm to the exterior girder. The change in bending stress at

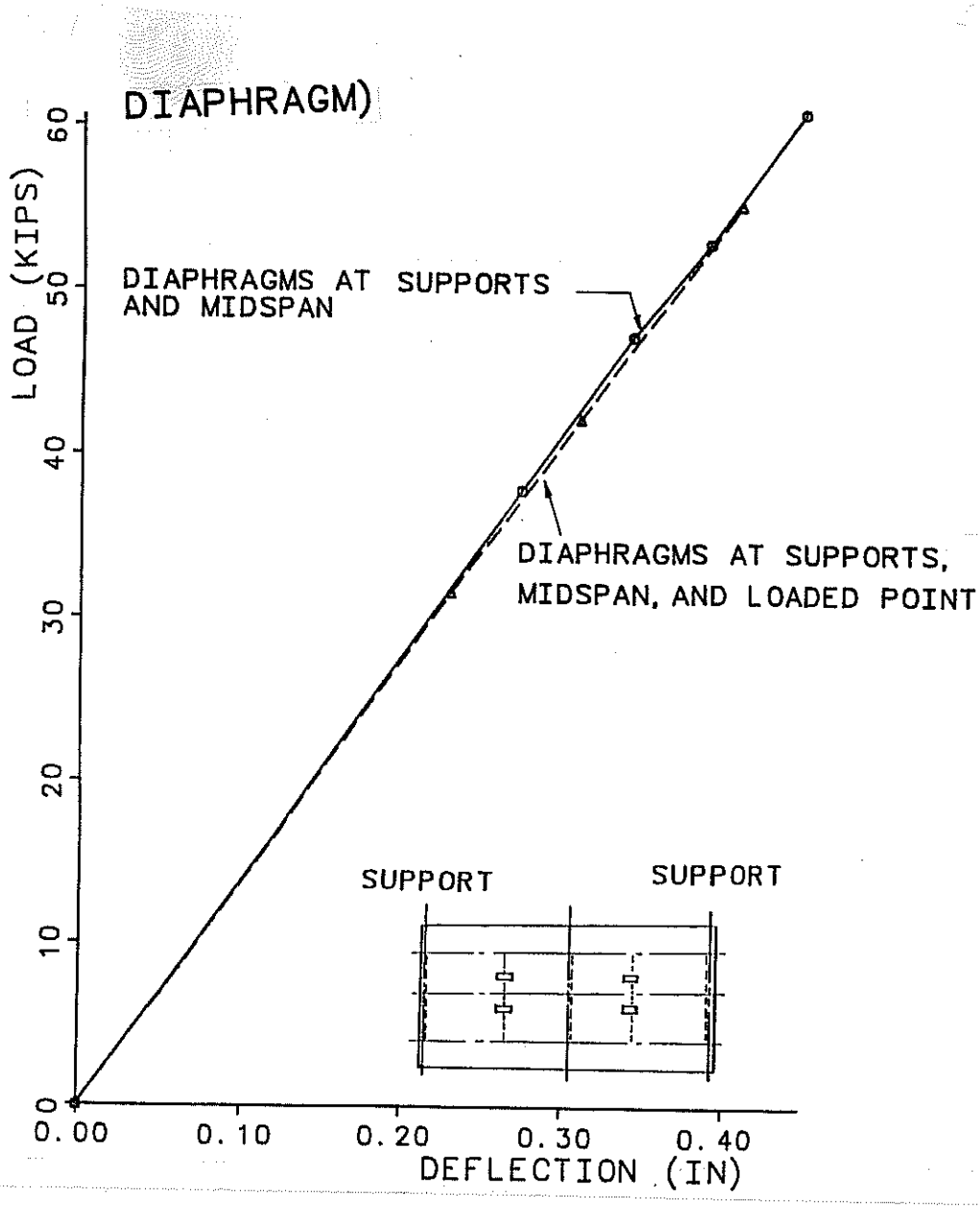

Fig. 7.3 Predicted deflection at loaded point of CIP deck with and without diaphragm at loaded point

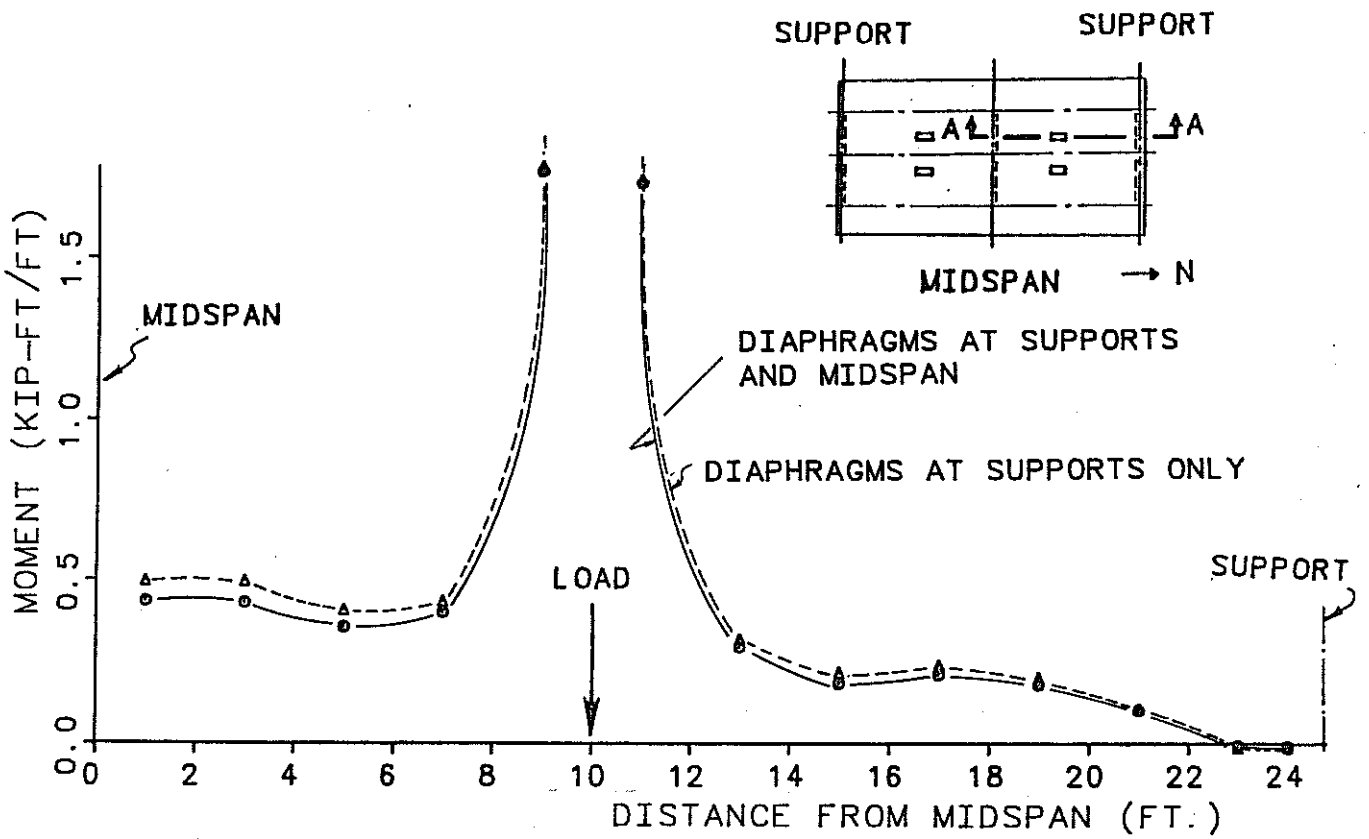

Fig. 7.4 Calculated longitudinal moment along load (section A-A) (pre-cracked results, CIP deck, 20 kips/ram)

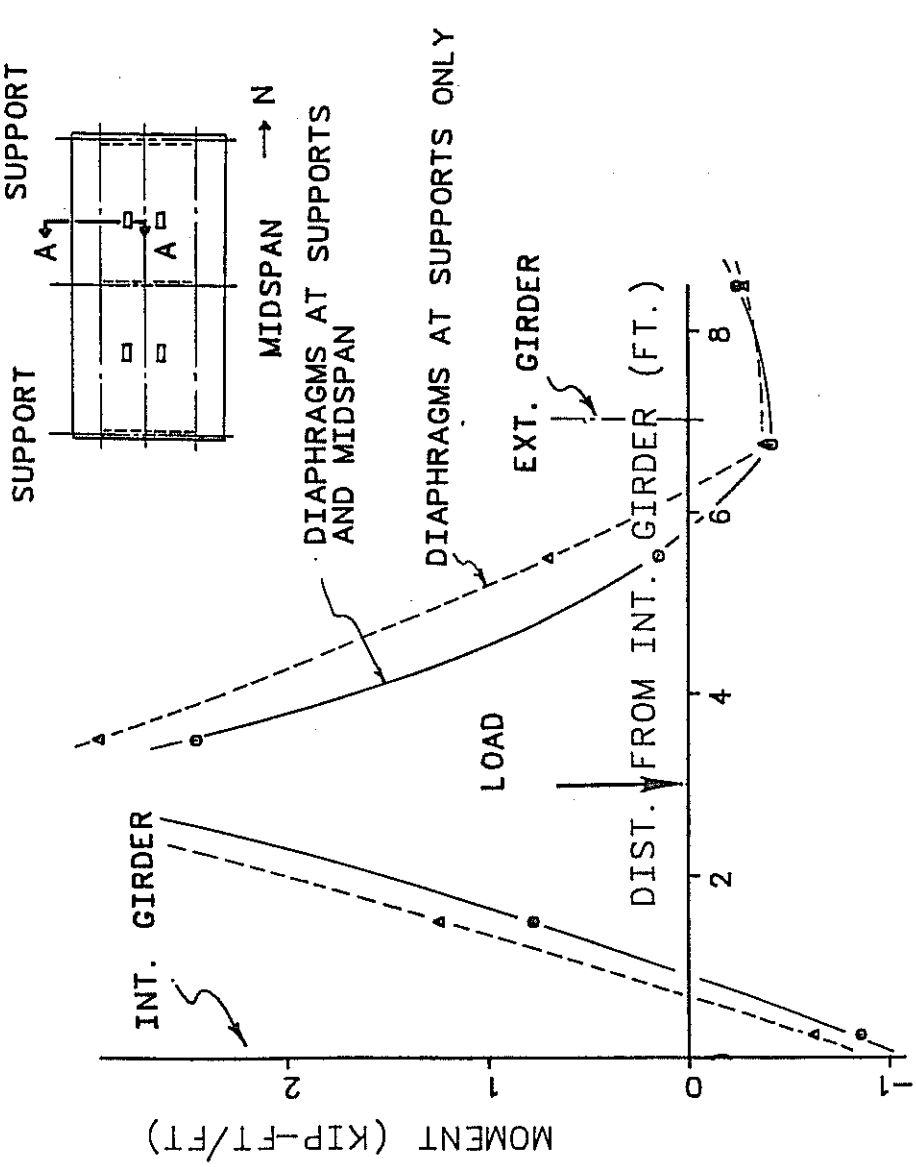

Fig. 7.5 Calculated transverse moment across load (section A-A) (pre-cracked results, CIP deck, 20 kips/ram)

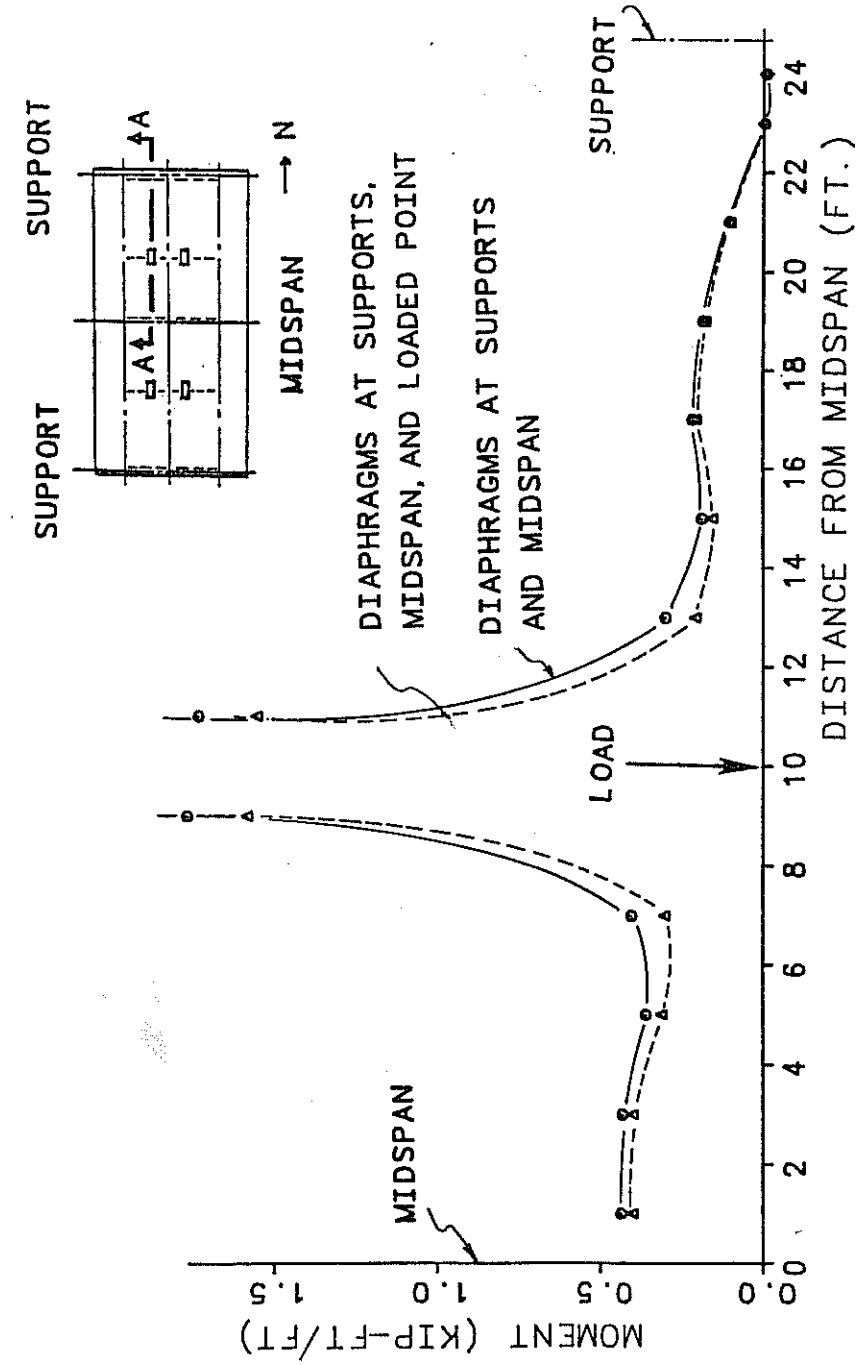

Fig. 7.6 Calculated longitudinal moment along load (section A-A) (pre-cracked results, CIP deck, 20 kips/ram)

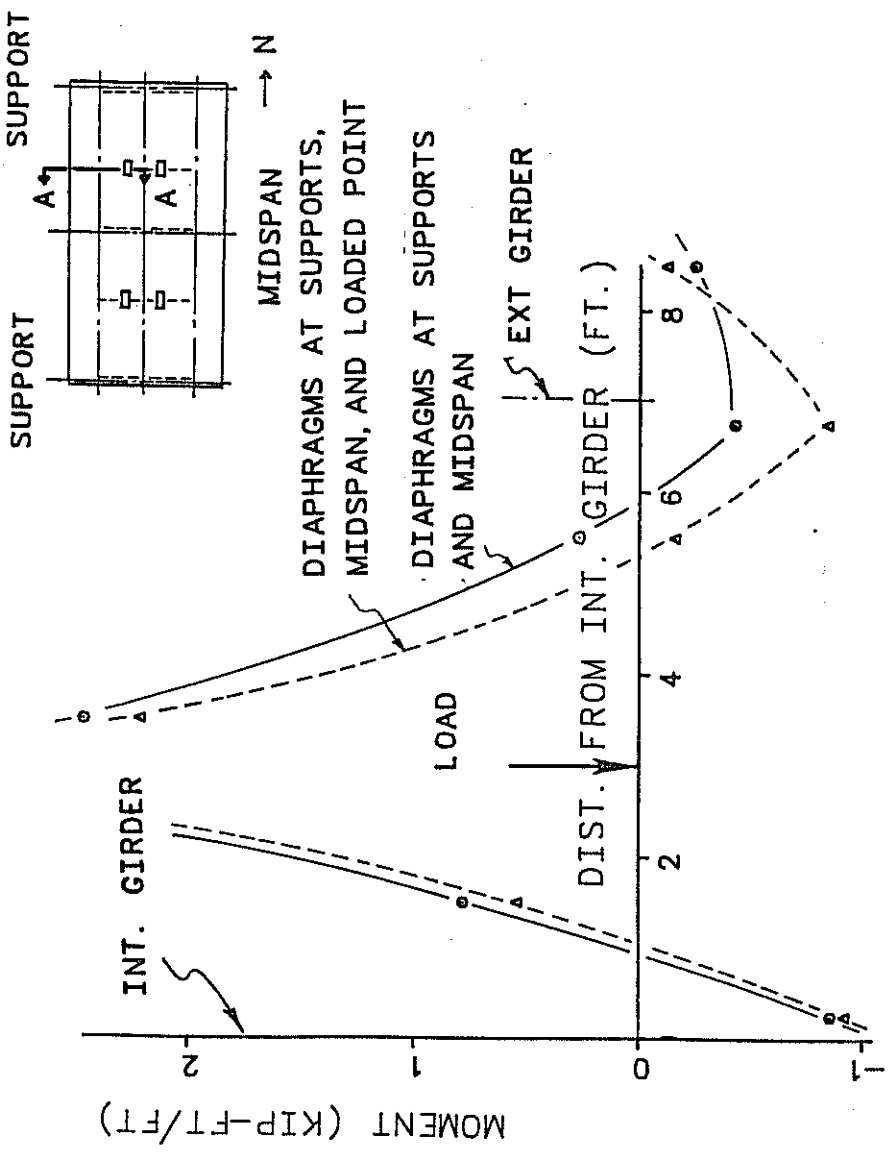

Fig. 7.7 Calculated transverse moment across load (section A-A)
(pre-cracked results, CIP deck, 20 kips/ram)

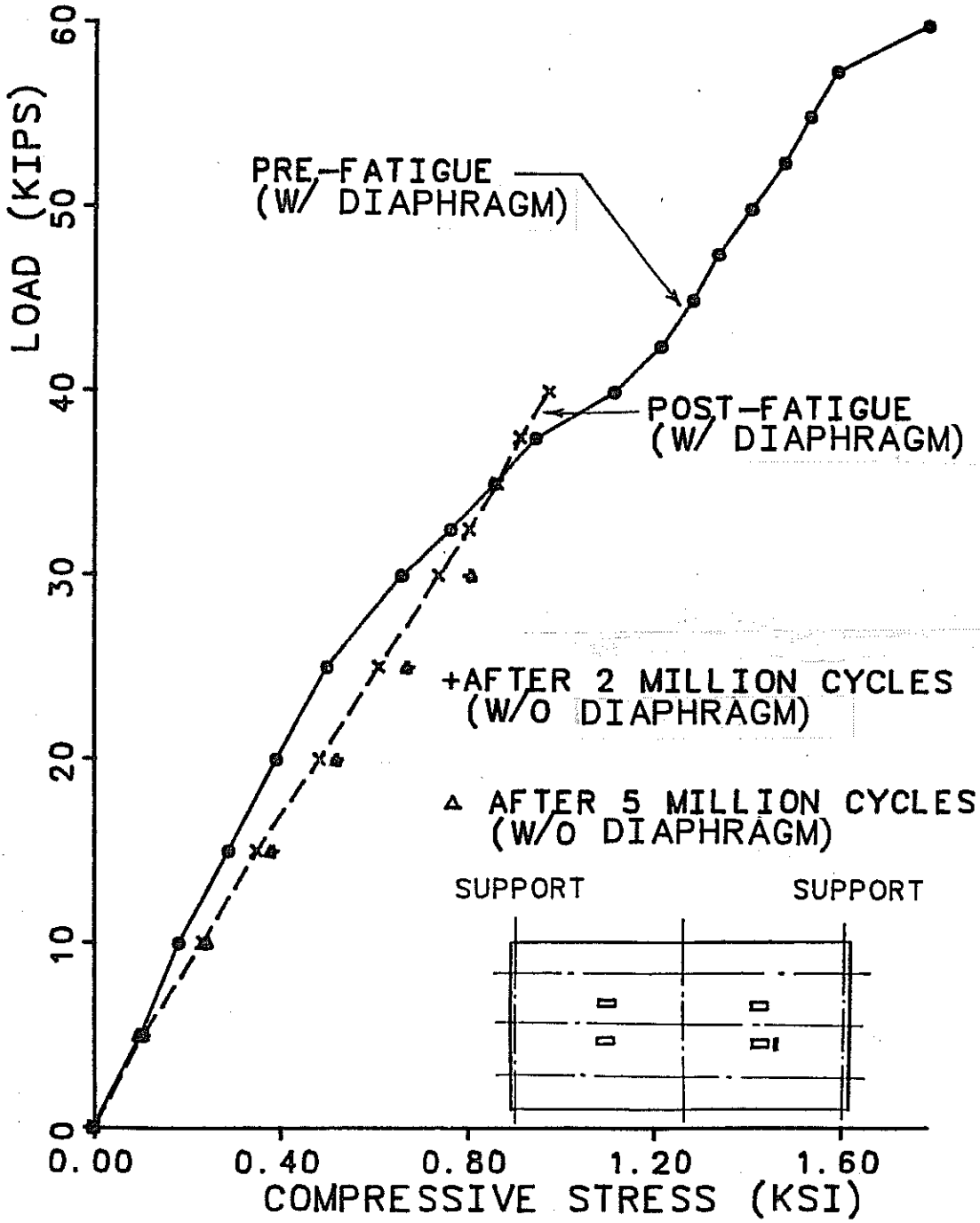

Fig. 7.8 Measured concrete stress in the transverse direction, CIP deck, at loaded point, with and without midspan diaphragm

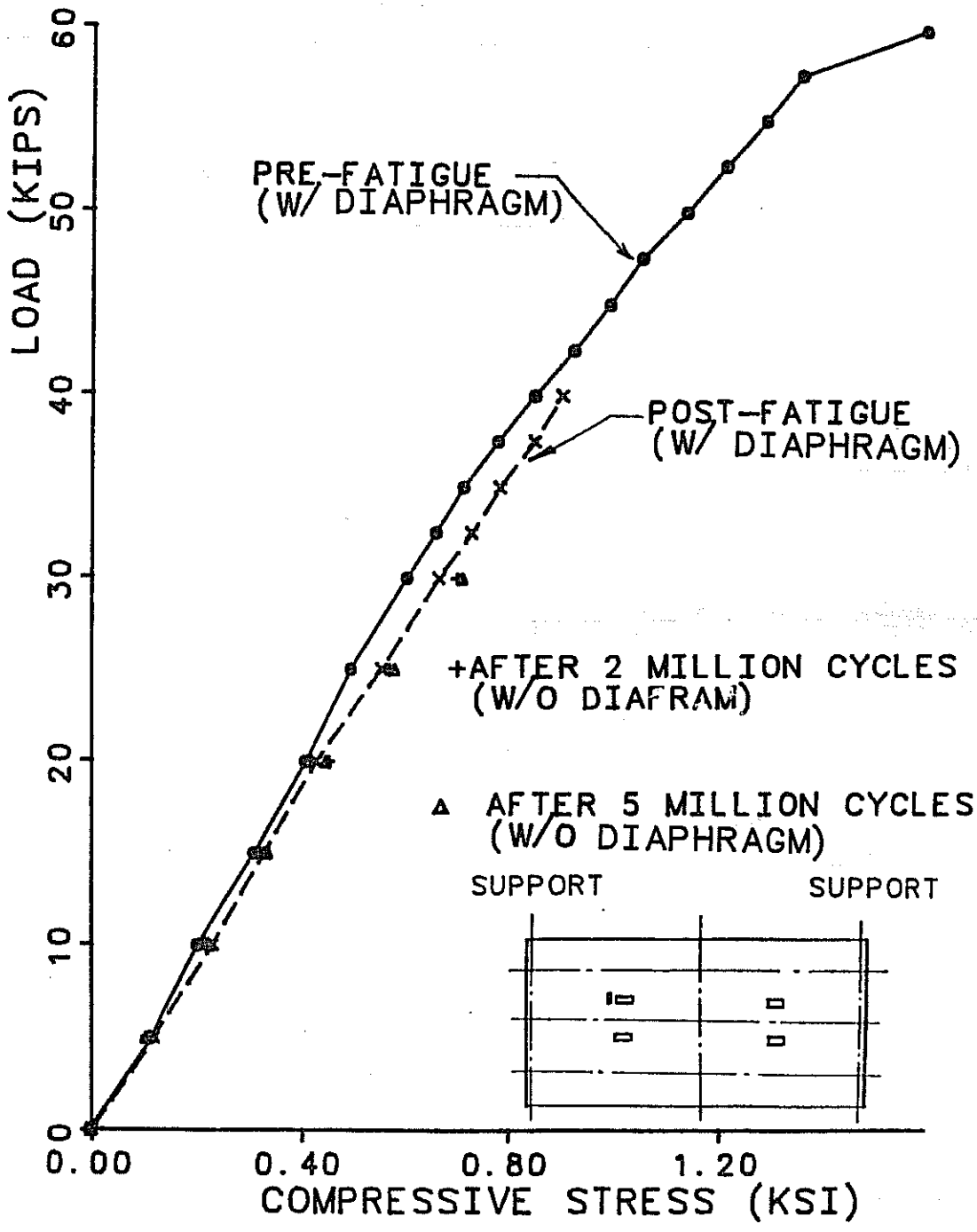

Fig. 7.9 Measured concrete stress in the transverse direction, panel end, at loaded points, with and without midspan diaphragm

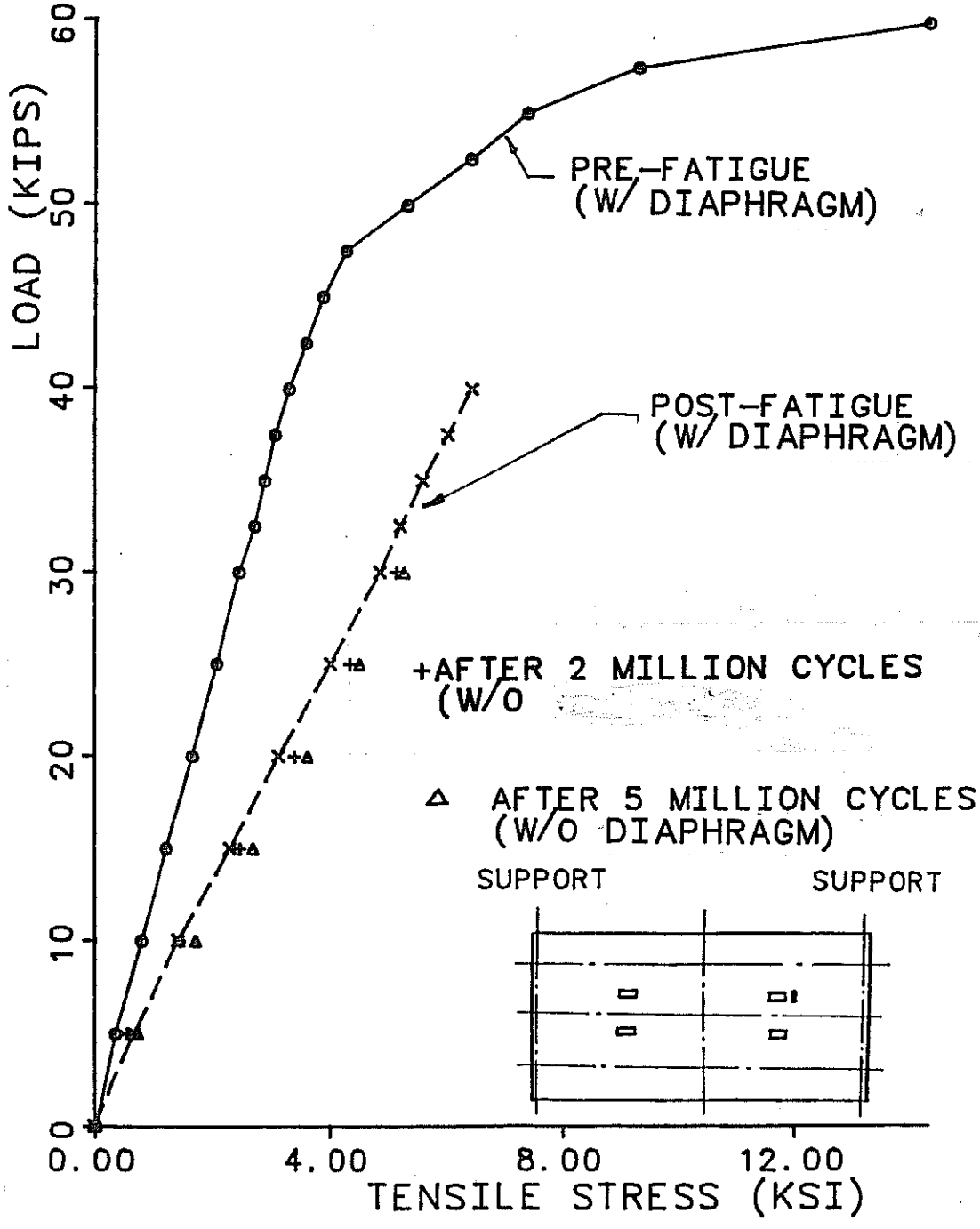

Fig. 7.10 Measured reinforced stress in the transverse direction, CIP deck, at loaded point, with and without midspan diaphragm

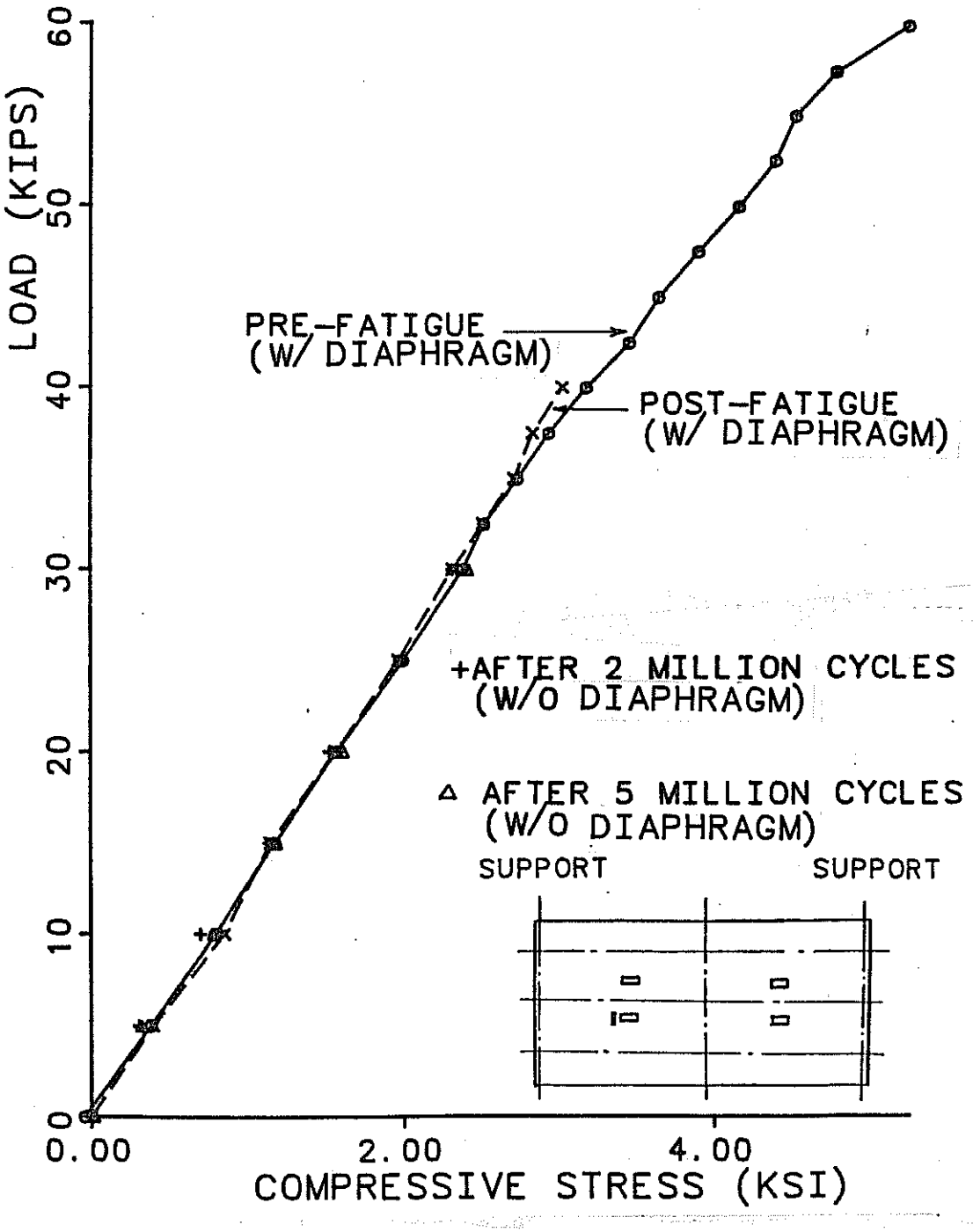

Fig. 7.11 Measured reinforced stress in the transverse direction, panel end, at loaded point, with and without midspan diaphragm

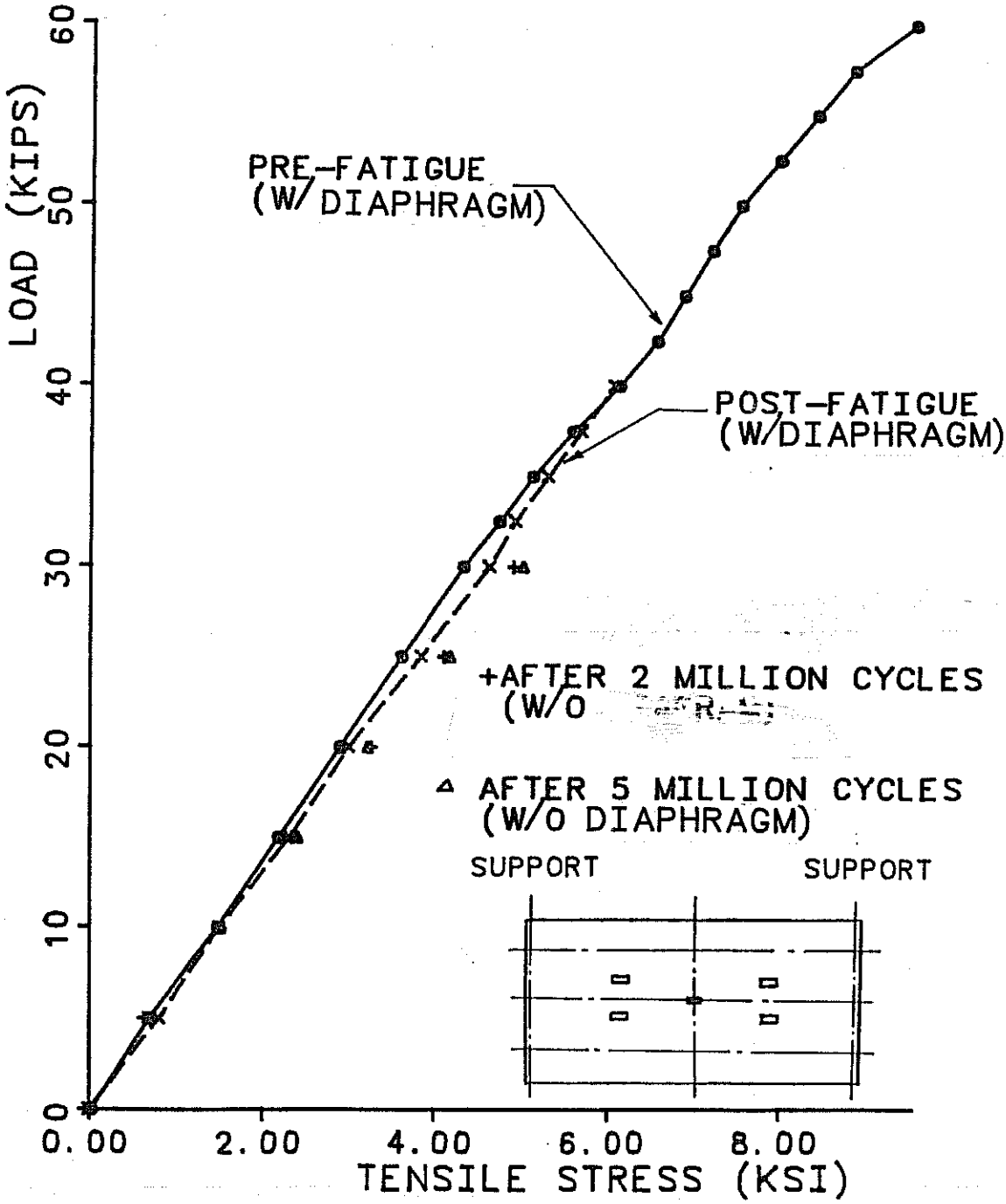

Fig. 7.12 Measured stress at midspan of interior girder, with and without midspan diaphragm

midspan of the exterior girder due to the pressure of the midspan diaphragm is shown in Fig. 7.13. From both Figs. 7.12 and 7.13, the presence of midspan diaphragms does not significantly affect girder stresses.

7.5 Effects of Intermediate Diaphragms on Membrane Force Distribution

The distribution of transverse membrane force along the interior girder was studied analytically, using the verified bridge model. Fig. 7.14 shows the distribution of membrane force for the bridge model with and without midspan diaphragms. The distribution and peak values of membrane force are not significantly altered by the presence of midspan diaphragms. As shown in Fig. 7.15, placement of additional diaphragms at the loaded points does not significantly affect the transverse membrane force distribution.

7.6 Conclusion

As shown by Figs. 7.1-7.14, midspan diaphragms and additional diaphragms placed at the loaded points do not significantly affect the behavior of the cracked or uncracked bridge deck. However, intermediate diaphragms would probably be required because of their effects on transverse load distribution (7.1, 7.2, 7.3, 7.4), and also for construction and overall stability considerations (7.5).

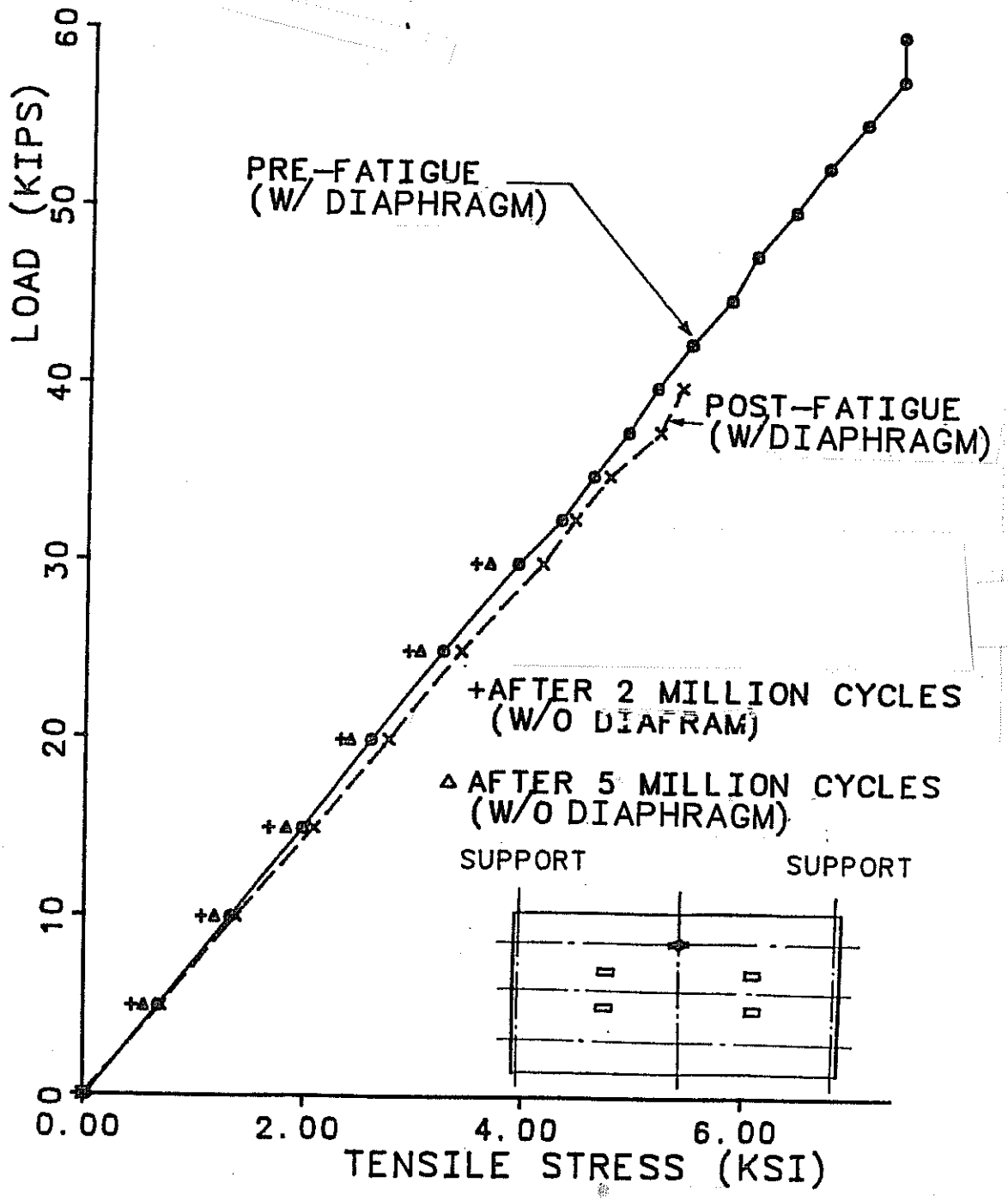

Fig. 7.13 Measured stress at midspan of exterior girder, with and without midspan diaphragm

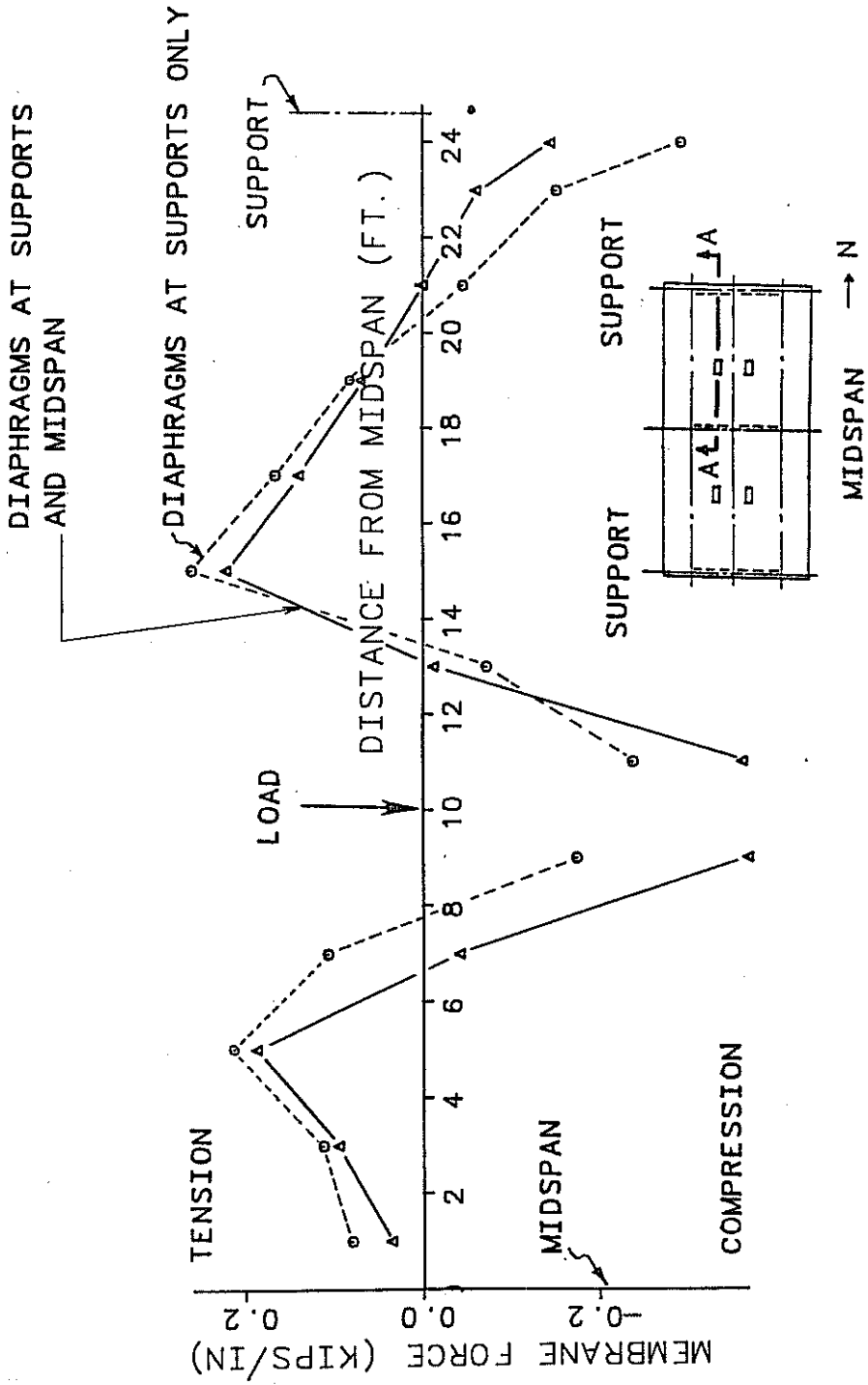

Fig. 7.14 Calculated distribution of transverse membrane force (post-cracked results, CIP deck, 20 kips/ram)

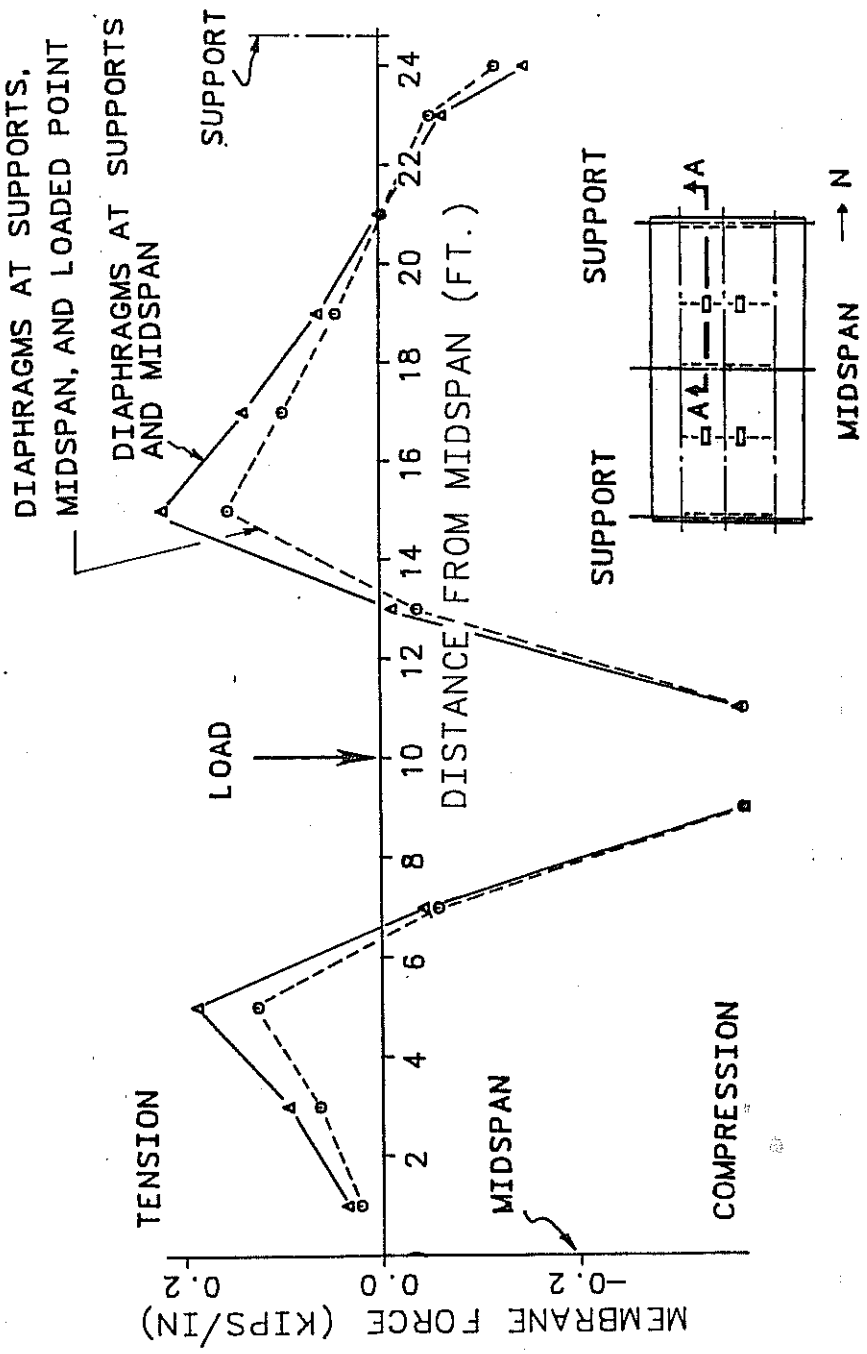

Fig. 7.15 Calculated distribution of transverse membrane force (post-cracked results, CIP deck, 20 kips/ram)

CHAPTER 8

SUMMARY

An experimental and analytical investigation was conducted regarding the behavior of reinforced concrete bridge decks designed in accordance with the Ontario Highway Bridge Deck Design Code.

8.1 Experimental Program

In the experimental part of the investigation, a 20- by 50-ft full-scale composite bridge (concrete deck on steel girders) was built and tested in the Ferguson Structural Engineering Laboratory of The University of Texas at Austin. The northern end of the 7-1/2 in. thick bridge deck was made of cast-in-place concrete, and the southern end, of precast prestressed panels (4 in. thick) with a cast-in-place topping (3-1/2 in. thick). The deck rested on three 36-in. deep steel girders. In this first phase of the experimental program, the bridge was simply supported on a 49-ft span, and loaded vertically at four points.

The bridge was first loaded statically to 60 kips per ram (about three times the current AASHTO design wheel load) to study its response under service and overload conditions, after which it was subjected to sinusoidal fatigue loading with a maximum of 26 kips per ram and a minimum of 5 kips per ram. During the fatigue cycling, the bridge was tested statically at intervals of about 1 million cycles to assess possible deterioration of the deck due to fatigue. After 5 million cycles of fatigue loading, the bridge was loaded statically to a maximum of 40 kips per ram to study its service and overload behavior after fatigue cracking.

8.2 Analytical Program

To check the experimental results and permit their extension to bridge decks other than the one studied experimentally, detailed finite element models of the specimen were developed using SAPIV, a widely available, non-proprietary structural analysis program. The reinforced concrete bridge deck was modeled using two layers of thick shell elements. The steel girder was modeled by three-dimensional beam elements.

Under the range of loads applied during the testing program, experimental results showed that stresses and deflections of the deck were small, and that the bridge behavior could be predicted using a sequence of linear elastic analyses. Cracking of the deck was followed using a smeared cracking model, extended to a three-dimensional stress state.

Two finite element models were developed, one idealizing a specimen with a wholly cast-in-place deck, and the other, with a precast panel deck. The precast panel deck model included the effects of transverse prestressing force in the panels, the different moduli of elasticity in CIP and precast panel concrete, and the gaps between panels.

8.3 Behavior of the Bridge Deck

8.3.1 Load-Deflection Relationships. Experimental results showed that load-deflection behavior at the exterior and interior girder, across the loaded section, is essentially linear up to about three times the design wheel load. Cracking of the CIP deck did not significantly change its stiffness at the loaded point, even after fatigue loading. Linear load-deflection behavior was also observed at the precast panel end. Experimentally measured and analytically predicted load-deflection relationships were almost identical.

8.3.2 Cracking of the Deck. Only a few shrinkage cracks were found on the top surface of the CIP deck. In the panel end, reflected shrinkage cracks less than 0.002 in. wide formed over the panel gaps.

The CIP deck first cracked at an applied load of 38 kips per ram, very close to what was predicted analytically. The precast panel deck developed very minor cracks at 60 kips per ram. The reduced amount of transverse reinforcement compared to AASHTO design requirements did not cause excessive cracking, even after 5 million cycles of fatigue loading. After initial cracking, crack propagation did not occur on the top surface of the CIP deck. However, propagation of minute cracks did occur on the bottom of the deck. On the precast panel end, cracks did not propagate signifiantly, either at the top or the bottom. The cracks above the panels gaps widened slightly, but crack widths were very small throughout all tests.

8.3.3 Local Stresses in the Deck. Numerous strain gages were installed on the bridge deck near the loaded points and along the steel girder. Under the design load of 20.8 kips per ram, the maximum concrete stress was only about 0.4 ksi in both the longitudinal and transverse directions, in both types of bridge deck.

Maximum stress in the transverse reinforcement near the load in the CIP deck reached about 1.8 ksi at that same design load level. Fatigue loading did not significantly change the local stresses in the deck. Stresses in concrete and reinforcement at other locations were relatively small compared to those near the loaded point.

8.3.4 Bending Moments in the Deck. At almost every gaged location, three strain gages were installed to measure the strain gradient. Using an assumed linearized strain gradient, the bending moment in the deck were obtained in both the transverse and longitudinal directions.

At the design load level of 20.8 kips per ram, peak transverse and longitudinal moments were about 2 kip-ft/ft, less than the current AASHTO design value. Peak moments increased slightly after the 5 million cycles of fatigue loading. The maximum longitudinal moment occurred in a very small region near the load, and dropped off rapidly away from the load.

8.3.5 Transverse Membrane Force in the Deck. From the strain gradient at each gaged location, transverse membrane forces were calculated for every load stage. At one location near the load in the CIP deck, transverse membrane forces were all tensile before the deck was significantly cracked. After the deck was significantly cracked, the transverse membrane forces near the load were all compressive, and increased as the load increased. The analytically predicted membrane force distribution agreed reasonably well with the experimental results. The total compressive membrane force near the load is approximately balanced by tensile membrane force in adjacent sections of the deck.

Since there was little cracking at the panel end, little compressive membrane force was found there, even though the deck was loaded up to about three times the service design load.

8.3.6 Effect of Intermediate Diaphragms on Bridge Deck Behavior. The effect of intermediate diaphragms on the bridge deck behavior was studied using the measured test results with and without midspan diaphragms, together with the verified analytical model. The presence of midspan diaphragms or additional diaphragms did not significantly change the local stiffness, local stresses, moment distribution, nor compressive membrane force of the deck. However, intermediate diaphragms might still be necessary for considerations beyond the scope of this report, such as lateral load distribution, construction purposes or overall stability.

8.4 Effects of Arching Action on Bridge Deck Performance

Significant membrane forces did not exist before the start of flexural cracking in the deck. Because significant cracking occurred only at the CIP end compressive membrane forces existed only at that end. It is probable that the ultimate flexural capacity of the CIP deck was significantly increased by arching action. Whether or not this increase in flexural capacity is actually reflected in the failure load of the deck, depends on the deck's punching shear resistance. These topics are outside the scope of this report, and will be discussed in further reports for this project. However, it is worth noting that even without taking arching action into account, current AASHTo requirements for slab flexural reinforcement were conservative in this case.

CHAPTER 9

CONCLUSIONS AND RECOMMENDATIONS

9.1 Conclusions

1. A full-scale, cast-in-place bridge deck on steel girders, detailed in accordance with the Ontario Highway Bridge Design provisions, performed satisfactorily under the current AASHTO design load levels, with respect to overall behavior of the bridge specimen, the local stiffness of the deck at the loaded point, crack widths, and bending moments in the deck.

2. A similarly detailed deck with precast, prestressed panels also performed satisfactorily.

3. Under overload conditions (about three times the current AASHTO design wheel load), the behavior of the deck slab was essentially linear, except for some nonlinearity due to minute tensile cracking of concrete. Fatigue loading did not significantly change the behavior of the deck under service load nor under overloads.

4. These bridge decks, which performed well, had about 60 percent of the reinforcement required by the current AASHTO code.

5. Analytical predictions and experimental results agreed closely, showing that the analytical models of the bridge specimen are satisfactory, and can be extended to other bridge configurations.

6. The presence of midspan diaphragms or additional diaphragms did not significantly change the local stiffness, local stresses, moment distribution, nor compressive membrane force of the deck.

7. Compressive mem brane forces did not significantly affect the performance of the bridge at loads below cracking. The effects of arching action on the ultimate capacity of the bridge deck will be discussed in further reports for this project.

9.2 Recommendations

Based on the results of this research, field use of Ontario-type decks, similar to the one tested in this investigation, seems fully justified. Their field performance should be evaluated by the Texas SDHPT. Further laboratory research should be conducted regarding the behavior of Ontario-type decks on skew bridges.

9.3 Further Research

This study is part of a series of investigations conducted in the Ferguson Structural Engineering Laboratory at The University of Texas at Austin. In this study, the service and overload behavior of two types of bridge deck was investigated, under static and fatigue loads. While both cast-in-place and panel decks were studied, a relatively narrow range of geometries was considered. To obtain a broader understanding of the behavior of bridge decks before the new deck design is completely incorporated in Texas SDHPT design provisions, parametric studies should be conducted involving variables such as the span to thickness ratio of the deck, the effects of line loads, skew bridge behavior, and the stiffness of integral barriers.

Work now in progress on the effects of arching action on ultimate capacity, needs to be completed. Further experimental study is also recommended on the effects of arching action on crack widths and reinforcement stresses at higher load levels.

APPENDIX A

CALCULATION OF REINFORCEMENT REQUIREMENT OF DECK SLAB ACCORDING TO AASHTO CODE AND EMPIRICAL METHOD OF OHBD CODE

This appendix is intended to show the calculation procedure of the reinforcement requirement of deck slab in accordance with the AASHTO design code and with the empirical method of the Ontario Highway Bridge Design Code. An 8-in. thick reinforced concrete deck slab supported by wide flange steel girders at 8 ft-7 in. spacing was used as an example. This example is not intended to duplicate the slab thickness of the test specimen. The 8-in. thickness is acceptable according to both the AASHTO Code and the Texas SDHPT's adaptation of the Ontario Code.

A.1 AASHTO Method

The example deck detailed in accordance with the AASHTO method is shown in Fig. A.1. The amount of reinforcement needed was calculated based on a unit strip of deck slab spanning transversely across the steel girders.

Transverse Reinforcement Needed (ft/ft)

No. 4 (Bars B)	12/9.5 x 8.57 = 10.83 ft
No. 5 (Bars A, C)	12/9.5 x 8.57 x 2 = 21.66 ft

Longitudinal Reinforcement Needed (ft/ft)

No. 4 Bars (Top)	1 ft x 9 = 9 ft
No. 5 Bars (Bottom)	1 ft x 9 = 9 ft

Total Amount of Reinforcement Needed

No. 4 Bars	19.82 ft x 0.668 lbs/ft =	13.25 lbs
No. 5 Bars	30.66 ft x 1.043 lbs/ft =	31.97 lbs
	Total Weight:	45.22

Required Reinforcement Per Unit Area

$45.22/(8.57 \times 1) = 5.28$ lbs/ft^2

A.2 Empirical Method of Ontario Code

The example deck which was detailed with the empirical method of the Ontario Code is shown in Fig. A.2. The amount of reinforcement required was calculated based on the following calculation:

b = 12 in., d = 5.75 in.

Required A_s = Pbd = 0.003)(12)(5.75) = 0.207 in^2/ft

Use No. 4 @ 11 in. top and bottom in both directions.

Actual A_s = 0.218 in^2/ft

Transverse Reinforcement Needed

12/11 x 8.57 x 2 = 18.70 ft (top and bottom)

Longitudinal Reinforcement Needed

(((8.57 x 12)/11) + 1 ft x 2 = 20.70 ft (top and bottom)

Total Amount of Reinforcement Needed

No. 4 Bars:

18.70 + 20.70 = 39.40 ft x 0.668 lbs/ft =

26.32 lbs

Required Reinforcement Per Unit Area

26.32/(8.57 x 1) = 3.07 lbs/ft^2

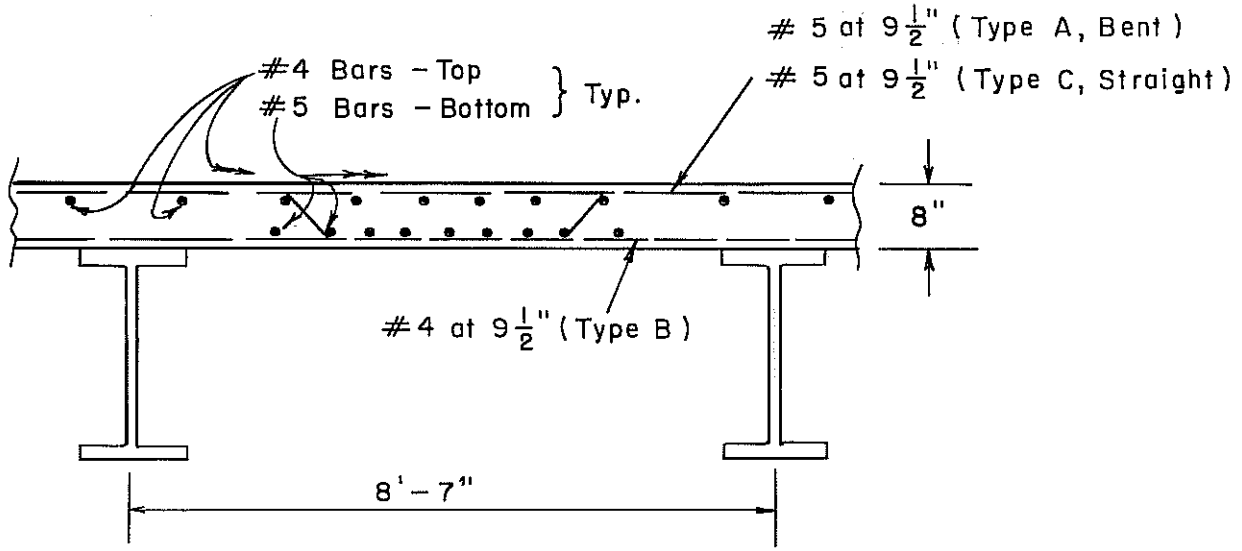

Fig. A.1 Section of example deck detailed with AASHTO method

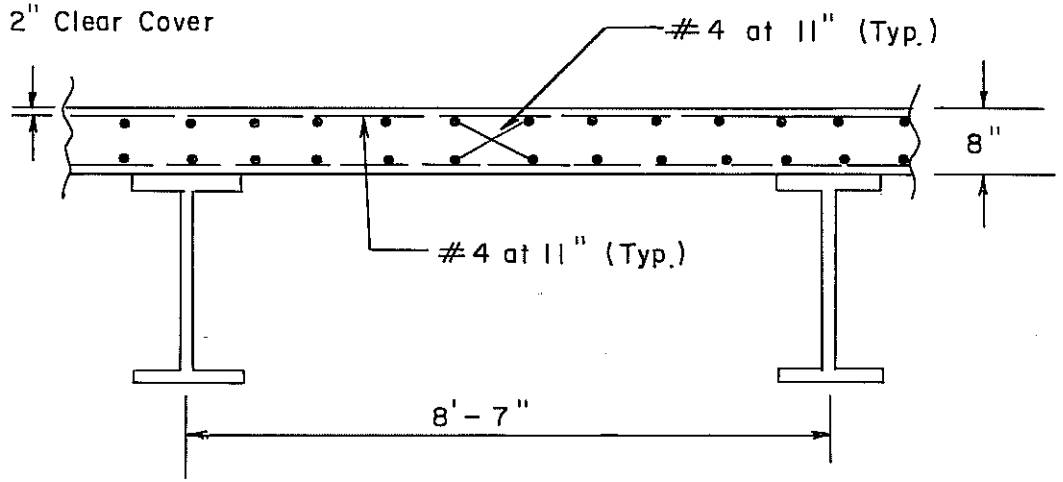

Fig. A.2 Section of example deck detailed with empirical method of Ontario Code

APPENDIX B

MATERIAL PROPERTIES

TABLE B.1 Concrete Mix Design for Cast-in-Place Deck

Design Strength:	3600 psi
Water-Cement Ratio:	0.485
Slump:	3 in.
Type I Cement:	0.36%
Water:	0.42%
Aggregate:	0.22%
Added Water:	0%
Admixture:	6% air entrained

TABLE B.2 Mechanical Characteristics of Cast-in-Place Deck

Concrete	
Casting Date:	2/28/84
f'_c: 14 day:	3510 psi
28 day:	4240 psi
180 day:	5160 psi
Slump:	3 in.
Steel	
Size:	#4
Grade:	60
Tested yield strength:	73 ksi

TABLE B.3 Seven-Day Modulus of Rupture Data,

Cast-in-Place Deck

1	3465	433
2	3470	434
3	4050	506
4	3890	486
5	2880	360
6	2080	385
7	3040	380
8	3580	448
9	3700	463

Average:	433 psi
Standard Deviation	49.6 psi

$ft = My/I = ((18P/4)3/(6^4/12) = P/8$ (psi)

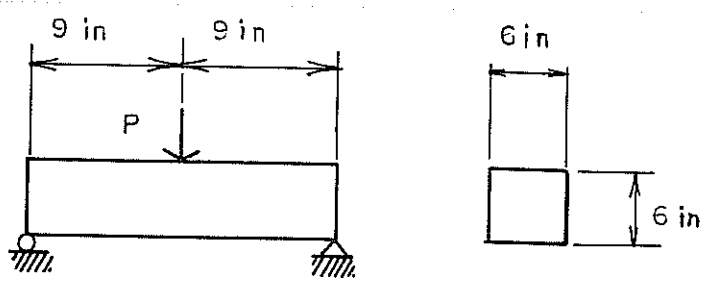

TABLE B.4 Mechanical Characteristics of Precast, Prestressed Panels

Concrete	
Release Strength:	4000 psi
Design Strength:	6000 psi
Type:	Texas Class H, Type III (high early strength) cement, 6-1/2 sacks/cu. yd.)
Casting date:	2/2/84
f'_c 48 hr:	5104 psi
7 day:	6593 psi
Slump:	4 in.
Prestressing Steel	
Size of strand:	3/8-in. diameter
Type:	7-wire
Grade:	270, stressed-relieved
Prestress force per strand:	16.1 kips

APPENDIX C

INPUT DATA CHECK FOR FINITE ELEMENT MODEL OF BRIDGE SPECIMEN

As developed in Chapter 4, the quarter-bridge model consisted of 156 thick shell elements, and 300 three-dimensional beam elements. A total of 937 nodes were used. In each thick shell element, there are 16 nodal numbers distributed at midsides and corners. In addition to these, different types of material properties and member properties are needed for the input of each type of elements. To facilitate generation and checking of input data, several accessory programs were therefore developed.

The finite element mesh at the top, middle and bottom surfaces of the deck were plotted. The nodal points with identical boundary conditions were plotted with the same color pen, permitting easy detection of input errors. The connectivity between nodal numbers and element number was checked by plotting the element number at the center of each element. Any errors in the location of the plotted element number could be clearly identified, and the connectivity between element number and associated nodal numbers can be examined. The input data for beam elements was checked similarly.

A known vertical load was applied to the model deck. The support reactions were compared with the externally applied load. The deformed shape of the bridge was checked in the transverse and longitudinal direction at various sections. Using the Zeta plotter and specially developed software the distribution of bending stresses in the deck slab in both directions were also plotted.

APPENDIX D

CALCULATION OF AXIAL FORCE AND MOMENT

The following example is used to explain the procedure for calculating axial force and moment from strain gage readings in concrete and reinforcement. Refer to Fig. D.1.

Example:

Measured concrete strain at compressive side:	36 $\mu\varepsilon$
Measured reinforcement strain on tension side:	298 $\mu\varepsilon$
Calculated reinforcement strain on other layer:	114 $\mu\varepsilon$
Calculated concrete srain at tension side:	465 $\mu\varepsilon$
f'_c at 28 days:	4240 psi
$E_c = 57{,}000\sqrt{f'_c}$	488 psi
Maximum allowable tensile strain of concrete:	132 $\mu\varepsilon$

Because the concrete tensile strain is greater than 132 $\mu\varepsilon$, C2 will be ignored.

Total axial force = S1+ S2 + C1

= 1.73 + 0.66 - 0.04

= 2.35 kips/in.

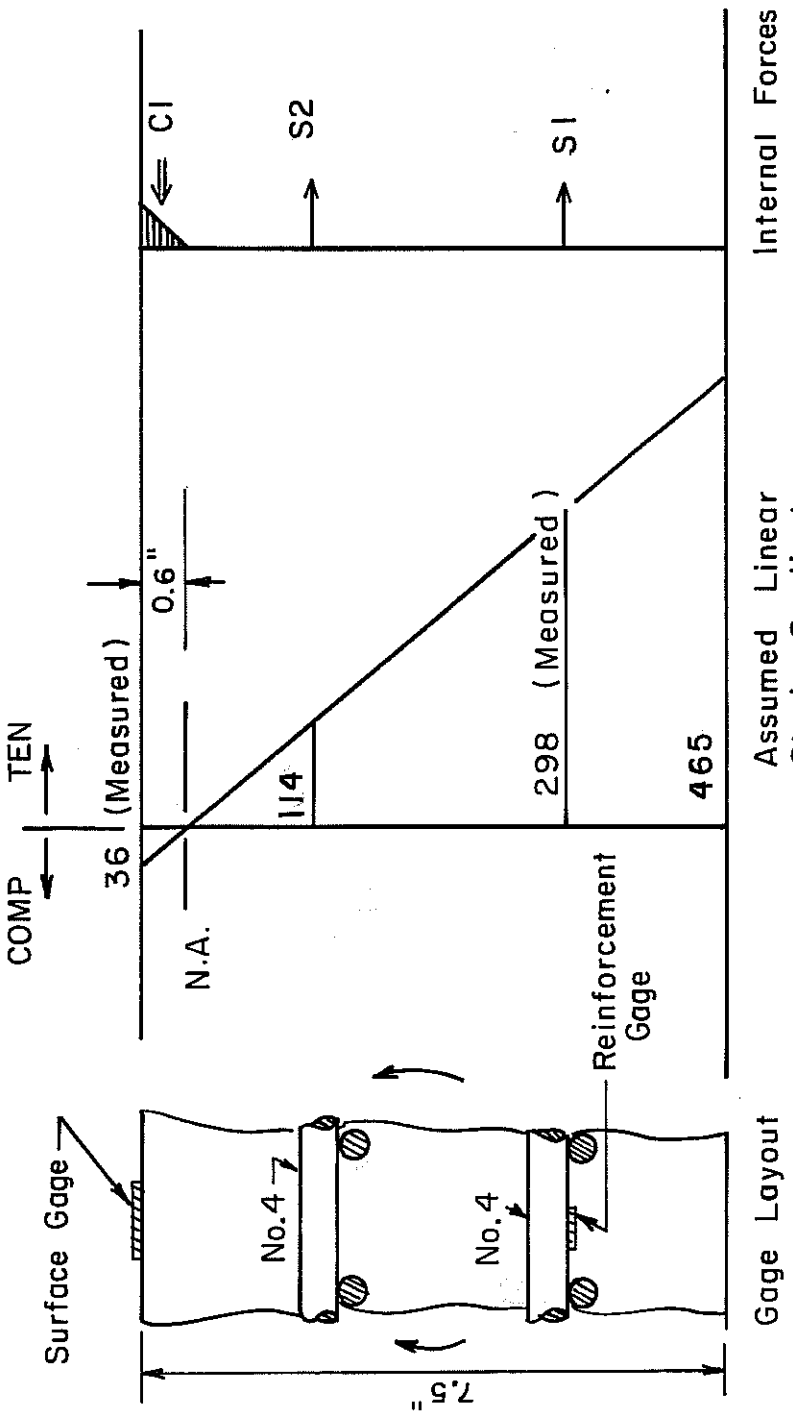

Fig. D.1 Calculation of axial force and moment from measured strain gage readings

R E F E R E N C E S

1.1 Standard Specifications for Highway Bridges, 13th Edition, American Association of State Highway and Transportation Officials, 1983.

1.2 Ontario Highway Bridge Design Code, Ontario Ministry of Transportation and Communications, 2nd Edition, 1983.

1.3 Elling, C.W., "Distribution of Girder Loads in a Composite Highway Bridge," Thesis presented to The University of Texas at Austin, Texas, in partial fulfillment of the requirements for the degree of Master of Science in Engineering, May, 1985.

1.4 Tsu, K. T., "A Study of the Negative Moment Region and the Strength of a Highway Bridge Deck", Thesis presented to the University of Texas at Austin, Texas, in partial fulfillment of the requirements for the degree of Master of Science in Engineering, May, 1985

2.1 Timoshenko, S. and Woinowsky-Krieger, S., Theory of Plates and Shells, 2nd Edition, McGraw-Hill Book Company, Inc., New York, 1959.

2.2 Ugural, A.C., Stresses in Plates and Shells, McGraw-Hill Book Company, Inc., New York, 1981.

2.3 Ockleston, A. J., "Load Tests on a Three Story Concrete Building in Johannesburg," The Structural Engineer, Vol. 33, No. 10, October 1955, pp. 304-322.

2.4 Ockleston, A.J., "Arching Action in Reinforced Concrete Slabs," The Structural Engineer, Vol. 36, No. 6, June 1958, pp. 197-201.

2.5 Leibenberg, A.C., "Arching Action in Concrete Slabs," National Building Research Institute, Council for Scientific and Industrial Research, Report 234, South Africa, 1966.

2.6 Guyon, Y., Prestressed Concrete, Vol. 2, New York, John Wiley & Sons, 1962.

2.7 Christiansen, K. P., "The Effect of Membrane Stresses on the Ultimate Strength of the Internal Panel in a Reinforced Concrete Slab," The Structural Engineer, Vol. 41, No. 8, August 1963, pp. 261-265.

2.8 Christiansen, K. P., "Experimental Investigation of Rectangular Concrete Slabs with Horizontal Restraints," Materials and Structures, Vol. 16, No. 93, May-June 1982, pp. 178-192.

2.9 Park, R., "The Lateral Stiffness and Strength Required to Ensure Membrane Action at the Ultimate Load of a Reinforced Concrete Slab-and-Beam Floor," Magazine of Concrete Research, Vol. 17, No. 50, March 1965, pp. 29-38.

2.10 Park, R., "Tensile Membrane Behaviour of Uniformly Loaded Rectangular Reinforced Concrete Slabs with Fully Restrained Edges," Magazine of Concrete Research, Vol. 16, No. 46, March 1964, pp. 39-44.

2.11 Park, R., "The Ultimate Strength and Long-Term Behavior of Uniformly Loaded, Two-Way Concrete Slabs with Partial Lateral Restraint at All Edges," Magazine of Concrete Research, Vol. 16, No. 48, September 1964, pp. 139-152.

2.12 Park, R., "Ultimate Strength of Rectangular Concrete Slabs Under Short-term Uniform Loading with Edges Restrained Against Lateral Movement," Proceeding of the Institute of Civil Engineers, Vol. 28, No. 6705, 1964, pp. 125-145.

2.13 Park, R., Gamble, W. L., Reinfored Concrete Slabs, 1980.

2.14 Girolami, A. G., Sozen, M. A., and Gamble, W. L., "Flexural Strength of Reinforced Concrete Slabs with Externally Applied In-Plane Forces," Report to the Defense Office of the Secretary of the Army and Office of Civil Defense, October 1970.

2.15 Gamble, W. L., Flug, H., and Sozen, M. A., "Strength of Slabs Subjected to Multiaxial Bending and Compression," Report to the Defense Office of the Secretary of the Army and Office of Civil Defense, October 1970.

2.16 Hopkins, David C., and Park, R., "Test on a Reinforced Concrete Slab and Beam Floor Designed with Allowance for Membrane Action," and "Cracking, Deflection and Ultimate Load of Concrete Slab Systems," Special Publication SP-30, American Concrete Institute, 1971, pp. 223-250.

2.17 Tong, P. Y., and Batchelor, B., deV., "Compressive Membrane Enhancement in Two-Way Bridge Slabs," Special Publication SP-30, American Concrete Institute, 1971, pp. 271-286.

2.18 Brotchie, J. F. and Holley, M. J., "Membrane Action in Slabs", Special Publication SP-30, American Concrete Institute, 191, pp. 345-377.

2.19 Csagoly, P. F. and Dorton, R. A., "The Development of the Ontario Highway Design Bridge Code," Transportation Research Record, No. 665, 1978, pp. 1-12.

2.20 Buckland, P. G. and Sexsmith, R. G., "A Comparison of Design Loads for Highway Bridges," Canadian Journal of Civil Engineering, Vol. 8, No. 1, 1981, pp. 16-21.

2.21 Bakht, B., Cheung, M. S., Dorton, R., "A Comparison of Design Loads for Highway Bridges: Discussion," Canadian Journal of Civil Engineering, Vol. 9, No. 1, 1982, pp. 138-140.

2.22 Ontario Highway Bridge Design Code, Ontario Ministry of Transportation and Communications, 2nd Edition, 1983.

2.23 Bekht, G. and Csagoly, P> F., "Bridge Testing," Research Report No. 79-SSR-10, Ministry of Transportation and Communications of Ontario, Downsview, August 1979, pp. 127.

2.24 Batchelor, B. deV., Hewitt, B. E., Csagoly, P., and Holowka, M., "Investigation of the Ultimate Strength of Deck Slabs of Composite Steel/Concrete Bridges," Transportation Research Record, No. 664, 1978, pp. 162-170.

2.25 Batchelor, B. deV., Hewitt, B.E., and Csagoly, P., "Investigation of the Fatigue Strength of Dek Slabs of Composite Steel/Concrete Bridges," Transportation Research Record, No. 664, 1978, pp. 153-161.

2.26 Hewitt, B. E. and Batchelor, B. deV., "Punching Shear Strength of Restrained Slabs," Proceedings, ASCE, ST9, September 1975, pp. 1827-1853.

2.27 Hewitt, B. E., "An Investigation of the Punching Strength of Restrained Slabs with Particular Reference to the Deck Slabs of Composite I-Beam Bridges," Thesis presented to Queen's University of Kingston, Canada, in 1972, in partial fulfillment of the requirements for the degree of Doctor of Philosophy.

2.28 Csagoly, P., Holowka, M., and Dorton, R. A., "The True Behavior of Thin Concrete Bridge Slabs," Transportation Researach Record, No. 664, 1978, pp. 171-179.

2.29 Dorton, R. A., and Holowka, M., "The Conestogo River Bridge -- Design and Testing," Canadian Journal of Civil Engineering, Vol. 4, No. 1, 1977, pp. 18-39.

2.30 Bakht, B., "Testing of the Manitou Bridge to Determine Its Safe Load Carrying Capacity," Canadian Journal of Civil Engineering, Vol. 8, No. 1, 1981, pp. 218-229.

2.31 Standard Specifications for Highway Bridges 13th Edition, American Association of Highway and Transportation Officials, 1983.

2.32 Holowka, M., "Testing of a Trapezoidal Box Girder Bridge," Structural Research Report RR221, Ontario Ministry of Transportation and Communications, November 1979.

2.33 Holowka, M. and Csagoly, P., "A Composite Prestressed Concrete AASHTO Girder Bridge," Research Report RR222, Ontario Ministry of Transportation and Communications, July 1980.

2.34 Beal, D. B., "Strength of Concrete Bridge Deck," Research Report 89, New York State Department of Transportation, July 1981.

3.1 Ontario Highway Bridge Design Code, Ontario Ministry of Transportation and Communications, Ontario, Canada, 1983, 357 pp. (with Commentary).

3.2 Drawings for "Proposed Bridge Deck Details (Ontario 1977 Bridge Code)," File No. 1284, Texas SDHPT, October 1981 (2 sheets).

3.3 Texas Highway Department, "Summary Report on Investigation to Determine Feasibility of Using In-Place Precast Prestressed Form Panels for Highway Bridge Decks," PCI Journal, Vol. 20, No. 3, May-June 1975, pp. 62-67.

3.4 Kluge, R. W. and Sawyer, H. A., "Interacting Pretensioned Concrete Form Panels for Bridge Decks," PCI Journal, Vol. 20, No. 3, May-June 1975, pp. 34-61.

3.5 Barnoff, R. M. and Orndorff, J. A., "Construction and Testing of an Experimental Prestressed Concrete Bridge," Report No. 1, The Pennsylvania State Univesity, University Park, Pennsylvania, 1974.

3.6 Barnoff, R. M. and Rainey, D. L., "Laboratory Tests of Prestressed Concrete Deck Planks and Deck Plank Assemblies," Report No. 2, The Pennsylvania Transportation Institute, The

Pennsylvania State University, University Park, Pennsylvania, 1974.

3.7 Jones, H. L. and Furr, H. L. "Study of In-Service Bridges Constructed with Prestressed Panel Subdecks," Research Report 145-1, Texas Transportation Institute, Texas A & M University, College Station, Texas, 1970.

3.8 Jones, H. L. and Furr, H. L., "Development of Length of Strands in Prestressed Panel Subdecks," Research Report 145-2, Texas Transportation Institute, Texas A & M University, College Station, Texas, 1970.

3.9 Buth, E., Furr, H. L., Jones, H. L., and Toprac, A. A., "Evaluation of a Prestressed Panel, Cast-in-Place Concrete Bridge," Research Report 145-3, Texas Transportation Institute, Texas A & M University, College Station, Texas, 1972.

3.10 Furr, H. L. and Ingram, Leonard L., "Cyclic Load Tests of Composite Prestressed-Reinforced Concrete Panels," Research Report 145-4, Texas Transportation Institute, Texas A & M University, College Station, Texas, 1972.

3.11 Barker, J. M., "Research, Adaptation and Experience with Precast Prestressed Bridge Deck Panels," PCI Journal, Vol. 20, No. 6, November-December, 1975, pp. 67-82.

3.12 Reed, R. L., "Application and Design of Prestressed Deck Panels," Transportation Research Record, No. 665, 1978, pp. 164-171.

3.13 Bieschke, L. A. and Klingner, R. E., "The Effect of Transverse Strand Extensions on the Behavior of Precast Prestressed Panel Bridges," Research Report No. 303-1F, Center for Transportation Research, The University of Texas at Austin, June 1982.

3.14 Texas Highway Department, "Standard Specifications for Construction of Highways, Streets, and Bridges," September 1, 1982.

4.1 Cusens, A. R. and Pama, R. P., Bridge Deck Analysis, John Wiley & Sons, Ltd., 1975.

4.2 Loo, Y. C. and Cusens, A. R., The Finite-Strip Method in Bridge Engineering, Cement and Concrete Association, 1975.

4.3 Cheung, M. S., Bakht, B., Jaeger, L. G., "Analysis of Box-Girder Bridges by Grillage and Orthotropic Plate Methods," Canadian Journal of Civil Engineering, Vol. 9, 1982, pp. 595-601.

4.4 Bathe, J. J., Wilson, E. L., and Peterson, F. E., "SAP IV: A Structural Analysis Program for Static and Dynamic Response of Linear Systems," Report No. EERC 73-11, Earthquake Engineering Research Center, University of California at Berkeley, 1973.

4.5 Finite Element Analysis of Reinforced Concrete, American Society of Civil Engineers, 1982.

4.6 Chen, W. F., Plasticity in Reinforced Concrete, McGraw-Hill Book Co., New York, 1981.

4.7 Bazant, A. P. and Cedolin, L., "Blunt Crack Band Propagation in Finite Element Analysis," Journal of the Engineering Mechanics Division, ASCE, Vol. 105, No. EM2, Proc. Paper 14529, April 1979, pp. 279-315.

4.8 Bazant, Z. P. and Cedolin, L., "Fraction Mechanics in Reinforced Concrete," Journal of Engineering Mechanics Division ASCE, Vol. 106, EM6, December 1980.

4.9 Gallagher, R. H., "A Review of Finite Element Techniques in Fracture Mechanics," Proceedings of the First International Conference on Numerical Methods in Fracture Mechanics, Swansea, January 9-13, 1978, pp. 1-25.

4.10 Kesler, C. E., Naus, D. J., and Lott, J. L., "Fracture Mechanics-Its Applicability to Concrete," Proceedings of the 1971 International Conference on Mechanical Behavior of Materials, Vol. IV, Japan, 1972, pp. 113-124.

4.11 Lynn, P. P. and Ingraffea, A. R., "Transition Elements to be Used with Quarter-Point Crack-Tip Elements," International Journal for Numerical Methods in Engineering, Vol. 12, No. 6, 1978, pp. 1031-1036.

4.12 Ngo, D., and Scordelis, A. C., "Finite Element Analysis of Reinforced Concrete Beams," Journal of the American Concrete Institute, Vol. 64, No. 3, March 1967, pp. 152-163.

4.13 Nilson, A. H., "Nonlinear Analysis of Reinforced Concrete by the Finite Element Method," Journal of the American Concrete Institute, Vol. 65, No. 9, September 1968, pp. 757-766.

4.14 Kupfer, H., Hilsdorf, H. K., and Rusch, H., "Behavior of Concrete Under Biaxial Stresses," Journal of the American Concrete Institute, August 1969, Vol. 66.

4.15 Rashid, Y. R., "Analysis of Prestressed Concrete Pressure Vessels," Nuclear Engineering and Design, Vol. 7, No. 4, April 1968, pp. 334-344.

4.16 Cervenka, V., "Inelastic Finite Element Analysis of Reinforced Concrete Panels Under In-Plane Loads," Thesis presented to the University of Colorado at Boulder, Colorado, in 1970, in partial fulfillment of the requirements for the degree of Doctor of Philosophy.

4.17 Cervenka, V. and Gerstle, K. H., "Inelastic Analysis of Reinforced Concrete Panels, Part I: Theory," International Association of Bridge and Structural Engineering Publications, Vol. 31-11, 1971, pp. 31-45, "Part II: Experimental Verification and Application,", Vol. 32-11, 1972, pp. 25-39.

4.18 Vallippan, s. and Doolan, T. F., "Nonlinear Stress Analysis of Reinforced Concrete," Journal of the Structural Division, ASCE, Vol. 98, No. Sta. 4, Proc. Paper 8845, April 1972, pp. 885-898.

4.19 Schnobrich, W. C., et al. Discussion of "Nonlinear Stress Analysis of Reinforced Concrete," by Vallippan and Doolan, Journal of the Structural Division, ASCE, Vol. 98, No. ST10, October 1972, pp. 2327-2328.

4.20 Lin, C. S. and Scordelis, A., "Nonlinear Analysis of RC Shells of General Form," Journal of the Structural Division, ASCE, No. ST3, Proc. Paper 11164, March 1975.

4.21 Hand, F. R., Pecknold, D. A. and Schnobrich, W. C., "Nonlinear Layered Analysis of RC Plates and Shells," Journal of the Structural Division, ASCE, Vol. 99, No. ST7, Proc. Paper 9860, July 1973 pp. 1491-1505.

4.22 Yuzugullu, O. and Schnobrich, W. C., "A Numerical Procedure for the Determination of the Behavior of a Shear Wall Frame System," Journal of the American Concrete Institute, Vol. 70, No. 7, July 1973, pp. 474-479.

4.23 Bashur, F. K. and Darwin, D., "Nonlinear Model for Reinforced Concrete Slabs," Journal of the Structural Division, ASCE, Vol. 104, No. ST1, Proc. Paper 13495, January 1978, pp. 157-170.

4.24 Darwin, D. and Pecknold, D. A., "Analysis of RC Shear Panels Under Cyclic Loading," Journal of the Structural Division, ASCE, Vol. 102, No. ST2, Proc. Paper 11896, february 1976, pp. 355-369.

4.25 Kabir, A. F., "Nonlinear Analysis of Reinforced concrete Panels, Slabs and Shells for Time Dependent Effects," UC-SESM Report No. 76-6, University of California at Berkeley, December 1976.

4.26 Salem, M. H. and Mohraz, B., "Nonlinear Analysis of Planar Reinforced Concrete Structures," Civil Engineering Studies, SRS No. 410, University of Illinois at Urbana-Champaign, Urbana, Illinois, July 1974.

4.27 Van Greunen, J., "Nonlinear Geometric, Material and Time Dependent analysis of Reinforced and Prestressed Concrete Slabs and Panels," UC-SESM Report No. 79-3, University of California at Berkeley, October 1979.

4.28 Bieschke, L. A. and Klingner, R. E., "The Effect of Transverse Strand Extensions on the Behavior of Precast Prestressed Panel Bridges," Research Report No. 303-1F, Center for Transportation Research, The University of Texas at Austin, June 1982

6.1 Ontario Highway Bridge Design Code, Ontario Ministry of Transportation and Communications, 1983.

6.2 Building Code Requirements for Reinforced Concrete, American Concrete Institute 318-83.pa

7.1 Lount, A.M., "Distribution of Loads on Bridge Decks," Journal of the Structural Division, ASCE, Vol. 83, ST4, July 1957, pp. 1303-23.

7.2 Wei, Benjamin, C.F., "Load Distribution of Diaphragm in I-Beam Bridges," Journal of the Structural Division, ASCE, Vol. 85, ST5, May 1959, pp. 17-55.

7.3 White, A. and Purnell, W.B., "Lateral Load Distribution Tests on I-Beam Bridge," Journal of the Structural Division, ASCE, Vol. 83, ST3, May 1957, pp. 1255-1-1255-20.

7.4 Sengputa, S. and Breen, J. E., "The Effect of Diaphragms in Prestressed Concrete Girder and Slab Bridges," Research Report No. 158-1F, Center for Highway Research, The University of Texas at Austin, October 1973, pp. 232.